



**MONASH** University

# **Towards the Development of Corrosion Resistant Aluminium Alloys**

A thesis submitted for the fulfilment of the degree of Doctor of Philosophy

by

**Nazatul Liana Sukiman**

ARC Centre of Excellence for Design in Light Materials

Department of Materials Engineering

Monash University

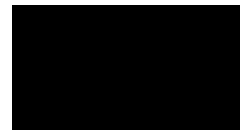
Australia

December 2013

## **Copyright Notice**

Under the Copyright Act 1968, this thesis must be used only under the normal conditions of scholarly fair dealing. In particular no results or conclusions should be extracted from it, nor should it be copied or closely paraphrased in whole or in part without the written consent from the author. Proper written acknowledgement should be made for any assistance obtained from this thesis.

I certify that I have made all reasonable efforts to secure copyright permissions for third party content included in this thesis and have not knowingly added copyright content to my work without the owner's permission.



.....

Nazatul Liana Sukiman



## **General Declaration**

### **Declaration for thesis based or partially based on conjointly published or unpublished work**

In accordance with Monash University Doctorate Regulation 17 Doctor of Philosophy and Research Master's regulations the following declarations are made:

I hereby declare that this thesis contains no material which has been accepted for the award of any other degree or diploma at any university or equivalent institution and that, to the best of my knowledge and belief, this thesis contains no material previously published or written by another person, except where due reference is made in the text of the thesis.

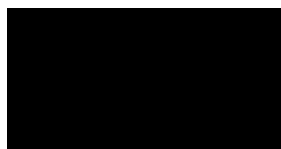
This thesis includes 7 original papers published in peer reviewed journals, 1 invited book chapter and 1 unpublished publication. The core theme of the thesis is “towards the development of corrosion resistant aluminium alloys”. The ideas, development and writing up of all the papers in the thesis were the principal responsibility of myself, the candidate, working within the Department of Materials Engineering under the supervision of Prof. Nick Birbilis.

The inclusion of co-authors reflects the fact that the work came from active collaboration between researchers and acknowledges input into team-based research.

The following international peer-reviewed academic journal articles are presented in this thesis:

<b>Item No</b>	<b>Thesis Chapter</b>	<b>Publication Title</b>	<b>Publication Status</b>	<b>Nature and extent of candidate's contribution</b>
1	2	Durability and corrosion of aluminium and its alloys: Overview, property space, techniques and developments	Aluminium Alloys, ISBN 980-953-307-512-4	Initiation, key ideas, experimental, development, results interpretations, writing up [75%]
2	4	A consolidated presentation of bulk chemical effects on the corrosion kinetics of some commercial wrought aluminium alloys	Corrosion (Submitted in December, 2013)	Initiation, key ideas, experimental, development, results interpretations, writing up [85%]
3	5	Influence of microalloying additions on Al-Mg alloy. Part 1: Corrosion and electrochemical response	Corrosion Engineering, Science and Technology, 49 (4), pp 254-262 (2014)	Initiation, key ideas, experimental, development, results interpretations, writing up [85%]
4	5	Electrochemical behavior and localised corrosion associated with Mg <sub>2</sub> Si Particles in Al and Mg Alloys	ECS Electrochemistry Letters, 1 (2012) B1-B3	Experimental, development, results interpretations [40%]
5	5	Metastable pitting characteristics of aluminium alloys measured using current transients during potentiostatic polarisation	Electrochimica Acta, 66 (2012) 245-254	Experimental, development, results interpretations [35%]
6	6	Influence of microalloying additions on Al-Mg alloy. Part 2: Phase analysis and sensitisation behaviour	Corrosion Engineering, Science and Technology, 49 (4), pp 263-268 (2014)	Initiation, key ideas, experimental, development, results interpretations, writing up [80%]
7	7	Electrochemical and corrosion response of commercially pure aluminium alloyed with binary additions of strontium	Journal of The Electrochemical Society, 160 (8) C299-C304 (2013)	Initiation, key ideas, experimental, development, results interpretations, writing up [80%]
8	7	Influence of alloyed Nd content on the corrosion of an Al-5Mg alloy	Corrosion Science, 73 (2013) 181-187	Experimental, development, results interpretations [30%]
9	7	Imparting sensitization resistance to an Al-5Mg alloy via Neodymium additions	Corrosion, 69 (1), pp. 4-8 (2013)	Experimental, development, results interpretations [30%]

I have renumbered sections of submitted or published papers in order to generate a consistent presentation within the thesis.



Signed: .....

Date: 18 June 2014

# Acknowledgement

---

This thesis would not have been possible without the help and guidance from many individuals. Here, I would like to express my sincere gratitude to them for lending me their support, share their experiences, knowledge and also expertise. Firstly I would like to thank my supervisor, Prof. Nick Birbilis, who have taken me under his wings and nurtured me throughout this experience. His never ending support and advice will never be forgotten. I would also like to acknowledge my co-supervisor, Prof. Rudy Buchheit who made my visit to the Ohio State University, USA possible and a rewarding one.

To the Postdocs in the group, Dr. Rajeev Gupta, Dr. Kevin Ralston and Dr. Marie Clancy who unselfishly aided me in the laboratory from the very start and were always ready to share their insights and thoughts in discussions regarding my project. To the ARC Centre of Excellence for Design in Light Metals, for their full support on my project, to the Victorian Facility for Light Metals Surface Technology for the lab provisions and to the RMIT Microscopy and Microanalysis Facility (RMMF) for providing high quality electron microscopy equipment.

Not to forget the Ministry of Higher Education Malaysia and University of Malaya who have provided me with the scholarship to pursue this project. Without their full support and funding, this project would have never taken place. To my friends and colleagues especially Kateryna Gusieva, Sebastian Thomas, Xian Zhou and Asyraf Kassim; who made my time in Monash University and Melbourne a joyful one. Last but not least, to my family for their endless encouragement and a special thank you goes out to Nadia, for giving me strength and standing by me through and through.

# Abstract

---

This dissertation reports some discrete developments towards more corrosion resistant Al-alloys by controlling alloy chemistry and microstructure. Al-alloys are generally passive and corrosion resistant due to the presence of a protective aluminium oxide film. However, on exposure to a corrosive environment (i.e. solution containing halide ions), Al-alloys are prone to localised attack, particularly pitting. The pits are typically initiated by the differing electrochemical interaction (and roles) of second phase particles with the surrounding Al-matrix, which can also contribute to pit propagation. The corrosion response of the alloys herein was evaluated with a combination of immersion and electrochemical tests, including potentiodynamic polarisation (PDP) and electrochemical impedance spectroscopy (EIS). Corrosion assessment was supplemented by surface analysis with scanning electron microscopy (SEM) and optical profilometry.

Development towards a more corrosion resistant Al-alloy was approached in stages, wherein the first stage involved characterising the corrosion response of commercial Al-alloys for the construction (i.e. revelation) of primitive property space (hardness vs. corrosion rate). This highlighted the opportunities in minimising corrosion whilst being aware of mechanical strength (albeit that hardness was used in this project as proxy to mechanical strength). A consolidated presentation of the role of chemistry on both the corrosion kinetics and hardness suggested that reducing/eliminating Cu and limiting microstructural heterogeneity (i.e. additional phases) are effective in minimising corrosion. It was empirically revealed that AA5083 (Al-4.4Mg-0.4Mn), which has medium strength and low corrosion rates, was the ‘best compromise’ (commercial) alloy and will be further explored in this project.

The next stage was to investigate the effect of alloying elements to the Al-4.0Mg-0.4Mn (similar to the AA5083 commercial alloy composition) system. This study was divided into two parts. The first part aimed to understand the effect of microalloying additions to the microstructure of Al-4.0Mg-0.4Mn in relation to the electrochemical response and subsequent corrosion morphology. The effect of microalloying upon the microstructure of the base alloy was demonstrated by the formation of additional intermetallic particles (be it dispersoids or constituent particles). The second part of the study was to investigate the effect of microalloying additions on the intergranular corrosion susceptibility. In the sensitised

condition, Al-4.0Mg-0.4Mn alloys are prone to intergranular attack, as the electrochemically active  $\beta$ -phase ( $\text{Mg}_2\text{Al}_3$ ) tends to precipitate at grain boundaries. A consolidated presentation of the outcomes from a number of corrosion measurement methods employed, revealed the alloying additions that can improve corrosion resistance of the Al-4.0Mg-0.4Mn alloy. For mass loss, Zn addition yields better resistance to corrosion, whereas PDP test indicates Si, Zr and Sr have lower  $i_{\text{corr}}$  than Al-4.0Mg-0.4Mn alloy. On the other hand, addition of Ti, Si and Sr reduce the susceptibility to intergranular corrosion. Sr was particularly effective due to its ability to modify the  $\beta$ -phase characteristics.

The corrosion response measured on the Al-4.0Mg-0.4Mn system, microalloyed with different elements, revealed that Sr and Nd imparted a good compromise between corrosion resistance and hardness. Therefore new Al-Mg alloys were studied from more systematic in-house production with different concentrations of Sr and Nd. For alloys containing Sr, the localised corrosion was not associated with the presence of the  $\text{Al}_4\text{Sr}$  intermetallic particles but rather the Fe-containing constituent particles (which are present in all commercial Al-alloys). The presence of Sr greatly retarded the precipitation of  $\beta$ -phase. The addition of Nd revealed a similar trend, where the presence of fine  $\text{Al}_{11}\text{Nd}_3$  intermetallics did not have a significant influence on localised corrosion. Transmission electron microscopy (TEM) analysis revealed fine  $\text{Al}_{11}\text{Nd}_3$  intermetallics, formed at the grain boundaries along with  $\beta$ -phase, may serve to increase the intergranular corrosion resistance.

The information from this project is intended to contribute to certain knowledge gaps in the literature on the background, basis, and development of more corrosion resistant Al-alloys; bearing in mind that the new alloys must retain or improve the mechanical properties.

# Table of Contents

---

<b>Acknowledgements</b>	<b>I</b>
<b>Abstract</b>	<b>II</b>
<b>List of Figures</b>	<b>VII</b>
<b>List of Tables</b>	<b>IX</b>
<b>List of Publications</b>	<b>X</b>
<b>Chapter 1      Introduction</b>	<b>1</b>
<b>Chapter 2      Literature Review</b>	
2.1 The origin of Aluminium	<b>4</b>
2.2 Physical metallurgy of aluminium alloys	<b>7</b>
2.2.1 Non-heat treatable alloys	<b>9</b>
2.2.2 Heat treatable alloys	<b>10</b>
2.2.3 Influence of strengthening mechanism on corrosion	<b>23</b>
2.3 Challenges in aluminium alloys applications	<b>24</b>
2.4 Methods to improve corrosion via alloying	<b>26</b>
2.5 Evaluation of Al-alloys corrosion via electrochemical polarisation technique	<b>30</b>
2.6 Durability and Corrosion of Aluminium and Its alloys: Overview, Property Space, Techniques and Developments	<b>34</b>
<b>Chapter 3      Research Aims and Dissertation Outline</b>	
3.1 Research Aims	<b>91</b>

	3.2 Dissertation Outline	93
	3.3 Laboratory testing and setup	95
<b>Chapter 4</b>	<b>The construction of Al-alloys property space</b>	
	4.1 A consolidated presentation of bulk chemical effects on the corrosion kinetics of some commercial wrought aluminium alloys	104
<b>Chapter 5</b>	<b>The role of chemistry in the general corrosion behaviour of Al-alloys</b>	
	5.1 The influence of microalloying additions on Al-Mg alloy (Al-4Mg-0.4Mn), Part 1: Corrosion and electrochemical response	130
	5.2 Electrochemical behavior and localised corrosion associated with Mg <sub>2</sub> Si Particles in Al and Mg Alloys	140
	5.3 Metastable pitting characteristics of aluminium alloys measured using current transients during potentiostatic polarisation	144
<b>Chapter 6</b>	<b>The role of chemistry in intergranular corrosion of Al-4Mg-0.5Mn</b>	
	6.1 The influence of microalloying additions on Al-Mg alloy (Al-4Mg-0.4Mn), Part 2: Phase analysis and sensitisation behaviour	156
<b>Chapter 7</b>	<b>Alloying additions to improve the corrosion performance of Al-Mg-Mn alloys</b>	
	7.1 Electrochemical and corrosion response of commercially pure aluminium alloyed with binary additions of strontium	165
	7.2 Influence of alloyed Nd content on the corrosion of an	172



	Al-5Mg alloy	
	7.3 Imparting sensitization resistance to an Al-5Mg alloy via Neodymium additions	<b>180</b>
<b>Chapter 8</b>	<b>Discussion and Future Works</b>	
	8.1 General Discussion	<b>185</b>
	8.2 Future Works	<b>190</b>
<b>Chapter 9</b>	<b>Conclusions</b>	<b>193</b>

# List of Figures

<b>Figure 2.1</b>	Flow diagram for integrated production of aluminium from bauxite	<b>5</b>
<b>Figure 2.2</b>	Schematic of Tafel extrapolation	<b>31</b>
<b>Figure 2.3:</b>	A schematic diagram of electric circuit for electrochemical polarisation of three-electrode corrosion cell	<b>32</b>
<b>Figure 3.1</b>	Work flow of the in-house alloy production process. The insert image in (i) shows the type of crucibles used in this study. The bigger crucible used for mixing and smaller crucible for casting. After homogenisation (ii), the cast alloy was cut into smaller pieces for further testing	<b>97</b>
<b>Figure 3.2</b>	Biologic VMP3 potentiostat	<b>98</b>
<b>Figure 3.3(a)</b>	A 3-electrode electrochemical cell for individual sample	<b>99</b>
<b>Figure 3.3(b)</b>	A custom version of the 3-electrode electrochemical cell for high throughput and long term testing of numerous specimens	<b>99</b>
<b>Figure 3.4</b>	Veeco Wyko NT1100 optical profilometry	<b>100</b>
<b>Figure 3.5</b>	FEI Quanta 200 Scanning Electron Microscopy	<b>101</b>
<b>Figure 3.6</b>	Duramin A300 hardness tester	<b>101</b>
<b>Figure 4.1</b>	(a) Typical potentiodynamic polarisation response of selected Al-alloys. (b) Typical Nyquist plots collected using electrochemical impedance spectroscopy for different samples the same alloys in (a)	<b>117</b>
<b>Figure 4.2</b>	The range of mass loss values collected for Al-alloys, presented versus the corresponding Hardness. Hardness was collected using a 1kg load. Mass loss determined from 2 weeks exposure in 0.1M NaCl. The inset is the same data as the main plot, but with a log axis on the x and y axis	<b>118</b>
<b>Figure 4.3</b>	The correlation between hardness and the average pit density. Hardness was collected using a 1kg load. Average pit density was determined using optical profilometry following 2 weeks exposure in 0.1M NaCl. Error bars omitted for clarity. The inset reveals the average pit depth values, showing little correlation between hardness and average pit depth	<b>119</b>
<b>Figure 4.4</b>	Correlation between electrochemically determined corrosion rates from short-term EIS testing and the mass loss determined from 2 weeks exposure in 0.1M NaCl. Error bars omitted for	<b>120</b>

clarity

- Figure 4.5** Schematic representation of the electrochemical impact of alloying elements studied. The plot depicts the ability of alloying additions to modify anodic or cathodic kinetics (or both), leading to changes in the resultant corrosion rate, along with changes in  $E_{\text{corr}}$  and  $E_{\text{pit}}$  **121**
- Figure 4.6** Fuzzy curve (a) and fuzzy curve range (b) for the empirically determined impact of alloying elements on the corrosion of aluminium **122**

# List of Tables

---

<b>Table 2.1</b>	Solid solubility of elements in Al	<b>7</b>
<b>Table 2.2</b>	Wrought Al alloys temper designation	<b>8</b>
<b>Table 2.3</b>	The typical microstructures for selected commercial of Al-alloys	<b>13</b>
<b>Table 2.4</b>	Property – microstructure relationships in Al alloys adapted from Starke	<b>26</b>
<b>Table 4.1</b>	Solubility of elements in pure aluminium. Elements classified according to soluble (S), slightly soluble (SS), insoluble (I) or unknown (U)	<b>115</b>
<b>Table 4.2</b>	Chemical composition from ICP-AES of the alloys tested in this study. All values in weight %	<b>116</b>

# List of Publications

---

The findings in this dissertation are comprised of 8 published and/or submitted papers in internationally recognised journals and 1 invited book chapter. The publications are organised in the order of appearance in the thesis.

## **Invited Book Chapter**

**N.L. Sukiman**, X. Zhou, N. Birbilis, A.E. Hughes, J.M.C. Mol, S.J. Garcia, X. Zhou, G.E. Thompson, Durability and Corrosion of Aluminium and Its alloys: Overview, Property Space, Techniques and Developments, In *Aluminium Alloys – New Trends in Fabrication and Applications*, InTech (2012) ISBN 980-953-307-512-4

## **Peer Reviewed Journal Papers**

1. **N.L. Sukiman**, R.K. Gupta, R.G. Buchheit, N. Birbilis, A consolidated presentation of bulk chemical effects on the corrosion kinetics of some commercial wrought aluminium alloys, *Corrosion*, (2013)
2. R.K. Gupta, **N.L. Sukiman**, K.M. Fleming, M.A. Gibson, N. Birbilis, Electrochemical behavior and localised corrosion associated with Mg<sub>2</sub>Si Particles in Al and Mg Alloys, *ECS Electrochemistry Letters*, 1 (2012) B1-B3
3. R.K. Gupta, **N.L. Sukiman**, M.K. Cavanaugh, B.R.W. Hinton, C.R. Hutchinson, N. Birbilis, Metastable pitting characteristics of aluminium alloys measured using current transients during potentiostatic polarisation, *Electrochimica Acta*, 66 (2012) 245-254
4. **N.L. Sukiman**, R.K. Gupta, R.G. Buchheit, N. Birbilis, The influence of microalloying additions on Al-Mg alloy (Al-4Mg-0.4Mn), Part 1: Corrosion and electrochemical response, *Corrosion Engineering, Science & Technology*, (2013)
5. **N.L. Sukiman**, R.K. Gupta, R.G. Buchheit, N. Birbilis, The influence of microalloying additions on Al-Mg alloy (Al-4Mg-0.4Mn), Part 2: Phase analysis and sensitisation behaviour, *Corrosion Engineering, Science & Technology*, (2013)
6. **N.L. Sukiman**, H. Shi, R.G. Buchheit, N. Birbilis, Electrochemical and corrosion response of commercially pure aluminium alloyed with binary additions of strontium, *Journal of Electrochemical Society*, 160 (8) C1-C6 (2013)

7. Y. Wang, R.K. Gupta, **N.L. Sukiman**, R. Zhang, C.H.J. Davies and N. Birbilis, Influence of alloyed Nd content on the corrosion of an Al-5Mg alloy, *Corrosion Science*, In Press (2013)
8. R.K. Gupta, Y. Wang, R. Zhang, **N.L. Sukiman**, C.H.J. Davies, N. Birbilis, Imparting sensitization resistance to an Al-5Mg alloy via Neodymium additions, *Corrosion*, 69 (1) (2013) 4-8

# Chapter 1

## Introduction

---

Aluminium (Al) alloys have been widely used in a number of applications over the last century, corresponding with their commercial viability. Al-alloys are readily available and can be processed to meet the materials requirements of many industries. This includes commodity applications such as foil and cutlery, to the most advanced aerospace alloys produced with complex compositions and tempers. The cost of Al is greater than that of steel, owing to the large amount of energy required for production, however the density of Al is a very attractive property, meaning that growth in the usage of Al has been steady, and that rate of growth in the past decade has escalated. In an era of light weighting for the purposes of energy reduction and emission reductions, the demand for Al alloys is due to their strength to density ratio, formability, toughness and relatively good corrosion resistance. Mechanical strength arises by the addition of alloying elements such as magnesium, copper, silicon, manganese and zinc. Many of the commercial high strength Al alloys are heavily alloyed such as the 2xxx (Al-Cu-Mg, Al-Cu-Li) and 7xxx series (Al-Zn-Mg-Cu) alloys. The alloy strength, when it arises from precipitates, increases the heterogeneity of the microstructure employing second phases to restrict dislocation movement. However, from a corrosion perspective, an increase in heterogeneity can reduce the corrosion resistance of Al. On the contrary to the higher strength Al alloys, medium to low strength Al alloys such as the 3xxx and 5xxx (and some 6xxx) series alloys which have a more homogeneous microstructure, remain more resistant to corrosion. In the presence of corrosive environments (i.e. high or low pH, or in the presence of halide ions such as chlorides) Al undergoes corrosion, nominally localised corrosion whereby the attack commences at defects in the nominally protective aluminium oxide surface. This localisation is accelerated and deterministic if the presence of second phases with different electrochemical characteristics to the surrounding matrix can contribute to the driving force for alloy corrosion.

In the rapidly changing consumer market, that includes more advanced vehicles, a rapid growth in portable electronics, and exposure of metals to harsher environments (be it atmospheric extremes or geological extremes), there demand for lighter, stronger and highly durable materials is assured. In particular the notion of more efficient and sustainable alloys,

particularly in transport, remains key. To make this challenge a realisation, Al-alloys with improved corrosion resistance (but equivalent or even improved mechanical performance) are required. Such a task is beyond that of a single (or numerous) PhD projects, however the project herein was developed as a discrete, and evolving effort, to research corrosion related aspects that could contribute towards the science base needed to develop Al-alloys that have reduced corrosion rates, bearing in mind some elementary retention of mechanical performance. In order to commence such a task, it was important to develop an understanding of the property space of corrosion performance for commercial Al-alloys. Whilst a prime focus is on the corrosion performance, there was hardness testing performed in all cases, as a proxy to yield strength, and in some cases yield strength. From such a primitive representation of the performance of Al-alloys, there were first order relationships that could be identified, such as elements that have a positive or neutral effect on both corrosion resistance, and those that do not. Various aspects were obvious, in that lower strength alloys occupied the low corrosion rate space, and those elements such as Cu stimulated corrosion, whilst precipitate containing alloys always showed higher corrosion rates. Of the approaches that could possibly be pursued in a PhD to seek developments and favourable deviation into new property space, it was decided that to minimise the variables involved, the effect of heat treatment (which is essential in precipitation hardenable alloys) was discounted from this project, aligning the project towards ‘new’ alloys being cast and studied for non-age-hardenable systems. The heat treatable systems involve significant processing post alloy production and worthy of a separate study.

It was deemed (hypothesis and review driven) that magnesium as the major alloying element has the potential to be further developed by ternary and quaternary additions of other elements to Al alloys. Of the commercial alloys, the best balance of corrosion resistance and strength may be deemed to be offered by AA5083 (Al-4.4Mg-0.5Mn). This was determined from the research work revealing elementary property space. As a result, subsequent work in the thesis explores a selection of targeted studies that seek to understand, and improve, the performance of the present Al-Mg alloys. A range of custom alloys were prepared to study the effect of additions including, neodymium, strontium, zirconium, etc. in the processed conditions (in the lab) that include wrought (hot and cold) work to simulate the route of 5xxx alloy production. This project combines the electrochemical analyses and microstructural characterisation to investigate the symbiotic effect of the alloying additions to corrosion. In



addition, further foundational works for laying the platform between electrochemical analysis and alloy performance, and isolated studies focusing (in-depth) on the effect of unique elemental additions are also include. The combined work in the thesis contributes towards a platform, including a first open holistic effort, and some key examples, for the future establishment of next generation, corrosion resistant, Al-alloys.

# Chapter 2

## Literature Review

---

### 2.1 The origin of aluminium

Aluminium (Al) occupies approximately 8% of the Earth's solid surface by weight and is the third most abundant element behind oxygen and silicon [1]. Al is listed in Group 13 of the periodic table, also known as the 'earth metals' group. Pure Al appears as a silvery white metal with high ductility. It is also one of the lightest metals having a density of  $2.3 \text{ g/cm}^3$  – significantly lower than ferrous alloys ( $\sim 7.8 \text{ g/cm}^3$ ) [2, 3]. Al is highly reactive and attracts oxygen forming aluminium oxide ( $\text{Al}_2\text{O}_3$ ). Therefore in its natural form, Al has to be extracted from bauxite ores which contain mainly hydrated alumina (40-60%) with other minerals such as iron oxides, silica and titania [1, 4, 5]. Al is also present in other minerals such as clays and shales but the extraction process from these minerals is twice as expensive as that from bauxite, hence is prohibitive [1, 6].

The extraction of Al was first attempted in 1808 by Humphry Davy through electrolysis but without much success [7]. In 1825, another attempt by Hans-Christian Oersted involved extracting the aluminium chloride ( $\text{AlCl}_3$ ), which then heated with potassium amalgam resulted in the production of a metal reported to be similar to tin [8]. Friedrich Wohler continued the work to produce Al ingot. The efficiency of the extraction process at the time was low but in 1855, H. Sainte-Claire Deville developed an industrially more efficient process [9]. The process used sodium for  $\text{AlCl}_3$  reduction instead of potassium. This process however produced less than 95% pure Al and the difficulty in Al extraction raised its cost higher than that of gold [1]. A more economical process to extract Al was developed 40 years later in 1885 independently by Charles Hall in the USA and Paul Heroult in France. The process was later named the Hall-Heroult process. The difficulty in processing the alumina was due to its high melting temperature of  $2040^\circ\text{C}$ . The problem was solved by dissolving the alumina in molten cryolite ( $\text{Na}_3\text{AlF}_6$ ) with additives such as aluminium fluoride ( $\text{AlF}_3$ ) and calcium fluoride ( $\text{CaF}_2$ ) followed by electrolysis between  $950^\circ\text{C}$  and  $980^\circ\text{C}$ . In 1888, Karl Josef Bayer developed a more efficient process to extract alumina from the ore. This process involves crushing the bauxite in strong sodium hydroxide ( $\text{NaOH}$ )

solution at 240°C. The alumina is obtained by precipitation of solid aluminium hydroxide from the aluminate containing solution by increasing the pH and adding some 'seed' crystal. After the separation of solid from the liquid by filtration, the aluminium hydroxide is then converted to alumina by calcination to drive off water.

Modern day Al production from bauxite ore combines the Bayer process and Hall-Heroult process. The flow diagram for the integrated production of aluminium from bauxite is shown in Figure 2.1.

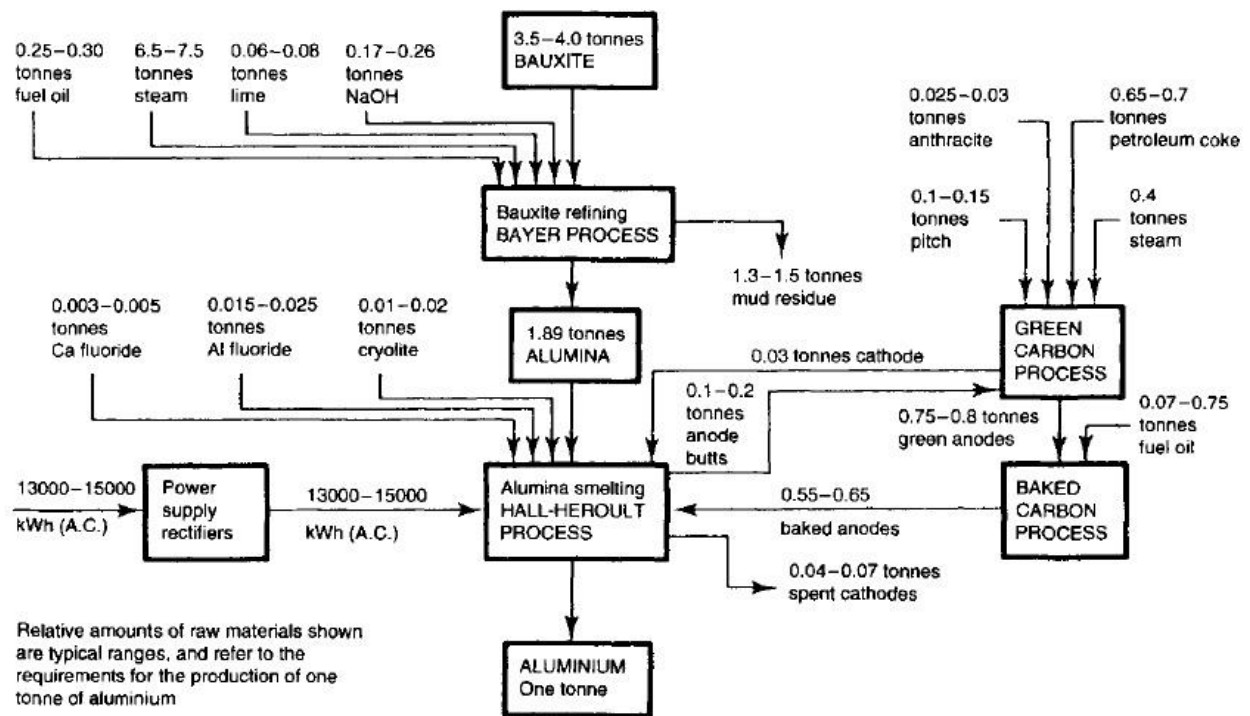


Figure 2.1: Flow diagram for integrated production of aluminium from bauxite [10]

Generally every 4 tonnes of bauxite will only produce 1 tonne of pure Al and consumes a massive amount of energy [1]. This indeed remains a concern with regards to the environmental aspect of the Al industry. In 2012, the world produced 45 million tonnes of Al and production is expected to soar in the coming years [11]. It is estimated that in Australia alone, 30% of the total greenhouse gas emission from all industries is contributed by Al production [10]. Nevertheless, Al could still contribute to the environment in several ways:

- *Recycling.* Al is 100% recyclable. The process of recycling Al consumes 95% less energy than producing Al, when compared to production from the ore itself [12, 13]. The sustainability initiative that started in the 1970s has seen around two-thirds of Al products at the moment produced from recycled Al [11].
- *Transportation efficiency.* The high strength to weight ratio of Al makes it possible to design lighter vehicles with less fuel consumption and lower carbon emission [14]. This helps to offset the carbon emission by using Al instead of steel (which is heavier).
- *Durability.* Al is not only lighter and stronger but also nominally resistant to corrosion making it more durable than other “light metals” in its class (e.g. Mg) [1, 14-16]. Durability contributes to a longer life span of the product in service hence reducing the need for replacements. The use of Al as a building material also has increased recently as it is more durable to endure the weather. It is also recyclable when the building is in need of remodelling [11, 17-19].

## 2.2 Physical metallurgy of aluminium alloys

Al in its pure form shows appreciable resistance to corrosion but lacks mechanical strength (i.e.  $\sigma_y \sim 20\text{MPa}$ ) [1, 2]. Improvements in strength can be achieved by solid solution strengthening, cold work, and the formation of finely dispersed precipitates within the matrix via precipitation hardening [1, 3, 20]. The most widely used alloying additions are magnesium (Mg), copper (Cu), zinc (Zn) and silicon (Si) due to their relatively significant solid solubilities with Al. Other elements with limited solubility such as titanium (Ti), chromium (Cr), manganese (Mn) or zirconium (Zr) are also added in small amounts to achieve certain properties - namely grain refinement and inoculation [1, 3]. The maximum solid solubility for elements that are typically added in Al is listed in Table 2.1.

Table 2.1: Solid solubility of elements in Al [2]

Element	Max. Solid Solubility (wt.%)
Copper	5.65
Chromium	0.77
Iron	0.05
Lithium	4.2
Magnesium	17.4
Manganese	1.82
Silicon	1.65
Silver	55.6
Tin	0.06
Titanium	1.3
Zinc	70
Zirconium	0.28

The Aluminium Association classifies commercial Al alloys into one of eight (8) series, depending on the major type of alloying element added [1]. Each alloy has a 4 digit numeric designation, the first digit reveals the major alloying element and the second digit nominally refers to alloy purity. The last two digits refer to the alloy number - which increases with the invention of new alloys. In order to give the reader an appreciation of the wide class of Al alloys, the designation system for wrought Al alloys is presented in Table 2.2.

Table 2.2: Wrought Al alloy temper designation [2]

Letter	First Digit	Second Digit
<b>F</b> As Fabricated		
<b>O</b> Annealed		
<b>H</b> Cold Worked	1 – cold worked only 2 – cold worked and partially annealed 3 – cold worked and stabilised	1 – annealed 2 – ¼ hard 4 – ½ hard 6 – ¾ hard 8 – hard 9 – extra hard
<b>T</b> Heat Treated	1 – partial solution and natural aging 2 – partial solution, cold work and natural aging 3 – solution, cold work and natural aging 4 – solution and natural aging 5 – partial solution and artificial aging 6 – solution and artificial aging 7 – solution and stabilising 8 – solution, cold work and artificial aging 9 – solution, artificial aging and cold work 10 – partial solution, cold work and artificial aging	

Al alloys are generally classified in two groups with respect to strengthening, i.e. heat treatable, and non – heat treatable.

### 2.2.1 Non – heat treatable alloys

Strengthening in non – heat treatable alloys occurs from alloying of the solid solution. It is coupled with grain refinement by dispersoids (to hinder recrystallisation more so than contribute to strength) and strain hardening (from either warm or cold work) to further increase the strength. Wrought alloys of this type are mainly those of the 3xxx, 5xxx and some 6xxx series (containing predominately Mg, Mn and Si) Al-alloys.

- *3xxx series alloys.* The major alloying element is Mn in the amount between 1 to 1.5 wt.% and the tensile strength is approximately 50 MPa [16]. To improve the mechanical strength, additional elements are typically added in conjunction with Mn. In AA3003-O for instance, addition of 0.2 wt.% Cu increased the tensile strength to 110 MPa. Also in AA3004-O with the addition of 1 wt.% Mg, the tensile strength is significantly increased to 180 MPa. In addition to having good formability and weldability, the alloys in this series are also stronger than the 1xxx series alloys. These alloys are popular as the general purpose alloys used in the manufacturing of kitchen utensils, food packaging and building materials [14, 16].
- *5xxx series alloys.* The major alloying element in this series is Mg, ranging from 0.8 wt% to 5 wt.%. The tensile strength in as-annealed condition for AA5005 is 125 MPa (when the Mg content is kept at a minimum). Strength increases with Mg content in the alloy. The addition of Mn and Cr, combined with appreciable cold-work, as in AA5456-H111 improves the tensile strength up to 324 MPa [2]. In general, 5xxx series alloys are widely used in transport applications, particularly in marine industry (e.g. 5083-H34) due to its outstanding corrosion resistance as well as good weldability and formability. Other applications include building materials, tanks and rivets for Mg [14, 16].

### 2.2.2 Heat treatable alloys

Heat treatable Al-alloys are strengthened by precipitation (age) hardening [1, 3, 21]. Such alloys contain elements that exceed their equilibrium solid solubility at room temperature (and aging temperatures). Prior to aging, a 'supersaturated solid solution' is formed during solution heat treatment where the alloy is annealed and quenched so that diffusion is impeded, causing retention of a solute rich single phase [22]. The formation of supersaturated solid solutions is essential for subsequent heat treatment process to create finely dispersed precipitates within the matrix. This process is called precipitation hardening. In the precipitation hardening process, aging time and temperature play a major role in determining the type of precipitates developed. However, this trend is visible only up until peak value which then the hardness decreases synonymous with 'overaging'. In the overaged condition, aging causes the precipitates to reach an equilibrium state which involves a loss of coherency with the matrix [22]. Thus coarsely dispersed precipitates and increased distance between the precipitates make dislocation movement possible by a 'by-pass' mechanism [23]. Dislocations are significantly less possible in the instance where a high number density of fine and dispersed precipitates were present. This phenomenon typifies the notion that precipitate presence alone is not solely responsible for strength increase, but the number density and size range distributions are also critical. Wrought alloys of this type are mainly those of the 6xxx, 7xxx and 8xxx series Al-alloys (containing predominately Cu, Zn and Si).

- *2xxx series alloys.* The major alloying element in this alloy series is Cu (typically between 1.9 wt.% to 6.8 wt.%) with minor additions of Mg and Mn. One of the earliest reports of Al-Cu alloys is on AA2017 (Al-3.5Cu-0.5Mg-0.5Mn), also known as Duralumin. The Al-Cu alloys were responsible of the first discovery of 'age hardening' (i.e. precipitation hardening) process. Shortly after this discovery, Al-alloys were subsequently (and expressly) used for aircraft structures [1]. The tensile strength for AA2017 with T4 temper at the time was 425 MPa. An improved version of the alloy has been developed throughout the years in order to achieve higher tensile strength (>480 MPa). For instance, the addition of higher Mg content (up to 1.8 wt%) enhances the precipitation process, giving higher tensile strength as in AA2124-T851. Addition of Si (0.5 wt% - 1.2 wt.%) is also common in this series such as in



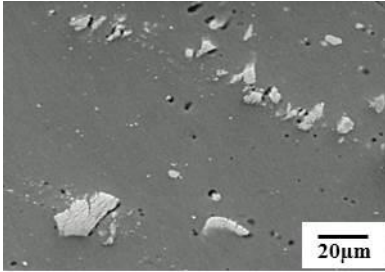
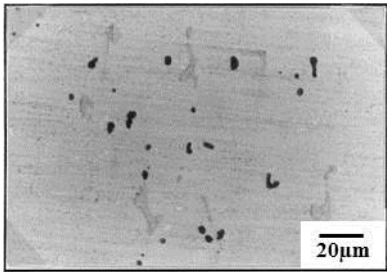
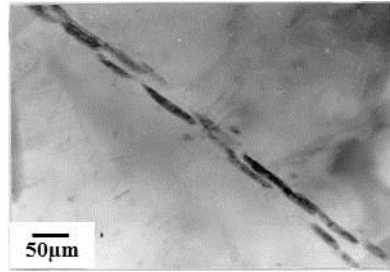
AA2014 and AA2214 with T6 temper that yields up to 500 MPa tensile strength. The AA2219 has the highest amount of Cu (6.8 wt.%) in this series and produce good mechanical properties at cryogenic temperatures (available at T3, T6 and T8 tempers) making it possible to be used as welded tanks for space launcher rockets [16].

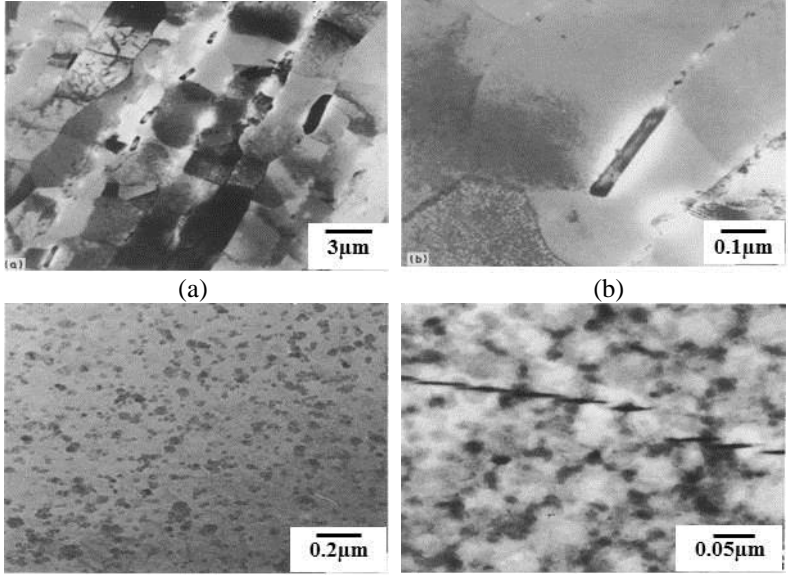
- *6xxx series alloys.* The major alloying element of this series is Si. The presence of Mg in addition to Si enables the precipitation hardening of the alloy. The amount of Mg and Si added in the system is usually balanced at ~1.73:1. An excess amount of Si will form the  $Mg_2Si$  phase which further increases the mechanical strength [16]. The tensile strength for alloy with balanced Mg and Si content as in AA6063-T6 is at 245 MPa. An increase in Si content with minor addition of Cu in AA6056-T6 alloy enhanced the tensile strength to the highest value at 470 MPa. This series of alloys has good corrosion resistance and weldability similar to the 5xxx series alloys. They can be thermo-mechanically processed, and thus subject to rolling, extrusion and forging. The applications include automotive panels, pipelines and building materials.
- *7xxx series alloys.* The major alloying element of this series is Zn with minor addition of Mg and Cu to further increase the strength. Alloys of this series without Cu such as in AA7020 (T5 or T6 temper) have appreciable tensile strength between 360 to 400 MPa. The presence of Cu enhances age-hardening of the alloy producing higher mechanical strength but subsequently increasing its resistance to stress corrosion cracking (SCC) [1]. AA7075 for instance, the tensile strength at T6 temper could reach up to 570 MPa. However, for T73 temper of the same alloy which has better resistance to SCC, possess lower tensile strength. In order to achieve balanced properties between T6 and T73, a new heat treatment known as retrogression and re-ageing (RRA) heat treatment (T77) was introduced to AA7055 alloy with higher Zn and Cu content [1]. Alloys in this series are heavily used in aircraft structural parts solely because of their high mechanical strength.

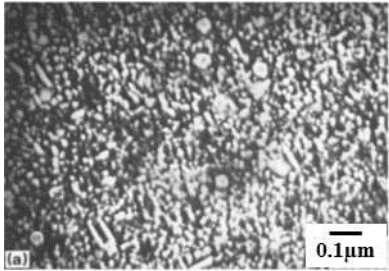
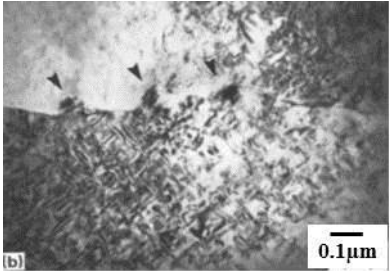
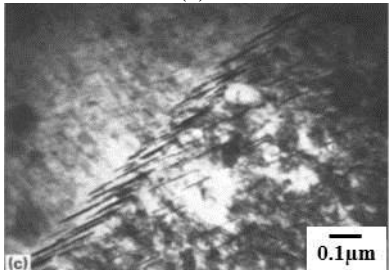
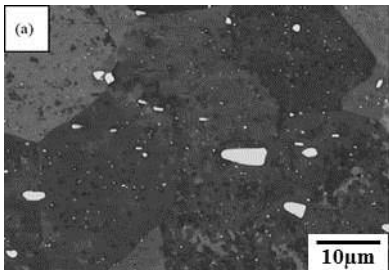
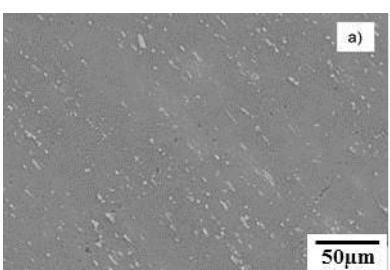
In the context of microstructurally influenced corrosion, the understanding of the

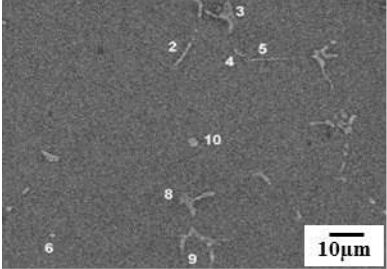
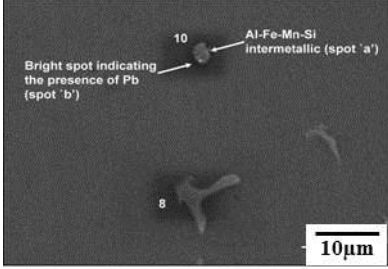
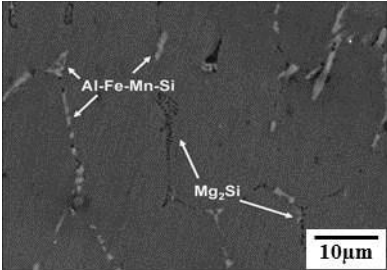
types and classes of particles that form in Al-alloys is also critical. As such, prior to presenting the microstructures formed, an important distinction needs to be made between the particle classes present in Al-alloys, and such terminology will be used throughout this project. Impurity elements such as Fe, Mn and Si can form insoluble compounds that are known as constituent particles. These are comparatively large and irregularly shaped with characteristic dimensions ranging from 1 to  $\sim 10\mu\text{m}$ . These particles are formed during alloy solidification and are not appreciably dissolved during subsequent thermo-mechanical processing. Rolling and extrusion tend to break-up and align constituent particles within the alloy. Often constituents are found in colonies made up of several different intermetallic compound types. Micro-alloying additions of Cr, Zr or Sc (for example) tend to promote sub-micron sized insoluble particles that subsequently can restrict or pin grain growth. Such particles are called *dispersoid particles*. Finally, intermetallics that are formed by precipitation processes (and hence can respond to heat treatment) are known as *precipitate particles*. To help in distinguishing the types and classes of particles, Table 2.3 summarised the typical microstructures that form in the selected commercial Al-alloys. In addition, the name, classification and type of particles observed have been added besides the corresponding micrograph to allow a ready understanding to be obtained for the reader.

Table 2.3: The typical microstructures for selected commercial of Al-alloys

Alloy	Nominal Composition	Microstructure	Comment on Microstructure
2024-T3	Al - 3.8-4.9Cu - 1.2-1.8Mg - 0.5Si - 0.5Fe	 <p>(a)</p>  <p>(b) [24]</p>  <p>(c) [24]</p>	<ul style="list-style-type: none"> <li>Commonly contains: <ul style="list-style-type: none"> <li><math>\text{Al}_2\text{CuMg}</math> (S-phase) as the strengthening precipitate phase on the submicron level (seen in (c))</li> <li><math>\text{Mg}_2\text{Si}</math> constituent particles that do not contribute to strength, but form due to Mg alloying additions and Si impurities (seen in (a, b)) Constituent particles owing to impurities, such as <math>\text{Al}_7\text{Cu}_2\text{Fe}</math> and <math>\text{Al}_3\text{Fe}</math> (seen in (a, b))</li> <li>Possibly some low levels of the <math>\text{Al}_{20}\text{Cu}_2\text{Mn}_3</math> dispersoid (rod shape) uniformly dispersed in matrix and rarely seen by microscopy.</li> </ul> </li> <li>In (c), <math>\text{Al}_2\text{CuMg}</math> along grain boundary [24].</li> </ul>

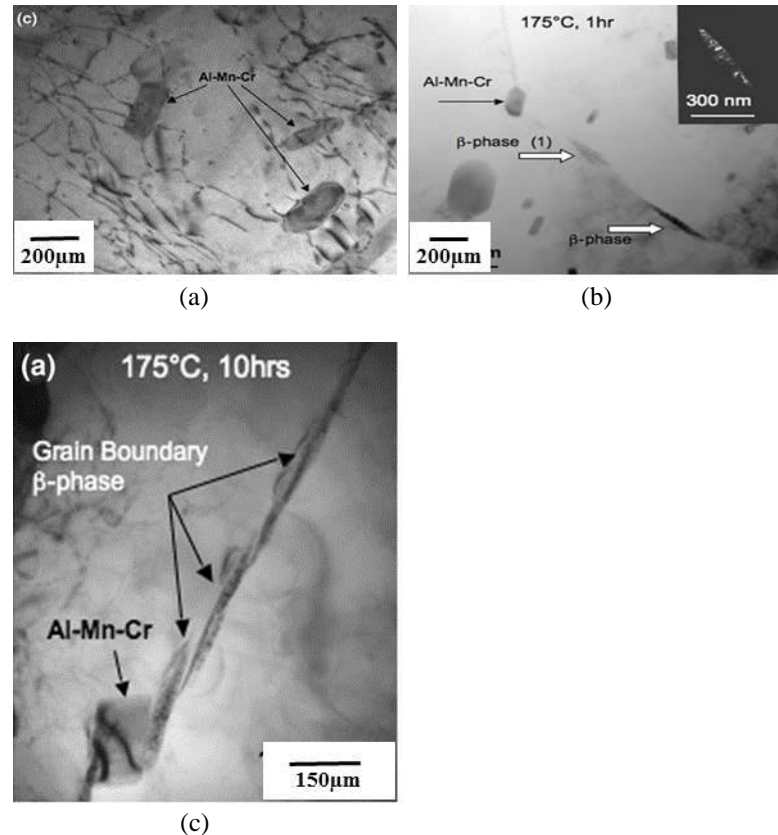
2124-T4	Al - 3.8-4.9Cu - 1.2-1.8Mg - 0.2Si - 0.3Fe	 <p>(a) (b)</p> <p>(c) (d)</p>	<ul style="list-style-type: none"> <li>• Particles present are similar as in 2024-T3</li> <li>• Bright-field transmission electron micrograph showing elongated grains with Fe-rich particle at the grain boundaries in (a) and a closer look at the particle in (b).</li> <li>• In (c), showing the morphology and distribution of Mn-rich dispersoids.</li> <li>• In (d), showing the morphology of S' strengthening precipitate [25].</li> <li>• All electron images are courtesy of Srivatsan et. al.[25]</li> </ul>
---------	--	--	--

2090	Al – 2.9Cu 2.2Li – 0.12Zr – 0.06Fe – 0.04Si	   <p>(a) (b) (c)</p>	<ul style="list-style-type: none"> <li>• The precipitates that typically present in this alloy are <math>\delta'</math> (<math>\text{Al}_3\text{Li}</math>), <math>\delta</math> (<math>\text{AlLi}</math>), <math>\theta'</math> (<math>\text{Al}_2\text{Cu}</math>) and <math>T_1</math></li> <li>• In (a), a homogeneous distribution of <math>\delta'</math> phase can be observed</li> <li>• A significant amount of <math>\delta</math> at the grain boundaries shown in (b). The size of the phase reaches <math>0.40\text{ }\mu\text{m}</math></li> <li>• The plate-like <math>T_1</math> phase precipitated uniformly on the <math>[111]</math> plane of the matrix displayed by (c) [26].</li> <li>• All electron images are courtesy of Dervenis et. al. [26]</li> </ul>
3003-O	Al – 1.0-1.5Mn – 0.1Zn – 0.6Si – 0.7Fe	  <p>(a) [27] (b) [28]</p>	<ul style="list-style-type: none"> <li>• There are 2 distinct type of IMP shown in (a); <ul style="list-style-type: none"> <li>- <math>\alpha\text{-Al}(\text{Mn,Fe})\text{Si}</math>; e.g. <math>\text{Al}_{15}(\text{Mn,Fe})_3\text{Si}_2</math></li> <li>- <math>\text{Al}(\text{Mn,Fe})</math>; e.g. <math>\text{Al}_6(\text{Mn,Fe})</math> [29]</li> </ul> </li> <li>• Both are coarse (<math>0.5\text{-}10\text{ }\mu\text{m}</math>) and appear as white particles in the backscattered SEM image.</li> <li>• It is possible to form finer IMP by heat treatment and contain only Al and Mn.</li> <li>• In (b), another SEM image showing <math>\text{Al}_x(\text{Fe,Mn})</math> second phase particles with an average diameter of <math>5\text{ }\mu\text{m}</math> [28].</li> </ul>

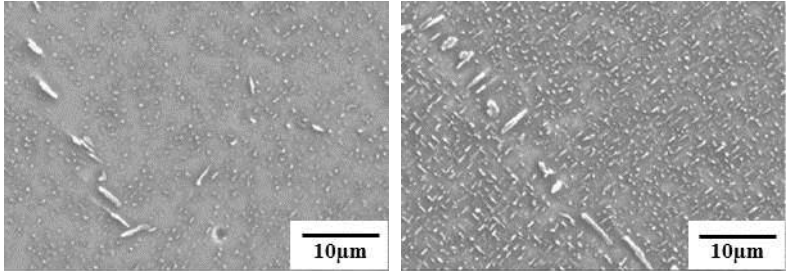
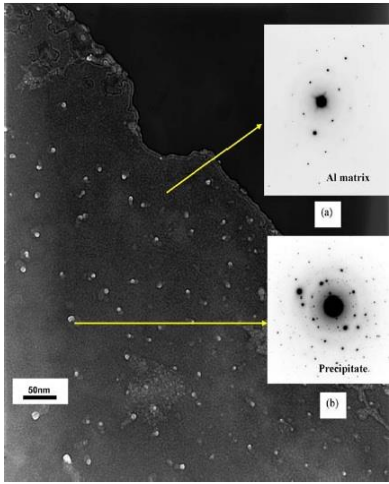
5005-O	Al – 1.22Mg – 0.75Fe – 0.37Mn – 0.36Si – 0.112Cu	 <p>(a)</p>  <p>(b)</p>  <p>(c)</p>	<ul style="list-style-type: none"> <li>• A distribution of second phase particles in the commercial AA5050 can be observed in (a). The intermetallics are mainly Al-Fe-Mn-Si phase.</li> <li>• The bright spot in (b) revealed the presence of Pb-rich particles in commercial AA5050.</li> <li>• In (c), apart from Al-Fe-Mn-Si phase, a smaller <math>Mg_2Si</math> phase formed at the grain boundaries [30]</li> <li>• All electron images are courtesy of Premendra et. al. [30]</li> </ul>
--------	--	--	--

5083-  
H34

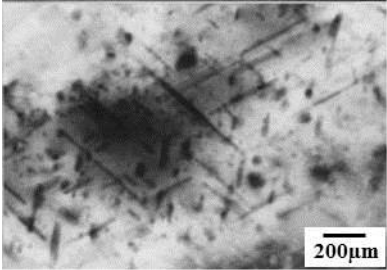
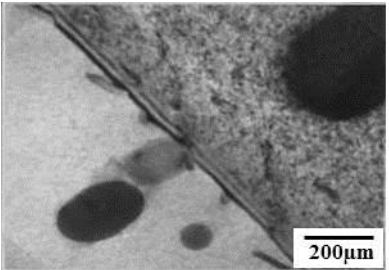
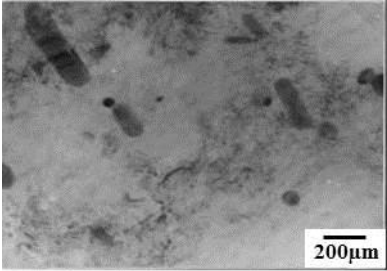
Al – 4.0-4.9Mg  
– 0.25Zn – 0.4-  
1.0Mn – 0.4Si  
– 0.4Fe

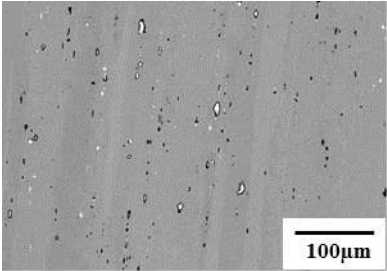
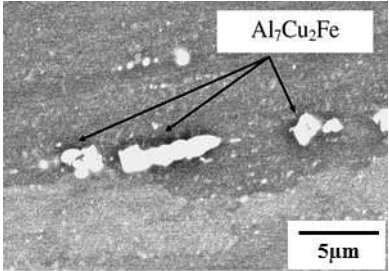
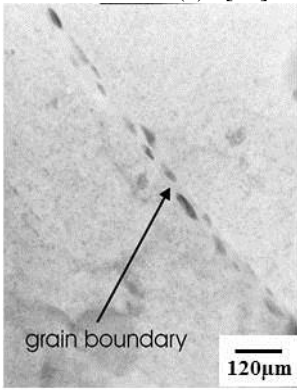


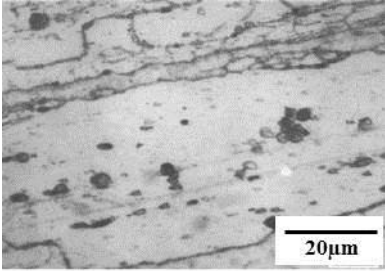
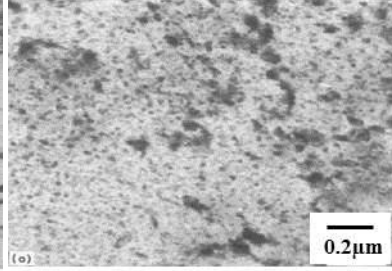
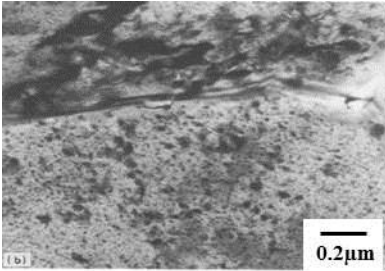
- This alloy is nominally a solid solution when Mg content is less than 5 wt.%.
- Mn and Cr are also typically present to increase the recrystallisation temperature. This leads to the formation of Al-Mn-Cr type particle and  $Al_6Mn$  dispersoids [1]
- Bright-field micrograph in (a) shows the Al-Mn-Cr type particles pinned down a number of dislocations [31]
- When the alloy is exposed to an elevated temperature (as low as 90°C) [32], β-phase forms at the grain boundaries seen in (b) and (c) as Mg content typically exceeds 3.5 wt.%.
- All electron images are courtesy of Goswami et. al. [31]

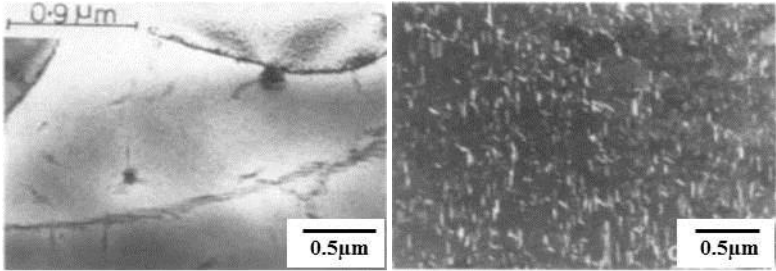
6016	Al – 1.0-1.5Si – 0.25-0.6Mg – 0.2Mn – 0.2Zn – 0.5Fe	 <p>(a) (b)</p>	<ul style="list-style-type: none"> <li>• Q-phase, metallic Si and <math>\beta</math>-phase present when Cu content between 0.2 – 0.5%</li> <li>• Longer heat treatment caused precipitates in matrix to enlarge</li> <li>• AlMgSiCu (Q-phase) may grow at the expense of <math>\beta</math> phase</li> <li>• It can be as large as 1 <math>\mu\text{m}</math></li> <li>• Q phase in grain boundary highly increase susceptibility to IGC and those in matrix caused pitting attack</li> <li>• These can be avoided by thermal treatment during fabrication</li> <li>• <math>\beta</math>-phase (<math>\text{Mg}_2\text{Si}</math>) may precipitate if Mg:Si ratio is low [33]</li> </ul>
6022	Al – 1.35Si – 0.58Mg – 0.04Mn – 0.2Zn – 0.14Fe	 <p>[34]</p>	<ul style="list-style-type: none"> <li>• The lath like precipitate is <math>\text{Al}_4\text{Cu}_2\text{Mg}_8\text{Si}_7</math> (Q-phase)</li> <li>• Excess Si reduces time to initiate strengthening during aging due to enhanced precipitation of fine and uniformly dispersed <math>\beta''</math> precipitates when Mg/Si ratio in GP zones and <math>\beta''</math> precipitates</li> <li>• If quench after solution heat treatment, resistant to IGC is higher because there's no Q-phase along grain boundary [34]</li> </ul>



6013-T6	Al – 0.92Si – 0.86Mg – 0.19Fe – 0.87Cu – 0.55Mn – 0.15Zn	 <p>(a)</p>  <p>(b)</p>  <p>(c)</p>	<ul style="list-style-type: none"> <li>• The hardening precipitates contain Al-Cu-Si formed in the matrix with the size up to 100nm shown in (a)</li> <li>• Dispersoids (round and rod shaped) are also present in the matrix displayed by (b) where the composition is mainly Al-Mn-Cu-Fe-Si</li> <li>• In (c), needle-like precipitates contain Al-Si-Cu formed at the grain boundaries. The size is up to 40nm wide [35]</li> <li>• All electron images are courtesy of Guillaumin et al. [35]</li> </ul>
---------	---	--	--

<p>7075-T651</p>	<p>Al – 1.2-2.0Cu – 2.1-2.9Mg – 5.1-6.1Zn – 0.3Mn – 0.4Si – 0.5Fe</p>	<div style="display: flex; flex-direction: column; align-items: center;">  <p>(a) [36]</p>  <p>(b) [36]</p>  <p>(c) [37]</p> </div>	<ul style="list-style-type: none"> <li>• AA7075 microstructure in (a) shows the presence of constituent type particles such as <math>\text{Al}_7\text{Cu}_2\text{Fe}</math>, <math>\text{Al}_7\text{CuMg}</math>, <math>\text{Mg}_2\text{Si}</math>, <math>\text{MgZn}_2</math>, <math>\text{Al}_2\text{Cu}</math> and <math>\text{Al}_3\text{Fe}</math> [36]</li> <li>• In (b), the <math>\text{Al}_7\text{Cu}_2\text{Fe}</math> particles known to cause localised attack. During fabrication, the particles fractured and aligned in the direction of work [1]</li> <li>• At T6 temper shown in (c), the matrix contains fine precipitation of <math>\text{MgZn}_2</math> particles. Whilst the large <math>\text{MgZn}_2</math> particles (~50nm) tend to form at the grain boundaries [37]</li> </ul>
------------------	---	---	--

7150-T773	Al – 1.9-2.5Cu – 2.0-2.7Mg – 5.9-6.9Zn – 0.1Mn – 0.12Si – 0.15Fe	   <p>(a) (b) (c)</p>	<ul style="list-style-type: none"> <li>• This alloy typically contains <math>\text{Al}_7\text{Cu}_2\text{Fe}</math>, <math>\text{Al}_7\text{CuMg}</math>, <math>\text{Al}_2\text{MgCu}</math>, <math>\text{Mg}_2\text{Si}</math> and <math>\text{MgZn}_2</math> phases.</li> <li>• It also contains an intermediate <math>\eta'</math> (<math>\text{MgZn}_2</math>) precipitates dispersed in matrix as shown in (b) and equilibrium <math>\eta</math> precipitates in matrix and grain boundary shown in (c) [38]</li> <li>• <math>\text{Al}_3\text{Zr}</math> also present as dispersoids distributed throughout the matrix.</li> <li>• All electron images are courtesy of Srivatsan et. al. [38]</li> </ul>
-----------	--	--	---

<p>8090 T8771</p>	<p>Al – 2.2-2.7Li – 1.0-1.6Cu – 0.6-1.3Mg – 0.2Si – 0.3Fe</p>	<div data-bbox="618 225 1391 531">  <div style="display: flex; justify-content: space-around; margin-top: 5px;"> (a) (b) </div> </div>	<ul style="list-style-type: none"> <li>• The presence of Li leads to the formation of <math>T_1</math> (<math>Al_2CuLi</math>), <math>S</math> (<math>Al_2CuMg</math>), <math>\delta</math> (<math>AlLi</math>) and <math>\delta'</math> (<math>Al_3Li</math>) phases.</li> <li>• Precipitation of <math>T_1</math> is influenced by <math>S</math>-phase for the availability of Cu atoms and heterogeneous nucleation sites [39]</li> <li>• Hence <math>S</math>-phase tends to form on grain boundaries or sub- grain boundaries as shown in (a).</li> <li>• Subsequent artificial aging results in more <math>S</math>-phase distributed throughout the matrix as shown in (b).</li> <li>• The electron images are courtesy of Martin [39]</li> </ul>
-----------------------	---	--	---

### 2.2.3 Influence of strengthening mechanism on corrosion

As discussed in section 2.2.1 and 2.2.2, there are several different approaches to increase the strength of Al-alloys. Each approach yields different sets of properties depending on the microstructures produced. For low to medium strength alloys, the main strengthening mechanism is by solid solution strengthening, often followed by strain hardening such as cold work. Alloying elements largely remain in solid solution therefore a homogeneous microstructure is achieved. Without the presence of particles in the microstructure and hence on the surface, possible sites for localised attack are reduced, though some appreciable amount of constituent particles such as  $\text{Al}_6(\text{Mn,Fe})$  or  $\text{Al}_{12}(\text{Mn,Fe})_3\text{Si}$  in 3xxx alloy may be present from solidification [27, 28, 40] and are unavoidable in low number densities. The cold work followed by solution treatment might influence the constituent particle morphology, re-aligning them in the direction of rolling or forming clusters of smaller constituent particles [41, 42].

As for 5xxx series alloys, precipitation of  $\beta$  phase ( $\text{Al}_8\text{Mg}_5$  or  $\text{Al}_3\text{Mg}_2$ ) may occur at ambient temperatures after prolonged periods if the alloy is in the heavily worked condition. The precipitation of  $\beta$  phase commonly occur along the slip bands and grain boundaries making them more prone to intergranular corrosion or stress corrosion cracking [43-46]. This process of unintended and deleterious precipitation is given the special name of ‘sensitisation’, as it is unwanted and does not contribute to strength.

For precipitation hardened alloys such as 2xxx, 6xxx and 7xxx, the precipitates significantly increase mechanical strength. In this type of strengthening mechanism, artificial ageing is carried out after the alloy is solution heat-treated. The type of microstructure relies on the ageing temperature and time. In 6xxx series alloys, the precipitation of  $\beta$ -phase ( $\text{Mg}_2\text{Si}$ ) and Q-phase ( $\text{Al}_4\text{Mg}_8\text{Si}_7\text{Cu}_2$ ) contribute to the increase in IGC [47-49]. The susceptibility to IGC can be reduced by ‘overaging’ and rapid quenching. However, it may cause other types of corrosion. For instance, increase in localised attack from the precipitation of large  $\beta$ -phase particles [50]; and introduction of residual stresses from quenching causing SCC [51]. In high strength aluminium alloys such as 2xxx and 7xxx, some of the common intermetallic particles present are  $\text{Al}_2\text{CuMg}$ ,  $\text{MgZn}_2$ ,  $\text{Al}_2\text{Cu}$ ,  $\text{Al}_7\text{Cu}_2\text{Fe}$ ,  $\text{Mg}_2\text{Si}$ ,  $\text{Al}_3\text{Fe}$  and  $\text{Al}_7\text{CuMg}$  [52-54]. These particles are known to increase the susceptibility to localised attack. The appropriate choice of ageing process is important to control the

evolution of these particles. The susceptibility towards pitting is lowest in the naturally aged condition (e.g. 2024-T4) and highest in the peak-aged condition (e.g. 7075-T651). The over-aged condition lies between these two [55].

### **2.3 Challenges in aluminium alloy applications**

Al alloys are heavily utilised in the transportation industry; namely for aerospace, marine and automotive applications [14, 56-59]. The combination of high specific strength and workability make Al an ideal material for these applications. Each application offers a rather diverse environment that showcases the versatility of Al alloys. In aircraft design, more than 70% of the structural materials are dominated by Al alloys, specifically the higher strength alloys [1, 14]. During operation, an aircraft has to endure radical loading conditions (including fatigue), an environment that reaches sub-zero temperatures and high ground temperatures in many instances. The evolution of aircraft alloy design started with the aim to improve the strength to weight ratio of the structural alloys, which resulted in the utilisation of 2xxx and 7xxx series alloys. These alloys include AA2024-T3 and AA7075-T6 used to manufacture commercial and military aircraft for many decades (and the subsequent evolution of AA7050/7150 and most recently, AA2099 and AA2050 as described below). The issue of damage tolerance was raised when a premature fatigue failure of pressurised fuselage caused multiple plane crashes in the 1950s [56]. The failures were attributed to SCC of the alloy used for the critical points of the planes (e.g. fuselage, wings). Up to 90% of SCC related failures of Al-alloys at the time was associated with AA7075-T6 and AA2024-T3 in the short transverse direction due to residual quenching stresses of thick product [56]. In order to overcome this problem, T73 temper for AA7075 alloy was developed but at the expense of strength when compared to the AA7079-T6 alloy. Alloy AA7050-T74 was also developed for better SCC resistance without loss of strength [14, 16, 56]. Over the years, more standards were introduced by aviation governing bodies that lead to the development of more durable Al-alloys. One of the key features is improving the fracture and fatigue characteristics. It can be done by the introduction of temper T76 on AA7050 alloy and also increasing the Cu content and Zn/Mg ratio of the alloys [60, 61].

The need for lighter aircraft for better fuel efficiency is the priority for every aircraft manufacturers due to the rising cost of fossil fuel. The reduction in density has the greatest

impact on reducing the weight [39, 59, 62]. The addition of lithium (Li) as low as 1 wt.% can reduce the alloy density by 3% and increase in the Young's modulus by 6% [62]. This has given stiff competition in the development of new alloys in the metal industry. Li containing Al alloys have been around for decades such as the AA8090-T86 and AA2090-T81. These alloys were developed in order to replace AA2024-T3 and AA7075-T6. However, Li alloying was found to be ineffective in improving the fracture toughness and corrosion resistance. Nevertheless, the use of Li containing alloys has expanded since the development of the third generation Al-Li base alloys. The alloys of this generation contain less than 2 wt.% Li along with silver (Ag) and zinc (Zn) [63, 64]. They include AA2050, AA2099, AA2195 and AA2297. According to Rioja [64], AA2099-T86 has outperformed the longest serving Al alloy, AA7050-T7451 in terms of fatigue resistance, exfoliation corrosion and SCC. The importance of improving the resistance to SCC is due to the severity of the damage caused to the structure. It is also more difficult to detect during regular maintenance. SCC is typically initiated by localised corrosion such as pitting or intergranular corrosion [65]. Both attacks can be minimised by surface treatment or cladding with more noble materials (e.g 1xxx series alloys) [14].

In the automotive industry, the need for fuel efficient vehicles to reduce carbon emission is the main motivation in reducing vehicle weight [57, 58]. As a result, the use of Al alloys has reached more than 80% throughout the years, not only as structural materials but engine components as well [1]. The utilisation of medium strength alloys, typically from the 5xxx and 6xxx series, is due to their good impact energy absorption and formability rather than the strength [58]. Alloy AA5052, AA5182, AA6022 in annealed condition (O) typically used as the inner body panels. Whereby the 6xxx series alloys are used as the outer body panels owing to higher strength and better surface finish [14, 16]. For engine and body components that require stronger materials, the AA5754-H28, AA6061-T4 and AA6262-T6 are used. Weldability of the 5xxx and 6xxx series alloys is beneficial for marine vessel components such as the hull, deckhouses and tanks, seeing an extensive use of AA5083-H116, AA5086-H32 and AA6063-O alloys. In general, the alloys have a good balance between mechanical strength, formability and corrosion resistance. However, the downside of 5xxx and 6xxx series alloys is the high susceptibility to intergranular attack at elevated temperature that can propagate to SCC [66-70]. This is due to the presence of Mg and its tendency to form  $\beta$ -phase ( $\text{Al}_3\text{Mg}_2$ ) at the grain boundaries [32, 44, 71].

In recent times, the focus has shifted in designing not only stronger alloys but also more durable and damage tolerant alloys. The presence of defects, crack growth from cyclic loading, and environmental interactions are typically initiated by the microstructural features of the alloy. The following table (Table 2.3) summarises the effect of microstructural features to the property of Al alloys as adapted from Starke [56]. One notable omission in the table is the presence of ‘cathodic’ particles, which can lead to well-documented circumferential attack [72], which have the potential to serve as fatigue crack initiation sites [73, 74].

Table 2.4: Property – microstructure relationships in Al alloys adapted from Starke [56]

<b>Property</b>	<b>Microstructural feature</b>	<b>Function of feature(s)</b>
Strength	Uniform dispersion of small, hard particles, fine grain size	Inhibit dislocation motion
Ductility and toughness	No large particles, clean grain boundaries, fine structure, no shearable particles	Encourage plasticity, inhibit void formation and growth, work harden
Fatigue crack initiation resistance	No shearable particles, fine grain size, no surface defects	Prevent strain localisation and slip steps on surface, prevent stress concentration
Fatigue crack propagation resistance	Shearable particles, no anodic phases or hydrogen traps, large grain size	Encourage crack closure, branching, deflection and slip reversibility
Pitting	No anodic phases	Prevent preferential dissolution of second phase particles
Stress corrosion cracking	No anodic phases, or interconnected hydrogen traps, hard particles	Prevent crack propagation due to anodic dissolution

## 2.4 Methods to improve corrosion via alloying

Discrete works aimed at improving corrosion resistance and mechanical performance through alloying have been documented since the 1920s [75-81]. Initially, studies were limited to a small range of Al-alloys used for the aircraft industry [81-83]. Some of the alloying elements studied at the time include copper, iron, silicon and manganese [75, 79, 84-90]. Since then, numerous works have been done on developing various types of alloys with different alloying elements. The addition of silver (Ag) for instance, improves the resistance to SCC in Al-Mg-Zn alloy [91-94] (noting that SCC resistance may not necessarily be synonymous with pitting resistance). More atypical elements were studied later such as Bi, V,



B, Ti, Zr, Co and Cr to improve resistance to localised attack, as well as SCC [95-100]. There however have been limited studies on improving corrosion resistance simultaneously with mechanical properties. Many of the studies are in relation to the 7xxx series alloys due to the extensive use of the alloy in aircraft structures. The addition of Zr, Cr and Mn for instance, improve resistance to SCC along with increase in yield and tensile properties [101, 102]. Similar results were achieved with the presence of Sc, Ni and Ce [103].

The Li containing alloys have been around for several decades. In recent years, an optimum amount of Li has been identified as being ideal for a balance of properties to modern Li-containing Al-alloys in the 2xxx series. The use of this alloy have suddenly expanded due to the development of third generation Al-Cu-Li such as the AA2050, AA2099, AA2195 and AA2297 [63, 64]. The improvement in mechanical strength is achieved from the formation of; i) Li-containing strengthening precipitates such as  $T_1$  ( $Al_2CuLi$ ),  $\delta$  ( $Al_3Ti$ ) and  $\theta$  ( $Al_2Cu$ ) [62, 104-106], and ii) strengthening dispersoids  $Al_3Zr$  and  $Al_{20}Cu_2Mn_3$ . The tensile strength can also be further improved by mechanical processing such as cold rolling prior to heat treatment for the refinement of  $T_1$  precipitates and to reduce precipitation at the grain boundaries during aging [107]. AA2099-T86 has better resistance to fatigue, exfoliation corrosion and SCC [64]. A similar trend is also observed for corrosion resistance of AA2050 in comparison to AA2024. However, it is very prudent to note that the number of independent, and characterisation based studies on such alloys do not exist in the open literature as yet – many of the reports being from alloy manufacturers. The addition of Li is not only limited to the high strength Al-alloys but also in non-heat treatable Al-alloys such as the 1xxx (e.g. AA1420) and 5xxx (e.g. AA5091) series [108]. Corrosion in Al-Li base alloys is typically associated with the presence of  $T_1$  ( $Al_2CuLi$ ),  $T_2$  ( $Al_6CuLi$ ) and  $\theta$  ( $Al_2Cu$ ) phases [26, 104, 109].  $T_1$  and  $T_2$  are highly anodic to the matrix at the beginning of exposure due to selective dissolution (dealloying) of Li. The dealloying of Li will leave Cu remnants at the bottom pits making it cathodic to the surrounding matrix [54]. The mechanism is similar to the dissolution of S-phase in Cu containing Al-alloys. The increase SCC and IGC are associated with these phases and also the dissolution of precipitate free zone along the grain boundaries [110].

As previously stated, localised attack is nominally caused by heterogeneity of the microstructure; with intermetallic particles acting as the initiation sites for pitting. The

susceptibility may be decreased by having finely dispersed sub-critical nano-scale precipitates within the matrix as suggested by Ralston [72]. It was found that embryonic precipitates from low heat treatment times can increase yield strength, even though not to the levels synonymous with peak aging. The precipitates however did not contribute to heterogeneity of the microstructure (in an electrochemical sense) hence this was shown to increase strength without increasing the susceptibility to pitting [111]. In that work, it was determined that the critical precipitate size is between 3 – 4 nm in size for an Al-Cu-Mg alloy. Once the precipitate grew beyond this size, a significant increase in pitting susceptibility was observed. Thus in other words, such alloys can be suggested to behave like solid solutions as far as corrosion is concerned, but as engineered solid solutions as far as strength development goes. Another suggested way in achieving nano-scale precipitates was rapid solidification. In this process, the cooling rate is greater than  $10^4$  K/s in order to achieve rapid extraction of thermal energy forming metastable crystalline phases incorporation of desirable fine second phases. Using the technique discussed here, it was found that pitting potential was significantly ennobled for Al alloys with the exception of alloys containing Mg, Fe or Zn [112].

In other works, the groups of Frankel [113, 114] and Shaw [50] independently studied the doping of Al with 'passive' elements such as Co, Mo, W, etc. These studies were conducted on sputtered thin films. The reason for this is for one; alloying with such elements is not possible by conventional means, since the melting point of such transition metals is close to temperatures where Al can undergo boiling; secondly, transition metals have very low solubility in Al - and hence appreciable alloying is only possible by sputtering. Such thin films studied showed increased resistance to pitting and enhanced passivity - making the studies very useful from a fundamental sense. None-the-less, from a practical alloy perspective such thin films cannot be up-scaled and are not viable engineering materials.

Studies have also shown that low levels of scandium (Sc) added in Al is found to contribute to grain refinement by the formation of  $\text{Al}_3\text{Sc}$  dispersoids. Dispersoids are effective in blocking dislocations. They also hinder grain growth and recrystallisation during thermomechanical processing, due to having coherency with the aluminium matrix but has high lattice mismatch [36]. Consequently, an increase in mechanical strength can be expected with low Sc additions. These effects are well known, but what makes Sc unique, is that although it can lead to development (of what are nominally considered deleterious) second

phase - for the case of  $\text{Al}_3\text{Sc}$  it has been found that the electrochemical properties do not significantly differ from Al - suggesting that this particle can be tolerated in the matrix as being electrochemically compatible [36]. It was also found in one recent study that Sc was able to enhance the properties of a high strength alloy with no significant degradation of corrosion performance [52]. This avenue is one that has not been exploited fully. At the time of this PhD, the cost of Sc in experimental quantities was in the vicinity of US\$1Million/kg (US\$1000/gram).

## **2.5 Evaluation of Al-alloy corrosion via electrochemical polarisation techniques**

Corrosion of Al alloys in aqueous solution is typically localised in nature, driven by heterogeneity of the microstructure during open circuit exposure. The degree of corrosion attack is governed by localisation of electrochemical reactions from the second phases and surrounding Al-matrix. In order to design Al-alloys with better corrosion resistance, kinetic parameters such as corrosion rate/electrode kinetics are of major interest in evaluating the corrosion performance rather than thermodynamic predictions [51]. One of the most common techniques to measure the electrochemical reaction kinetics is potentiodynamic polarisation [115-118]. This technique involves application of potential to an electrode (i.e. specimen under study), which results in current flow. The deviation of potential from the open circuit potential is the overpotential, which usually expressed in volts. Polarisation allows the user to drive the anodic or cathodic reactions, to be evaluated separately.

Tafel extrapolation is typically used to measure corrosion rate. The technique was first used by Wagner and Traud to verify the mixed potential theory. As will be seen in this thesis, polarisation curves are generally very useful in enabling one to observe any windows of passivity, comparison of electrode kinetics over a range of potentials, and also for providing an estimation of corrosion rate via Tafel extrapolation [119], as seen in Figure 2.2.

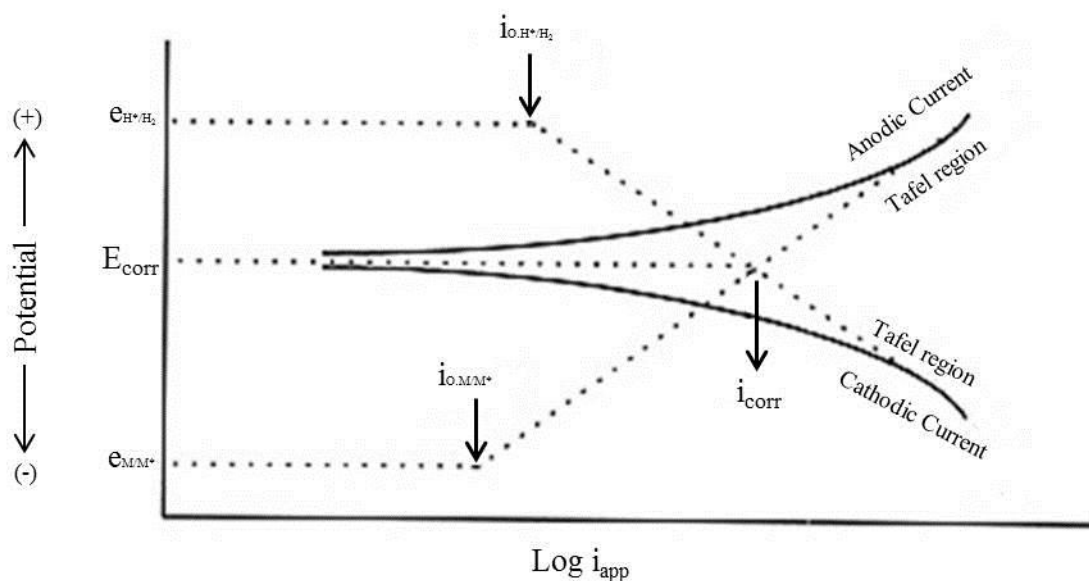


Figure 2.2: Schematic of Tafel extrapolation [15]

The Tafel plot provides an instant measurement of corrosion current density ( $i_{\text{corr}}$ ) representing the corrosion rate of the system.  $i_{\text{corr}}$  is obtained at the intersection between the anodic and cathodic reactions where the total rates of oxidation and reduction are equal. The corrosion rate acquired by Tafel extrapolation have compared favourably with other method such as weight loss, depth of penetration measurement and hydrogen evolution measurement [51, 120]. However, careful qualification is needed in instances where the response deviates from Tafel-like behaviour. There are several basic steps for good interpretation of a Tafel slope. It is important that extrapolation commence at least 50 to 100mV away from the  $E_{\text{corr}}$  and to ensure one of the slopes exhibits Tafel behaviour (e.g. linear or semi-logarithmic). A bad interpretation of the slopes could change the  $i_{\text{corr}}$  reading by a factor of 5 to 10. The sensitivity of electrochemical measurements and its data analysis, it is important to compare the data with other types of corrosion measurements such as the mass loss values from immersion test.

In a laboratory setting, electrochemical polarisation is carried out with a potentiostat that controls the potential of a test electrode in an electrolyte. The typical electrochemical corrosion test cell setup consisting of three electrodes submerged in an electrolyte and connected to a potentiostat is presented in Figure 2.3. The degree of polarisation is measured

by the potential difference between reference and test electrode. The potential for reference electrode always remains at its open circuit potential (OCP) to act as a fixed reference point and provide feedback to the potentiostat. Depending on the range of potential supplied the resulting a polarisation plot can be utilised for interpretation of corrosion data such as passivity, pitting potential, coating performance, corrosion rates and corrosion resistance. Sample preparation for electrochemical tests is also important. The surface finish of the test electrode should be as smooth as possible according to ASTM G1-03 standard. It suggests that at least a 1200 grit finish (1200 grit corresponds to 1200 abrasive particles per lineal inch of abrasive paper) is achieved [121]. An uneven surface can influence current density, leading to electrochemical data that does not reflect the actual corrosion behaviour.

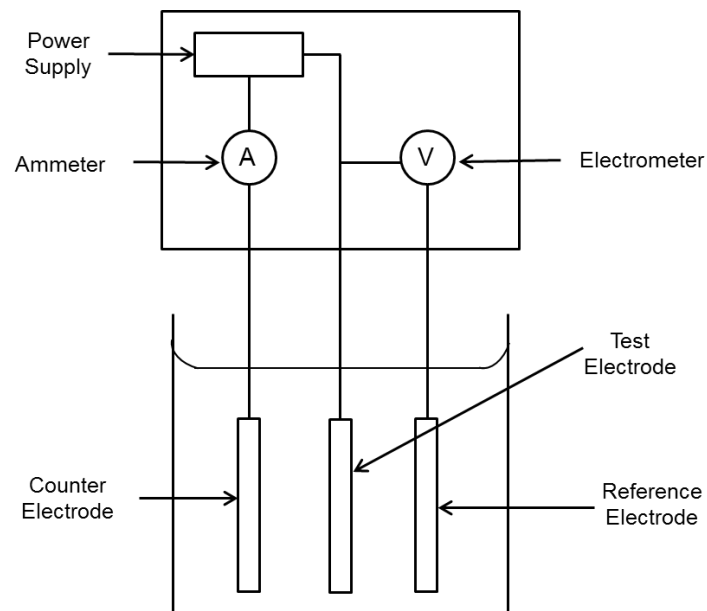


Figure 2.3: A schematic diagram of a three electrode cell for electrochemical polarisation testing [122]

Generally, electrochemical testing results in the determination of distributed values, perhaps more so than non-electrochemical tests such as mass loss measurements. The data variability is influenced not only by the experimental set-up but also the metal itself. The inconsistency of data distribution often makes it difficult to evaluate the actual corrosion response of the system – particularly since polarisation test are more of an ‘instant’ as opposed to cumulative term. A statistical formula to estimate number of repetition suggested by Miller [123] given in the following equation;

$$Er^* = \frac{Z\sigma}{\sqrt{n}}$$

where,  $Er^*$  is the difference between the true mean and the mean estimated from a group of repetitions,  $\sigma$  is standard deviation of the repetitions,  $n$  is number of repetitive measurements and  $Z$  is the desired statistical confidence level. Caution also has to be applied in using this equation as the number of repetitions depends on how much error is accepted in the experiment.

In the study of systems that are prone to localised corrosion,  $E_{pit}$  [111, 124] is often used as an indication of pitting susceptibility [125]. However, care should be taken as the  $E_{pit}$  value can be misleading as it only indicates the occurrence of stable pits, but insufficient to holistically determine pitting or pitting resistance. For example, a more noble  $E_{pit}$  value does not necessarily mean the alloy has better resistance but consideration also has to be given to the damage accumulation (e.g. density and depth of pits) before the pitting resistance can be determined.

## **2.6 Durability and Corrosion of Aluminium and Its Alloys**

This section comprises of a book chapter in ‘Aluminium Alloys - New Trends in Fabrication and Applications’ published by InTech (2012). The chapter covers a more detailed discussion of the Al-alloys in regards to corrosion. It includes recent advances in aspects related to corrosion protection, corrosion assessment methods and the development towards better corrosion resistance Al-alloys. The PhD candidate was the principal author and responsible for the compilation / review.



## Monash University

### Declaration for Thesis Section 2.6

In the case of Section 2.6, the nature and extent of my contribution to the work was the following:

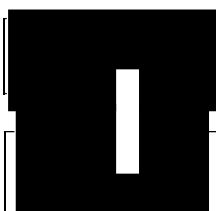
Nature of contribution	Extent of contribution (%)
Initiation, key ideas, experimental, development, results interpretations, writing up	75

The following co-authors contributed to the work. If co-authors are students at Monash University, the extent of their contribution in percentage terms must be stated:

Name	Nature of contribution	Extent of contribution (%) for student co-authors only
Nick Birbilis	Initiation, key ideas, experimental, development, results interpretations, writing up	5
Xian Zhou	Results interpretations, writing up	5
Anthony Hughes	Results interpretations, writing up	5
Arjan Mol	Results interpretations, writing up	5
Santiago Garcia	Results interpretations, writing up	5 (combined)
Xiaorong Zhou	Results interpretations, writing up	
George Thompson	Results interpretations, writing up	

The undersigned hereby certify that the above declaration correctly reflects the nature and extent of the candidate's and co-authors' contributions to this work.

**Candidate's  
Signature**



**Date**

18 June 2014

**Main  
Supervisor's  
Signature**



**Date**

18 June 2014

---

# Durability and Corrosion of Aluminium and Its Alloys: Overview, Property Space, Techniques and Developments

---

N. L. Sukiman, X. Zhou, N. Birbilis, A.E. Hughes,  
J. M. C. Mol, S. J. Garcia, X. Zhou and G. E. Thompson

Additional information is available at the end of the chapter

<http://dx.doi.org/10.5772/53752>

---

## 1. Introduction

Aluminium (Al) is an important structural engineering material, its usage ranking only behind ferrous alloys (Birbilis, Muster et al. 2011). The growth in usage and production of Al continues to increase (Davis 1999). The extensive use of Al lies in its strength: density ratio, toughness, and to some degree, its corrosion resistance. From a corrosion perspective, which is most relevant to this chapter, Al has been a successful metal used in a number of applications from commodity roles, to structural components of aircraft. A number of Al alloys can be satisfactorily deployed in environmental/atmospheric conditions in their conventional form, leaving the corrosion protection industry to focus on market needs in more demanding applications (such as those which require coating systems, for example, the aerospace industry).

Relatively pure aluminium presents good corrosion resistance due to the formation of a barrier oxide film that is bonded strongly to its surface (passive layer) and, that if damaged, reforms immediately in most environments; i.e. re-passivation (Davis 1999). This protective oxide layer is especially stable in near-neutral solutions of most non-halide salts leading to excellent pitting resistance. Nevertheless, in open air solutions containing halide ions, with Cl<sup>-</sup> being the most common, aluminium is susceptible to pitting corrosion. This process occurs, because in the presence of oxygen, the metal is readily polarised to its pitting potential,

and because chlorides contribute to the formation of soluble chlorinated aluminium (hydr)oxide which interferes with the formation of a stable oxide on the aluminium surface.

Aluminium and its alloys readily oxidises, including when Al is present in either in solid solution or in intermetallic (IM) particles. Industrial alloy surfaces however, tend to be as heterogeneous as their underlying microstructures. The surface of a wrought or cast alloy is likely to contain not only aluminium oxide alone, but may for example contain a fragment of a mixed Al-Mg oxide for alloys rich in Mg (Harvey, Hughes et al. 2008)). This is primarily because of the heat of segregation of Mg is high and it has a favorable free energy for oxide formation. If however an Al surface is mechanically undisturbed - then the surface oxide is relatively protective. Though, most real surfaces have some sort of mechanical finishing which results in the formation of a near surface deformed layer (NSDL) and shingling. Shingling occurs where the alloy matrix is spread across the surface including IM particles in abrasion and milling (Scholes, Furman et al. 2006; Muster, Hughes et al. 2009). This is because the IM particles are harder than the surrounding matrix and less susceptible to deformation (Zhou, Liu et al. 2011). Even on polished surfaces, the matrix and the IM particles rapidly form different oxide structures (Juffs, Hughes et al. 2001; Juffs, Hughes et al. 2002). This is almost certainly due to different chemical environments and different electrochemical reactions over the IM particles compared to the matrix. Furthermore, the morphology and the oxide are not continuous from the IM particles to the matrix and this represents a potential defect site in the context of corrosion. For the purposes of descriptions herein, IM particles can be classified into three main types; i) precipitates, ii) constituent particles and iii) dispersoids. Precipitates are typically in the shape of needles, laths, plates or spherical with the size ranging from Angstroms to fractions of a micrometer. They are formed by nucleation and growth from a supersaturated solid solution during low temperature aging and may be concentrated along the grain boundaries. Constituent particles however, are relatively large with irregular shape and the size can be up to 10 micrometers. This type of particle forms during solidification of the alloy and is not fully dissolved by subsequent thermomechanical processing (including solution heat treatments). They can be found in colonies of several IM crystals or different compound types. On the contrary, dispersoids are small particles with size ranging from 0.05 to 0.5 micrometers. They are thermally stable intermetallics of a fine size that are functional for controlling grain size and recrystallisation behavior. Dispersoids form by low level additions of highly insoluble elements such as Cr, Mn or Zr.

This chapter will aim to cover some of the important aspects related to the corrosion of Al-alloys, bearing in mind the role of alloy chemistry. In addition, some of the topical aspects related to techniques and ongoing developments in the general field of Al-alloy corrosion are presented. An attempt has been made to give the reader an overview of the key technical aspects, but unfortunately for comprehensive insight into the topic overall, the size of this chapter alone cannot be a replacement to dedicated monographs on the specific topics at hand; nor the ever-evolving journal literature that represents the state of the art. To aid in the transfer of information, this chapter has been divided into a number of sections to treat the widely varying topics independently.

### 1.1. The general performance of the Al-alloy classes

The corrosion potential of an aluminium alloy in a given environment is primarily determined by the composition of the aluminium rich solid solution, which constitutes the predominant volume fraction and area fraction of the alloy microstructure (Davis 1999). While the potential is not affected significantly by second phase IM particles of microscopic size, these particles frequently have corrosion potentials (when measured in isolation) differing from that of the solid solution matrix resulting in local (micro-) galvanic cells, when IMs are polarised to the corrosion potential of the alloy. The result is that local currents on the alloy surface differ, establishing anodes and cathodes. Since most of the commercial aluminium alloys contain additions of more than one type of alloying element, the effects of multiple elements on solution potential are approximately additive. The amounts retained in solid solution, particularly for more highly alloyed compositions, depend on production and thermal processing so that the heat treatment and other processing variables influence the final electrode potential of the product.

By measuring the potentials of grain boundaries and grain bodies separately, the difference in potential responsible for local types of corrosion such as intergranular corrosion, exfoliation, and stress corrosion cracking (SCC) can be quantified (Guillaumin and Mankowski 1998; Zhang and Frankel 2003). By measuring the corrosion potential of IMs (Buchheit 1995), and indeed by measurement of the polarisation response of IMs, even more significant insights into localised corrosion can be gained (Birbilis and Buchheit 2005). Such specialist topics are not dealt with in their entirety herein, however an abridged written summary of the performance of the key Al-alloy classes (as outlined by the Aluminium Association (Hatch 1984)) is provided below.

#### 1.1.1. 1xxx series alloys

Corrosion resistance of aluminium increases with increasing metal purity, however the use of the >99.8% grades is usually confined to those applications where very high corrosion resistance or ductility is required. In regards to such specialist applications however, the actual number of applications are very few. Consequently 1xxx series alloys are not commonly used or sold (but do serve as important feedstock to secondary alloy producers or production). In the instance where general-purpose alloys for lightly stressed applications are required, such alloys are approximately 99% pure aluminium and offer adequate corrosion resistance in near neutral environments. 1xxx is also sometimes used in cladding for example AA1230 is used as clad on AA2024 (Hatch 1984)

#### 1.1.2. 2xxx series alloys

Copper is one of the most common alloying additions - since it has appreciable solubility and can impart significant strengthening by promotion of age hardening (in fact, the Al-Cu system was the classical/original age hardening system (Hatch 1984)). These alloys were the foundation of the modern aerospace construction industry and, for example AA2024 (Al-4.4Cu-1.5Mg-0.8Mn), which is still used in many applications to this day, can achieve strengths in excess of 500MPa depending on temper (Polmear 2006).

### 1.1.3. 3xxx series alloys

The 3xxx series alloys are a commodity product that is nominally available in the form of thin sheet (for beverage can usage). The key alloying element, Manganese, has a relatively low solubility in aluminium but can improve corrosion resistance when remaining in solid solution. Additions of manganese of up to about 1% form the basis of the non-heat treatable wrought alloys with good corrosion resistance, moderate strength (i.e. AA3003 tensile strength ~110MPa) and exceptionally high formability (Polmear 2006).

### 1.1.4. 5xxx series alloys

Magnesium has significant solubility in aluminium and imparts substantial solid solution strengthening (which can also contribute to enhanced work hardening characteristics) (Davis 1999; Polmear 2006). The 5xxx series alloys (containing <~6% Mg) do not age harden. Whilst it is possible for  $\beta$ -phase ( $\text{Mg}_2\text{Al}_3$ ) to precipitate in systems with above ~3%Mg, the  $\beta$ -phase is not a strengthening precipitate and actually weakens the alloy (by depleting the solute of Mg). Nominally, the corrosion resistance of 5xxx series alloys is good and their mechanical properties make them ideally suited for structural use in aggressive conditions (such as marine vessels). Fully work-hardened AA5456 (Al-4.7Mg-0.7Mn-0.12Cr) has a tensile strength of >380MPa. One corrosion issue with fully work-hardened 5xxx series alloys is that the heavy dislocation density (and supersaturation of the solid solution with Mg) can permit the sensitization of the microstructure by precipitation of deleterious  $\beta$ -phase ( $\text{Mg}_2\text{Al}_3$ ) during sustained high temperature exposure (i.e. in service) (Baer, Windisch et al. 2000; Searles, Gouma et al. 2002; Davenport, Yuan et al. 2006; Goswami, Spanos et al. 2010).

### 1.1.5. 6xxx series alloys

Silicon additions alone can lower the melting point of aluminium whilst simultaneously increasing fluidity (which is why the vast majority of cast Al products contain various amounts of Si). These alloys are increasing in importance in automotive applications for engine and drive train components – however are yet to realise the majority of market share. Heat-treatable Al-Mg-Si are predominantly structural materials (strengths >300MPa are possible), all of which have an appreciable resistance to corrosion, immunity to SCC and are weldable. To date, 6xxx series alloys are mainly used in extruded form, although increasing amounts of sheet are being produced (Birbilis, Muster et al. 2011). Magnesium and silicon additions are made in balanced amounts to form quasi-binary Al-Mg<sub>2</sub>Si alloys, or excess silicon additions are made beyond the level required to form Mg<sub>2</sub>Si. Alloys containing magnesium and silicon in excess of 1.4% develop higher strength upon aging.

### 1.1.6. 7xxx series alloys

The Al-Zn-Mg alloy system provides a range of commercial compositions, primarily where strength is the key requirement (and this can be achieved without relatively high cost or complex alloying). Al-Zn-Mg-Cu alloys have traditionally offered the greatest potential for age hardening and as early as 1917 a tensile strength of 580MPa was achieved, however,

such alloys were not suitable for commercial use until their high susceptibility to stress corrosion cracking could be moderated (Song, Dietzel et al. 2004; Birbilis, Cavanaugh et al. 2006; Lin, Liao et al. 2006; Lynch, Knight et al. 2009). Aerospace needs led to the introduction of a range of high strength aerospace alloys of which AA7075 (Al-5.6Zn-2.5Mg-1.6Cu-0.4Si-0.5Fe-0.3Mn-0.2Cr-0.2Ti) is perhaps the most well-known, and which is now essentially wholly superseded by AA7150 (or the 7x50 family). The high strength 7xxx series alloys derive their strength from the precipitation of  $\eta$ -phase ( $\text{MgZn}_2$ ) and its precursor forms. The heat treatment of the 7xxx series alloys is complex, involving a range of heat treatments that have been developed to balance strength and stress corrosion cracking performance - including secondary (or more) heat treatments that can include retrogression and re-aging (Fleck, Calleros et al. 2000; Ferrer, Koul et al. 2003; Zieliński, Chrzanowski et al. 2004; Marlaud, Deschamps et al. 2010).

#### 1.1.7. 8xxx series alloys

Nominally reserved for the sundry alloys, 8xxx series alloys include a number of Lithium (Li) containing alloys. Li is soluble in aluminium to  $\sim 4$  wt% (corresponding to  $\sim 16$  at%). As these alloys of high specific strength and stiffness readily respond to heat treatment, research and development has intensified due to their potential for widespread usage in aerospace applications (Lavernia and Grant 1987; Dorward and Pritchett 1988; Giummarra, Thomas et al. 2007). Based on the impressive lightweight of such alloys, present day aircraft are comprised of some portion of Al-Li based alloys (modern generations of which actually include low Li levels and hence are nowadays designated as 2xxx alloys (Ambat and Dwarakadasa 1992; Garrard 1994; Semenov 2001; Giummarra, Thomas et al. 2007). First generation Li-containing alloys displayed some of the highest corrosion rates of all aluminium alloys, where susceptibility to intergranular corrosion was challenging. Modern Al-Cu-Li seem to have overcome this challenge; however it is also important to recognise that production requires specialised melting and casting, not presently available in most commercial facilities.

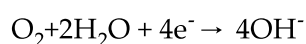
## 2. Corrosion of aluminium and its alloys in aqueous environment

### 2.1. Environmental corrosion of aluminium

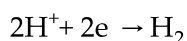
Corrosion in aluminium alloys is generally of a local nature, because of the separation of anodic and cathodic reactions and solution resistance limiting the galvanic cell size. The basic anodic reaction is metal dissolution:



While the cathodic reactions are oxygen reduction:



or hydrogen reduction in acidified solution such as in a pit environment as a result of aluminium ion hydrolysis:



It is the interaction between local cathodes and anodes and the alloy matrix that leads to nearly all forms of corrosion in aluminium alloys. These include pitting corrosion, selective dissolution, trenching, intermetallic particle etchout, intergranular attack and exfoliation corrosion. Surface and subsurface grain etchout is also influenced by grain energy which is derived from grain defect density. Grain etchout, has a significant role in exfoliation corrosion since the volume of hydrated aluminium oxide generated during dissolution is larger than the original volume of the grain.

The general consensus for Al and its alloys is that they are resistant towards corrosion in mildly aggressive aqueous environments. The protective oxide layer represents the thermodynamic stability of Al alloys in corrosive environment - acting as a physical barrier as well as capable to repair itself in oxidizing environments if damaged. While the passive layer breakdown mechanism by chloride ions is still in debate (Sato 1990; McCafferty 2010) due to the complexity of the process (Szklarska-Smialowska 2002), the general consensus is that localized attack starts by adsorption of aggressive anions and formation of soluble transitional complexes with the cations at the oxide surface. Thermodynamic principles to explain and predict the passivity phenomenon that controls the corrosion behavior of Al are summarised by Pourbaix-type analysis. This results in a plot of potential vs. pH based on the electrochemical reaction of the species involved, the representation known as a Pourbaix diagram (Pourbaix 1974) as shown in Figure 1.

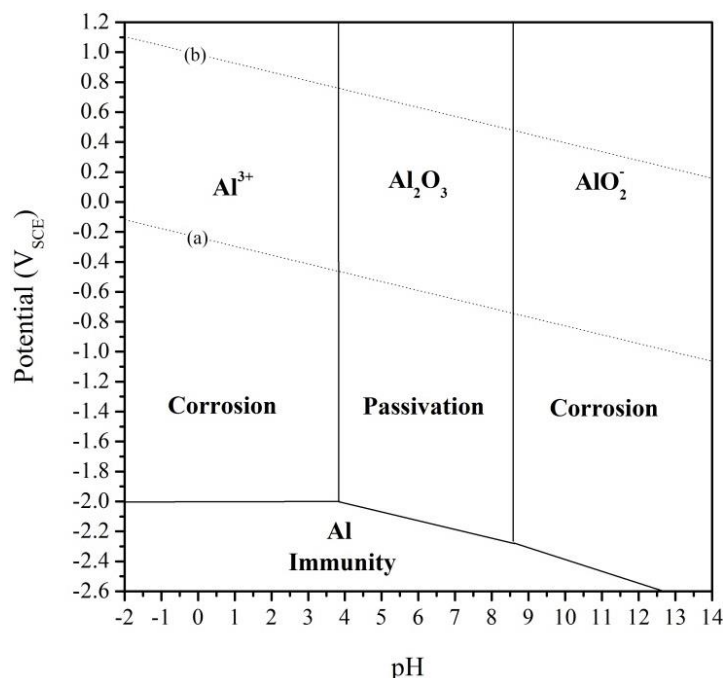


**Figure 1.** E-pH diagram for pure Al at 25°C in aqueous solution (adapted from Pourbaix 1974). The lines (a) and (b) correspond to water stability and its decomposed product.

It is seen that Al is nominally passive in the pH range of ~4 to 9 due to the presence of an  $\text{Al}_2\text{O}_3$  film. In environments that deviate from the near neutral range, the continuity of this film can be disrupted in which the film becomes soluble, facilitating the relatively rapid dissolution of the alloy. In the acidic range, Al is oxidised by forming  $\text{Al}^{3+}$ , whilst  $\text{AlO}_2^-$  occurs in alkaline range.

The E-pH diagram gives an impression that corrosion prediction is a straightforward process, however in actual engineering applications, there are several variables that weren't considered by Pourbaix. These include (i) the presence of alloying elements in most engineering metals (ii) the presence of substances in the electrolyte such as chloride (albeit that this has been addressed in more modern computations), (iii) the operating temperature of the alloy, (iv) the mode of corrosion, and (v) the rate of reaction. Taking these factors into account is nominally done on a case by case (i.e. alloy by alloy) basis, and a revised version of an E-pH diagram for 5xxx series alloys in 0.5M sodium chloride is given in Figure 2.

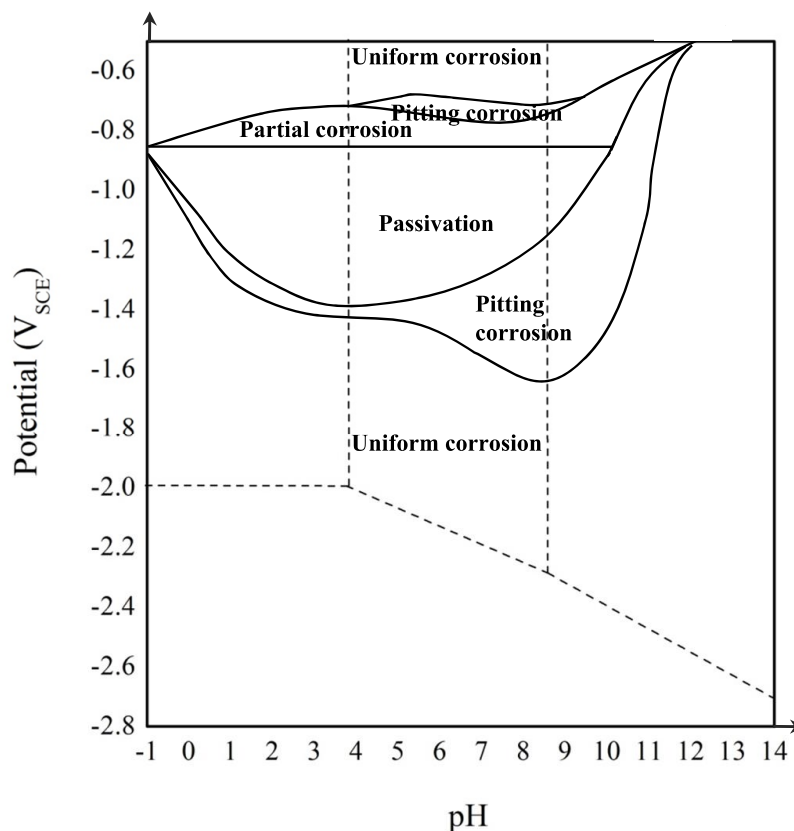


**Figure 2.** Mode of corrosion based on experimental data for AA5086 in the presence of 0.5M sodium chloride (adapted from Gimenez, Rameau et al. 1981)

Figure 2 indicates windows where localized attack is highly possible in the supposed passive region (Gimenez, Rameau et al. 1981). It is also seen that localised attack is possible across the whole range of pH depending on the specific potential. One should therefore not rely solely on



the Pourbaix diagram as a direct index to actual corrosion rates, with rates needing to be independently measured for a given alloy-electrolyte combination (Ambat and Dwarakadasa 1992). Finally, whilst not to be discussed in detail here, it is prudent to indicate that effectively all Al-alloys do not attain practical/empirical immunity as evidence in Figure 1. Cathodic polarisation tends to contribute to alloy deterioration by two modes. Firstly, the accumulation of hydroxyl ions at the Al-surface will cause chemical dissolution of the Al. Secondly, Al is a very strong hydride former, and hydrogen from the cathodic reaction at such negative potentials will serve combine with Al to form hydrides (Perrault 1979).

## 2.2. Kinetic stability of aluminium alloys

Kinetics represents the rate of reaction during corrosion. When exposed to an aqueous environment, metals stabilise to a value of electrochemical potential that is characteristic of the material and its composition for a given electrolyte. This potential is the potential at which anodic and cathodic reactions upon the metal surface are equal, and the value of this potential is thus significantly influenced by factors that can alter the relative rates of anodic or cathodic reaction efficiency upon the metal surface (i.e. alloying, precipitate state, etc.).

Most typically, the potentiodynamic polarisation test is used to characterise the corrosion performance of an alloy (as far as determination of mechanistic aspects from an instantaneous test). This method gives vital kinetic information such as current density over a range of potentials, pitting potential (if it exists), corrosion potential, the passive current density and potentially more information in reverse scans, etc. Thus factors affecting corrosion as discussed in the previous sections can be evaluated with much higher confidence. For example, Figure 3 shows a polarisation curve of Pure Al compare to AA2024-T3 (Al-4.3Cu-1.5Mg-0.6Mn) in 0.1M NaCl.

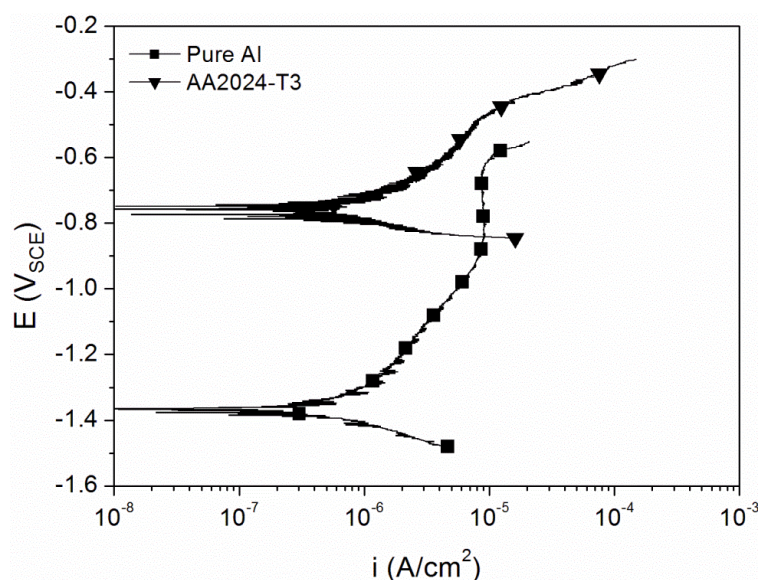


**Figure 3.** Polarisation curve of pure Al and AA2024-T3 exposed to 0.1M NaCl for 7 days collected at 1mV/s<sup>-1</sup> (adapted from (Sukiman, Birbilis et al. 2010))

Comparison of alloy behavior and dominant reactions can be made in a quantitative manner. The anodic branch of the polarisation curve gives information related to the anodic/dissolution reaction while the cathodic branch represents the reduction reaction (nominally oxygen reduction, but at lower potentials or in strong acids, water reduction). The addition of more noble alloying elements typically increases the corrosion potential to more noble values (Davis 1999) and this is dramatically observed in Figure 3. This ennoblement however does not correlate to the rate of corrosion (as judged by Figure 3), whereby we see the pure Al versus AA2024-T3 has a difference in potential of  $\sim 0.5\text{V}$ . In addition, the main practical threat for Al alloys is localised attack such as pitting, so in that vein, a more noble value of pitting potential does not necessarily signify a better corrosion resistance (Frankel 1998; Birbilis and Buchheit 2005). Rather generally, the electrochemical reactions upon Al-alloys are heavily influenced by the chemistry and microstructure of the alloy – which we attempt to discuss in the following section.

Moving beyond potentiodynamic polarisation towards a true measure of kinetic stability in the E-pH domain (similar in concept to Pourbaix diagrams however which give ‘speed’ and not just thermodynamic likelihood) there are tests which can be done in this regard. In order to develop an improved understanding of overall kinetic stability of a metal over the potential-pH space, methods including the staircase potentiodynamic electrochemical impedance spectroscopy (SPEIS) can be used to establish so-called kinetic stability diagrams, as previously demonstrated for pure Al (Zhou, Birbilis et al. 2010) and depicted in Figure 4. The specifics of SPEIS will be introduced in section 5.3.

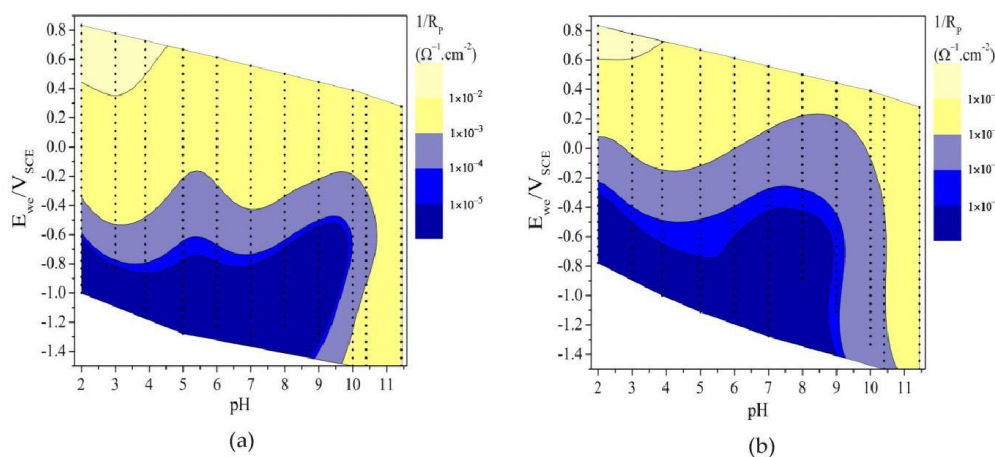


**Figure 4.** Contour plots of  $1/R_p$  for the E-pH space and their data for (a) A portion of a 99.9999% Al ingot single crystal and (b) a polycrystalline specimen from the identical ingot in (a) (adapted from (Zhou, Birbilis et al. 2010))

In Figure 4, presentation of the reciprocal of polarisation resistance ( $1/R_p$ ) is the metric of reaction ‘speed’, as it is proportional to the reaction rate at a given condition. The influence of potential and pH is presented not only for pure Al in the sample which was single crystal,

but also for a polycrystalline sample. As a result, one is also able to assess the effect of grain structure from Figure 4. Most importantly however, Figure 4 reveals that the rate of reaction stays in a low range in areas that extend beyond that of the Pourbaix diagram in terms of certain E-pH combinations – indicating that although Al may be in a thermodynamically unstable region, the reaction rate can be maintained to be low enough to make it still be useful in an engineering context. Similarly, there are regions of high potential where pure aluminium may be in a thermodynamically stable region, but unusable – owing to transpassive dissolution. Finally, in terms of microstructure effects, it is seen that the exact same material can have a different kinetic response based on structural factors alone. Such differences are not detectable or predicted from thermodynamic analysis in any way, and this highlights the importance of approaches which provide kinetic information to meet demands of engineering applications.

### 2.3. The property space and corrosion property profile of aluminium alloys

As technologies continue to advance with more challenging applications and environments, a general understanding of durability limits across the class of Al-alloys is essential. Durability needed in a broad sense is the ability to withstand an environment while maintaining mechanical integrity. This indicates a requirement to understand the property space for Al and its alloys. Figure 5 shows a trend that is in line with the notion that increases in hardness (used here as a proxy to yield strength) show increases in corrosion rate.

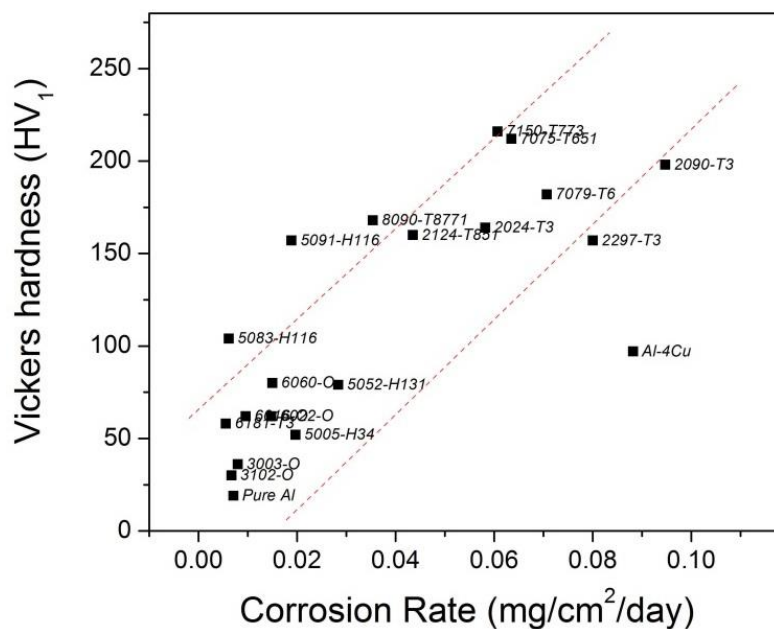


**Figure 5.** Corrosion rate as determined from weight loss data for commercial Al alloys collected after 14 days exposure in quiescent 0.1M NaCl presented against alloy hardness.

From Figure 5, it can be argued that the data is divided into two main groups, one at each end of the corrosion rate spectrum. High hardness/strength aluminium alloys were found to populate the high corrosion rate space. This is in contrast to the medium to low hardness/strength alloys that revealed considerably lower corrosion rates. The alloys that show the highest corrosion rates are the 'precipitation hardenable' family. Besides the high number density of precipitate particles in such alloys, they also contain an appreciable population of constituent type particles (Chen, Gao et al. 1996; Wei 2001; Andreatta, Terryn et al. 2004; Ilievbare, Schneider et al. 2004; Birbilis, Cavanaugh et al. 2006; Boag, Hughes et al. 2009; Hughes, MacRae et al. 2010; Xu, Birbilis et al. 2011). These particles are industrially necessary, since the complex chemistry of precipitation hardenable alloys (that can contain up to 10 alloying elements) have significant alloying additions added via alloy rich master alloys. It is also observed that the alloys that show the highest corrosion rates also contain appreciable amount of copper.

The plot in Figure 5 allows one to identify a region of property space (at the top left corner) that has potential for future alloys, with ongoing efforts aiming to reach such space (in addition to controlling ductility). Efforts that regard in are underway, focusing on corrosion rate (Carroll, Gouma et al. 2000; Norova, Ganiev et al. 2003; Rosalbino, Angelini et al. 2003; Cavanaugh, Birbilis et al. 2007; Lucente and Scully 2007; Fang, Chen et al. 2009; Graver, Pedersen et al. 2009; Ralston, Birbilis et al. 2010; Tan and Allen 2010; Xu, Birbilis et al. 2011; Brunner, Birbilis et al. 2012) and strength (Poole, Seter et al. 2000; Pedersen and Arnberg 2001; Fuller, Krause et al. 2002; Raviprasad, Hutchinson et al. 2003; Lee, Shin et al. 2004; Oliveira Jr, de Barros et al. 2004; Zhao, Liao et al. 2004; Kim, Kim et al. 2005; Teixeira, Bourgeois et al. 2007; McKenzie and Lapovok 2010; Wang, Zhang et al. 2010; Puga, Costa et al. 2011; Zhong, Feng et al. 2011; Westermann, Hopperstad et al. 2012). However, such studies are done independently of both properties thus the symbiotic effect can't be readily evaluated to date.

### 3. Corrosion of aluminium and its alloys in aqueous environment

#### 3.1. The role of chemistry on corrosion

Alloying elements are added to aluminium for various reasons, with improving mechanical properties the principal reason. These elements introduce heterogeneity into the microstructure, which is the main cause of localised corrosion that initiates in the form of pitting. Each alloying element has a different effect on the corrosion of Al, and in this section we *briefly* discuss the role of alloying elements on corrosion of Al.

##### 3.1.1. Influence of magnesium

Mg is one of the major elements added to Al to improve mechanical properties by solid solution strengthening – and can be found in 5xxx alloys, as well as 2xxx, 3xxx, 6xxx and 7xxx commercial alloys. Mg can stabilize GP zones, has a high solubility in Al and decreases the alloy density. Muller and Galvele showed that Mg when present in solid solution does not

have a significant effect on the pitting corrosion of Al which can be understood on the basis of standard potentials of Al and Mg (Muller and Galvele 1977). Moreover, Mg decreases the rate of the cathodic reaction when present in solid solution, increasing corrosion resistance, which may appear counterintuitive, but is rather obvious (as Mg has a very low exchange current density and hence retards the cathodic reaction). In contrast, excess amounts of Mg in the alloy or a long term exposure to elevated temperature will cause the precipitation of either  $\text{Al}_8\text{Mg}_2$  or  $\text{Al}_3\text{Mg}_2$  (Searles, Gouma et al. 2002; Davenport, Yuan et al. 2006; Oguocha, Adigun et al. 2008; Jain, Lim et al. 2012). These phases form typically along grain boundaries (Baer, Windisch et al. 2000; Goswami, Spanos et al. 2010) and are known to be anodic with respect to Al matrix therefore prone to localized corrosion (Vetrano, Williford et al. 1997; Aballe, Bethencourt et al. 2001; Jones, Baer et al. 2001; Brunner, May et al. 2010). Mg in 2xxx, 6xxx and 7xxx alloys however, forms precipitates with other alloying elements to strengthen the alloy where role of Mg mainly depends upon the other alloying additions (Ringer, Hono et al. 1996; Buchheit, Grant et al. 1997; Campestrini, van Westing et al. 2000; Guillaumin and Mankowski 2000; Eckermann, Suter et al. 2008).

### 3.1.2. Influence of silicon

The addition of Si in conjunction with Mg, which is typical in 6xxx series Al alloys, allows  $\text{Mg}_2\text{Si}$  particles to precipitate. There is vast literature on the chemical composition of the Mg-Si phase and its role on mechanical properties (Hirth, Marshall et al. 2001; Usta, Glicksman et al. 2004; Stelling, Irrerier et al. 2006; Eckermann, Suter et al. 2008; Zeng, Wei et al. 2011). This particle is beneficial in terms of increasing strength but renders the alloy prone to localised corrosion (Eckermann, Suter et al. 2008). The electrochemical behavior of  $\text{Mg}_2\text{Si}$  was investigated recently and it was shown that  $\text{Mg}_2\text{Si}$  remains more 'anodic' (i.e., less noble) than the matrix in Al-alloys. As a consequence of this,  $\text{Mg}_2\text{Si}$  remains anodic and undergoes selective dissolution in the Al-matrix. Some 6xxx series alloys contain excess Si. Excess amount of Si however increases the cathodic reaction rate (Eckermann, Suter et al. 2008) and are unfavorable since Si tends to be present along the grain boundary and this may lead to intergranular corrosion and stress corrosion cracking (Guillaumin and Mankowski 2000; Larsen, Walmsley et al. 2008; Zeng, Wei et al. 2011).

### 3.1.3. Influence of copper

The presence of Cu is viewed as detrimental to corrosion due to the formation of cathodic particles capable of sustaining the cathodic reaction locally and efficiently, such as  $\text{Al}_2\text{Cu}$  and  $\text{AlCu}_2\text{Mg}$ . In some cases where low Cu content is used, the impact of Cu is minimal, however given that corrosion is not the principal alloy design criteria in most instance, Cu is common in many (most) Al-alloys. The 2xxx series alloys are Cu rich, however Cu is added to other alloy classes such as the 6xxx series where it can increase strength when present in trace amounts, and also enhance precipitation hardening. The same is true in 7xxx alloys, with most modern aerospace alloys having appreciable amounts of Cu that can increase strength by modifying precipitation and minimising SCC via incorporation into precipitates (such as  $\text{Mg}(\text{Zn},\text{Cu})_2$ ).



In general however, there is still some debate on the precise role of Cu, which also depends on the temper condition. Muller and Buchheit found that Cu in the form of solid solution decreases pitting susceptibility through the ennoblement of pitting potential. While Muller and Galvele reported an increase in pitting potential for solid solution content of Cu up to 5 wt%. In the case of Al-Cu-Mg alloys which contain  $S$  phase ( $\text{Al}_2\text{CuMg}$ ), large differences in solution potential between Cu (highly noble) and Mg exist, with significant focus on corrosion of  $S$  phase (Buchheit, Grant et al. 1997; Guillaumin and Mankowski 1998; Buchheit, Montes et al. 1999; Ilevbare, Schneider et al. 2004; Boag, Hughes et al. 2011) revealing dealloying and selective dissolution that leads to preferential dissolution of Mg and Al with Cu remnant being redistributed at or near the site of the  $\text{Al}_2\text{CuMg}$ . A range of other particles associated with Cu have been reported such as  $\text{Al}_7\text{Cu}_2\text{Fe}$ . However recent microprobe studies of a number of batches of AA2024-T351 indicate five common compositions across modern alloys which do not have the same composition as older alloy stock indicating that this is still an active area of research (Hughes, Glenn et al. 2012). In general, Cu, or Cu containing particles are capable of supporting high oxygen reductions rates and hence undesirable from corrosion perspective (Mazurkiewicz and Piotrowski 1983; Scully, Knight et al. 1993; Buchheit 2000; Birbilis, Cavanaugh et al. 2006).

#### 3.1.4. Influence of zinc

In high strength commercial aluminium alloys such 7xxx series alloys, Zn is added to stimulate precipitation hardening. Alloys containing high levels of Zn such as the modern aerospace alloys 7050 and 7150 are amongst the highest strengths of Al-alloys owing to the high number density of precipitates such as  $\text{MgZn}_2$  which is evenly distributed throughout the Al matrix (Ringer, Hono et al. 1996; Andreatta, Terryn et al. 2004; Sha and Cerezo 2004; Birbilis and Buchheit 2005; Polmear 2006) in 5xxx alloys. The addition of Zn to Al-Mg alloys was reported to improve resistance against SCC (Unocic, Kobe et al. 2006) where a small amount of Zn added into AA5083 alloy was found to reduce the corrosion - reporting that Zn can promote the formation of Al-Mg-Zn ( $\tau$  phase) instead of  $\text{Al}_3\text{Mg}_2$  ( $\beta$  phase) the latter of which is responsible for stress corrosion cracking (Carroll, Gouma et al. 2000; Carroll, Gouma et al. 2001).

#### 3.1.5. Influence of iron

Iron is typically present as an impurity in all commercial Al alloys due to the production process of Al alloys. Unless specifically required for specialist applications, it is simply too expensive to remove all iron (even in aluminium destined for aerospace applications). Despite having a small fraction of the composition, iron is detrimental to corrosion due to its low solubility and hence ability to form constituent particles which are cathodic to the Al-matrix such as  $\text{Al}_3\text{Fe}$  (Nisancioglu 1990). Additionally, iron is capable of sustaining cathodic reactions more efficiently than Al (Galvele 1976; Szklarska-Smialowska 1999). In more complex alloys, Fe can also combine with other alloying elements such as Mn or Cu (in the latter case forming  $\text{Al}_7\text{Cu}_2\text{Fe}$ ), which are also a major issue for corrosion (Birbilis, Cavanaugh et al. 2006) since the combination of Fe and Cu provides even greater cathodic efficiency for such particles. Corrosion associated with such noble cathodic constituents/intermetallics leads to

an increase in local pH of the solution further enhancing anodic dissolution of the Al matrix adjacent to say,  $\text{Al}_3\text{Fe}$  (Seri 1994; Park, Paik et al. 1999; Birbilis and Buchheit 2005; Ambat, Davenport et al. 2006).

### 3.1.6. Influence of manganese

The addition of Mn is effective in reducing the pitting susceptibility of Al alloys particularly in the context of modifying Fe containing intermetallic particles (Nisancioglu 1990) (where Mn can substitute for Fe, rendering the resulting constituent particle somewhat less noble). The presence of Mn has been noted as reducing the concentration of Fe and reducing the degree of resultant corrosion (Koroleva, Thompson et al. 1999); owing to the formation of  $\text{Al}_6\text{MnFe}$  has a similar electrochemical potential with that of the Al matrix. However, it has also been noted that an excess of Mn can lead to an increase in the cathodic activity when beyond the solubility limit (solubility of Mn in Al is 1.25 wt%) – with constituents such as  $\text{Al}_6\text{Mn}$  readily forming (Liu and Cheng 2010). Generally however, the presence of Mn constituent particles are not as detrimental as particles rich in Fe or Cu (Birbilis and Buchheit 2005; Cavanaugh, Birbilis et al. 2007), which is evidenced by the reliable corrosion performance of 3xxx commercial Al alloy (Zamin 1981; Seri and Tagashira 1986; Tahani, Chaieb et al. 2003; Liu and Cheng 2011).

### 3.1.7. Influence of lithium

The addition of Li in Al alloys is efficient at significantly reducing alloy density whilst increasing strength – making it an obvious contender in the range of transport, namely aero, applications. Al-Li alloys are a rather specialised field that spans the past five decades, with descriptions originally in the 8xxx series compositional space (with principally Li rich compositions). Such so-called 1<sup>st</sup> generation Al-Li alloys were only used in specialised applications owing to their susceptibility to cracking. The cracking issue was later managed via new alloy compositions and thermomechanical processing (2<sup>nd</sup> generation Al-Li alloys), however until relatively recently Al-Li alloys were not so popular owing to relatively high corrosion rates and localised forms of corrosion propagation. Most recently, the 3<sup>rd</sup> generation of Al-Li alloys has gained significant attention and growing usage in commodity aerospace applications. These 3<sup>rd</sup> generation alloys are actually 2xxx series alloys, with less Li than Cu. These new 2xxx series alloys will be a significant alloy of the future, whilst still further research is required (from a corrosion perspective) to fully understand the performance, particularly as a function of thermomechanical treatment. Some abridged information regarding the role of Li upon corrosion is included here. In Li rich alloys, the formation of strengthening phase,  $\text{Al}_3\text{Li}$  which is dispersed homogeneously throughout the matrix, is responsible for the increase in strength (Lavernia and Grant 1987). It is however detrimental to corrosion as  $\text{Al}_3\text{Li}$  initially form along the grain boundaries. As Li is an active (i.e. less noble) element, this will localise dissolution to Li rich regions and therefore susceptibility to attack such as intergranular corrosion is high (Martin 1988). When Cu is also added in conjunction with Li (in alloys such as AA2090) the precipitation of phases such as  $T_1$  ( $\text{Al}_2\text{CuLi}$ ) occurs. There are two modes of attack associated with  $T_1$ , one of which  $T_1$  at the precipitate free

zone is dissolved forming small pits, while the other is when  $T_1$  undergo selective dissolution along with dissolution of the adjacent Al matrix leaving larger pits (Buis and Schijve 1992; Buchheit, Wall et al. 1995).

### 3.1.8. Influence of activating elements (i.e. Pb, Sn)

Lead (Pb) and tin (Sn) are usually present in low levels as trace elements (Gundersen, Aytaç et al. 2004; Premendra, Terryn et al. 2009). When present in trace amounts, their influence is minimal or negligible. When (by say, recycling or contamination) the levels rise above the solubility limits, the presence of Pb leads to segregation that results in Pb-rich film at the metal - oxide interface when the alloy is heat treated at elevated temperature (Sævik, Yu et al. 2005) causing the Al oxide film to destabilise particularly in the presence of chloride. The disruption of Al oxide film leads to an increase in anodic reaction rate which not only increases the pitting susceptibility, but can activate the entire surface. This process is called anodic activation, and has been well documented for a number of years by studies from the group of Nisancioglu (Keuon, Nordlien et al. 2003; Gundersen, Aytaç et al. 2004; Yu, Sævik et al. 2004; Yu, Sævik et al. 2005; Walmsley, Sævik et al. 2007; Jia, Graver et al. 2008; Graver, Pedersen et al. 2009; Anawati, Graver et al. 2010; Graver, van Helvoort et al. 2010; Anawati, Diplas et al. 2011). There have been some efforts to reduce the activation effect of Pb by addition of more noble alloying elements such as Cu in the hope that the addition of Cu may alter the surface potential - hence reducing the activation (Anawati, Diplas et al. 2011). A similar result was observed for the addition of Mg (Jia, Graver et al. 2008), however, such methods are not viable on the basis that the Pb interfering with the oxide is an effect in addition to any changes in the alloy potential. The presence of Sn along with Pb however reduces the dissolution rate when annealed at the maximum temperature of 600°C for an hour at which Sn is found to dissolve in the aluminium solid solution diluting the Sn concentration on the surface (Graver, Pedersen et al. 2009).

### 3.1.9. Influence of other element, including Zr, Cr, Sc, Ti, W and Sr

These elements are typically added independently in small amounts (i.e. <0.2 wt%) for the purpose of grain refinement, to reduce recrystallisation as well as minimising the effect of intermetallic compounds (Vetrano, Henager Jr et al. 1998). Elements such as Zr and Ti are able to form intermetallics at high temperatures in the Al melt, and persist as finely dispersed particles of  $Al_3Zr$  and  $Al_3Ti$  within the solidified matrix, which, based on their fine size (i.e.  $\ll 1 \mu m$ ), have a minimal impact on corrosion (Scully, Knight et al. 1993). Similarly with scandium (Sc) additions above the solubility limit the formation of  $Al_3Sc$  will occur, contributing to the strength and significantly reducing recrystallisation during thermomechanical processing (Cavanaugh, Birbilis et al. 2007). In general, and neglecting  $Al_3Fe$ , such dispersoids are based on the  $Al_3X$  system where X is Zr, Ti, Sc, Er, etc, and taking the form of fine insoluble dispersoids which are functional in grain inoculation and refinement. As such, there are specific alloying additions of Ti and Zr to high strength alloys such as AA7075 (Senkov, Bhat et al. 2005; Zou, Pan et al. 2007; He, Zhang et al. 2010).



Whilst not studied in detail, it has been posited that the ability to suppress recrystallisation leads to lower corrosion rates by avoiding the formation of high angle grain boundaries (Fang, Chen et al. 2009). Furthermore, there are also complex second and third order interactions between sparingly soluble elements that extend beyond the predictions of simple phase diagrams. An example is that the addition of Sr will impact intermetallics such as  $\text{Al}_5\text{FeSi}$ , making them smaller in both their size and volume fraction (Ashtari, Tezuka et al. 2003; Eidhed 2008). Such an effect has a role in corrosion by minimising the number of intermetallic sites. The purpose however of this section, is not to describe the metallurgy, as that has been done classically as far back as Mondolfo (Mondolfo 1971; Mondolfo and Barlock 1975), but to emphasise the microstructures direct impact on corrosion.

In common alloys prepared by conventional casting technologies, transition metals (TMs) such as W, Mo and Cr are not employed owing to their very low solubility limits. However it is important to note that when prepared in sputtered or thin film forms, such Al-TM alloys display the lowest corrosion rates of all the Al-alloys. Shaw successfully produced the alloys by sputter deposition and found that these elements increased the pitting potential and passivity of the alloys as well as inability to form second phase upon heat treatment (Shaw, Fritz et al. 1990; Shaw, Davis et al. 1991). The work of Frankel also showed promising results (Frankel, Russak et al. 1989; Frankel, Davenport et al. 1992; TAILLEART, Gauthier et al. 2009).

### 3.2. The role of microstructure on corrosion

In order to understand the corrosion performance of Al alloys, and following on from the previous section, an appreciation of the microstructure is vital. Alloying elements and thermomechanical processing play an important role in dictating the type of microstructure produced. For homogeneous alloys, such as pure Al or 5xxx series alloys, corrosion susceptibility is low due to lack of pre-existing microstructural attack sites. The main concern however is regarding heterogeneous alloys, particularly the higher strength Al alloys such as the 2xxx, 7xxx and heat-treatable 6xxx series, where microstructural heterogeneity is a necessity. The most common features of a microstructure are the intermetallic particles which are classified into precipitates (forming from nucleation and growth, nominally 1nm to 300nm in diameter), constituent particles (from insoluble or impurity elements, unable to redissolve, nominally a few microns, to a few tens of microns, in size) and dispersoids (nominally  $\ll 1$  micron in size) (Polmear 2006). Each of these features consists of different electrochemical characteristics (including their native electrochemical potential and the currents they can sustain at a given potential characteristic of the alloy which they populate) and act as the sites which dictate the severity of corrosion attack. Work on categorising such intermetallics in relation to corrosion is plentiful and now has been going on for several decades (Mazurkiewicz and Piotrowski 1983; Scully, Knight et al. 1993; Buchheit, Grant et al. 1997; Birbilis and Buchheit 2005; Eckermann, Suter et al. 2008; Goswami, Spanos et al. 2010; Boag, Hughes et al. 2011; Hughes, Boag et al. 2011). We make the distinction in this chapter that whilst such intermetallics are responsible for corrosion initiation steps, including pitting, we will not cover corrosion propagation in detail (i.e. stress corrosion, or intergranular corrosion) since they would require a dedicated chapter.

The knowledge of intermetallic chemistry and the electrochemistry allows a prediction of the mode of corrosion and the propensity of the attack (Cavanaugh, Buchheit et al. 2009). Theoretically, a more active particle (i.e. less noble) will become a local anode and consequently corrode while the more noble particles become cathodes (Szklańska-Smiałowska 1999). This is not always a true reflection of kinetics however, as reported by Birbilis where the capability of the element to sustain the cathodic reduction process can not be deduced by relative nobility as well (Birbilis and Buchheit 2005). As corrosion occurs upon Al alloys, particularly pitting and early damage accumulation, two types of corrosion mode are identified. In one mode of attack where the intermetallic is classified as a cathode, the surrounding matrix tends to corrode leaving a ring shape around the particle or also called trenching. There is still some uncertainty on whether or not the trench itself is a result of microgalvanic coupling alone, or if the major contributor is local pH elevation, however a good treatise of this topic was given in a multi-part series of papers by the group at Virginia (Ilevbare, Schneider et al. 2004; Schneider, Ilevbare et al. 2004; Schneider, Ilevbare et al. 2007). In some cases damage may propagate to the base of the particle and eventually lead to particle fall out (Buchheit, Grant et al. 1997). The other mode of attack is when the intermetallic acts as anode and matrix as cathode; whereby the intermetallic will corrode leaving a cavity on the surface. Finally, in some microstructurally complex systems with ternary and above alloying additions, another type of attack found to not follow the traditional way of determining anode and cathode is incongruent dissolution commonly found in 2xxx and 7xxx due to the presence of S phase ( $\text{Al}_2\text{CuMg}$ ) (Buchheit, Grant et al. 1997; Guillaumin and Mankowski 1998). This intermetallic contains Cu and Mg, whereby (Blanc, Lavelle et al. 1997; Buchheit, Martinez et al. 2000), S phase experiences selective dissolution of the highly active Mg hence leaving Cu remnants at the bottom of the pit (Buchheit, Grant et al. 1997; Büchler, Wataari et al. 2000) or redistributed near the particle site. Although the more detailed study of Boag et al. indicated that Al might be preferentially removed in the initial stages of attack on S-phase (first 2.5 minutes) as both Cu and Mg were observed to be present after Al dissolution at 5 minutes. This may have been due to a combination of the types of aluminium hydroxyl-chloro complexes that form and the partial switching of the areas of S-phase to Cu remnants where cathodic reactions lead to the formation of insoluble  $\text{Mg}(\text{OH})_2$  (Boag, Hughes et al. 2011). After 15 minutes the Mg is removed as well and no chloride was detected on these particles. The attack then continues with the dissolution of Al matrix (Buchheit, Grant et al. 1997; Guillaumin and Mankowski 1998). Localized attack of the intermetallic also influenced by the chloride content and pH of the electrolyte. Higher chloride content is widely reported to have higher pitting occurrence due to passive layer disruption of chloride ions (Seri 1994; Blanc, Lavelle et al. 1997; Ilevbare, Schneider et al. 2004) but this does not necessarily mean the pit will propagate deeper (Cavanaugh, Buchheit et al. 2010). There exists a dedicated monograph on this topic (Muster, Hughes et al. 2009). It has also been noted that the intermetallic  $\text{Mg}_2\text{Si}$  can undergo similar incongruent dissolution, whereby Si enrichment occurs at the expense of dissolving Mg (Birbilis and Buchheit 2005; Jain, 2006; Eckermann, Suter et al. 2008; Gupta, Sukiman et al. 2012).

The revelation of a large number of microstructure vs. corrosion micrographs will not be done herein, however if the readers are interested, a nice expose of such images exists in

Cavanaugh (Cavanaugh 2009). Instead, a demonstration is given here. Figure 6 shows the micron scale microstructure for 2024-T3 and 5083-H116 before and after corrosion exposure in 0.1M NaCl for 14 days. These relatively low magnification images do not reveal the precipitate structure in AA2024-T3, instead showing the coarse intermetallics that exist in the alloys. What is observed is that a higher intermetallic density gives more possible sites for localised attack. In the relatively widely studied 2024-T3 (Guillaumin and Mankowski 1998; Schmutz and Frankel 1998; Campestrini, van Westing et al. 2000; Leblanc and Frankel 2002; Boag, Hughes et al. 2009; Hughes, MacRae et al. 2010; Ralston, Biribilis et al. 2010; Boag, Hughes et al. 2011; Hughes, Boag et al. 2011; Zhou, Luo et al. 2012), pitting attack is associated with the Cu containing intermetallic such as S phase (coarse and precipitated) and the intermetallic density in AA2024-T3 is high, owing to the very large number of alloying elements which can leave the possibility of forming constituent particles based on Fe, or Si, or Cu, or Mn, etc. In contrast to AA2024, the alloy 5083-H116 with a smaller number of alloying elements, and Cu free, has a lower constituent number density. In addition to the Mg remaining in solid solution and reduces the susceptibility to localised attack (Vetrano, Williford et al. 1997; Aballe, Bethencourt et al. 2001; Yasakau, Zheludkevich et al. 2007).

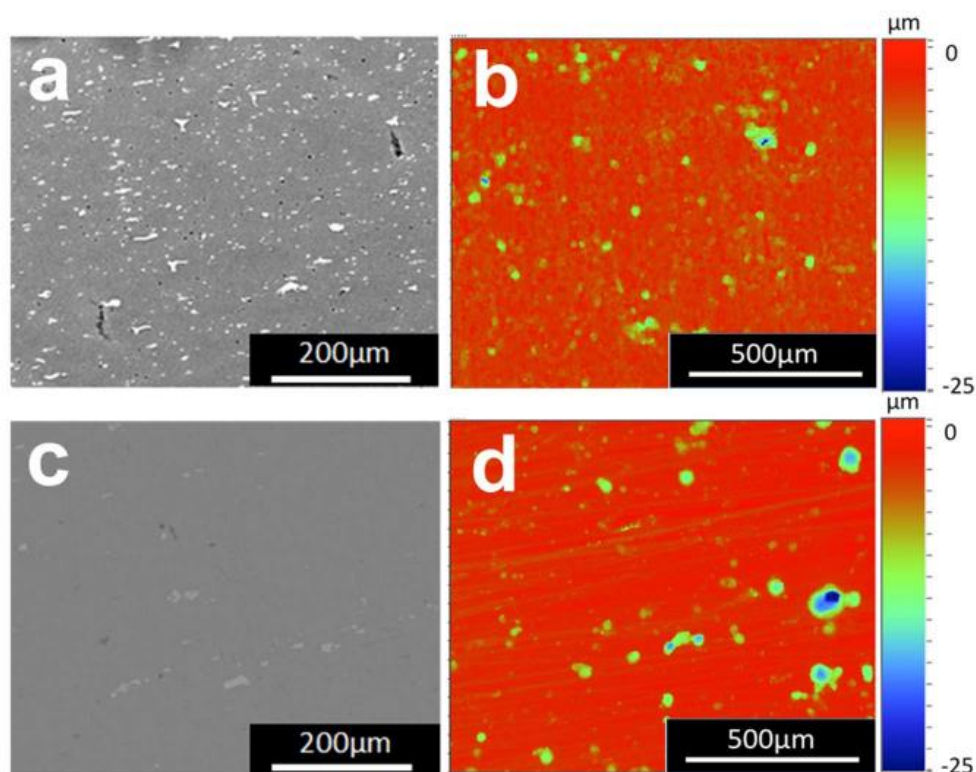


**Figure 6.** SEM images for AA2024-T3 and AA5083-H116 before exposure in (a) and (c) and after exposure in 0.1M NaCl for 14 days in (b) and (d). These are comparative images to show the extent of damage following immersion.

## 4. Corrosion protection

This section covers general approaches to protection of aluminium alloys in view of recent advances in the understanding of alloy microstructure. It includes an overview of pretreatment processes such as anodising, conversion coating and organic coatings (barrier and inhibitor combinations). It will examine recent advances in inhibitor design such as building in multifunctionality and touch upon self-healing coating systems. Approaches using multifunctionality can target anodic and cathodic reactions more effectively than using individual monofunctional inhibitors.

Standard metal finishing processes, which have been used for many years, are likely to continue to be used into the future unless they contain chemicals that are targeted for replacement such as chromium. The function of these coatings is primarily to provide better adhesion properties for paint coatings and a secondary role is to provide corrosion protection. The general approach for applying these coatings relies on metal finishing treatments (treatment prior to painting involving immersion in acidic and alkaline baths) with the objective of reducing the heterogeneous nature of the metal surface such as removing the NSDL and second phase particles (Muster 2009). This is achieved in multistep treatment processes for metal protection (Twite and Bierwagen 1998; Buchheit 2003; Muster 2009) as for instance:

- selective deoxidation (IM particle removal and surface etching);
- deposition or growth of a manufactured oxide via electrochemical (anodising) or chemical (conversion coating) means;
- use of an organic coating for specific applications, normally including a primer and a top-coat.

On aluminium, most anodised coating processes produce an outer oxide with a cellular structure on top of a thin barrier layer that provides some protection against corrosion. Inhibitors can be incorporated into the outer porous layer of the anodized layer during formation or as a seal after formation to offer some extra protection upon damage. Chromic acid anodizing is one of a number of processes that are available for electrochemical growth of surface protective oxides. More environmentally friendly alternatives to chromic acid anodizing such as sulfuric, sulfuric-boric, sulphuric-tartaric and phosphoric based processes have been available for a long time. There have been a number of recent advances in reducing the energy consumption of anodizing processes as well as improving coating properties. These advances are based on an improved understanding of the alloy microstructure described above and involve selective removal of second phase particles as part of the anodising process.

An alternative approach to anodizing is to precipitate a coating on a surface through chemical means called conversion coatings. For high strength Al-alloys such as 2xxx and 7xxx series chromate conversion coating (CrCC) is still the preferred process. Replacements for the toxic chromate-based conversion coatings include a range of treatments based on self-assembled monolayers, sol-gel chemistries, Ti/Z oxyfluorides, rare earth, cobalt, vanadates,

molybdates and permanganate processes (Twite and Bierwagen 1998; Buchheit 2003; Kendig and Buchheit 2003). These processes are widely developed for chemically pretreated surfaces that have nearly all the IM particles removed (by chemical pretreatment) and are not specifically designed to address electrochemical and compositional variations found for a heterogeneous surface such as when the IM phases are present. Work like that in (Buchheit and Birbilis 2010) depicting the reaction rate variation across the surface, however, opens an avenue to start designing inhibitors where the initial reaction rate distribution across a surface can be significantly reduced to limit the overall activity of the surface. In this context reaction of inhibitive phases with manufactured IM compounds as well as IM particles within the alloy have been studied for a number of systems (Juffs, Hughes et al. 2001; Juffs 2002; Juffs, Hughes et al. 2002; Birbilis, Buchheit et al. 2005; Scholes, Hughes et al. 2009).

Once the anodised or conversion coating is applied, the surface is ready to receive the organic coating. There are many different types of organic coatings, however because of the focus on 2xxx and 7xxx alloy used in the aerospace industry this section will only deal with that application area. The organic coating system usually consists of a primer and a topcoat. The primer is the main protective layer including corrosion inhibitors that can be released when corrosive species or water reach the metal. From the perspective of providing protection for the underlying aluminium alloy, the inhibitor needs to be available during a corrosion event at a concentration higher than the minimum concentration at which the inhibitor stops corrosion (critical concentration). While this sounds obvious, the critical inhibitor concentration needs to be maintained over many years for structures such as airframes, where maintenance may not be possible in parts of the aircraft because of poor access. The chromate systems itself provide continuous protection and repair to the surface for as long as the dose of chromate remains above the critical concentration. This mechanism of inhibitor release and metal protection is recognized as a self-healing mechanism, since the release of the active species recovers the protective layer on top of the metal.

The search for green inhibitors as replacements for chromate has been driven by legislative imperatives for a number of years. Needless to say, replacement inhibitors do not have the same intrinsic inhibitive power at low solubility as chromate. Thus solubility, inhibitive power and transport within the primer system (which consists of a number of inorganic phases as well as the epoxy) ultimately mean that finding a replacement for chromate is difficult. This means that alternatives must be present at higher concentration leading to the use of more soluble compounds and consequently encapsulation as a method of regulating the response to external or internal triggers emerges as a prospective way to achieve this objective.

Many current inhibitors are water soluble salts and thus ionic. Consequently, they exist as either anions or cation in solution and perform the single function of anodic or cathodic inhibition. So the simplest improvement to inhibitor design is to increase the functionality by finding compounds which play both a cationic and anionic inhibitive role. A large range of cations including Zn, Ca, and rare earths (Bohm, McMurray et al. 2001; Du, Damron et al. 2001; Kendig and Buchheit 2003; Taylor and Chambers 2008; Muster, Hughes et al. 2009) have been combined with either organic (Osborne, Blohowiak et al. 2001; Sinko 2001; Voevo-

din, Balbyshev et al. 2003; Khramov, Voevodin et al. 2004; Blin, Koutsoukos et al. 2007; Taylor and Chambers 2008; Muster, Hughes et al. 2009) or inorganic (oxyanions, carbonates, phosphates, phosphites, nitrates, nitrites, silicate (Bohm, McMurray et al. 2001; Sinko 2001; Blin, Koutsoukos et al. 2007; Taylor and Chambers 2008) compounds.

Anions with dual functionality, such as some of the transition metal oxyanions which are both oxidants and anions, have been investigated extensively. The oxidizing oxyanions or some organophosphates have some degree of bio-inhibition required for some applications. Substitution of different organophosphates into rare earth-based inhibitors provide versatility in designing inhibitors for specific applications (Birbilis, Buchheit et al. 2005; Hinton, Dubrulle et al. 2006; Ho, Brack et al. 2006; Blin, Koutsoukos et al. 2007; Markley, Forsyth et al. 2007; Markley, Hughes et al. 2007; Forsyth, Markley et al. 2008; Deacon, Forsyth et al. 2009; Scholes, Hughes et al. 2009). Thus Ce(di-butyl phosphate)<sub>3</sub> is a good inhibitor and relatively “green” whereas Ce(di-phenyl phosphate)<sub>3</sub> is also a good inhibitor, but the diphenyl phosphate also has strong bio-inhibition characteristics (García 2011). However, good bio-inhibition usually means that there are increased environmental and health risks. Obviously the number of cathodic and anodic inhibitors means that there are an enormous number of possible combinations, particularly if ternary and quaternary combinations are considered. Hence high-throughput techniques are being used to assess new inhibitor.

As pointed out above, the kinetics of inhibitor release are of the utmost importance since the inhibitor should be available at levels above the critical inhibitor concentration. Optimization of the release kinetics by novel delivery systems becomes integral to incorporation of new inhibitors.

There are a number of different mechanisms investigated for release of healing agents or corrosion inhibitors which can be incorporated into organic coatings. Both mechanical damage and water are triggers for inhibitor release. In the former case mechanical damage breaks capsules containing water soluble inhibitors. In the latter case water dissolves inhibitor directly incorporated in the primer. Droplet formation within defects such as scratches means that the inhibitor is only released when required i.e., when the defect is moist (Furman, Scholes et al. 2006). There is some evidence to suggest that initial high release of inhibitors may be facilitated through atmospheric exposure of the intact paint where penetration of water into the film “prepares” the inhibitor, probably via surface hydrolysis reactions, within the paint, for diffusion and release into the defect (Joshua Du, Damron et al. 2001; Furman, Scholes et al. 2006; Scholes, Furman et al. 2006; Souto, González-García et al. 2010). The presence of water in the film allows soluble inhibitor species to be released into the paint system and diffuse to the metal/coating interface to provide in-situ corrosion prevention or repair called pre-emptive healing (Zin, Howard et al. 1998; Osborne, Blohowiak et al. 2001; Mardel, Garcia et al. 2011). Thus it has been demonstrated that water can trigger cerium dibutylphosphate (Ce(dbp)<sub>3</sub>) release into an epoxy matrix resulting in improved adhesion and resistance to filiform corrosion attack through interfacial modification (Mardel, Garcia et al. 2011)

In terms of delivery systems, hard capsules, which have been used in polymer healing (Dry 1996; White, Sottos et al. 2001; Mookhoek, Mayo et al. 2010) need to be smaller for paint systems particularly in the aerospace industry where coatings are typically 20  $\mu\text{m}$  or less (Yin, Rong et al. 2007; Fischer 2010; Hughes, Coles et al. 2010; Mookhoek, Mayo et al. 2010). In polymer applications, capsules up to a few hundred microns can be accommodated (Yin, Rong et al. 2007; Wu, Meure et al. 2008; Tedim, Poznyak et al. 2010). The concept of encapsulation has already been successfully applied to protective organic coatings under different concepts: i) liquids filling completely the void created by the damage by adopting a bi-component systems where one component is encapsulated and the other distributed in the matrix (Cho, White et al. 2009), or single based components with water reactive oils like linseed and tung oils (Suryanarayana, Rao et al. 2008; Samadzadeh, Boura et al. 2010) and ii) liquids (i.e. silyl esters) forming a hydrophobic and highly adhesive layer covering the metallic surface by reaction with the underlying metal and the humidity in air (García, Fischer et al. 2011). One adaption for capsules is to increase the volume of self-healing material by manufacturing rods instead of spheres. Rods with the same cross-sections as spheres can deliver larger volumes of material (Bon, Mookhoek et al. 2007; Mookhoek, Fischer et al. 2009). For inhibitors, their role is to prevent a surface reaction (corrosion) and therefore, the volume of material required is much smaller than that required to actually fill the defect. Consequently, there has been considerable effort looking at “nano-containers” (Voevodin, Balbyshev et al. 2003; Raps, Hack et al. 2009; Tedim, Poznyak et al. 2010).

Water is the most obvious trigger since it can permeate most polymers. pH variations are more specific and respond to the pH excursions that occur in corrosion reactions and by an understanding reactions that occur at different sites in the alloy microstructure. The presence of chloride ions (and other anions) within the coating can be used as specific triggers for the release of corrosion inhibitors and uptake of corrodents using anion exchange materials, such as layered double hydroxides (e.g. hydrotalcites) (Tedim, Poznyak et al. 2010) (Bohm, McMurray et al. 2001; Buchheit, Guan et al. 2003; Williams and McMurray 2003; Zheludkevich, Salvado et al. 2005; Mahajanarn and Buchheit 2008). In this context hydrotalcites have been loaded with vanadate, chromate, nitrate and carbonate which exchange for chloride ions and prevent interfacial damage (Bohm, McMurray et al. 2001; Williams and McMurray 2003; Mahajanarn and Buchheit 2008). The incorporation of Mg particles into paint act as sacrificial anodes to protect Al alloys and steels (Battocchi, Simoes et al. 2006).

## 5. Recent advances in aspects related to corrosion of aluminium alloys

The search for new multifunctional inhibitors has led to the development of high throughput and combinatorial assessment of new combination of inhibitors. These include multielectrode techniques, and high throughput versions of standard corrosion tests. A range of new electrochemical techniques including AC/DC/AC, SVET, LEIS, SECM and SIET will also be described.

Since corrosion of aluminium alloys tends to be dominated by electrochemical processes, most of the techniques employed for the evaluation of corrosion and protection are based on electrochemical approaches. Furthermore, combining electrochemical techniques with other microscopic, analytical and spectroscopic techniques enables the identification of corrosion products in solution (such as inductive coupled plasma (ICP) and UV-Vis). This combination provides an even broader mechanistic understanding of the level of corrosion and/or corrosion protection.

The increasing number of corrosion inhibitor alternatives to chromates has boosted interest in developing high-throughput techniques and combinatorial assessment of new corrosion inhibitors in aqueous solution. At the same time, the traditional techniques (accelerated or not) employed in the evaluation of the performance of organic coatings require long evaluation periods and are relatively expensive to run, and only offer qualitative or semi-quantitative information at best (e.g. salt fog spray tests). For these reasons, new accelerated techniques for the evaluation of coating performance that offer quantitative results are needed.

Figure 7 shows a simplified flowchart for the formulation of anticorrosive (organic) coatings. The chart includes some of the most common techniques employed in corrosion inhibitor and coating performance evaluation. In the figure, the parallel and complex line of the development of the polymeric matrix (i.e. organic coating) is not included, but awareness of its existence is important, since factors such as the corrosion inhibitor/coating matrix compatibility should be taken into account. For the development of anticorrosive organic coatings, several steps are proposed:

**a. Formulation of inhibitors:**

The number of corrosion inhibitor candidates is virtually unlimited, and is motivated by the urgent need to replace chromate based inhibitors by environmentally friendly and non-toxic ones, as well as the development of new concepts such as self-healing and synergies between anodic and cathodic inhibitors which open up the broad range of possibilities of organic chemistry. One example of the complexity of the introduction of organic compounds as corrosion inhibitors is the effect that the position of certain groups in a cyclic organic compound can have in the corrosion protection efficiency (Harvey, Hardin et al. 2011).

**b. Evaluation in aqueous solution:**

Once the inhibitors have been formulated, they can be tested by means of traditional aqueous solution tests such as electrochemical impedance spectroscopy (EIS), potentiodynamic polarisation (PP), immersion tests and weight loss/gain. Also local electrochemical techniques (see point 4-evaluation of organic coatings) give very important information of the mechanisms of corrosion protection offered by the different species in solution. Since traditional techniques require long periods of time and a large number of samples, the introduction of high-throughput techniques as a preceding step is important in order to reduce the number of inhibitors that enter further evaluation processes using traditional aqueous solution tests. It is necessary to highlight that high-throughput techniques are not aimed at re-



placing traditional tests but at complementing them in order to reduce cost and time in the corrosion inhibitor selection process. Some examples are: single metal, multielectrode array (Chambers, Taylor et al. 2005; Chambers and Taylor 2007), microchannels (White, Hughes et al. 2009) and multi metal multielectrode (Muster, Hughes et al. 2009; García, Muster et al. 2010; Kallip, Bastos et al. 2010).

**c. Introduction into an organic matrix:**

The introduction of pigments into organic coatings adds some extra difficulties to the whole process, leading to a lot of extra research to avoid undesirable reactions between the polymer matrix and the inhibitors. Some of the parameters to take into account are the ratio between the pigment volume concentration (PVC) and the critical pigment volume concentration (CPVC), the possible side reactions between the polymer and the pigment, with consequences in parameters like the barrier properties, gloss, active corrosion protection, and adhesion amongst others. At the same time, parameters such as contaminant reduction and parameters related to the polymeric matrix itself (such as adhesion and the glass transition temperature ( $T_g$ )) should be considered. In any case, once the pigments have been introduced into the organic coating, the coating's performance has to be tested for protection efficiency and if results are promising, then start the optimization process.

**d. Evaluation of the performance of organic coatings:**

As in the case of aqueous solution tests for evaluation of corrosion inhibitors, the introduction of accelerated tests to evaluate coatings performance is necessary to reduce the amount of time and number of samples that move into traditional assessment. Several techniques have been proposed in this direction, such as the technique AC/DC/AC (Hollaender 1997; Bethencourt, Botana et al. 2004; Rodriguez, Gracenea et al. 2004; Garcia and Suay 2006; Garcia and Suay 2006) (García, Rodríguez et al. 2007; Garcia and Suay 2007) (Garcia and Suay 2007; García and Suay 2007; García and Suay 2009), (Poelman, Olivier et al. 2005; Allahar, Bierwagen et al. 2010; Allahar, Wang et al. 2010), and thermal cycling (Bierwagen, He et al. 2000). Also new concepts like the use of flow induced degradation (Wang 2009) are interesting for developing accelerated testing techniques.

**e. Optimisation:**

Before entering the pre-commercialization phase, the final step of anticorrosive coatings formulation is the optimization, which is the improvement of the system by modifying pigments concentration, type, and delivery systems to improve and extend the service lifetime protection and compatibility with the matrix. This step is iterative as shown in Figure 7. The whole process from conception to commercialization of the system can take several years.

Due to the impossibility to cover the broad amount of existing (new) high-throughput techniques for selection of corrosion inhibitors for aluminium alloys and accelerated tests for evaluation of protective organic coatings on aluminium alloys, we focus on two electrochemical techniques that have attracted a broad interest most recently due to their high potential and relatively well understood evaluation procedure.

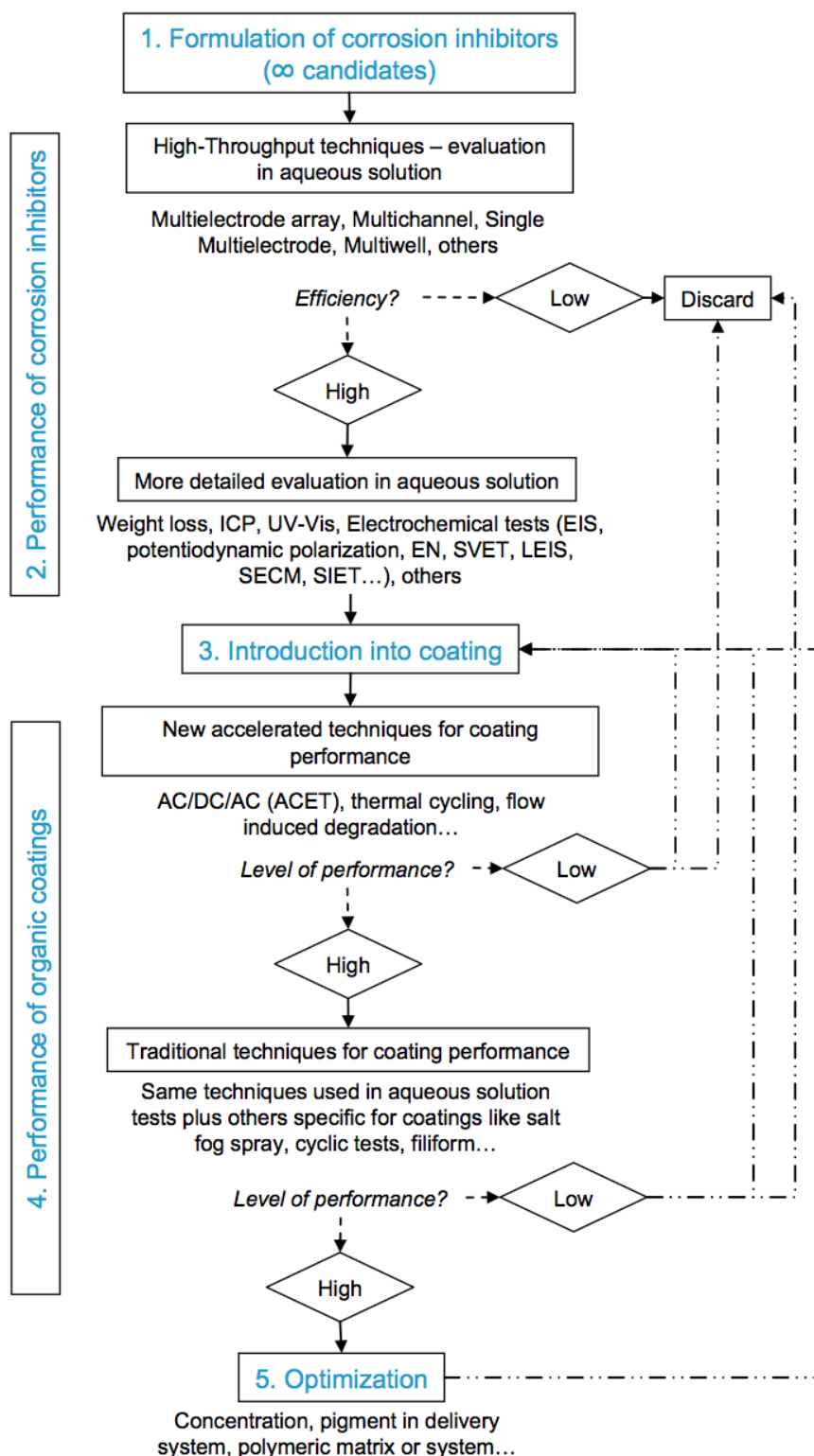


**Figure 7.** Simplified flowchart for anticorrosive coatings development departing from the inhibitor design or formula-  
 tion.

### 5.1. High throughput assessment

In terms of high-throughput techniques, those based on electrochemical approaches are of most interest, since their measurement principles are closely related to familiar research techniques such as Electrochemical Impedance Spectroscopy (EIS) and potentiodynamic polarisation (PP), while at the same time offer quantitative information about the corrosion and corrosion protection mechanisms.

Chambers and Taylor (Chambers, Taylor et al. 2005; Chambers and Taylor 2007) first presented the use of multi-electrode arrays for rapid screening of corrosion inhibitors in different concentrations and pHs, putting identical pairs of AA2024-T3 wires into a large number of separate reaction cells containing different inhibitive solutions and applying a 100mV potential between the two wires in each cell (Figure 8(a)). The current between both electrodes was used to determine the polarisation resistance. With this set-up they were able to evaluate for one metal many different combinations of inhibitors and their synergistic behavior, while at the same time showing its possible application for evaluating the influence of the pH on inhibitors' efficiency.

Based on the work of Taylor and Chambers, Muster et al. (Muster, Hughes et al. 2009) proposed a variation of the method using a combination of different pairs of metals assembled together (Figure 8(b)) to form what was presented as a multielectrode (ME). The basic idea of this ME was to test a combination of nine pairs (or as many as are interesting) of different metals in the same electrode configuration connected by means of a multiplexer to a potentiostat/galvanostat. Measurements consist of applying 100mV between a selected pair of the same metals within the ME and measure the current flow between them, repeating afterwards the same procedure for the other metal pairs. This set up was employed to rapidly evaluate, without removing the ME from the solution, the concentration range at which a particular inhibitor or combination of inhibitors were offering corrosion protection. Hence, the setup allowed the determination of optimal metal-inhibitor combinations, while significantly reducing the evaluation time with respect to conventional PP tests, without the need of a reference electrode, which simplifies the experimental setup.

In a second paper (Garcia, Muster et al. 2010), the authors studied the effect of the pH and inhibitor type on the correlation between the ME and PP for AA2024-T3. The findings were promising due to the high level of correlation between the ME and traditional techniques, although some discrepancies were found for corrosion inhibitors that can speciate or precipitate at certain pHs. Nevertheless, the non-correlation was assumed to be dependent on the type of corrosion inhibitors and not due to conceptual or experimental mismatching between techniques.

A second concern with the ME was the possibility of cross-contamination due to the presence of several metals in one solution. Garcia et al. (Garcia, Muster et al. 2010) also addressed this problem studying the effect of cross-contamination for the AA2024-T3 wires within the ME. This study showed that if there was cross-contamination then it was not significant enough to influence the results. Despite these results, some more studies should be performed with the ME to check cross-contaminations for other metals such as AA7075-T6

which could be more susceptible to copper plating coming from other metals such as AA2024-T3.

The results obtained so far with multielectrodes (multielectrode array and ME) are very promising and relatively extended information can be found in literature. Nevertheless, more studies and data treatment simplification need to be performed to completely validate these techniques and lead them to an industrial application level.

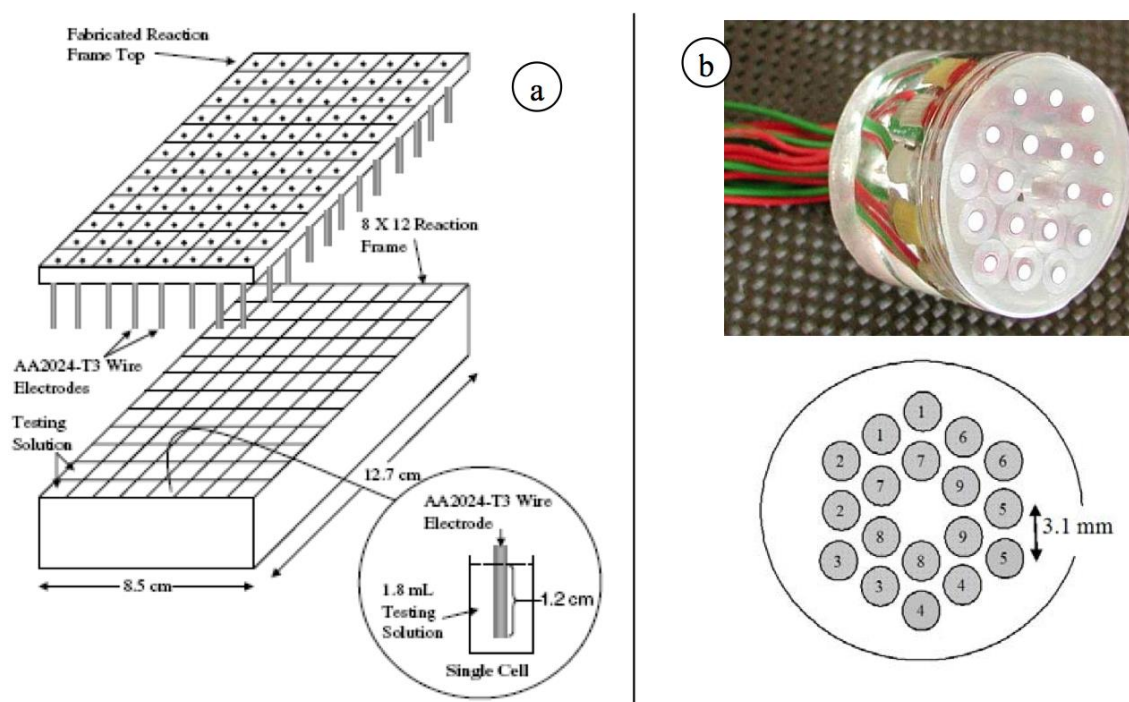


**Figure 8.** a) single metal multiarray (Chambers and Taylor 2007); b) multimetal multielectrode (Muster, Hughes et al. 2009)

## 5.2. AC/DC/AC accelerated technique for coating evaluation

This technique has already reached its maturity and is actually employed at an industrial level under the name of accelerated electrochemical technique (ACET) (Medco). Although the industrial application differs from the research technique (AC/DC/AC), the evaluation and testing are conceptually similar. The early version of the AC/DC/AC technique was performed for the packaging industry (Hollaender 1997). The accelerated technique developed by Hollaender (named AC/DC/AC) was based on the use of temporary stresses to accelerate degradation, and consisted of a first EIS test (AC) to evaluate the initial state of the coating, followed by a cathodic polarisation (DC) and a new EIS (AC) to detect the degradation of the lacquer.

The work initiated by Hollaender was further developed by Suay, Garcia and Rodriguez who successfully applied a modified version of the AC/DC/AC technique to evaluate the performance of organic coatings for carbon steel protection and compared the obtained re-

sults with EIS, salt-fog spray, and cyclic tests. The technique was then tested for liquid paints (Bethencourt, Botana et al. 2004; Rodríguez, Gracenea et al. 2004), powder coatings (García and Suay 2006; García and Suay 2006; García and Suay 2007; García and Suay 2007) and cathaphoretic paints to optimize parameters such as cathaphoretic potential and curing time (Poelman, Olivier et al. 2005; García, Rodríguez et al. 2007; García and Suay 2007; García and Suay 2009). The new version of the technique included a crucial step: the relaxation of potentials (open circuit potential relaxation) after the application of each cathodic polarisation. Furthermore, the potentials applied during the cathodic polarisation depended on the type of coating that was studied, although  $-4\text{V}$  for 20 minutes was preferred. Figure 9(a) shows a schematic of the AC/DC/AC technique procedure, including the relaxation step proposed by Garcia and Suay. The AC/DC/AC cycle is repeated 6 times (6 cycles) leading to a testing time per sample of around 24 hours, which is a significant improvement when compared to traditional EIS and salt-fog tests which require weeks or months. Nevertheless, depending on the quality of the coatings the number of cycles could be increased and the relaxation time reduced or extended.

The cathodic polarisation aims to degrade the coating and coating-metal interface (e.g. pore formation and delamination) due to hydrogen and  $\text{OH}^-$  production. If the coating is good then it has a higher number of cycles to degrade and the effects in the impedance and potentials relaxation are less pronounced, while a lower quality coating will display a faster degradation. An example of these effects compared to traditional EIS and salt-fog spray is presented by Garcia et al. (García and Suay 2009)

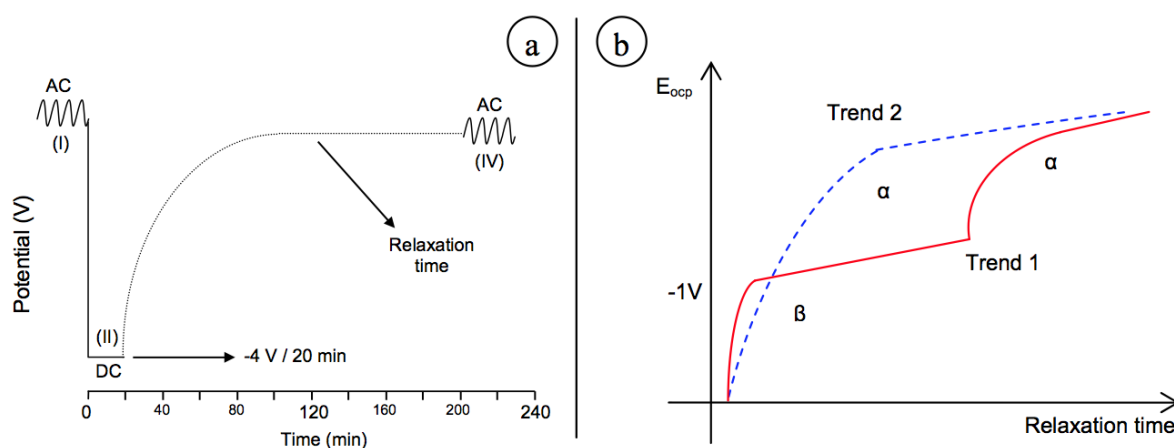


**Figure 9.** a) AC/DC/AC testing scheme (García and Suay 2009); b) Trends in relaxation of potentials.

Apart from the EIS spectral evolution with cycles, for which a higher drop of impedance is related to higher degradation, the evolution of the open circuit potential after polarisation (relaxation of potentials with time) provides extra crucial information about the degradation of the systems under study (García and Suay 2006). When the cathodic polarisation finishes, the potential of the system relaxes leading to two types of trends depending on the quality of the film (Figure 9(b)):

- a. Strongly degraded systems (Trend 1, Figure 9(b)), show two time relaxations of the potential, namely  $\alpha$  and  $\beta$ . The first relaxation in time ( $\beta$ ) is related to the end of the cathodic reactions that took place at the metallic surface. This relaxation is observed as a quick relaxation around  $-1V$  (with small variations depending on the system). The second relaxation ( $\alpha$ ), which occurs later in time, corresponds to ions and electrolyte leaving the coating. The relaxation ( $\beta$ ) could not be detected in all cases due to extremely long relaxation times, although if enough time was allowed this relaxation was then detected, supporting the idea of the two relaxation processes (García and Suay 2009)
- b. Less degraded systems (Trend 2, Figure 9(b)), only show relaxation  $\alpha$  which is detected at relatively short times of relaxation. This relaxation will take place at longer times as ions and electrolyte penetrate deeper into the film. More recently, Allahar et al. (Allahar, Wang et al. 2009; Allahar, Upadhyay et al. 2010; Wang, Battocchi et al. 2010) have performed an extensive study on the understanding of the AC/DC/AC technique and its principles, leading to a broader understanding of the relaxation of potentials and supporting previous theories, while at the same time further validating the technique.

In this section we have highlighted the complexity of the selection of corrosion inhibitors and anticorrosive coatings formulation leading to the design and validation of high-throughput and accelerated techniques, which at a certain stage can become commercial techniques. The interest in developing new techniques and understanding those already existing is indeed growing in recent years due to the need of developing environmentally friendly and non-toxic systems.

### 5.3. Staircase impedance

Staircase potenti-electrochemical impedance spectroscopy (SPEIS) is based on EIS, nowadays common for investigating electrochemical and corrosion system. The basis of EIS is by measuring impedance over a range of frequency and the data obtained is expressed graphically in Bode or Nyquist plot format. As for SPEIS, it is designed for impedance measurements over a range of frequency as well as over a range of voltages (similar to the signal sequence used for Mott-Schottky analysis (Barsoukov and Macdonald 2005; Orazem and Tribollet 2008)). The potential range is divided into several potential steps and each step contains a DC relaxation period for a given rest time ( $T_R$ ) to allow the current to stabilize; subsequently followed by an EIS test (Zhou, Birbilis et al. 2010). During the DC potential signal, the current at each potential is also recorded. Figure 10 demonstrates this process.

This method is used to assess the kinetic stability of electrochemical reactions over a range of potentials and pH, which gives a rather detailed insight into the corrosion behavior. In SPEIS however, by setting a range of voltage allows more details observation of how the system response at a particular voltage or 'step', even though it is not sufficient to explain the kinetic processes occurring. As reported by Zhou, SPEIS is able to illustrate the effect of pH and potential on the corrosion kinetics with clarity and able to obtain more information beyond the Pourbaix diagram (Zhou, Birbilis et al. 2010), including structural effects such as alloying, etc.

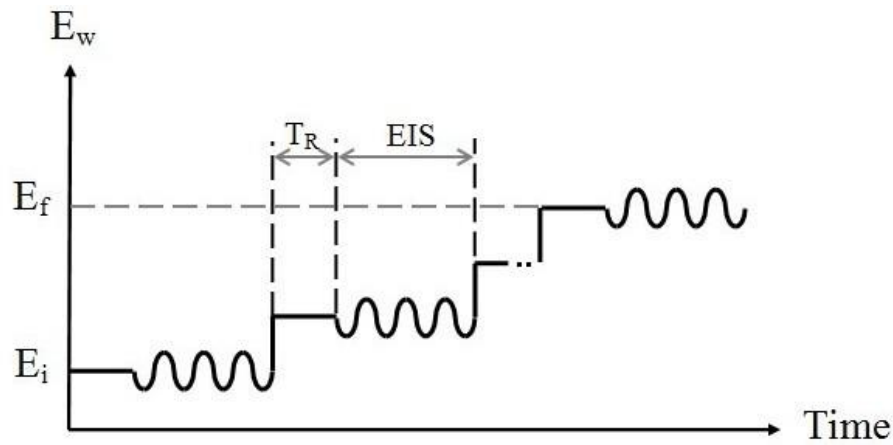


**Figure 10.** Illustration of polarizing signal during SPEIS

#### 5.4. Potentiostatic transients for determination of metastable and stable pitting

Since pitting is the most common type of corrosion in Al alloys, researchers commonly default to the investigation of pitting potential,  $E_{\text{pit}}$  as a means for evaluating the corrosion performance. A more noble  $E_{\text{pit}}$  is often accepted as better resistance to pitting. However, there are some significant limitations in such simple assessments (Gupta, Sukiman et al. 2012). For example, the pitting potential yields no information regarding how many pits form or how large pits may be. Additionally, the environment plays a key role in the severity of pitting damage (i.e. pit depth, pit size) (Cavanaugh 2009).

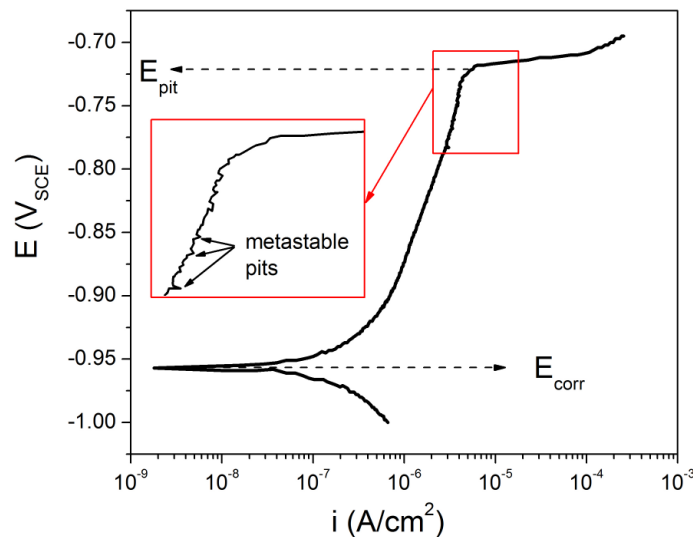


**Figure 11.** Polarisation curve indicating the corrosion potential  $E_{\text{corr}}$  and  $E_{\text{pit}}$  with metastable pits region prior to  $E_{\text{pit}}$  highlighted in the inset (adapted from (Cavanaugh 2009))



Pits that form at pitting potential are known as stable pits. However, at potentials slightly below pits stabilization (at  $E_{\text{pit}}$ ), pitting like events occur that are known as metastable pit (small surges of current that repassivate). Wu suggested that individual metastable pitting events influence subsequent events (Wu, Scully et al. 1997), and such events are readily observed in Al-alloys. Figure 11 indicates the metastable pitting region in a typical potentiodynamic polarisation curve, where  $E_{\text{pit}}$  is also depicted.

In order to measure metastable pitting, a potentiostatic value is selected at a potential just below  $E_{\text{pit}}$  where the metastable pitting events are the most frequent (while still in the passive region) (Cavanaugh 2009). Metastable pitting events are measured by counting the current fluctuations when an alloy is held potentiostatically for a period of time. The transient currents as shown in Figure 12 depend on the nucleation, growth and repassivation of the metastable pits.

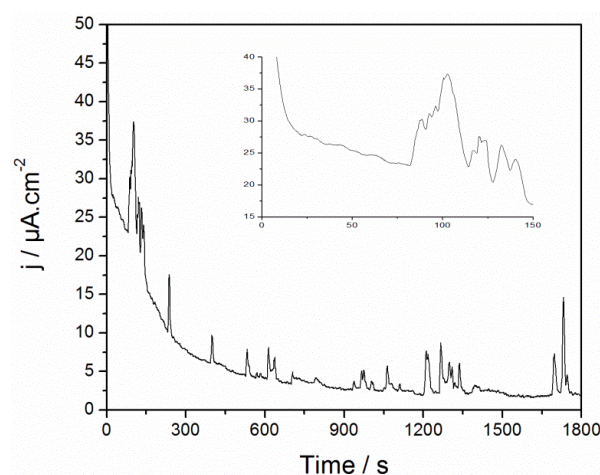


**Figure 12.** Current transient for AA5083-H116 obtained at 25mV below  $E_{\text{pit}}$ . Inset shows a zoom of a region of interest that represents the typical transient features (adapted from (Gupta, Sukiman et al. 2012))

The number of metastable pitting is expected to be proportional to the amount of pits formed (Williams, Stewart et al. 1994; Cavanaugh, Birbilis et al. 2012). This is confirmed by (Gupta, Sukiman et al. 2012), where the numbers of metastable pitting from potentiostatic test for various commercial Al alloys correlate with stable pitting tested in a long term immersion test. Ilevbare and Burstein however, stated that multiple metastable events may correspond to only one pit site (Burstein, Liu et al. 2004; Ilevbare, Schneider et al. 2004; Sasaki and Isaacs 2004; Trueman 2005; Speckert and Burstein 2011), however most of such analyses were not performed on Al-alloys. Since there are few studies on metastable pitting of Al alloy, the associated theory and principles will evolve in the coming decade. It is however obvious that metastable pitting analysis can be used to compare the pitting susceptibility between different environments [Cavanaugh 2009] and alloy systems [Gupta, Sukiman et al. 2012] more effectively than an examination of ( $E_{\text{pit}}$ ) alone.



Aside from the methods described above, the use of modern tests does not exclude the use of other traditional tests that require longer testing times and samples such as salt fog spray tests, weight determination, outdoor exposure, or cyclic salt fog-climatic chamber tests, but they aim at providing unique insights that are relevant to specific problems at hand such as pitting germination and inhibitor selection.

It is also worth mentioning here, the great interest that local electrochemical techniques have recently attracted to evaluate the corrosion protection offered when the coatings are damaged (i.e. self-healing). These techniques have been successfully applied to several conceptually different self-healing systems like scanning vibrating electrode technique (SVET) for encapsulated agents (Hughes, Cole et al. 2010; García, Fischer et al. 2011), scanning electrochemical microscope (SECM) for shape memory polymers, selective ion electrode technique (SIET) to evaluate activity of metals (Lamaka, Karavai et al. 2008), and local electrochemical impedance spectroscopy (LEIS) for evaluation of corrosion protection by inhibitor release from coatings (Jorcin, Aragon et al. 2006)

## 6. Summary and challenges

This chapter has given an abridged and focused treatment of the corrosion behavior of Al alloys on the basis of chemistry, microstructure and environment. Understanding these parameters is crucial in deployment of Al-alloys, but also in the development of more durable Al-alloys. It is obvious that alloying (i.e. chemistry) and microstructure dictates not only mechanical strength – but also corrosion performance. In this chapter we stopped short of discussing corrosion propagation such as intergranular corrosion, exfoliation corrosion and stress corrosion cracking – given space constraints, however such topics (along with hydrogen embrittlement) remain critical for structural alloy deployment.

In regards to corrosion protection, we have attempted to cover some modern developments and present some new techniques to assess the corrosion behavior designed to meet the more complicated and challenging requirements of inhibitor selection / chromate replacement. The information gathered from these techniques is beneficial for future protection and alloy development.

Looking to the future, the current strategy to increase strength by precipitation hardening of a crystalline matrix may no longer be feasible if an alloy with strength higher than 1000MPa is required. Methods to meet this threshold include (the un-upscalable) severe plastic deformation method such as High Pressure Torsion (Liddicoat, Liao et al. 2010) – however the thermal stability of these structures is low. Alternatively the strength of Al based metals could be significantly enhanced (up to 1500MPa) when rapidly quenched to form amorphous alloys (Masumoto 1994; Inoue and Takeuchi 2004; Li, Li et al. 2009; Yang, Yao et al. 2009). Such alloys typically use transition metals such as Zr, Ti, Nb, La, etc (Inoue, Gook et al. 1995; Zawrah and Shaw 2003; Rizzi and Battezzati 2004; Samanta, Manna et al. 2007; Huang, Li et al. 2008; Li, Li et al. 2009), however, again – the stability of such structures is unknown, and the ability form large components is also a challenge. From a corrosion point

of view, amorphous Al-alloys appear promising (Manna, Chattopadhyay et al. 2004; Lucente and Scully 2007; Lucente and Scully 2008; Tailleart, Huang et al. 2012) with the corrosion behavior of such alloys is not widely explored therefore leaves a lot of opportunities for new discoveries.

## Author details

N. L. Sukiman<sup>1,6</sup>, X. Zhou<sup>1</sup>, N. Birbilis<sup>1</sup>, A.E. Hughes<sup>2</sup>, J. M. C. Mol<sup>3</sup>, S. J. Garcia<sup>4</sup>, X. Zhou<sup>5</sup> and G. E. Thompson<sup>5</sup>

1 Department of Materials Engineering, Monash University, Clayton, Australia

2 CSIRO Materials Science and Technology, Melbourne, Australia

3 TU Delft, Materials Department, Delft, Netherlands

4 TU Delft, Aerospace Engineering, Delft, Netherlands

5 School of Materials, The University of Manchester, Manchester, United Kingdom

6 Department of Mechanical Engineering, University of Malaya, Kuala Lumpur, Malaysia

## References

- [1] Aballe, A., M. Bethencourt, et al. (2001). "Localized alkaline corrosion of alloy AA5083 in neutral 3.5% NaCl solution." *Corrosion Science* 43(9): 1657-1674.
- [2] Allahar, K. N., V. Upadhyay, et al. (2010). "Characterizing the relaxation of the open-circuit potential during an AC-DC-AC accelerated test." *Corrosion* 66(9): 0950011-09500111.
- [3] Allahar, K. N., D. Wang, et al. (2009). Real time monitoring of an air force topcoat/mg-rich primer system in b117 exposure by -embedded electrodes.
- [4] Ambat, R., A. J. Davenport, et al. (2006). "Effect of iron-containing intermetallic particles on the corrosion behaviour of aluminium." *Corrosion Science* 48(11): 3455-3471.
- [5] Ambat, R. and E. S. Dwarakadasa (1992). "The Influence of PH on the Corrosion of Medium Strength Aerospace Alloy-8090, Alloy-2091 And Alloy-2014." *Corrosion Science* 33(5): 681-690.
- [6] Anawati, S. Diplas, et al. (2011). "Effect of copper on anodic activity of aluminum-lead model alloy in chloride solution." *Journal of The Electrochemical Society* 158(5): C158-C163.

- [7] Anawati, S. Diplas, et al. (2011). "Surface Characterization of Heat Treated AlPbCu Model Alloys." *Journal of The Electrochemical Society* 158(6): C178-C184.
- [8] Anawati, B. Graver, et al. (2010). "Multilayer corrosion of aluminum activated by lead." *Journal of The Electrochemical Society* 157(10): C313-C320.
- [9] Andreatta, F., H. Terry, et al. (2004). "Corrosion behaviour of different tempers of AA7075 aluminium alloy." *Electrochimica Acta* 49(17-18): 2851-2862.
- [10] Ashtari, P., H. Tezuka, et al. (2003). "Influence of Sr and Mn additions on intermetallic compound morphologies in Al-Si-Cu-Fe cast alloys." *Materials Transactions* 44(12): 2611-2616.
- [11] Baer, D. R., C. F. Windisch, et al. (2000). "Influence of Mg on the corrosion of Al." *Journal of Vacuum Science & Technology a-Vacuum Surfaces and Films* 18(1): 131-136.
- [12] Barsoukov, E. and J. R. Macdonald (2005). *Solid State Devices, in Impedance spectroscopy: theory, experiment, and applications*, Wiley-Interscience, Inc.
- [13] Battocchi, D., A. M. Simoes, et al. (2006). "Comparison of testing solutions on the protection of Al-alloys using a Mg-rich primer." *Corrosion Science* 48(8): 2226-2240.
- [14] Bethencourt, M., F. J. Botana, et al. (2004). "Lifetime prediction of waterborne acrylic paints with the AC-DC-AC method." *Progress in Organic Coatings* 49(3): 275-281.
- [15] Birbilis, N. and R. G. Buchheit (2005). "Electrochemical Characteristics of Intermetallic Phases in Aluminum Alloys." *Journal of The Electrochemical Society* 152(4): B140.
- [16] Birbilis, N., R. G. Buchheit, et al. (2005). "Inhibition of AA2024-T3 on a phase-by-phase basis using an environmentally benign inhibitor, cerium dibutyl phosphate." *Electrochemical and Solid State Letters* 8(11): C180-C183.
- [17] Birbilis, N., M. K. Cavanaugh, et al. (2006). "Electrochemical behavior and localized corrosion associated with Al<sub>7</sub>Cu<sub>2</sub>Fe particles in aluminum alloy 7075-T651." *Corrosion Science* 48(12): 4202-4215.
- [18] Birbilis, N., T. Muster, et al. (2011). *Corrosion of Aluminum Alloys. Corrosion Mechanisms in Theory and Practice*, Third Edition, CRC Press: 705-736.
- [19] Blanc, C., B. Lavelle, et al. (1997). "The role of precipitates enriched with copper on the susceptibility to pitting corrosion of the 2024 aluminium alloy." *Corrosion Science* 39(3): 495-510.
- [20] Blin, F., P. Koutsoukos, et al. (2007). "The corrosion inhibition mechanism of new rare earth cinnamate compounds - Electrochemical studies." *Electrochimica Acta* 52(21): 6212-6220.
- [21] Boag, A., A. E. Hughes, et al. (2011). "Corrosion of AA2024-T3 Part I: Localised corrosion of isolated IM particles." *Corrosion Science* 53(1): 17-26.

- [22] Boag, A., A. E. Hughes, et al. (2009). "How complex is the microstructure of AA2024-T3?" *Corrosion Science* 51(8): 1565-1568.
- [23] Bohm, S., H. N. McMurray, et al. (2001). "Novel environment friendly corrosion inhibitor pigments based on naturally occurring clay minerals." *Materials and Corrosion-Werkstoffe Und Korrosion* 52(12): 896-903.
- [24] Bon, S. A. F., S. D. Mookhoek, et al. (2007). "Route to stable non-spherical emulsion droplets." *European Polymer Journal* 43(11): 4839-4842.
- [25] Brunner, J. G., J. May, et al. (2010). "Localized corrosion of ultrafine-grained Al-Mg model alloys." *Electrochimica Acta* 55(6): 1966-1970.
- [26] Buchheit, R. G. (1995). "A Compilation of Corrosion Potentials Reported for Intermetallic Phases in Aluminum-Alloys." *Journal of The Electrochemical Society* 142(11): 3994-3996.
- [27] Buchheit, R. G. (2000). "Electrochemistry of  $\theta$  ( $\text{Al}_2\text{Cu}$ ),  $\text{S}$  ( $\text{Al}_2\text{CuMg}$ ) and  $\text{T1}$  ( $\text{Al}_2\text{Cu-Li}$ ) and localized corrosion and environment assisted cracking in high strength Al alloys." *Materials Science Forum* 331: II/.
- [28] Buchheit, R. G. and N. Birbilis (2010). "Electrochemical microscopy: An approach for understanding localized corrosion in microstructurally complex metallic alloys." *Electrochimica Acta* 55(27): 7853-7859.
- [29] Buchheit, R. G., R. P. Grant, et al. (1997). "Local Dissolution Phenomena Associated with  $\text{S}$  Phase ( $\text{Al}_2\text{CuMg}$ ) Particles in Aluminum Alloy 2024-T3." *Journal of The Electrochemical Society* 144(8): 2621-2628.
- [30] Buchheit, R. G., H. Guan, et al. (2003). "Active corrosion protection and corrosion sensing in chromate-free organic coatings." *Progress in Organic Coatings* 47(3-4): 174-182.
- [31] Buchheit, R. G., Hughes, A.E. (2003). *Chromate and Chromate-Free Coatings. Corrosion: Fundamentals, Testing and Protection*. C. Moosbrugger. Mterials Park, Oh, USA, ASM International. 13A: 720 -735.
- [32] Buchheit, R. G., M. A. Martinez, et al. (2000). "Evidence for Cu Ion Formation by Dissolution and Dealloying the  $\text{Al}_2\text{CuMg}$  Intermetallic Compound in Rotating Ring-Disk Collection Experiments." *Journal of The Electrochemical Society* 147(1): 119-124.
- [33] Buchheit, R. G., L. P. Montes, et al. (1999). "The Electrochemical Characteristics of Bulk-Synthesized  $\text{Al}_{\text{sub } 2}\text{CuMg}$ ." *Journal of The Electrochemical Society* 146(12): 4424-4428.
- [34] Buchheit, R. G., F. D. Wall, et al. (1995). "Anodic Dissolution-Based Mechanism for the Rapid Cracking, Preexposure Phenomenon Demonstrated by Aluminum-Lithium-Copper Alloys." *Corrosion* 51(6): 417-428.

- [35] Büchler, M., T. Watari, et al. (2000). "Investigation of the initiation of localized corrosion on aluminum alloys by using fluorescence microscopy." *Corrosion Science* 42(9): 1661-1668.
- [36] Buis, A. and J. Schijve (1992). "Stress-Corrosion Cracking Behavior of Al Li-2090-T83 In Artificial Seawater." *Corrosion* 48(11): 898-909.
- [37] Burstein, G. T., C. Liu, et al. (2004). "Origins of pitting corrosion." *Corrosion Engineering Science and Technology* 39(1): 25-30.
- [38] Campestrini, P., E. P. M. van Westing, et al. (2000). "Relation between microstructural aspects of AA2024 and its corrosion behaviour investigated using AFM scanning potential technique." *Corrosion Science* 42(11): 1853-1861.
- [39] Carroll, M. C., P. I. Gouma, et al. (2001). "Effects of minor Cu additions on a Zn-modified Al-5083 alloy." *Materials Science and Engineering: A* 319–321(0): 425-428.
- [40] Carroll, M. C., P. I. Gouma, et al. (2000). "Effects of Zn additions on the grain boundary precipitation and corrosion of Al-5083." *Scripta Materialia* 42(4): 335-340.
- [41] Cavanaugh, M., N. Birbilis, et al. (2007). "Investigating localized corrosion susceptibility arising from Sc containing intermetallic Al3Sc in high strength Al-alloys." *Scripta Materialia* 56(11): 995-998.
- [42] Cavanaugh, M. K. (2009). *Modelling the environmental dependence of localized corrosion evolution in AA7075-T651*, Ohio State University.
- [43] Cavanaugh, M., N. Birbilis, et al. (2007). "Investigating localized corrosion susceptibility arising from Sc containing intermetallic Al3Sc in high strength Al-alloys." *Scripta Materialia* 56(11): 995-998.
- [44] Cavanaugh, M. K., N. Birbilis, et al. (2009). "A Quantitative Study on the Effects of Environment and Microstructure on Pit Initiation in Al-alloys." *ECS Transactions* 16(52): 1-11.
- [45] Cavanaugh, M. K., N. Birbilis, et al. (2012). "Modeling pit initiation rate as a function of environment for Aluminum alloy 7075-T651." *Electrochimica Acta* 59: 336-345.
- [46] Cavanaugh, M. K., R. G. Buchheit, et al. (2009). "Evaluation of a simple microstructural-electrochemical model for corrosion damage accumulation in microstructurally complex aluminum alloys." *Engineering Fracture Mechanics* 76(5): 641-650.
- [47] Cavanaugh, M. K., R. G. Buchheit, et al. (2010). "Modeling the environmental dependence of pit growth using neural network approaches." *Corrosion Science* 52(9): 3070-3077.
- [48] Chambers, B. D. and S. R. Taylor (2007). "High-Throughput Assessment of Inhibitor Synergies on Aluminum Alloy 2024-T3 Through Measurement of Surface Copper Enrichment." *Corrosion* 63(3): 268-276.

- [49] Chambers, B. D., S. R. Taylor, et al. (2005). "Rapid Discovery of Corrosion Inhibitors and Synergistic Combinations Using High-Throughput Screening Methods." *Corrosion* 61(5): 480-489.
- [50] Chen, G. S., M. Gao, et al. (1996). "Microconstituent-Induced Pitting Corrosion in Aluminum Alloy 2024-T3." *Corrosion (Houston)* 52(1): 8-15.
- [51] Cho, S. H., S. R. White, et al. (2009). "Self-Healing Polymer Coatings." *Advanced Materials* 21(6): 645-+.
- [52] Davenport, A. J., Y. Yuan, et al. (2006). "Intergranular Corrosion and Stress Corrosion Cracking of Sensitised AA5182." *Materials Science Forum* 519-521: 641-646.
- [53] Davis, J. R. (1999). *Corrosion of aluminum and aluminum alloys*, Materials Park, OH : ASM International.
- [54] Deacon, G. B., M. Forsyth, et al. (2009). "Synthesis and Characterisation of Rare Earth Complexes Supported by para-Substituted Cinnamate Ligands." *Zeitschrift Fur Anorganische Und Allgemeine Chemie* 635(6-7): 833-839.
- [55] Dorward, R. C. and T. R. Pritchett (1988). "Advanced aluminium alloys for aircraft and aerospace applications." *Materials & Design* 9(2): 63-69.
- [56] Dry, C. (1996). "Procedures developed for self-repair of polymer matrix composite materials." *Composite Structures* 35(3): 263-269.
- [57] Du, Y. J., M. Damron, et al. (2001). "Inorganic/organic hybrid coatings for aircraft aluminum alloy substrates." *Progress in Organic Coatings* 41(4): 226-232.
- [58] Eckermann, F., T. Suter, et al. (2008). "The influence of MgSi particle reactivity and dissolution processes on corrosion in Al-Mg-Si alloys." *Electrochimica Acta* 54(2): 844-855.
- [59] Eidhed, W. (2008). "Effects of solution treatment time and Sr-modification on microstructure and mechanical property of Al-Si piston alloy." *Journal of Materials Science and Technology* 24(1): 29-32.
- [60] Fang, H. C., K. H. Chen, et al. (2009). "Effect of Cr, Yb and Zr additions on localized corrosion of Al-Zn-Mg-Cu alloy." *Corrosion Science* 51(12): 2872-2877.
- [61] Ferrer, C. P., M. G. Koul, et al. (2003). "Improvements in strength and stress corrosion cracking properties in aluminum alloy 7075 via low-temperature retrogression and re-aging heat treatments." *Corrosion* 59(6): 520-528.
- [62] Fischer, H. R. (2010). *natural Science* 2: 873-901.
- [63] Fleck, P., D. Calleros, et al. (2000). "Retrogression and reaging of 7075 T6 aluminum alloy." *Materials Science Forum* 331: I/.
- [64] Forsyth, M., T. Markley, et al. (2008). "Inhibition of corrosion on AA2024-T3 by new environmentally friendly rare earth organophosphate compounds." *Corrosion* 64(3): 191-197.

- [65] Frankel, G. S. (1998). "Pitting Corrosion of Metals." *Journal of The Electrochemical Society* 145(6): 2186-2198.
- [66] Frankel, G. S., A. J. Davenport, et al. (1992). "X-ray absorption study of electrochemically grown oxide films on Al-Cr sputtered alloys." *Journal of The Electrochemical Society* 139(7): 1812-1820.
- [67] Frankel, G. S., M. A. Russak, et al. (1989). "Pitting of Sputtered Aluminum Alloy Thin Films." *Journal of The Electrochemical Society* 136(4): 1243-1244.
- [68] Fuller, C. B., A. R. Krause, et al. (2002). "Microstructure and mechanical properties of a 5754 aluminum alloy modified by Sc and Zr additions." *Materials Science and Engineering A* 338(1-2): 8-16.
- [69] Furman, S. A., F. H. Scholes, et al. (2006). "Corrosion in artificial defects. II. Chromate reactions." *Corrosion Science* 48(7): 1827-1847.
- [70] Galvele, J. R. (1976). "Transport Processes and the Mechanism of Pitting of Metals." *Journal of The Electrochemical Society* 123(4): 464-474.
- [71] García, S. J., H. R. Fischer, et al. (2011). "Self-healing anticorrosive organic coating based on an encapsulated water reactive silyl ester: Synthesis and proof of concept." *Progress in Organic Coatings* 70(2-3): 142-149.
- [72] García, S. J., Mol, J.M.C., Muster, T.H., Hughes, A.E., Mardel, J., Miller, T., Markely, T., Terryn, H., de Wit, J.H.W. (2011). *Advances in the Selection and use of Rare-Earth-Based Inhibitors for Self Healing Organic Coatings*, Accepted for publication in *Self-Healing Properties of New Surface Treatments. Green Inhibitors*. L. Fedrizzi, EFC-Maney Publishing. 58.
- [73] García, S. J., T. H. Muster, et al. (2010). "The influence of pH on corrosion inhibitor selection for 2024-T3 aluminium alloy assessed by high-throughput multielectrode and potentiodynamic testing." *Electrochimica Acta* 55(7): 2457-2465.
- [74] García, S. J., M. T. Rodríguez, et al. (2007). "Evaluation of cure temperature effects in cathaphoretic automotive primers by electrochemical techniques." *Progress in Organic Coatings* 60(4): 303-311.
- [75] García, S. J. and J. Suay (2006). "Anticorrosive properties of an epoxy-Meldrum acid cured system catalyzed by erbium III trifluoromethanesulfonate." *Progress in Organic Coatings* 57(4): 319-331.
- [76] García, S. J. and J. Suay (2006). "Application of electrochemical techniques to study the effect on the anticorrosive properties of the addition of ytterbium and erbium triflates as catalysts on a powder epoxy network." *Progress in Organic Coatings* 57(3): 273-281.
- [77] García, S. J. and J. Suay (2007). "A comparative study between the results of different electrochemical techniques (EIS and AC/DC/AC). Application to the optimisation of

- the cataphoretic and curing parameters of a primer for the automotive industry." *Progress in Organic Coatings* 59(3): 251-258.
- [78] García, S. J. and J. Suay (2007). "Influence on the anticorrosive properties of the use of erbium (III) trifluoromethanesulfonate as initiator in an epoxy powder clearcoat." *Corrosion Science* 49(8): 3256-3275.
- [79] García, S. J. and J. Suay (2009). "Optimization of deposition voltage of cataphoretic automotive primers assessed by EIS and AC/DC/AC." *Progress in Organic Coatings* 66(3): 306-313.
- [80] Garrard, W. N. (1994). "Corrosion Behavior of Aluminum-Lithium Alloys." *Corrosion* 50(3): 215-225.
- [81] Gimenez, P., J. J. Rameau, et al. (1981). "Experimental pH potential diagram of aluminium for seawater." *Corrosion* 37: 673-682.
- [82] Giummarra, C., B. Thomas, et al. (2007). "New Al-Li Alloys for Aerospace Applications." *Proceedings of the Light Metals Technology Conference*.
- [83] Goswami, R., G. Spanos, et al. (2010). "Precipitation behavior of the  $\beta$  phase in Al-5083." *Materials Science and Engineering: A* 527(4-5): 1089-1095.
- [84] Graver, B., A. M. Pedersen, et al. (2009). "Anodic Activation of Aluminum by Trace Element Tin." *ECS Transactions* 16(52): 55-69.
- [85] Graver, B., A. T. J. van Helvoort, et al. (2010). "Effect of heat treatment on anodic activation of aluminium by trace element indium." *Corrosion Science* 52(11): 3774-3781.
- [86] Guillaumin, V. and G. Mankowski (1998). "Localized corrosion of 2024 T351 aluminium alloy in chloride media." *Corrosion Science* 41(3): 421-438.
- [87] Guillaumin, V. and G. Mankowski (2000). "Localized corrosion of 6056 T6 aluminium alloy in chloride media." *Corrosion Science* 42(1): 105-125.
- [88] Gundersen, J. T. B., A. Aytaç, et al. (2004). "Effect of heat treatment on electrochemical behaviour of binary aluminium model alloys." *Corrosion Science* 46(3): 697-714.
- [89] Gupta, R. K., N. L. Sukiman, et al. (2012). "Metastable pitting characteristics of aluminium alloys measured using current transients during potentiostatic polarisation." *Electrochimica Acta* 66: 245-254.
- [90] Gupta, R. K., N. L. Sukiman, et al. (2012). "Electrochemical Behavior and Localized Corrosion Associated with Mg<sub>2</sub>Si Particles in Al and Mg Alloys." *ECS Electrochemistry Letters* 1(1): B1-B3.
- [91] Harvey, T. G., S. G. Hardin, et al. (2011). "The effect of inhibitor structure on the corrosion of AA2024 and AA7075." *Corrosion Science* 53(6): 2184-2190.
- [92] Harvey, T. G., A. E. Hughes, et al. (2008). "Non-chromate deoxidation of AA2024-T3: Sodium bromate–nitric acid (20–60)." *Applied Surface Science* 254(11): 3562-3575.



- [93] Hatch, J. E. (1984). *Aluminum: properties and physical metallurgy*, Metals Park, Ohio : American Society for Metals.
- [94] He, Y., X. Zhang, et al. (2010). "Effect of minor Cr, Mn, Zr, Ti and B on grain refinement of as-cast Al-Zn-Mg-Cu alloys." *Xiyou Jinshu Cailiao Yu Gongcheng/Rare Metal Materials and Engineering* 39(7): 1135-1140.
- [95] Hinton, B. R. W., N. Dubrule, et al. (2006). Raman, EDS and SEM studies of the interaction of corrosion inhibitor Ce(dbp)<sub>3</sub> with AA2024-T3. 4th International Symposium on Aluminium Surface Science and Technology. Beaune, France.
- [96] Hirth, S. M., G. J. Marshall, et al. (2001). "Effects of Si on the aging behaviour and formability of aluminium alloys based on AA6016." *Materials Science and Engineering A* 319-321: 452-456.
- [97] Ho, D., N. Brack, et al. (2006). "Cerium dibutylphosphate as a corrosion inhibitor for AA2024-T3 aluminum alloys." *Journal of the Electrochemical Society* 153(9): B392-B401.
- [98] Hollaender, J. (1997). "Rapid assessment of food/package interactions by electrochemical impedance spectroscopy (EIS)." *Food Additives and Contaminants* 14(6-7): 617-626.
- [99] Huang, Z. H., J. F. Li, et al. (2008). "Primary crystallization of Al-Ni-RE amorphous alloys with different type and content of RE." *Materials Science and Engineering: A* 489(1-2): 380-388.
- [100] Hughes, A. E., A. Boag, et al. (2011). "Corrosion of AA2024-T3 Part II: Co-operative corrosion." *Corrosion Science* 53(1): 27-39.
- [101] Hughes, A. E., A. M. Glenn, et al. (2012). A Consistent Description of Intermetallic Particle Composition: An analysis of 10 Batches of AA2024-T3. *Aluminium Surface Science & Technology*, Sorrento, Italy.
- [102] Hughes, A. E., C. MacRae, et al. (2010). "Sheet AA2024-T3: A new investigation of microstructure and composition." *Surface and Interface Analysis* 42(4): 334-338.
- [103] Hughes, A. E., I. S. Cole, et al. (2010). "Designing green, self-healing coatings for metal protection." *NPG Asia Materials* 2(4): 143-151.
- [104] Hughes, A. E., I. S. Coles, et al. (2010). "Combining Green and Self Healing for a new Generation of Coatings for Metal Protection." *Nature Asia Materials* 2(4): 143-151.
- [105] Ilevbare, G. O., O. Schneider, et al. (2004). "In Situ Confocal Laser Scanning Microscopy of AA 2024-T3 Corrosion Metrology." *Journal of The Electrochemical Society* 151(8): B453.
- [106] Inoue, A., J. S. Gook, et al. (1995). "New amorphous alloys in Al-Mg-Ln (Ln = La, Ce or Nd) systems prepared by rapid solidification (rapid publication)." *Materials Transactions, JIM* 36(7): 794-796.

- [107] Inoue, A. and A. Takeuchi (2004). "Recent progress in bulk glassy, nanoquasicrystalline and nanocrystalline alloys." *Materials Science and Engineering: A* 375–377(0): 16-30.
- [108] Jain, S. (2006). Corrosion and protection of heterogeneous cast Al-Si (356) and Al-Si-Fe-Cu (380) alloys by chromate and cerium inhibitors, Ohio State University.
- [109] Jain, S., M. L. C. Lim, et al. (2012). "Spreading of intergranular corrosion on the surface of sensitized Al-4.4Mg alloys: A general finding." *Corrosion Science* 59: 136-147.
- [110] Jia, Z., B. Graver, et al. (2008). "Effect of magnesium on segregation of trace element lead and anodic activation in aluminum Alloys." *Journal of The Electrochemical Society* 155(1): C1-C7.
- [111] Jones, R. H., D. R. Baer, et al. (2001). "Role of Mg in the stress corrosion cracking of an Al-Mg alloy." *Metallurgical and Materials Transactions A: Physical Metallurgy and Materials Science* 32(7): 1699-1711.
- [112] Jorcin, J. B., E. Aragon, et al. (2006). "Delaminated areas beneath organic coating: A local electrochemical impedance approach." *Corrosion Science* 48(7): 1779-1790.
- [113] Joshua Du, Y., M. Damron, et al. (2001). "Inorganic/organic hybrid coatings for aircraft aluminum alloy substrates." *Progress in Organic Coatings* 41(4): 226-232.
- [114] Juffs, L. (2002). Investigation of Corrosion Coating Deposition on Microscopic and Macroscopic Intermetallic Phases of Aluminium Alloys. Master of Science, RMIT.
- [115] Juffs, L., A. E. Hughes, et al. (2002). "The use of macroscopic modelling of intermetallic phases in aluminium alloys in the study of ferricyanide accelerated chromate conversion coatings." *Corrosion Science* 44(8): 1755-1781.
- [116] Juffs, L., A. E. Hughes, et al. (2001). "The use of macroscopic modelling of intermetallic phases in aluminium alloys in the study of ferricyanide accelerated chromate conversion coatings." *Micron* 32(8): 777-787.
- [117] Kallip, S., A. C. Bastos, et al. (2010). "A multi-electrode cell for high-throughput SVET screening of corrosion inhibitors." *Corrosion Science* 52(9): 3146-3149.
- [118] Kannan, M. B. and V. S. Raja (2010). Enhancing the localized corrosion resistance of high strength 7010 Al-alloy. 138: 1-6.
- [119] Kendig, M. W. and R. G. Buchheit (2003). "Corrosion Inhibition of Aluminum and Aluminum Alloys by Soluble Chromates, Chromate Coatings, and Chromate-Free Coatings." *Corrosion* 59(5): 379-400.
- [120] Keuon, Y. W., J. H. Nordlien, et al. (2003). "Electrochemical activation of aluminum by trace element lead." *Journal of The Electrochemical Society* 150(11): B547-B551.
- [121] Khramov, A. N., N. N. Voevodin, et al. (2004). "Hybrid organo-ceramic corrosion protection coatings with encapsulated organic corrosion inhibitors." *Thin Solid Films* 447–448(0): 549-557.

- [122] Kim, K. T., J. M. Kim, et al. (2005). Effect of alloying elements on the strength and casting characteristics of high strength Al-Zn-Mg-Cu alloys. 475-479: 2539-2542.
- [123] Kim, W. J., C. S. Chung, et al. (2003). "Optimization of strength and ductility of 2024 Al by equal channel angular pressing (ECAP) and post-ECAP aging." *Scripta Materialia* 49(4): 333-338.
- [124] Koroleva, E. v., G. e. Thompson, et al. (1999). "Surface morphological changes of aluminium alloys in alkaline solution:: effect of second phase material." *Corrosion Science* 41(8): 1475-1495.
- [125] Lamaka, S. V., O. V. Karavai, et al. (2008). "Monitoring local spatial distribution of Mg<sup>2+</sup>, pH and ionic currents." *Electrochemistry Communications* 10(2): 259-262.
- [126] Larsen, M. H., J. C. Walmsley, et al. (2008). "Intergranular corrosion of copper-containing AA6xxx AlMgSi aluminum alloys." *Journal of The Electrochemical Society* 155(11): C550-C556.
- [127] Lavernia, E. J. and N. J. Grant (1987). "Aluminum Lithium Alloys." *Journal of Materials Science* 22(5): 1521-1529.
- [128] Leblanc, P. and G. S. Frankel (2002). "A study of corrosion and pitting initiation of AA2024-T3 using atomic force microscopy." *Journal of The Electrochemical Society* 149(6): B239-B247.
- [129] Lee, Y. B., D. H. Shin, et al. (2004). "Effect of annealing temperature on microstructures and mechanical properties of a 5083 Al alloy deformed at cryogenic temperature." *Scripta Materialia* 51(4): 355-359.
- [130] Li, C., D. Y. Li, et al. (2009). "Microstructure and mechanical properties of multicomponent aluminum alloy by rapid solidification." *Journal of Materials Engineering and Performance* 18(1): 79-82.
- [131] Li, J. F., Z. Q. Zheng, et al. (2007). "Exfoliation corrosion and electrochemical impedance spectroscopy of an Al-Li alloy in EXCO solution." *Materials and Corrosion* 58(4): 273-279.
- [132] Liddicoat, P. V., X.-z. Liao, et al. (2010). "Nanostructural hierarchy increases the strength of aluminium alloys." *Nature Communications* 1(6): 63-63.
- [133] Lin, J. C., H. L. Liao, et al. (2006). "Effect of heat treatments on the tensile strength and SCC-resistance of AA7050 in an alkaline saline solution." *Corrosion Science* 48(10): 3139-3156.
- [134] Liu, Y. and Y. F. Cheng (2010). "Role of second phase particles in pitting corrosion of 3003 Al alloy in NaCl solution." *Materials and Corrosion* 61(3): 211-217.
- [135] Liu, Y. and Y. F. Cheng (2011). "Characterization of passivity and pitting corrosion of 3003 aluminum alloy in ethylene glycol-water solutions." *Journal of Applied Electrochemistry* 41(2): 151-159.

- [136] Lucente, A. M. and J. R. Scully (2007). "Pitting of Al-based amorphous-nanocrystalline alloys with solute-lean nanocrystals." *Electrochemical and Solid-State Letters* 10(5): 39-43.
- [137] Lucente, A. M. and J. R. Scully (2008). "Localized corrosion of Al-based amorphous-nanocrystalline alloys with solute-lean nanocrystals: Pit stabilization." *Journal of The Electrochemical Society* 155(5): C234-C243.
- [138] Lynch, S. P., S. P. Knight, et al. (2009). Stress-corrosion cracking of Al-Zn-Mg-Cu alloys effects of composition and heat-treatment.
- [139] Mahajanarn, S. P. V. and R. G. Buchheit (2008). "Characterization of inhibitor release from Zn-Al- V10O28 (6-) hydrotalcite pigments and corrosion protection from hydrotalcite-pigmented epoxy coatings." *Corrosion* 64(3): 230-240.
- [140] Manna, I., P. P. Chattopadhyay, et al. (2004). "Development of amorphous and nanocrystalline Al<sub>65</sub>Cu<sub>35-x</sub>Zr<sub>x</sub> alloys by mechanical alloying." *Materials Science and Engineering: A* 379(1-2): 360-365.
- [141] Mardel, J., S. J. Garcia, et al. (2011). "The characterisation and performance of Ce(dbp)<sub>3</sub>-inhibited epoxy coatings." *Progress in Organic Coatings* 70(2-3): 91-101.
- [142] Markley, T. A., M. Forsyth, et al. (2007). "Corrosion protection of AA2024-T3 using rare earth diphenyl phosphates." *Electrochimica Acta* 52(12): 4024-4031.
- [143] Markley, T. A., A. E. Hughes, et al. (2007). "Influence of praseodymium - Synergistic corrosion inhibition in mixed rare-earth diphenyl phosphate systems." *Electrochemical and Solid State Letters* 10(12): C72-C75.
- [144] Marlaud, T., A. Deschamps, et al. (2010). "Evolution of precipitate microstructures during the retrogression and re-ageing heat treatment of an Al-Zn-Mg-Cu alloy." *Acta Materialia* 58(14): 4814-4826.
- [145] Martin, J. W. (1988). "Aluminum-Lithium Alloys." *Annual Review of Materials Science* 18: 101-119.
- [146] Masumoto, T. (1994). "Recent progress in amorphous metallic materials in Japan." *Materials Science and Engineering: A* 179-180, Part 1(0): 8-16.
- [147] Mazurkiewicz, B. and A. Piotrowski (1983). "The electrochemical behaviour of the Al<sub>2</sub>Cu intermetallic compound." *Corrosion Science* 23(7): 697-707.
- [148] McCafferty, E. (2010). Passivity
- [149] Introduction to Corrosion Science, Springer New York: 209-262.
- [150] McKenzie, P. W. J. and R. Lapovok (2010). "ECAP with back pressure for optimum strength and ductility in aluminium alloy 6016. Part 2: Mechanical properties and texture." *Acta Materialia* 58(9): 3212-3222.
- [151] Medco.

- [152] Mondolfo, L. F. (1971). "Discussion of "grain-size refining of primary crystals in hypereutectic Al-Si and Al-Ge alloys"." *Metallurgical Transactions* 2(4): 1254.
- [153] Mondolfo, L. F. and J. G. Barlock (1975). "Effect of superheating on structure of some aluminum alloys." *Metallurgical Transactions B* 6(4): 565-572.
- [154] Mookhoek, S. D., H. R. Fischer, et al. (2009). "A numerical study into the effects of elongated capsules on the healing efficiency of liquid-based systems." *Computational Materials Science* 47(2): 506-511.
- [155] Mookhoek, S. D., S. C. Mayo, et al. (2010). "Applying SEM-Based X-ray Microtomography to Observe Self-Healing in Solvent Encapsulated Thermoplastic Materials." *Advanced Engineering Materials* 12(3): 228-234.
- [156] Muller, I. L. and J. R. Galvele (1977). "Pitting potential of high purity binary aluminium alloys—II. AlMg and AlZn alloys." *Corrosion Science* 17(12): 995-1007.
- [157] Muster, T. H., A. E. Hughes, et al. (2009). "A rapid screening multi-electrode method for the evaluation of corrosion inhibitors." *Electrochimica Acta* 54(12): 3402-3411.
- [158] Muster, T. H., A. E. Hughes, et al. (2009). *Cu Distributions in Aluminium Alloys*, New York, Nova Science Publishers.
- [159] Muster, T. H., Hughes, A.E., Thompson, G.E. (2009). *Cu Distributions in Aluminium Alloys*. New York, Nova Science Publishers.
- [160] Nisancioglu, K. (1990). "Electrochemical Behavior of Aluminum-Base Intermetallics Containing Iron." *Journal of The Electrochemical Society* 137(1): 69-77.
- [161] Nisancioglu, K. and H. Holtan (1978). "Measurement of the critical pitting potential of aluminium." *Corrosion Science* 18(9): 835-849.
- [162] Norova, M. T., I. N. Ganiev, et al. (2003). "Enhancement of the corrosion resistance of aluminum-lithium alloys by microalloying with calcium." *Russian Journal of Applied Chemistry* 76(4): 547-549.
- [163] Oguocha, I., O. Adigun, et al. (2008). "Effect of sensitization heat treatment on properties of Al-Mg alloy AA5083-H116." *Journal of Materials Science* 43(12): 4208-4214.
- [164] Oliveira Jr, A. F., M. C. de Barros, et al. (2004). "The effect of RRA on the strength and SCC resistance on AA7050 and AA7150 aluminium alloys." *Materials Science and Engineering A* 379(1-2): 321-326.
- [165] Orazem, M. E. and B. Tribollet (2008). *Semiconducting Systems, in Electrochemical Impedance Spectroscopy*, John Wiley & Sons.
- [166] Osborne, J. H., K. Y. Blohowiak, et al. (2001). "Testing and evaluation of nonchromated coating systems for aerospace applications." *Progress in Organic Coatings* 41(4): 217-225.

- [167] Park, J. O., C. H. Paik, et al. (1999). "Influence of Fe-Rich Intermetallic Inclusions on Pit Initiation on Aluminum Alloys in Aerated NaCl." *Journal of The Electrochemical Society* 146(2): 517-523.
- [168] Pedersen, L. and L. Arnberg (2001). "The effect of solution heat treatment and quenching rates on mechanical properties and microstructures in AlSiMg foundry alloys." *Metallurgical and Materials Transactions A: Physical Metallurgy and Materials Science* 32(3): 525-532.
- [169] Perrault, G. G. (1979). "Role of Hydrides in the Equilibrium of Aluminum in Aqueous Solutions." *J Electrochem Soc* 126(2): 199-204.
- [170] Poelman, M., M. G. Olivier, et al. (2005). "Electrochemical study of different ageing tests for the evaluation of a cataphoretic epoxy primer on aluminium." *Progress in Organic Coatings* 54(1): 55-62.
- [171] Polmear, I. J. (2006). *Light alloys : from traditional alloys to nanocrystals*, Oxford ; Burlington, MA : Elsevier/Butterworth-Heinemann.
- [172] Poole, W. J., J. A. Seter, et al. (2000). "A model for predicting the effect of deformation after solution treatment on the subsequent artificial aging behavior of AA7030 and AA7108 alloys." *Metallurgical and Materials Transactions A: Physical Metallurgy and Materials Science* 31(9): 2327-2338.
- [173] Pourbaix, M. (1974). *Atlas of Electrochemical Equilibria in Aqueous Solutions*. National Association of Corrosion Engineers, Houston, TX, USA.
- [174] Premendra, P., H. Terryn, et al. (2009). "A comparative electrochemical study of commercial and model aluminium alloy (AA5050)." *Materials and Corrosion* 60(6): 399-406.
- [175] Puga, H., S. Costa, et al. (2011). "Influence of ultrasonic melt treatment on microstructure and mechanical properties of AlSi9Cu3 alloy." *Journal of Materials Processing Technology* 211(11): 1729-1735.
- [176] Ralston, K. D., N. Birbilis, et al. (2010). "Role of nanostructure in pitting of Al-Cu-Mg alloys." *Electrochimica Acta* 55(27): 7834-7842.
- [177] Ralston, K. D., N. Birbilis, et al. (2010). "Revealing the relationship between grain size and corrosion rate of metals." *Scripta Materialia* 63(12): 1201-1204.
- [178] Raps, D., T. Hack, et al. (2009). "Electrochemical study of inhibitor-containing organic-inorganic hybrid coatings on AA2024." *Corrosion Science* 51(5): 1012-1021.
- [179] Raviprasad, K., C. R. Hutchinson, et al. (2003). "Precipitation processes in an Al-2.5Cu-1.5Mg (wt. %) alloy microalloyed with Ag and Si." *Acta Materialia* 51(17): 5037-5050.
- [180] Ringer, S. P., K. Hono, et al. (1996). "Nucleation of precipitates in aged AlCuMg(Ag) alloys with high Cu:Mg ratios." *Acta Materialia* 44(5): 1883-1898.

- [181] Rizzi, P. and L. Battezzati (2004). "Mechanical properties of Al based amorphous and devitrified alloys containing different rare earth elements." *Journal of Non-Crystalline Solids* 344(1–2): 94-100.
- [182] Rodríguez, M. T., J. J. Gracenea, et al. (2004). "Testing the influence of the plasticizers addition on the anticorrosive properties of an epoxy primer by means of electrochemical techniques." *Progress in Organic Coatings* 50(2): 123-131.
- [183] Rosalbino, F., E. Angelini, et al. (2003). "Influence of the rare earth content on the electrochemical behaviour of Al-Mg-Er alloys." *Intermetallics* 11(5): 435-441.
- [184] Sævik, Ø., Y. Yu, et al. (2005). "Characterization of lead enrichment on electrochemically active AlPb model alloy." *Journal of The Electrochemical Society* 152(9): B334-B341.
- [185] Samadzadeh, M., S. H. Boura, et al. (2010). "A review on self-healing coatings based on micro/nanocapsules." *Progress in Organic Coatings* 68(3): 159-164.
- [186] Samanta, A., I. Manna, et al. (2007). "Phase evolution in Al-Ni-(Ti, Nb, Zr) powder blends by mechanical alloying." *Materials Science and Engineering A* 464(1-2): 306-314.
- [187] Sasaki, K. and H. S. Isaacs (2004). "Origins of Electrochemical Noise during Pitting Corrosion of Aluminum." *Journal of The Electrochemical Society* 151(3): B124-B133.
- [188] Sato, N. (1990). "An overview on the passivity of metals." *Corrosion Science* 31(0): 1-19.
- [189] Schmutz, P. and G. S. Frankel (1998). "Characterization of AA2024-T3 by scanning Kelvin probe force microscopy." *Journal of The Electrochemical Society* 145(7): 2285-2295.
- [190] Schneider, O., G. O. Ilevbare, et al. (2007). "In situ confocal laser scanning microscopy of AA2024-T3 corrosion metrology: III. Underfilm corrosion of epoxy-coated AA2024-T3." *Journal of The Electrochemical Society* 154(8): C397-C410.
- [191] Schneider, O., G. O. Ilevbare, et al. (2004). "In situ confocal laser scanning microscopy of AA 2024-T3 corrosion metrology II. Trench formation around particles." *Journal of The Electrochemical Society* 151(8): B465-B472.
- [192] Scholes, F. H., S. A. Furman, et al. (2006). "Chromate leaching from inhibited primers: Part I. Characterisation of leaching." *Progress in Organic Coatings* 56(1): 23-32.
- [193] Scholes, F. H., S. A. Furman, et al. (2006). "Corrosion in artificial defects. I: Development of corrosion." *Corrosion Science* 48(7): 1812-1826.
- [194] Scholes, F. H., A. E. Hughes, et al. (2009). "Interaction of Ce(dbp)(3) with surface of aluminium alloy 2024-T3 using macroscopic models of intermetallic phases." *Corrosion Engineering Science and Technology* 44(6): 416-424.

- [195] Scully, J. R., T. O. Knight, et al. (1993). "Electrochemical characteristics of the Al<sub>2</sub>Cu, Al<sub>3</sub>Ta and Al<sub>3</sub>Zr intermetallic phases and their relevancy to the localized corrosion of Al alloys." *Corrosion Science* 35(1–4): 185-195.
- [196] Searles, J. L., P. I. Gouma, et al. (2002). "Stress Corrosion Cracking of Sensitized AA5083 (Al-4.5Mg-1.0Mn)." *Materials Science Forum* 396-402: 1437-1442.
- [197] Semenov, A. M. (2001). "Effect of Mg additions and thermal treatment on corrosion properties of Al-Li-Cu-base alloys." *Protection of Metals* 37(2): 126-131.
- [198] Senkov, O., R. Bhat, et al. (2005). "Microstructure and properties of cast ingots of Al-Zn-Mg-Cu alloys modified with Sc and Zr." *Metallurgical and Materials Transactions A* 36(8): 2115-2126.
- [199] Seri, O. (1994). "The effect of NaCl concentration on the corrosion behavior of aluminum containing iron." *Corrosion Science* 36(10): 1789-1803.
- [200] Seri, O. and K. Tagashira (1986). "Effect of Manganese Content on Corrosion Characteristics of Al-Mn Alloys." *Keikinzoku/Journal of Japan Institute of Light Metals* 36(12): 806-812.
- [201] Sha, G. and A. Cerezo (2004). "Characterization of precipitates in an aged 7xxx series Al alloy." *Surface and Interface Analysis* 36(5-6): 564-568.
- [202] Shaw, B. A., G. D. Davis, et al. (1991). "The Influence of Tungsten Alloying Additions on the Passivity of Aluminum." *Journal of The Electrochemical Society* 138(11): 3288-3295.
- [203] Shaw, B. A., T. L. Fritz, et al. (1990). "The Influence of Tungsten on the Pitting of Aluminum Films." *Journal of The Electrochemical Society* 137(4): 1317-1318.
- [204] Sinko, J. (2001). "Challenges of chromate inhibitor pigments replacement in organic coatings." *Progress in Organic Coatings* 42(3–4): 267-282.
- [205] Song, R. G., W. Dietzel, et al. (2004). "Stress corrosion cracking and hydrogen embrittlement of an Al-Zn-Mg-Cu alloy." *Acta Materialia* 52(16): 4727-4743.
- [206] Souto, R. M., Y. González-García, et al. (2010). "Examination of organic coatings on metallic substrates by scanning electrochemical microscopy in feedback mode: Revealing the early stages of coating breakdown in corrosive environments." *Corrosion Science* 52(3): 748-753.
- [207] Speckert, L. and G. T. Burstein (2011). "Combined anodic/cathodic transient currents within nucleating pits on Al-Fe alloy surfaces." *Corrosion Science* 53(2): 534-539.
- [208] Stelling, O., A. Irretier, et al. (2006). "New light-weight aluminum alloys with high Mg<sub>2</sub>Si-content by spray forming." *Materials Science Forum* 519-521: 1245-1250.
- [209] Sukiman, N. L., N. Birbilis, et al. (2010). *Corrosion Maps For Aluminium Alloys*. Proc. Conf. Corrosion And Prevention '10. Adelaide, Australia, Australasian Corrosion Association (ACA).



- [210] Suryanarayana, C., K. C. Rao, et al. (2008). "Preparation and characterization of microcapsules containing linseed oil and its use in self-healing coatings." *Progress in Organic Coatings* 63(1): 72-78.
- [211] Szklarska-Smialowska, Z. (1999). "Pitting corrosion of aluminum." *Corrosion Science* 41(9): 1743-1767.
- [212] Szklarska-Smialowska, Z. (2002). "Mechanism of pit nucleation by electrical breakdown of the passive film." *Corrosion Science* 44(5): 1143-1149.
- [213] Tahani, A., E. Chaieb, et al. (2003). "Electrochemical study of the influence of rolling on the resistance. The corrosion of alloy of aluminium 3003 in milieu 3% NaCl." *Transactions of the SAEST (Society for Advancement of Electrochemical Science and Technology)* 38(1): 43-46.
- [214] Tailleart, N., B. Gauthier, et al. (2009). Metallurgical and physical factors in improving the corrosion resistance of thermally sprayed semi-amorphous Al-Co-Ce coatings.
- [215] Tan, L. and T. R. Allen (2010). "Effect of thermomechanical treatment on the corrosion of AA5083." *Corrosion Science* 52(2): 548-554.
- [216] Taylor, S. R. and B. D. Chambers (2008). "Identification and Characterization of Non-chromate Corrosion Inhibitor Synergies Using High-Throughput Methods." *Corrosion* 64(3): 255-270.
- [217] Tedim, J., S. K. Poznyak, et al. (2010). "Enhancement of Active Corrosion Protection via Combination of Inhibitor-Loaded Nanocontainers." *Acs Applied Materials & Interfaces* 2(5): 1528-1535.
- [218] Teixeira, J. D. C., L. Bourgeois, et al. (2007). A study of the microstructural evolution and strengthening effects of non-spherical precipitates in an al-cu-based alloy. 561-565: 2317-2320.
- [219] Trueman, A. R. (2005). "Determining the probability of stable pit initiation on aluminium alloys using potentiostatic electrochemical measurements." *Corrosion Science* 47(9): 2240-2256.
- [220] Twite, R. L. and G. P. Bierwagen (1998). "Review of Alternatives to Chromate for Corrosion Protection of Aluminum Aerospace Alloys." *Progress in Organic Coatings* 33(2): 91-100.
- [221] Unocic, K. A., P. Kobe, et al. (2006). "Grain Boundary Precipitate Modification for Improved Intergranular Corrosion Resistance." *Materials Science Forum* 519-521: 327-332.
- [222] Usta, M., M. E. Glicksman, et al. (2004). "The effect of heat treatment on Mg<sub>2</sub>Si coarsening in aluminum 6105 alloy." *Metallurgical and Materials Transactions A: Physical Metallurgy and Materials Science* 35 A(2): 435-438.

- [223] Vetrano, J. S., C. H. Henager Jr, et al. (1998). Use of Sc, Zr and Mn for grain size control in Al-Mg alloys.
- [224] Vetrano, J. S., R. E. Williford, et al. (1997). Influence of microstructure and thermal history on the corrosion susceptibility of AA5083. TMS Annual Meeting, Orlando, FL, USA.
- [225] Voevodin, N. N., V. N. Balbyshev, et al. (2003). "Nanostructured coatings approach for corrosion protection." *Progress in Organic Coatings* 47(3–4): 416-423.
- [226] Walmsley, J. C., Ø. Sævik, et al. (2007). "Nature of segregated lead on electrochemically active AlPb model alloy." *Journal of The Electrochemical Society* 154(1): C28-C35.
- [227] Wang, D., D. Battocchi, et al. (2010). "In situ monitoring of a Mg-rich primer beneath a topcoat exposed to Prohesion conditions." *Corrosion Science* 52(2): 441-448.
- [228] Wang, W. t., X. m. Zhang, et al. (2010). "Influences of Ce addition on the microstructures and mechanical properties of 2519A aluminum alloy plate." *Journal of Alloys and Compounds* 491(1-2): 366-371.
- [229] Wei, R. P. (2001). "A model for particle-induced pit growth in aluminum alloys." *Scripta Materialia* 44(11): 2647-2652.
- [230] Westermann, I., O. S. Hopperstad, et al. (2012). "Effect of alloying elements on stage-III work-hardening behaviour of Al -Zn-Mg(-Cu) alloys." *International Journal of Materials Research* 103(5): 603-608.
- [231] White, P. A., A. E. Hughes, et al. (2009). "High-throughput channel arrays for inhibitor testing: Proof of concept for AA2024-T3." *Corrosion Science* 51(10): 2279-2290.
- [232] White, S. R., N. R. Sottos, et al. (2001). "Autonomic healing of polymer composites." *Nature* 409(6822): 794-797.
- [233] Williams, D. E., J. Stewart, et al. (1994). "The nucleation, growth and stability of micropits in stainless steel." *Corrosion Science* 36(7): 1213-1235.
- [234] Williams, G. and H. N. McMurray (2003). "Anion-exchange inhibition of filiform corrosion on organic coated AA2024-T3 aluminum alloy by hydrotalcite-like pigments." *Electrochemical and Solid State Letters* 6(3): B9-B11.
- [235] Wu, B., J. R. Scully, et al. (1997). "Cooperative stochastic behavior in localized corrosion: I. Model." *Journal of The Electrochemical Society* 144(5): 1614-1620.
- [236] Wu, D. Y., S. Meure, et al. (2008). "Self-healing polymeric materials: A review of recent developments." *Progress in Polymer Science* 33(5): 479-522.
- [237] Xu, D. K., N. Birbilis, et al. (2011). "Effect of solution treatment on the corrosion behaviour of aluminium alloy AA7150: Optimisation for corrosion resistance." *Corrosion Science* 53(1): 217-225.

- [238] Yang, B. J., J. H. Yao, et al. (2009). "Al-rich bulk metallic glasses with plasticity and ultrahigh specific strength." *Scripta Materialia* 61(4): 423-426.
- [239] Yasakau, K. A., M. L. Zheludkevich, et al. (2007). "Role of intermetallic phases in localized corrosion of AA5083." *Electrochimica Acta* 52(27 SPEC. ISS.): 7651-7659.
- [240] Yin, T., M. Z. Rong, et al. (2007). "Self-healing epoxy composites - Preparation and effect of the healant consisting of microencapsulated epoxy and latent curing agent." *Composites Science and Technology* 67(2): 201-212.
- [241] Yu, Y., Ø. Sævik, et al. (2005). "Effect of annealing temperature on anodic activation of rolled AA8006 aluminum alloy by trace element lead." *Journal of The Electrochemical Society* 152(9): B327-B333.
- [242] Yu, Y., Ø. Sævik, et al. (2004). "Characterization of lead enrichment on electrochemically activated binary Al-Pb model alloy." *Materials Forum* 28: 270-276.
- [243] Zamin, M. (1981). "ROLE OF Mn In the Corrosion Behavior of Al-Mn Alloys." *Corrosion* 37(11): 627-632.
- [244] Zawrah, M. and L. Shaw (2003). "Microstructure and hardness of nanostructured Al-Fe-Cr-Ti alloys through mechanical alloying." *Materials Science and Engineering: A* 355(1-2): 37-49.
- [245] Zeng, F.-l., Z.-l. Wei, et al. (2011). "Corrosion mechanism associated with Mg<sub>2</sub>Si and Si particles in Al-Mg-Si alloys." *Transactions of Nonferrous Metals Society of China* 21(12): 2559-2567.
- [246] Zhang, W. and G. S. Frankel (2003). "Transitions between pitting and intergranular corrosion in AA2024." *Electrochimica Acta* 48(9): 1193-1210.
- [247] Zhao, Y. H., X. Z. Liao, et al. (2004). "Microstructures and mechanical properties of ultrafine grained 7075 Al alloy processed by ECAP and their evolutions during annealing." *Acta Materialia* 52(15): 4589-4599.
- [248] Zheludkevich, M. L., I. M. Salvado, et al. (2005). "Sol-gel coatings for corrosion protection of metals." *Journal of Materials Chemistry* 15(48): 5099-5111.
- [249] Zhong, J., K. Feng, et al. (2011). Effect of RE on the mechanical properties of 7075 Al alloy. 150-151: 1286-1289.
- [250] Zhou, X., N. Birbilis, et al. (2010). "Kinetic Stability of Aluminium." *Corrosion & Prevention Corrosion*, Adelaide, Australia.
- [251] Zhou, X., Y. Liu, et al. (2011). "Near-Surface Deformed Layers on Rolled Aluminum Alloys." *Metallurgical and Materials Transactions A* 42(5): 1373-1385.
- [252] Zhou, X., C. Luo, et al. (2012). "Study of localized corrosion in AA2024 aluminium alloy using electron tomography." *Corrosion Science* 58: 299-306.

- [253] Zieliński, A., J. Chrzanowski, et al. (2004). "Influence of retrogression and reaging on microstructure, mechanical properties and susceptibility to stress corrosion cracking of an Al-Zn-Mg alloy." *Materials and Corrosion* 55(2): 77-87.
- [254] Zin, I. M., R. L. Howard, et al. (1998). "The mode of action of chromate inhibitor in epoxy primer on galvanized steel." *Progress in Organic Coatings* 33(3-4): 203-210.
- [255] Zou, L., Q.-l. Pan, et al. (2007). "Effect of minor Sc and Zr addition on microstructures and mechanical properties of Al-Zn-Mg-Cu alloys." *Transactions of Nonferrous Metals Society of China* 17(2): 340-345.

## References

- [1] I.J. Polmear, *Light alloys : from traditional alloys to nanocrystals*, 4th ed., Oxford ; Burlington, MA : Elsevier/Butterworth-Heinemann, 2006.
- [2] ASM Handbook, Volume 02 - Properties and Selection: Nonferrous Alloys and Special-Purpose Materials, 1990.
- [3] J.E. Hatch, *Aluminum: properties and physical metallurgy*, Metals Park, Ohio : American Society for Metals, 1984.
- [4] S.M. Mehta, S.R. Patel, *Journal of the American Chemical Society*, 73 (1951) 226-227.
- [5] D.C. Wysor, *Economic Geology*, 11 (1916) 42-50.
- [6] E.P. Flint, W.F. Clarke, *J. Res. Natl. Bur. Stand.*, 36 (1946) 63-106.
- [7] H. Davy, *Elements of Chemical Philosophy: Part 1*, Bradford and Inskeep, New York, 1812.
- [8] F. Wöhler, *Annalen der Physik und Chemie*, 11 (1827) 146-161.
- [9] H.E. Sainte-Claire Deville, *De l'aluminium, ses propriétés, sa fabrication*, Mallet-Bachelier, Paris, 1859.
- [10] in.
- [11] in.
- [12] R.U. Ayres, *Resources, Conservation and Recycling*, 21 (1997) 145-173.
- [13] A.L. Craighill, J.C. Powell, *Resources, Conservation and Recycling*, 17 (1996) 75-96.
- [14] J.R. Davis, *Corrosion of aluminum and aluminum alloys*, Materials Park, OH : ASM International, 1999.
- [15] D.A. Jones, *Principles and Prevention of Corrosion*, 2nd ed., Upper Saddle River, NJ : Prentice Hall, 1996.
- [16] C. Vargel, *Corrosion of Aluminium*, Elsevier, 2004.
- [17] P. Brimblecombe, C.M. Grossi, *TheScientificWorldJournal*, 10 (2010) 116-125.
- [18] E. Dienes, C. Radlbeck, D. Kostas, in, Innsbruck, 2005, pp. 547-554.
- [19] L. Yuan, Z. Han, L. Gao, in, Guilin, 2013, pp. 655-657.
- [20] L.F. Mondolfo, *Aluminium Alloys: Structure and Properties*, Butterworths, 1976.
- [21] J.R. Davis, *Aluminum and Aluminum Alloys*, ASM International, 1993.
- [22] C.R. Brooks, *Heat treatment, structure, and properties of nonferrous alloys* American Society for Metals, Metals Park, OH, 1982.
- [23] J.W. Martin, *Micromechanisms in particle-hardened alloys*, Cambridge University Press, 1980.
- [24] V. Guillaumin, G. Mankowski, *Corrosion Science*, 41 (1998) 421-438.
- [25] T. Srivatsan, D. Lanning, K. Soni, *Journal of Materials Science*, 28 (1993) 3205-3213.
- [26] C.P. Dervenis, E.I. Meletis, R.F. Hochman, *Materials Science and Engineering a-Structural Materials Properties Microstructure and Processing*, 102 (1988) 151-160.
- [27] A. Davoodi, J. Pan, C. Leygraf, S. Norgren, *Journal of The Electrochemical Society*, 155 (2008) C211.
- [28] Y. Liu, Y.F. Cheng, *Materials and Corrosion*, 61 (2010) 211-217.
- [29] A. Davoodi, J. Pan, C. Leygraf, S. Norgren, *Electrochimica Acta*, 52 (2007) 7697-7705.
- [30] P. Premendra, H. Terryn, J.M.C. Mol, J.H.W. de Wit, L. Katgerman, *Materials and Corrosion*, 60 (2009) 399-406.
- [31] R. Goswami, G. Spanos, P.S. Pao, R.L. Holtz, *Metallurgical and Materials Transactions A*, 42 (2010) 348-355.

- [32] D.R. Baer, C.F. Windisch, M.H. Engelhard, M.J. Danielson, R.H. Jones, J.S. Vetrano, *Journal of Vacuum Science & Technology a-Vacuum Surfaces and Films*, 18 (2000) 131-136.
- [33] G. Svenningsen, M.H. Larsen, J.H. Nordlien, K. Nisancioglu, *Corrosion Science*, 48 (2006) 3969-3987.
- [34] S. Ramachandran, K. Jung, J. Narayan, H. Conrad, *Materials Science and Engineering: A*, 435-436 (2006) 693-697.
- [35] V. Guillaumin, G. Mankowski, *Corrosion Science*, 42 (2000) 105-125.
- [36] N. Birbilis, M.K. Cavanaugh, R.G. Buchheit, *Corrosion Science*, 48 (2006) 4202-4215.
- [37] F. Andreatta, H. Terryn, J.H.W. de Wit, *Electrochimica Acta*, 49 (2004) 2851-2862.
- [38] T.S. Srivatsan, *Journal of Materials Science*, 27 (1992) 4772-4781.
- [39] J.W. Martin, *Annual Review of Materials Science*, 18 (1988) 101-119.
- [40] A. Afseth, J.H. Nordlien, G.M. Scamans, K. Nisancioglu, *Corrosion Science*, 44 (2002) 145-162.
- [41] R. Braun, T. Hack, in, 1996, pp. 1635-1640.
- [42] P. Brenner, G.J. Metcalfe, *Journal of the Institute of Metals*, 81 (1953) 261-&.
- [43] D.-H. Choi, B.-W. Ahn, D.J. Quesnel, S.-B. Jung, *Intermetallics*, 35 (2013) 120-127.
- [44] R. Goswami, G. Spanos, P.S. Pao, R.L. Holtz, *Materials Science and Engineering: A*, 527 (2010) 1089-1095.
- [45] I. Oguocha, O. Adigun, S. Yannacopoulos, *Journal of Materials Science*, 43 (2008) 4208-4214.
- [46] J.L. Searles, P.I. Gouma, R.G. Buchheit, *Materials Science Forum*, 396-402 (2002) 1437-1442.
- [47] C. Blanc, G. Mankowski, *Corrosion Science*, 39 (1997) 949-959.
- [48] F. Eckermann, T. Suter, P.J. Uggowitzer, A. Afseth, P. Schmutz, *Electrochimica Acta*, 54 (2008) 844-855.
- [49] G. Svenningsen, M.H. Larsen, J.C. Walmsley, J.H. Nordlien, K. Nisancioglu, *Corrosion Science*, 48 (2006) 1528-1543.
- [50] K.-H. Na, S.-I. Pyun, *Corrosion Science*, 50 (2008) 248-258.
- [51] M.G. Fontana, *Corrosion Engineering*, McGraw-Hill, 1987.
- [52] N. Birbilis, R.G. Buchheit, *Journal of The Electrochemical Society*, 152 (2005) B140.
- [53] R. Ambat, A.J. Davenport, G.M. Scamans, A. Afseth, *Corrosion Science*, 48 (2006) 3455-3471.
- [54] R.G. Buchheit, *Materials Science Forum*, 331 (2000) II/.
- [55] J.F. Li, Z.Q. Jia, C.X. Li, N. Birbilis, C. Cai, *Materials and Corrosion*, 60 (2009) 407-414.
- [56] E.A. Starke Jr, J.T. Staley, *Progress in Aerospace Sciences*, 32 (1996) 131-172.
- [57] I.N. Fridlyander, *Metal Science and Heat Treatment*, 44 (2002) 3-9.
- [58] W.S. Miller, L. Zhuang, J. Bottema, A.J. Wittebrood, P. De Smet, A. Haszler, A. Vieregge, *Materials Science and Engineering: A*, 280 (2000) 37-49.
- [59] R.C. Dorward, T.R. Pritchett, *Materials & Design*, 9 (1988) 63-69.
- [60] M.D. Halliday, C. Cooper, P. Bowen, *International Journal of Fatigue*, 29 (2007) 1195-1207.
- [61] P.S. Pao, S.J. Gill, C.R. Feng, *Scripta Materialia*, 43 (2000) 391-396.
- [62] E.J. Lavernia, N.J. Grant, *Journal of Materials Science*, 22 (1987) 1521-1529.
- [63] C. Giummarra, B. Thomas, R.J. Rioja, *Proceedings of the Light Metals Technology Conference*, (2007).
- [64] R. Rioja, J. Liu, *Metallurgical and Materials Transactions A*, 43 (2012) 3325-3337.

- [65] V.S. Sinyavskii, *Protection of Metals*, 37 (2001) 469-478.
- [66] M.H. Larsen, J.C. Walmsley, O. Lunder, R.H. Mathiesen, K. Nisancioglu, *Journal of The Electrochemical Society*, 155 (2008) C550-C556.
- [67] J. Gao, D.J. Quesnel, *Metallurgical and Materials Transactions A*, 42 (2010) 356-364.
- [68] R. Goswami, G. Spanos, P.S. Pao, R.L. Holtz, *Metallurgical and Materials Transactions A: Physical Metallurgy and Materials Science*, 42 (2011) 348-355.
- [69] S. Jain, M.L.C. Lim, J.L. Hudson, J.R. Scully, *Corrosion Science*, 59 (2012) 136-147.
- [70] M.L.C. Lim, J.R. Scully, R.G. Kelly, *Corrosion*, (2012).
- [71] R.H. Jones, D.R. Baer, M.J. Danielson, J.S. Vetrano, *Metallurgical and Materials Transactions A: Physical Metallurgy and Materials Science*, 32 (2001) 1699-1711.
- [72] M.K. Cavanaugh, in: *Materials Engineering Department, Ohio State University*, 2009.
- [73] K. Jones, D.W. Hoepfner, *International Journal of Fatigue*, 31 (2009) 686-692.
- [74] K. Jones, S.R. Shinde, P.N. Clark, D.W. Hoepfner, *Corrosion Science*, 50 (2008) 2588-2595.
- [75] P.D. Merica, R.G. Waltenberg, A.N. Finn, *Transactions of the American Institute of Mining and Metallurgical Engineers*, 64 (1921) 29-40.
- [76] A.C. Zimmerman, *Industrial and Engineering Chemistry*, 17 (1925) 359-362.
- [77] E. Wilson, *Proc. Phys. Soc. Lond.*, 39 (1927) 0015-0025.
- [78] H. Sutton, K.J. Sidery, *Journal of the Institute of Metals*, 38 (1927) 241-257.
- [79] E.H. Dix, J.J. Bowman, *Transactions of the American Institute of Mining and Metallurgical Engineers*, 117 (1935) 357-368.
- [80] F.A. Champion, *Journal of the Institute of Metals*, 83 (1955) 385-&.
- [81] W.D. Robertson, *Transactions of the American Institute of Mining and Metallurgical Engineers*, 166 (1946) 216-228.
- [82] P. Brenner, W. Roth, *Journal of the Institute of Metals*, 74 (1948) 159-&.
- [83] E. Herzog, G. Chaudron, *Comptes Rendus Hebdomadaires Des Seances De L Academie Des Sciences*, 196 (1933) 2002-2003.
- [84] G. Siebel, H. Vosskuhler, H. Sutton, *Journal of the Institute of Metals*, 74 (1948) 646-652.
- [85] B.M. Thall, B. Chalmers, *Journal of the Institute of Metals*, 77 (1950) 79-&.
- [86] M. Shibata, S. Mishi, *Keikinzoku/Journal of Japan Institute of Light Metals*, 33 (1983) 131-136.
- [87] H.S. Campbell, *Ocean Engineering*, 1 (1969) 387-&.
- [88] L.F. Mondolfo, *Light Met Age*, 37 (1979) 20, 22-24.
- [89] O. Seri, K. Tagashira, *Keikinzoku/Journal of Japan Institute of Light Metals*, 36 (1986) 806-812.
- [90] D.L. Robinson, M.S. Hunter, *Metall Trans*, 3 (1972) 1147-1155.
- [91] J. Busby, J.F. Cleave, R.L. Cudd, *J Inst Metals*, 99 (1971) 41-49.
- [92] J.M. Truscott, D.S. Calvert, *Journal of the Institute of Metals*, 95 (1967) 289-&.
- [93] P. Doig, J.W. Edington, *British Corrosion Journal*, 9 (1974) 22-25.
- [94] M.A. Reynolds, J.G. Harris, *Aluminium*, 50 (1974) 592-597.
- [95] K. Sugimoto, Y. Sawada, S. Morioka, *Trans Jap Inst Met*, 13 (1972) 345-351.
- [96] Y. Baba, M. Hagiwara, J. Hamada, *J Inst Met (London)*, 100 (1972) 309-312.
- [97] Z. Ahmad, A. Afshar, *Anti-Corrosion Methods and Materials*, 25 (1978) 10-13.
- [98] T. Saito, *J Jap Inst Light Met*, 22 (1972) 403-416.
- [99] H. Yoshida, Y. Baba, *Journal of Japan Institute of Light Metals*, 31 (1981) 20-29.
- [100] R.L. Jones, S. Murphy, *British Corrosion Journal*, 18 (1983) 123-131.
- [101] H. Yoshida, T. Uno, Y. Baba, *Sumitomo Keikinzoku Giho/Sumitomo Light Metal*

Technical Reports, 25 (1984) 1-17.

[102] Y. Kishi, Y. Hirose, I. Tsukuda, S. Nagai, K. Higashi, *Zairyo/Journal of the Society of Materials Science, Japan*, 43 (1994) 1113-1119.

[103] Y.L. Wu, F.H. Froes, C. Li, A. Alvarez, *Metallurgical and Materials Transactions A: Physical Metallurgy and Materials Science*, 30 (1999) 1017-1024.

[104] W.N. Garrard, *Corrosion*, 50 (1994) 215-225.

[105] Ø. Sævik, Y. Yu, J.H. Nordlien, K. Nisancioglu, *Journal of The Electrochemical Society*, 152 (2005) B334-B341.

[106] T.S. Srivatsan, E.J. Coyne, E.A. Starke, *Journal of Materials Science*, 21 (1986) 1553-1560.

[107] W.A. Cassada, G.J. Shiflet, E.A. Starke, *MTA*, 22 (1991) 287-297.

[108] J.-f. Li, W.-j. Chen, X.-s. Zhao, W.-d. Ren, Z.-q. Zheng, *Transactions of Nonferrous Metals Society of China*, 16 (2006) 1171-1177.

[109] R.G. Buchheit, F.D. Wall, G.E. Stoner, J.P. Moran, *Corrosion*, 51 (1995) 417-428.

[110] C. Kumai, J. Kusinski, G. Thomas, T.M. Devine, *Corrosion*, 45 (1989) 294-302.

[111] G. Scamans, N. Birbilis, R.G. Buchheit, *Corrosion of Aluminium and Aluminium Alloys in: Shrier's Corrosion*. (Eds. T. Richardson). Elsevier, 2010.

[112] E.J. Lavernia, T.S. Srivatsan, *Journal of Materials Science*, 45 (2010) 287-325.

[113] R.G. Buchheit, *Journal of The Electrochemical Society*, 142 (1995) 3994-3996.

[114] G.O. Ilevbare, O. Schneider, R.G. Kelly, J.R. Scully, *Journal of The Electrochemical Society*, 151 (2004) B453-B464.

[115] S. Evans, E.L. Koehler, *Journal of The Electrochemical Society*, 108 (1961) 509-514.

[116] S.W. Dean Jr, in, *NACE*, Boston, MA, USA, 1985, pp. 76. 71-76. 20.

[117] S.B. Brummer, F.H. Cocks, Bradspie.Ji, *Electrochimica Acta*, 16 (1971) 2005-&.

[118] F. Øvari, L. Tomcsányi, T. Túrmezey, *Electrochimica Acta*, 33 (1988) 323-326.

[119] W.S. Tait, *An Introduction to Electrochemical Corrosion Testing for Practicing Engineers and Scientists*, Pair O Docs Publications, Racine, Wisconsin, 1994.

[120] E. McCafferty, *Corrosion Science*, 47 (2005) 3202-3215.

[121] A. International, in: *ASTM Standard G1-03*, ASTM International, West Conshohocken, PA, 2011.

[122] A.J. Bard, L.R. Faulkner, *Electrochemical Methods*, John Wiley & Sons Inc., New York, 2001.

[123] I. Miller, *Probability and Statistics for Engineers*, Prentice-Hall, Englewood Cliffs, NJ, 1985.

[124] G.S. Frankel, *Journal of The Electrochemical Society*, 145 (1998) 2186-2198.

[125] Z. Szklarska-Smialowska, *Corrosion Science*, 41 (1999) 1743-1767.



# Chapter 3

## Research Aims

---

### 3.1 Research Aims

The literature review reveals that, in spite of the wide usage of aluminium, a paucity of reported archival work exists which has focused on the development of more corrosion resistant Al-alloys; particularly in regards to compositional selection or balancing industrially useful properties. Whilst this may be occurring in the laboratories of the aluminium producers, it has not been reported in the readily available literature. Instead, what is observed in the literature is a focus on the understanding of the corrosion of existing commercial alloys, as opposed to the use of corrosion engineering to produce new Al-alloys. It is hypothesised that by controlling chemistry and microstructure it is possible to develop Al-alloys that are more corrosion resistant for equivalent or better mechanical properties. This statement is all encompassing, and obviously includes such wide notions that cannot be met in a single doctoral thesis. Therefore, a distinct effort has been made in this thesis to concentrate on aspects that are either foundational, or focused, in order to contribute towards the rationalisation of the hypothesis.

As such, the thesis, within limits, seeks to understand the key role of chemical variables in affecting electrochemical / corrosion behaviour, and use this as a basis to establish an elementary foundation for the improvement / development of an experimental, optimised, alloy.

The objectives of this project can be summarised as the following:

1. Understanding the corrosion rate vs. hardness property space in order to rationalise the development of new Al-alloys with superior corrosion resistance while maintaining one mechanical metric (we have not considered multiple properties such as ductility or fracture). This aim will require parallel testing to determine which corrosion metric is most appropriate for determination of this property space.
2. Understanding the effect of alloying elements in relation to the electrochemical

response of Al-alloys. This aim will involve a round-robin of electrochemical tests and a broad range of alloying elements to demonstrate the changes of anodic and cathodic kinetics with alloying.

3. An understanding of the effect of alloying elements upon the microstructure of Al-alloys. This involves electron microscopy imaging of a wide range of experimental alloys. Corrosion tests couple with characterisation allowing for a rationalisation of corrosion response.
4. Understanding the effect of alloying elements to the extent and morphology of corrosion that will occur. This aim will involve different type of corrosion testing methods and subsequent profilometry
5. Production of experimental Al-alloys with beneficial alloying elements (or exclusion of deleterious alloying elements) from points 1 to 4. This will form the basis of the latter portion of the work.

Whilst the work and its purpose are consolidated in each subsequent chapter, to orient the reader, an important explanatory introduction should be given here.

The work in this thesis continued to evolve with the learning's from initial experiments. It was determined in the attainment of the primitive property space (in Chapter 4) that there exists some opportunities for optimising (i.e. minimising) the corrosion of Al-alloys. This included reducing Cu, and avoiding microstructural heterogeneity. Also identified as the current 'best compromise' alloy was AA5083, which has medium strength and low corrosion rates. The realisation of property space suggested that efforts should either be focused on reducing corrosion rates of age hardenable alloys (i.e. 2xxx or 7xxx series), or increasing the strength of non-age hardenable alloys (i.e. 5xxx) series, with the 6xxx series being somewhere in between. For the purposes of avoiding additional experimental variables such as heat treatments and complex thermal and thermomechanical schedules. It was decided (after an initial attempt with 6xxx series documented in Chapter 4), that the remainder of the work would focus on the non-heat treatable 5xxx Al-Mg-Mn system.

## 3.2 Dissertation Outline

This dissertation consists of nine chapters and the findings of this work are presented in published and/or submitted papers in internationally recognised journals and one invited book chapter. The papers and chapter are worked into the thesis in the relevant sections, including co-authored papers where the work was carried out under the auspices of the activity in the PhD. The detailed descriptions of the chapters are as the following:

### Chapter 1: Introduction

This chapter provides a general overview of the project that serves as an introduction to the initial ideas, background concept and the rationale of this work.

### Chapter 2: Literature review

In this chapter, an extensive coverage of the literature on Al-alloys and corrosion behaviour is reviewed. This includes discussion on the role of chemistry and microstructure on corrosion, electrochemical aspect of corrosion and methods to improve corrosion resistance of Al-alloys.

### Chapter 3: Research Aims

The research aims of this project are listed in this chapter. It also includes the outline of the dissertation and a brief section on the methodology of this project.

### Chapter 4:

This chapter demonstrates the effect of chemistry on the corrosion kinetics of commercial Al-alloys. A detailed discussion on the electrochemical response of microstructurally driven localised attack is also included.

### Chapter 5

This chapter discusses the general corrosion behaviour in relation to microalloying of the 5xxx Al-alloy with a broad range of alloying elements. The work also covers the results from initial works that would have included 6xxx alloys (and hence the study of the Mg<sub>2</sub>Si phase). This was included on the basis that it is another demonstration of the role of microstructure and microstructural heterogeneity. This then leads into the work that investigated the microstructure-corrosion relationship in some quantitative detail (via potentiostatic

transients), emphasising the key points made in Chapter 4 via original research.

#### Chapter 6

A more focused appraisal on the effect of microalloying to intergranular corrosion of 5xxx Al-alloys is deliberated with a focus on phase analysis and sensitisation behaviour.

#### Chapter 7

This chapter focuses on specific alloying elements that improve corrosion resistance of 5xxx Al-alloys while retaining the other properties on par with a benchmark alloy (AA5083).

#### Chapter 8

A consolidating discussion that relates the findings described in the body of work to the literature on this subject. Several recommendations on future work are also deliberated.

#### Chapter 9

This chapter presents the Conclusions of the overall findings and accomplishment of the research aims listed in Chapter 3.

### 3.3 Laboratory Testing and Setup

In order to augment the limited experimental details in the subsequent sections, a supplementary section here provides some further experimental details and imagery for the purposes of reproduction and disclosure.

#### 3.3.1 Materials

The alloys (in the form of commercial or master alloys) for this project were sourced from a combination of:

- Alcan (Canada), Courtesy of Dr. Nick Parson
- Chalco (China), Courtesy of ICLAR collaboration
- DSTO (Fishermans Bend, Australia), Courtesy Prof. Stan Lynch
- Alcoa (United States), Alfa-Aeser (United States), Delphi (United States) or Airport Metals (Tullamarine, Australia), acquired commercially

#### 3.3.2 Alloy Production

To meet the aim of this project, a range of experimental alloys have been produced at Monash using open air casting using a muffle furnace, housed in the Department of Materials Engineering, Monash University.

Alloy production involved the introduction of solid feedstock in the form of pellets  $\leq 1\text{cm}\varnothing$ . In all cases, pure Al 99.95 (Alfa-Aeser) is blended with master alloys to form the final composition. Master alloys include Al-4Cu, Al-2Sc, Mg-9Al, Mg-10Si, Al-2.5Sr; which are blended with pure Al and in some instances, portions of commercial alloys, to achieve the final target composition. Images of the relevant aspects of alloy production and processing are shown overleaf. Melting was carried out in a muffle furnace. Regular stirring of the melt was carried out, followed by casting into a pre-heated (at  $\sim 300^\circ\text{C}$ ) graphite crucible to prevent shrinkage. Cast alloys were homogenised below the liquidus temperature (nominally at  $400^\circ\text{C}$ ) for two days, and then cold rolled to a 50 % thickness reduction. The work flow of the in-house alloy making process is shown in Figure 3.1.

In all cases where composition of alloys is given within this report, the compositions were measured by an accredited external laboratory; Spectrometer Services (Coburg, Australia). The testing method was ICP-AES (inductively coupled plasma atomic emission

spectroscopy).

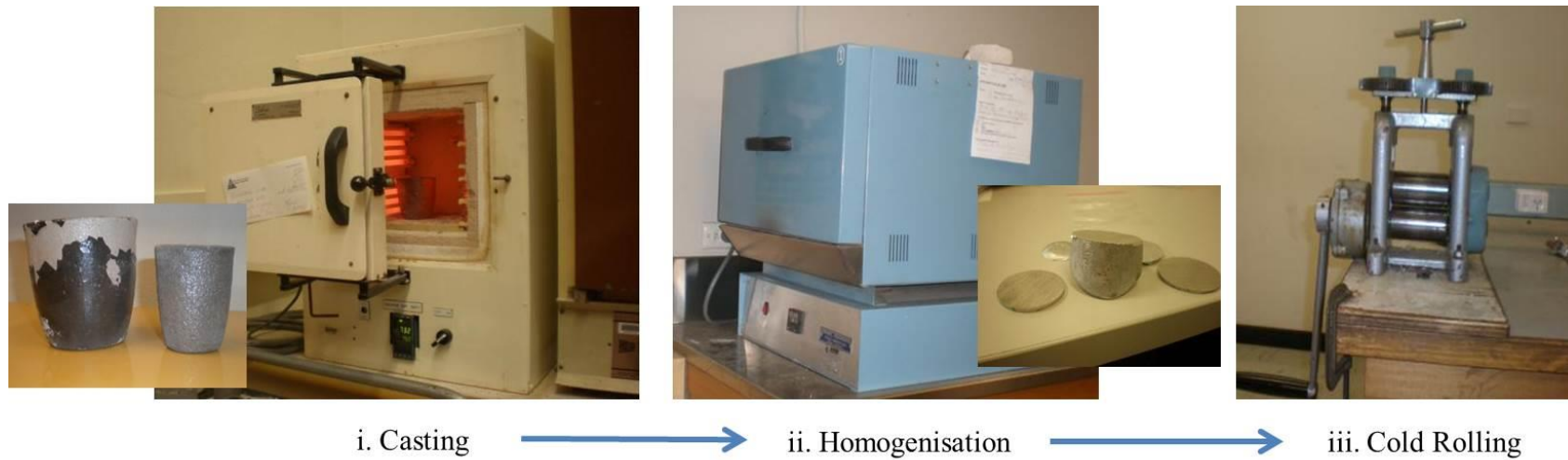


Figure 3.1: Work flow of the in-house alloy production process. The insert image in (i) shows the type of crucibles used in this study. The bigger crucible used for mixing and smaller crucible for casting. After homogenisation (ii), the cast alloy was cut into smaller pieces for further testing.

### 3.3.3 Electrochemical Testing

Potentiodynamic polarisation (PDP) tests were performed using a standard 3-electrode flat-cell (supplied by PAR) and a Biologic VMP3 potentiostat under the control of EC-Lab<sup>®</sup> software shown in Figure 3.2. A saturated calomel electrode (SCE) was used as a reference electrode and platinum mesh was used as a counter electrode. The electrolyte used in all test was 0.1M NaCl. This electrolyte was chosen as it represents a moderately aggressive environment (which will allow discrimination of comparative alloy performance), it is also considered a first order simulant to atmospheric exposure, and it also allows for comparison between results of others in the literature. For PDP tests, potential was scanned at  $1\text{mV.s}^{-1}$ . Such testing is destructive and hence samples were tested in a 'one off' manner. Additionally, electrochemical impedance spectroscopy (EIS) was also performed on samples and EIS spectra were collected over the range of 500kHz to 5mHz in the potential range of OCP $\pm$ 10mV, and analysed using EC-Lab<sup>®</sup> software.



Figure 3.2: Biologic VMP3 potentiostat

The set-up in Figure 3.3(a) is typically used for an individual sample for a short term test. However, in some circumstances, a large amount of samples are required to be tested particularly after a long term exposure. An improvised version of electrochemical cell that able to fit up to 16 samples at a time was fabricated as demonstrated in Figure 3.3(b). This set-up was found to tremendously increase the productivity of the testing.



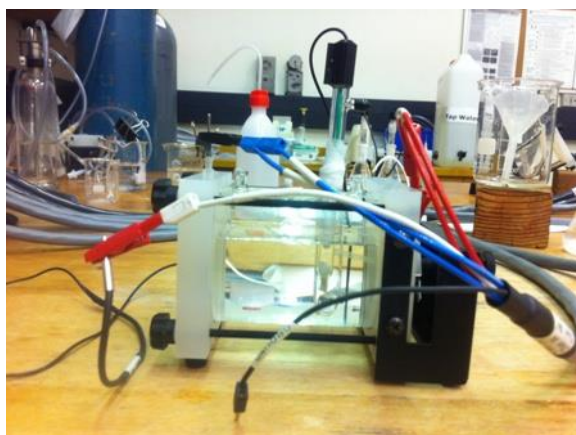


Figure 3.3(a): A 3-electrode electrochemical cell for individual sample

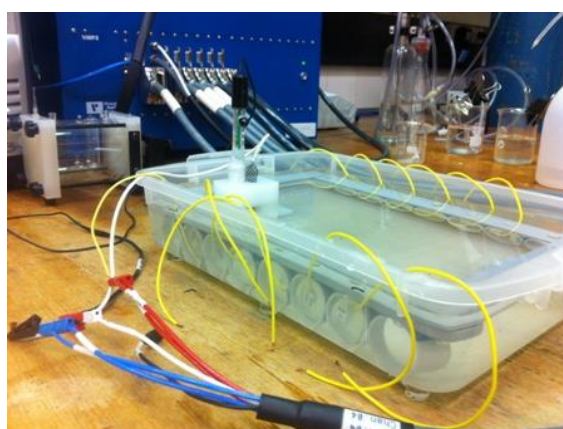


Figure 3.3(b): A custom version of the 3-electrode electrochemical cell for high throughput and long term testing of numerous specimens

### 3.3.4 Mass Loss Testing

Immersion (mass loss) tests were performed for samples immersed in 0.1M NaCl for 14 days. Following immersion, corrosion products were removed by a short immersion (~15s) and light rubbing with a soft-bristle brush in 7% nitric acid solution prior to final weighing. This solution was used in order to preserve the original morphology of the corrosion attack for subsequent profilometry.

### 3.3.5 Surface Characterisation

#### *Optical Profilometry*

The morphology of the immersion samples were analysed using optical profilometry (Veeco Wyko) shown in Figure 3.4. Pitting attributes such as average pit depth, number of pits and the volume of pits were calculated with the assistance of Veeco Vision software package.

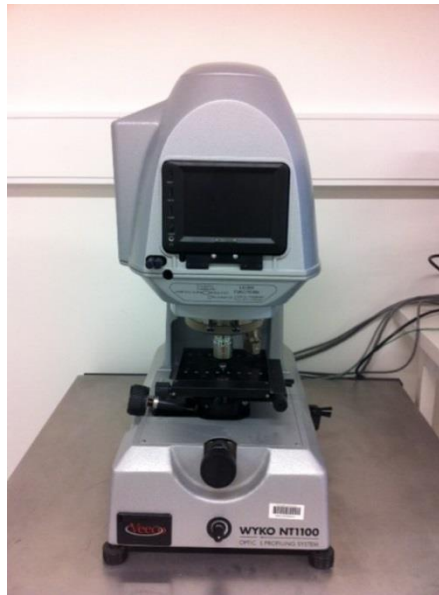


Figure 3.4: Veeco Wyko NT1100 optical profilometry

#### *Scanning Electron Microscopy (SEM)*

Selected microstructures were characterised using a FEI Quanta 200 SEM at The Ohio State University and Royal Melbourne Institute of Technology (RMIT) to identify the presence and nature of particles within the microstructure. All samples were prepared by metallographic polishing down to a 1 $\mu$ m finish followed by ultrasonic cleaning. The images were observed using back-scattered electron (BSE) mode and the chemical composition of the particles was analysed with energy-dispersive X-ray (EDX) spectroscopy.

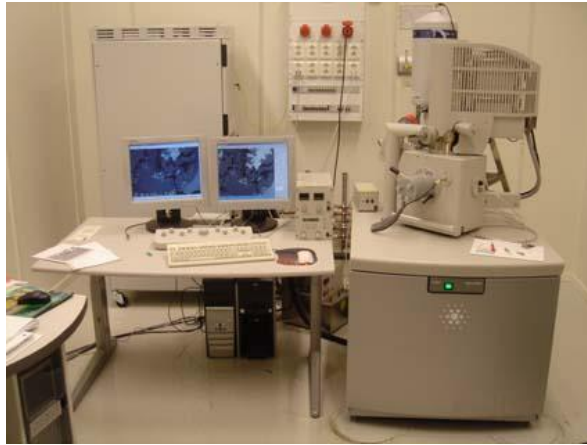


Figure 3.5: FEI Quanta 200 Scanning Electron Microscope

### 3.3.6 Hardness Testing

Vickers hardness testing was performed using a Duramin A300 Hardness Tester employing a 1 kg load. This method of mechanical testing was preferred, as a number of duplicate measurements were possible, and the testing could be performed in house on all specimens.

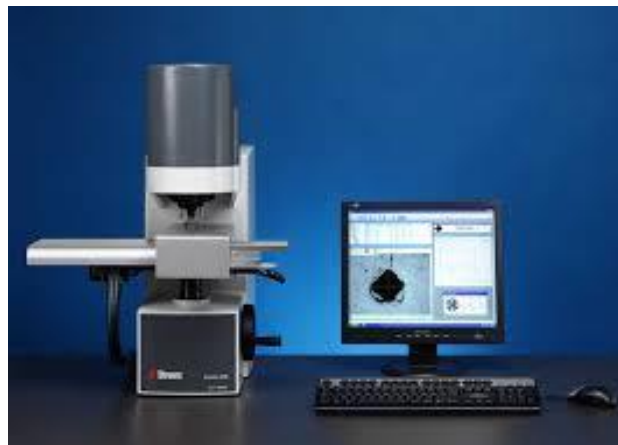


Figure 3.6: Duramin A300 hardness tester

### 3.3.7 Calculation of Phase Diagrams (CALPHAD)

To assist in interpretation of alloy characterisation, CALPHAD and phase analysis was carried out using Pandat® software package (CompuTherm LLC, Madison, WI). This software is capable of calculating the most stable phase equilibrium without requiring prior knowledge of the diagram by using algorithm that is based on the mathematical and thermodynamic properties between the Gibbs free energy and stable phase equilibrium [1, 2]. The PanAluminum database was used for thermodynamic calculations in this work.

### **References**

- [1] W. Cao, S.L. Chen, F. Zhang, K. Wu, Y. Yang, Y.A. Chang, R. Schmid-Fetzer, W.A. Oates, Calphad, 33 (2009) 328-342.
- [2] S.L. Chen, S. Daniel, F. Zhang, Y.A. Chang, X.Y. Yan, F.Y. Xie, R. Schmid-Fetzer, W.A. Oates, Calphad, 26 (2002) 175-188.

# Chapter 4

## The construction of Al-alloy property space

---

This chapter is presented in the format of a research paper. The purpose of this was to provide the relevant flow and experimental variables for a consolidated presentation. The works in this chapter include characterising the corrosion response (using a variety of laboratory methods) of commercial Al-alloys towards the construction of a primitive property space as a first order means of highlighting opportunities in minimising corrosion whilst being aware of mechanical strength. Combination of immersion tests and electrochemical tests including potentiodynamic polarisation and electrochemical impedance spectroscopy (EIS) were carried out on various commercial Al-alloys which were acquired from a number of wide sources. A consolidated presentation of the role of chemistry on the corrosion kinetics and hardness (used herein as a simplistic proxy to strength) suggested that reducing/eliminating Cu and limiting microstructural heterogeneity are effective in minimising corrosion (as discussed). It was empirically revealed that AA5083 (Al-4.4Mg-0.5Mn), which has medium strength and low corrosion rates, was evident as the ‘best compromise’ (commercial) alloy; further explored in this project with the following chapters of this thesis will focus on works to understand and improve the performance of the non-heat treatable Al-Mg-Mn alloy system.

This chapter (Chapter 4), in spite of being a wide empirical study, has revealed significant insights that are previously unreported, and hence serves as one of the original outcomes to the field arising from this thesis.

#### **4.1 A consolidated presentation of bulk chemical effects on the corrosion kinetics of some commercial wrought aluminium alloys**

##### **Introduction**

Aluminium (Al) alloys can be found in various applications ranging from household items to aerospace alloys. The role of alloying elements is critical in achieving a range of physical properties including strength, ductility, fracture and fatigue properties. It is established that relatively pure aluminium presents high corrosion resistance. Nevertheless, in open-air solutions or atmospheric conditions containing halide ions, aluminium is susceptible to pitting corrosion [1-3]. Alloys with heterogeneous microstructures arising from alloying can also possess localised corrosion susceptibility, even in benign aqueous environments [4-7]. Further practical reasons why aluminium can undergo corrosion include the formation of a near surface deformed layer (NSDL) from mechanical finishing [8], and shingling [9].

Al-alloys are prone to all known forms of corrosion including pitting, crevice, general, filiform, and intergranular forms. It is acknowledged that a large number of physical and environmental variables play a key role in the corrosion of Al-alloys, from alloy casting and processing, to electrolyte chemistry. In this study, we do not (and cannot) attempt to do all such relevant aspects justice, and instead attempt to focus on the basic influence of chemical effects as studied from commercially available alloys for the following specific outcome.

1. A paucity in consolidated information regarding the solubility of elements in Al (this aspect being a review exercise).
2. A need to holistically represent the electrochemical impact of alloying elements upon reaction kinetics. Herein we reveal a phenomenological representation of this based on a large database of tests (and supplemented by review) to reveal the impact on anodic and cathodic branches of the polarisation curves at room temperature.
3. A sensitivity analysis of the influence of alloying elements for alloy corrosion based on the alloys studied herein at room temperature.

As described above, this work here is concerned with the determination of relatively short-term corrosion (from electrochemical and mass loss tests in 0.1M NaCl at room temperature)

and is not targeted towards the information from long term exposure site testing or environmentally assisted cracking; with such information available from handbooks reporting results from standard ASTM tests [10-12]. Furthermore, the relationships regarding corrosion propagation in the form of environmentally assisted cracking are indeed unique and complex, as recently pointed out by an excellent review by Holroyd and Scamans for Al-Zn-Mg-Cu alloys [13]. The most common alloying elements in commercial aluminium alloys are magnesium, copper, silicon, manganese, and zinc [14]. Alloying elements can increase heterogeneity of the microstructure by introducing precipitate particles (when they stimulate a second phase), along with the potential presence of constituent particles that arise from impurities, or dispersoid particles used for grain size control. These phases have different electrochemical characteristics than the surrounding matrix, and can be classified as either 'cathodic' or 'anodic' with respect to the alloy matrix, which then relates to the subsequent corrosion damage morphology. A comprehensive background to aluminium metallurgy has been given by Polmear [14], Hatch [15] and Mondolfo [16]. Such monographs, in conjunction with the relevant phase diagrams, reveal the types of second phases that may form in aluminium alloys as a function of chemistry and thermomechanical processing. However, herein we present the solubility of elements in Al, from a review of the relevant literature – and present it in a unique manner in Figure 1. The information in Figure 1 classifies each element as to whether it is soluble (i.e. > 1wt.%), slightly soluble (i.e. < 1 wt.%), insoluble, or unknown. The extent of solubility is also given. We believe that this presentation is of general utility to the Al corrosion community, as the consolidated presentation does not exist elsewhere.

#### *Influence of thermomechanical processing and temper.*

A detailed description of thermomechanical processing and temper effects is not included herein, however to provide a balanced view, such aspects merit comment. Of the aluminium alloys, whilst a large number of commercial alloys, there is only a finite number of precipitation hardening systems that are common to commercial alloys. These include systems that stimulate the development of the following phases;  $\text{Al}_2\text{CuMg}$  (in 2xxx alloys),  $\text{Mg}_2\text{Si}$  (in 6xxx alloys),  $\text{MgZn}_2$  (in 7xxx alloys), and to a lesser volume,  $\text{Al}_2\text{CuLi}$  (in 2xxx alloys). The corrosion of these alloys is influenced by the number density and size range of the precipitates. The number density and size range is dictated by the thermomechanical processing (i.e. extent of reduction which can influence dislocation density and grain size)

and the temper (which can dictate the precipitate size and volume fraction). In addition, the above finite precipitate systems are also complicated by minor compositional variations of the precipitates themselves, which is pronounced in their influence upon corrosion propagation. Classic examples include the doping of  $\text{MgZn}_2$  with Cu (in Cu rich 7xxx alloys) to moderate IGC and SCC [13, 17, 18], and the modification of the Mg/Si ratio in 6xxx alloys [19-21].

As a consequence, for age hardenable systems, the corrosion response is a continuum that scales with precipitate size and volume, and the possible dynamic evolution of precipitate chemistry. Of studies which offer electrochemical insight into the evolution of corrosion response with precipitate evolution, there is significant paucity of information in the open literature. Some studies that have coupled high-resolution characterisation (a requirement in such works) with corrosion response in tracking corrosion as a function precipitate characteristics involve the work of Ralston *et al.* (tracking the evolution of  $\text{Al}_2\text{CuMg}$ ) [6, 22] and Gupta *et al.* (tracking the evolution of  $\text{MgZn}_2$ ) [17], additionally Liang *et al.* have also done a similar study for 6xxx alloys (tracking  $\text{Mg}_2\text{Si}$ ), however characterisation in that work remains pending. What was observed in such works is that pitting susceptibility was dictated when a critical precipitate size distribution was reached (in all cases) and the extent of the susceptibility was dictated by the precipitate chemistry. It was also shown that there is a relationship between the precipitate state and alloy strength [22], which is an important link. Such studies were complex, and indicate that there is still significant future work remaining to unravel the microstructural effects on corrosion of Al-alloys generally, however a precursor to such a deterministic achievement is the basic holistic presentation of chemical effects on corrosion of Al-alloys; the goal of this study. We again emphasise that the work herein is focused on relatively short-term corrosion results at room temperature, and does not tackle corrosion propagation modes such as IGC and SCC; more specifically the superficial and pitting responses are studied (being the precursors to propagation modes of attack).



## Experimental

The materials tested herein were acquired from a variety of sources including Alfa-Aesar, Alcan, Comalco (which is now part of the Rio Tinto group, for some legacy alloys) and DSTO. The alloys tested are listed in the corresponding figures, however the compositions as determined from ICP-AES (Spectrometer Services, VIC, Australia) are presented in the Table 2.

All samples used were ground under ethanol to 1200 grit using SiC paper prior to testing. The electrolyte used in all test was quiescent 0.1M NaCl. Potentiodynamic polarisation tests were performed using a scan rate of at  $1\text{mV.s}^{-1}$  and a standard 3-electrode flat-cell (PAR) employing a saturated calomel reference electrode and Pt-mesh counter electrode. Electrochemical impedance spectroscopy was also performed on samples continuously immersed for a period of 1, 3, 7 and 14 days. EIS spectra were collected over the range of 500kHz to 5mHz in the potential range of OCP $\pm$ 10mV, and analysed using EC-Lab<sup>®</sup>.

Immersion (mass loss) tests were performed for samples immersed in 0.1M NaCl for 14 days. Following immersion, corrosion products were removed by a short immersion (~15s) and light rubbing with a soft-bristle brush in 7% nitric acid solution prior to final weighing. This solution was used in order to preserve the original morphology of the corrosion attack for subsequent profilometry (shown to be effective in [23, 24]). The microstructure and morphology of the immersion samples were analysed using SEM and optical profilometry (Veeco Wyko). Pitting attributes such as average pit depth, number of pits and the volume of pits were calculated with the assistance of Veeco Vision software package.

Vickers hardness testing was performed using a Duramin A300 Hardness Tester using a 1kg load. This method of mechanical testing was preferred, as a large number of replicate measurements were possible, and the testing could be performed in-house on all specimens. Further, many of the alloy geometries (small ingots or thin sheets) were incompatible to tensile testing. For some representative yield strength values, readers are referred to [10, 25] and alloy manufacturer spec-sheets [26].

## Results & Discussion

### *Electrochemical characteristics of Al-alloys*

To represent the general electrochemical response of some typical Al-alloys, the polarisation response is shown in Figure 1.

From Figure 1a we observe that differing alloys have rather different electrochemical characteristics, namely in the  $E_{\text{corr}}$  value, and when viewed in summary, in the relative rates of cathodic reactions and to a lesser extent, anodic reactions. It is observed that pure Al has the least noble  $E_{\text{corr}}$  by several hundreds of millivolts for the examples given. The  $E_{\text{corr}}$  values increase with increasing alloying additions used as examples here and this ennoblement is not due to a retardation of the anodic reaction, but largely due to an increase in the cathodic reaction kinetics. AA2024-T3 and AA7150-T773 show significantly higher  $E_{\text{corr}}$  values owing to the heavy alloying additions that include appreciable levels of Cu (and significant levels of Zn, Mg and Cu in the latter), and to the obvious existence of constituent and precipitate particles (discussed further below) [27-32]. From Figure 1a, there is minimal alteration in the  $E_{\text{pit}}$  value between the alloys, however the difference between  $E_{\text{corr}}$  and  $E_{\text{pit}}$  is significantly diminished with increasing alloying additions [33-36]. A slight decrease in the anodic kinetics is seen in the case of alloying, suggesting that alloying additions in the matrix may moderate the dissolution of pure Al to an extent. The purpose of Figure 1a is not to contribute significant mechanistic interpretation that can be deduced from various works that study Al electrochemistry in detail [30, 37-46], along with the associated electrochemistry of intermetallics [4, 7, 44, 47-53], but to show the general trends in the form of the electrochemical data.

An alternate approach regarding electrochemical analysis is to measure the impedance of alloys as seen in Figure 1b. The Nyquist plot provides the charge transfer resistance measurement of the alloys tested in this work. The trends from impedance data were seen in this work to mimic those of polarisation tests (and indeed immersion tests as discussed in the following section). Impedance data was collected herein in addition to potentiodynamic polarisation and mass loss to establish the basic link between alteration of anodic / cathodic kinetics and ground truth data (mass loss). Further, profilometry also gives information regarding localisation of corrosion. As such, of the many hundreds of tests that have contributed to this study, the combination of methods has itself been illuminating – with each

test has its relative merits and demerits – however the combination of tests providing a holistic picture.

### *Corrosion survey of Al-alloys*

Figure 2 represents the consolidated presentation of the mass loss values determined for the alloys tested in this work. In order to show the data as a spread of results as opposed to a table or bar chart, we have plotted the mass loss versus the alloy hardness as determined herein. This does not necessarily imply a relationship between the parameters, but it is of interest to note that for finite range of commercial alloys tested in this work, there is a correlation between higher mass loss being associated with alloys that have the highest measured hardness (the inset of Figure 2 shows the data on a log-log plot of the same data, to indicate the data spread). In this case we show mass loss following 2 weeks immersion; however we correlate this with pitting and electrochemistry further below.

Figure 2 is illuminating on the basis that a spread of an order of magnitude was determined for corrosion levels realised of the commercial alloys surveyed. A more detailed correlation between the parameters plotted will not be given, as the corrosion varies with aging time in alloys [50, 54-59] that undergo age hardening. As such, temper dependant variations would be seen in such alloys with a finite window. This temper dependence will influence both mechanical and corrosion properties, as shown by Ralston *et al.* [22], however in such individual instances there is also a correlation reported in specific detail regarding mechanical and corrosion performance. None the less, the data in Figure 2 is accurate for a given set of known conditions and alloys in their commercially available form, and for the alloys that have been tested. The information it is possible to deduce the following, independently of the reported hardness values:

- a) Pure Al and solid solution alloys occupy the low corrosion / mass loss space
- b) Alloys that contain some Cu occupy the medium to high corrosion / mass loss space
- c) Alloys that are age hardenable occupy the high corrosion / mass loss space
- d) 7xxx and 2xxx series alloys show high corrosion / occupy the high mass loss space

Interested readers may seek the strength (in MPa) or elongation, or even fracture toughness, of the alloys presented Figure 2 from other sources, and could use the results herein as a basis for the representation of primitive property space.

The corrosion of Al-alloys is well appreciated in the literature to proceed via localised modes of corrosion that are reliant on the microstructure of the alloy [7, 33, 42, 60-63]. As such, to gain an appreciation of this, Figure 3 plots the pitting measured, again for comparison with the information in Figure 2, against the measured Hardness. Figure 3 indicates the average pit density (i.e. number of pits per unit area) as measured by Optical Profilometry following 2 weeks of immersion in 0.1M NaCl. In addition the maximum pit depths are also presented in the inset. We observe from Figure 3 there is significant scatter, however generally speaking the alloys with the highest hardness (and mass loss) also present the highest pit density. In the medium to low hardness range however, there were some alloys that had moderate hardness and high pit density (such as certain 6xxx alloys) and alloys with a moderate hardness and low pit density (such as certain 3xxx and 5xxx alloys, known for their corrosion resistance).

In order to correlate the mass loss data to an electrochemical measurement and to provide the readers with a general set of data for commercial alloys, we plot the EIS determined reciprocal of polarisation resistance ( $1/R_p$ , determined following stabilisation of the open circuit potential after immersion in 0.1M NaCl) versus the mass loss data in Figure 4. What is observed is that there is a general trend for the body of data in that a low mass loss corresponds to a low value of  $1/R_p$ . There is significant scatter in the data as previously mentioned, but rather than focus on individual systems, the general trend is sought and presented. Of the large number of alloys tested however, 2297-T3, 6360-T3 and 2090-T3 where the three that revealed significant mass loss, but low values of  $1/R_p$  in short term tests, these alloys stood out in this regard and hence this is reported explicitly. The results in Figure 4 are presented as a consolidated data set, as opposed to focusing on the composition of individual alloys, in order to show any global trends.

### ***Influence of alloying elements in the corrosion of Al***

In assessing the polarisation curves of many replicate tests, for the many alloys tested, it is possible to extract some general trends in a holistic sense. Polarisation curves, although instantaneous in nature, are advantageous from the point of view that they can provide information on the electrochemical aspects (i.e. relative rates of anodic or cathodic reactions) that dictate corrosion. Such information cannot be assessed from EIS or mass loss tests.

To represent the influence of alloying elements on the corrosion (more specifically, the reaction kinetics) of Al, a phenomenological plot is given in Figure 5. This plot is derived

from the observation of experimental data that includes not only binary alloys, but higher order systems (ternaries, quaternaries, etc.) and commercial alloys. As such, Figure 5 is representative, as opposed to quantitatively definitive. The arrows on Figure 5 indicate the direction of the reactions, but not the extent of difference.

Figure 5 reveals the impact of the elements tested herein. The impact is conveniently represented as the relative movement on the anodic or cathodic branch that the alloying element induces. The distance associated with the relative movement is a representation of how significant the effect is. The information in Figure 5 can be considered a map as far as corrosion engineering of Al alloys is concerned. As such, we have also supplemented the plot with data from [4, 27, 34, 38, 44, 46, 48, 51, 52, 59, 63-79] where interpretable polarisation data is given. Some of the significant observations included in Figure 5 include:

- i. Below their solubility limit, many elements are benign and even beneficial
- ii. Mg can retard cathodic kinetics making the alloy less noble, but with lower corrosion rates. This is offset when too much Mg is added and Mg-rich second phases suffer anodic dissolution
- iii. Cu increased  $E_{\text{corr}}$  and pitting potential but enhances cathodic kinetics and leads to higher corrosion rates
- iv. Zn decreases  $E_{\text{corr}}$  and lowers the pitting potential
- v. Many elements increase the cathodic kinetics of Al, and hence, corrosion rates (Mn, Fe, Cu, Ti, etc.)
- vi. Si is rather inert in its impact on either anodic or cathodic kinetics
- vii. Pb and Sn enhance the anodic reaction dramatically [71, 80]
- viii. Li is rather inert unless present in appreciable concentrations

Whilst not part of this study, it is possible to see how the information in Figure 5 may be used to select inhibitors, or rationalise corrosion rates seen in certain (if not most) Al-alloy systems. Of the alloys studied in the work, a statistical analysis was carried out. Fuzzy curves were used to study the sensitivity and significance of each input variable. This technique was also used in previous corrosion studies [81]. Fuzzy curves, developed by Lin and Cunningham [82], are generated based on the Gaussian function [151]:

$$\varphi_{ik}(X_i) = e^{-\left(\frac{X_{ik}-X_i}{b}\right)^2} \quad \text{Eqn. 1}$$

where  $\varphi_{ik}$  is the membership function used to form the fuzzy curve for each input candidate,  $x_i$ . According to Lin and Cunningham [82], a fuzzy curve ( $C_i$ ), for each input ( $x_i$ ) can be constructed by employing the centre of area method for defuzzification:

$$C_i(X_i) = \frac{\sum_{k=1}^m \varphi_{ik}(x_i) \cdot y_k}{\sum_{k=1}^m \varphi_{ik}(x_i)} \quad \text{Eqn. 2}$$

Figure 6a reveals the fuzzy curves for the alloying additions tested herein. This can be considered to be ‘sensitivity’ analysis, whereby the sensitivity of the output (corrosion rate) to the input (variably we are altering, being composition) is given by the  $C_{xi}$  parameter. A large range of  $C_{xi}$  indicates that corrosion rate varies significantly with an element that causes such a large range, whereas a low range of  $C_{xi}$  means that an element has no significant influence on corrosion rate.  $C_{xi}$  can vary between 0 and 1. Again, to re-iterate, if the variation in  $C_{xi}$  over the range of compositions studied is high (i.e. close to 1) then corrosion rate has a large dependence on that element, and if  $C_{xi}$  is low (i.e. close to 0) then the corrosion rate will not alter significantly as a result of alloying with that element. As a result, a convenient way of assessing fuzzy curves is by studying the fuzzy curve range (Figure 6b), where it is seen that each element tested has a different range.

Corrosion rate is seen to be highly sensitive to amount of Cu, and not sensitive to the amount of Sc. Of the major alloy elements, we see that corrosion is least sensitive to Si. It is pointed out that the fuzzy curve range doesn’t indicate if the element is beneficial or detrimental, and hence should be viewed with some caution (i.e. Mg shows a relatively high sensitivity, but it is beneficial in low concentrations for reducing cathodic rates, but detrimental at higher concentrations where it enhances anodic rates). The slopes on the fuzzy curves themselves can illuminate changes in response however, i.e. relative little change in the influence of Mn until a certain concentration is reached and a large change in  $C_{xi}$  occurs. The data in Figure 6 is useful to those wishing to correlate other properties with corrosion performance and who wish to conduct further analysis by way of consideration of elemental solubilities.

### ***General discussion***

The combination of the solubility data (Table 1) [83-88], the realisation of a the spread of observed corrosion rates, (Figure 2), the phenomenological map indicating influence on

reaction kinetics (Figure 5), and sensitivity analysis (Figure 6) has added a consolidated body of knowledge to the basic/elementary understanding of corrosion of Al-alloys. Many prior studies have previously indicated a correlation between chemistry and structure (and elemental solubility) of Al-alloys with corrosion rates [7, 31, 34, 42, 46, 53, 59, 61, 89-94] – however a wider study of alloys as herein, has provided a general validation of many aspects of Al-alloy corrosion that were previously anecdotal. These aspects are summarised by the relevant bullet points made in the two sections above (a. to d., and i. to vii.).

Whilst the many families of Al-alloys which exist are chemically complex and there are second order effects other than chemistry (such as thermomechanical processing and temper) that can dictate microstructure and hence also influence corrosion, the effect of chemistry is (from a free energy perspective) major – as seen herein. Other works have shown – in addition to the work here – that as the heterogeneity of the alloy microstructure increases, the corrosion rate and pitting density tends to increase (concomitant with electrochemical heterogeneity). The lowest corrosion rates are realised by pure Al and Al-solid solutions, and corrosion rates tend to increase with the presence of second phases. Precipitates nominally serve to increase anodic dissolution kinetics in most cases, such as when precipitation occurs yielding  $\text{MgZn}_2$ ,  $\text{Mg}_2\text{Si}$ ,  $(\text{Mg}_2\text{Al}_3$ , which is not a hardening phase), or  $\text{Al}_2\text{CuLi}$ , with the partial exception being  $\text{Al}_2\text{CuMg}$  which is initially cathodic, but later anodic [60, 95, 96]. For information about the corrosion of a specific alloy, readers are directed to dedicated studies that include specific variables such as heat treatment and electrolyte variations.

## Conclusions

The study herein has provided a significant amount of consolidated information of the corrosion behaviour in a standard electrolyte (0.1M NaCl) at room temperature, in a quantitative sense. The work combines review and experiment, however all reported data is from original tests conducted in this study.

We have reported a consolidated diagram with the solubility of elements in Al, which is of general utility to the Al-corrosion field.

We have also presented schematically, the phenomenological effect on the relative anodic and cathodic reactions as imparted by a large number of typical alloying additions to aluminium, which we believe is significant to those researching Al-alloy corrosion, and serves as an important benchmark. This also serves as a phenomenological framework for corrosion of Al-alloys revealing the kinetic impact (as overlaid upon a polarisation schematic) of alloying elements.

The identification of coarse level findings was readily possible; such as

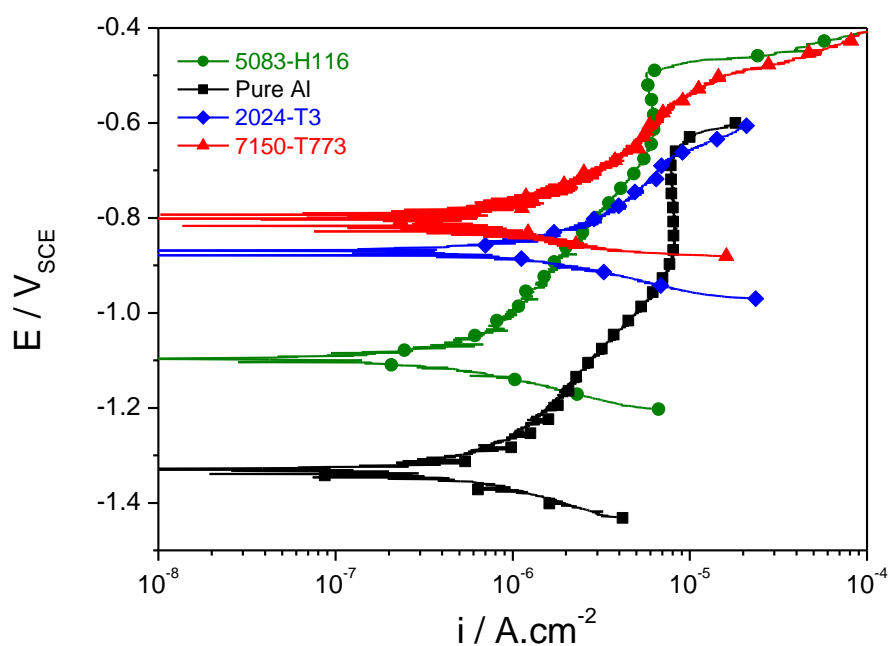
- Pure Al and Al-solid solutions occupy the low corrosion / mass loss space (1xxx, 3xxx, 5xxx). Below their solubility limit, many elements are benign and even beneficial. However, alloys in the low corrosion / mass loss space were generally seen to be Cu and Zn free. Mg can retard cathodic kinetics making the alloy less noble, but with lower corrosion rates.
- Alloys that contain some Cu occupy the medium to high corrosion / mass loss space. Cu increased  $E_{\text{corr}}$  and pitting potential but enhances cathodic kinetics and leads to higher corrosion rates. Zn decreases  $E_{\text{corr}}$  and lowers the pitting potential
- Alloys that are age hardenable occupy the high corrosion / mass loss space. 7xxx and 2xxx series alloys show highest corrosion and occupy the high mass loss space
- Many elements increase the cathodic kinetics of Al, and hence, corrosion rates (Mn, Fe, Cu, Ti, etc.). Si is rather inert in its impact on either anodic or cathodic kinetics



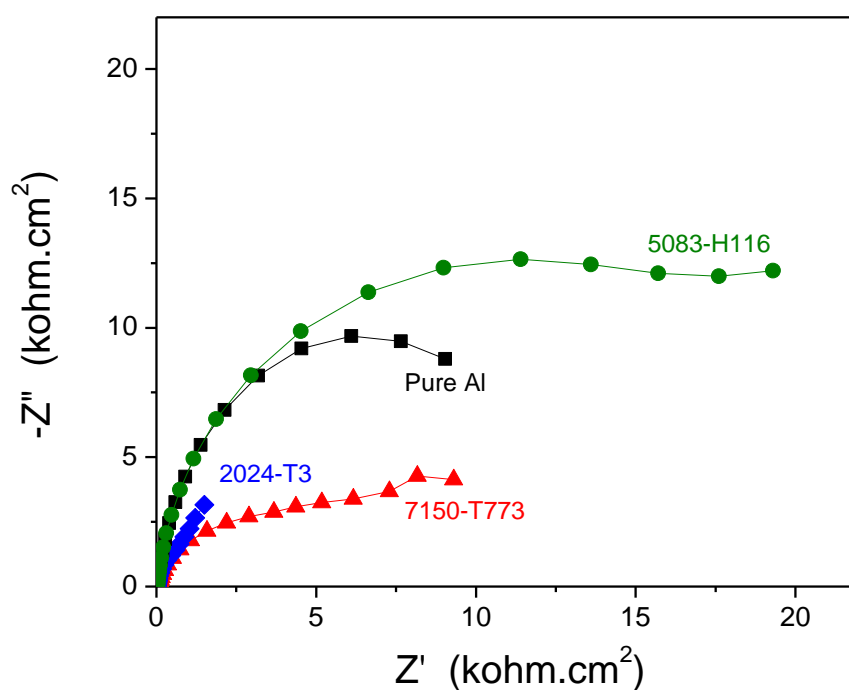


	Si	Fe	Cu	Mn	Mg	Cr	Zn	Ti	Zr	Li	Ni	Sr	Sc
Pure Al	0.03	0.03	0.01	0.01	0.01	0.01	0.02	0.01	0.005	-	0.01	0.001	-
2024-T3	0.5	0.5	4.2	0.5	1.6	0.10	0.25	0.15	-	-	-	-	-
2090-T3	0.15	0.03	2.70	0.01	0.01	0.01	0.01	0.01	0.07	2.05	0.01	0.001	-
2124-T851	0.20	0.30	4.5	0.6	1.7	0.10	0.25	0.15	-	-	-	-	-
2297-T3	0.10	0.10	2.9	0.35	0.25	-	0.05	0.12	0.11	1.6	-	-	-
3003-O	0.60	0.70	0.12	1.2	-	-	0.10	-	-	-	-	-	-
3102-O	0.40	0.70	0.10	0.25	-	-	0.30	0.10	-	-	-	-	-
5005-H34	0.30	0.70	0.20	0.20	0.50	0.10	0.25	-	-	-	-	-	-
5052-H131	0.25	0.40	0.10	0.10	2.5	0.2	0.10	-	-	-	-	-	-
5083-H116	0.40	0.40	0.10	0.6	4.8	0.15	0.25	0.15	-	-	-	-	-
5091-H116	0.05	0.12	0.01	0.01	4.04	0.01	0.02	0.01	0.01	1.12	0.01	0.001	-
6016-O	1.2	0.50	0.20	0.20	0.4	0.10	0.20	0.15	-	-	-	-	-
6022-O	1.35	0.14	0.04	0.04	0.58	0.10	0.21	0.10	-	-	-	-	-
6060-O	0.53	0.17	0.10	0.03	0.37	0.05	0.15	0.02	-	-	-	-	-
6181-T3	0.95	0.45	0.10	0.15	0.77	0.10	0.20	0.10	-	-	-	-	-
6360-T3	0.4	0.15	0.10	0.10	0.5	0.05	0.15						-
7075-T651	0.40	0.50	1.3	0.30	2.4	0.19	5.5	0.20	-	-	-	-	-
7079-T6	0.30	0.40	0.39	0.17	3.2	0.15	4.2	0.10					-
7150-T773	0.12	0.15	2.4	0.10	2.45	0.04	6.1	0.06	0.1	-	-	-	-
8090-T8771	0.20	0.30	1.35	0.10	0.9	0.10	0.25	0.10	0.07	2.4	-	-	-
AS40	12.60	0.46	0.35	0.34	0.13	0.02	0.05	0.02	0.005	-	0.01	0.051	-
AS303	5.29	0.77	3.40	0.31	0.02	0.01	0.09	0.03	0.005	0.005	0.01	0.001	-
CP401	0.14	0.13	5.03	0.01	0.01	0.01	0.01	0.01	0.005	0.005	0.01	0.001	-
LM5	0.13	0.36	0.01	0.49	4.01	0.01	0.01	0.02	0.005	-	0.01	0.001	-
LM8	5.98	0.55	0.07	0.35	0.38	0.01	0.05	0.06	0.005	0.005	0.01	0.001	-
LM20	12.70	0.49	0.38	0.39	0.14	0.02	0.06	0.02	0.005	0.005	0.01	0.001	-
LM25	7.06	0.54	0.09	0.32	0.46	0.02	0.09	0.07	0.005	0.005	0.01	0.001	-
AlZy	6.89	0.16	0.01	0.01	0.37	0.01	0.01	0.01	0.005	-	0.01	0.02	-
Al-6Ti	0.05	0.14	0.10	0.01	0.01	0.01	0.01	6.01	0.005	0.005	0.01	0.001	-
Al-4Cu	0.05	0.4	3.83	0.005	0.01	0.005	0.005	0.038	0.005	-	0.005	0.001	-
Al-Sr	0.11	0.17	0.01	0.01	0.01	0.01	0.01	0.01	0.005	-	0.01	2.45	-
UL40	0.05	0.05	0.01	0.01	0.02	0.01	0.02	0.01	0.19	3.85	0.01	0.00	-
Al-2Sc	0.06	0.04	0.02	0.01	0.02	-	0.01	0.02	-	-	-	-	1.38

Table 2: Chemical composition from ICP-AES of the alloys tested in this study. All values in weight %.



(a)



(b)

Figure 1: (a) Typical potentiodynamic polarisation response of selected Al-alloys. (b) Typical Nyquist plots collected using electrochemical impedance spectroscopy for different samples the same alloys in (a).

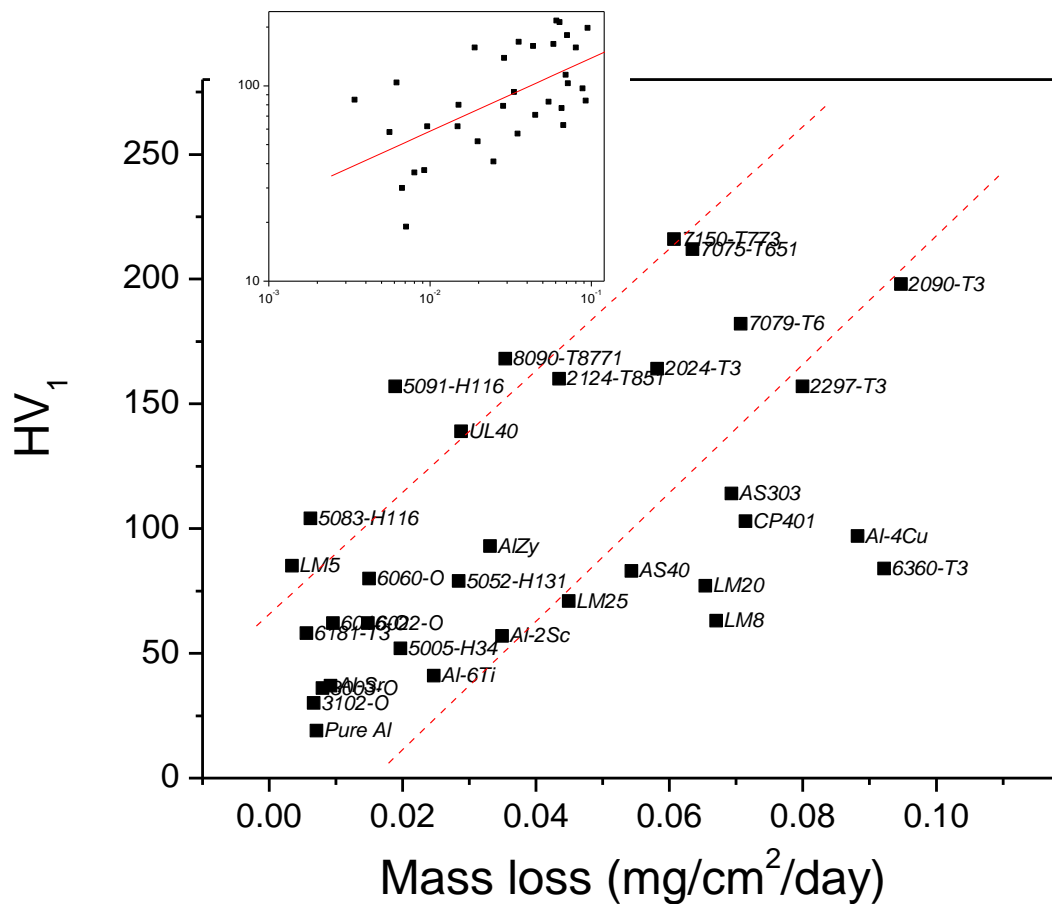


Figure 2: The range of mass loss values collected for Al-alloys, presented versus the corresponding Hardness. Hardness was collected using a 1kg load. Mass loss determined from 2 weeks exposure in 0.1M NaCl. The inset is the same data as the main plot, but with a log axis on the x and y axis.

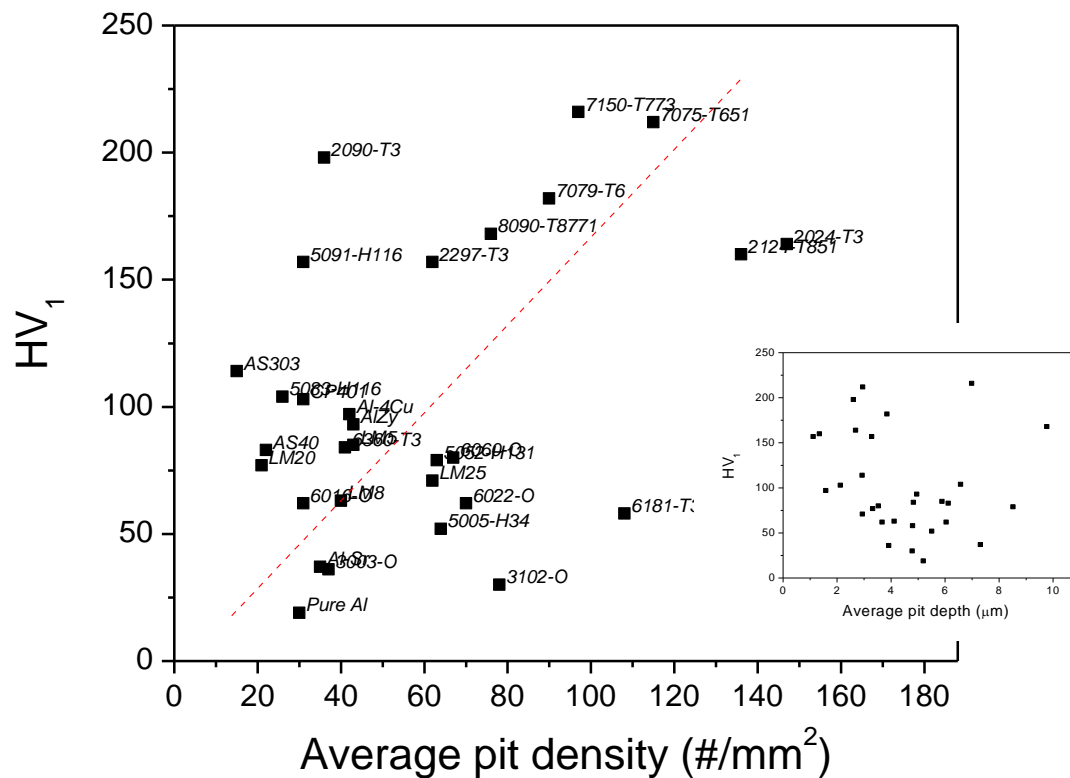


Figure 3: The correlation between hardness and the average pit density. Hardness was collected using a 1kg load. Average pit density was determined using optical profilometry following 2 weeks exposure in 0.1M NaCl. Error bars omitted for clarity. The inset reveals the average pit depth values, showing little correlation between hardness and average pit depth.

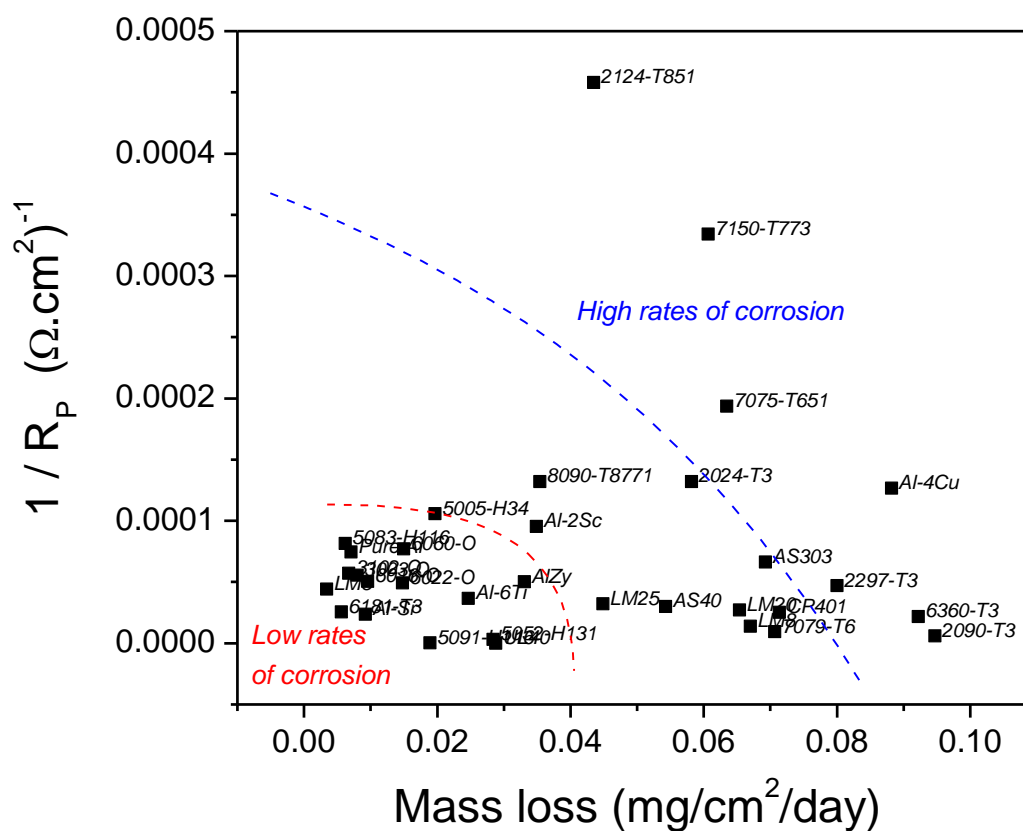


Figure 4: Correlation between electrochemically determined corrosion rates from short-term EIS testing and the mass loss determined from 2 weeks exposure in 0.1M NaCl. Error bars omitted for clarity.

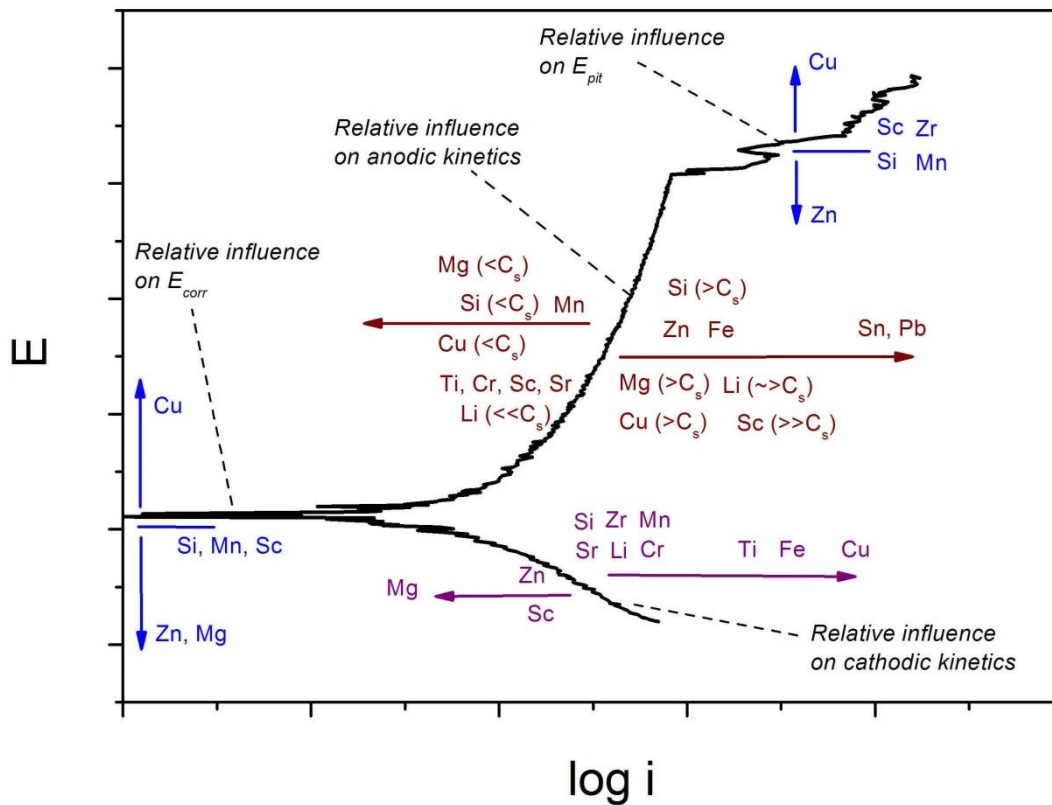
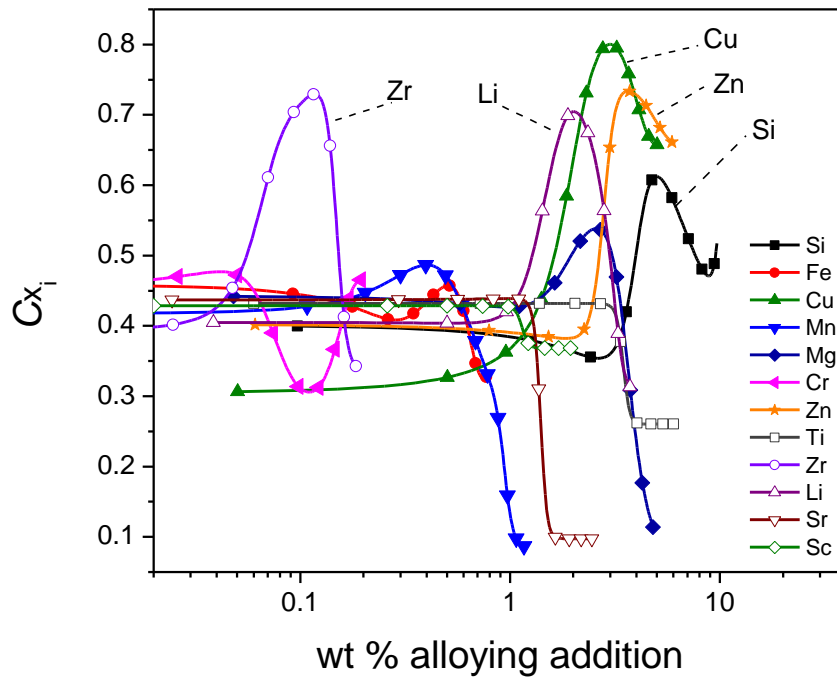
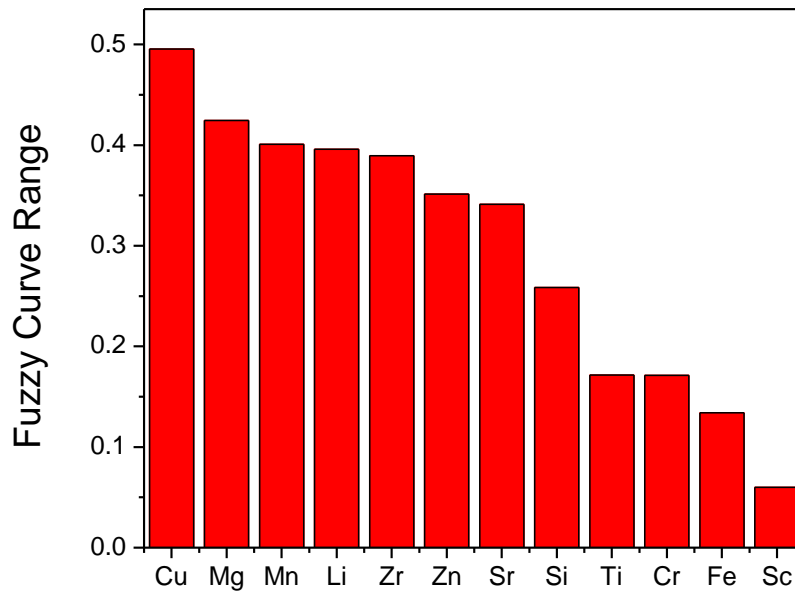


Figure 5: Schematic representation of the electrochemical impact of alloying elements studied. The plot depicts the ability of alloying additions to modify anodic or cathodic kinetics (or both), leading to changes in the resultant corrosion rate, along with changes in  $E_{corr}$  and  $E_{pit}$ .



(a)



(b)

Figure 6: Fuzzy curve (a) and fuzzy curve range (b) for the empirically determined impact of alloying elements on the corrosion of aluminium.



## References

- [1] N. Birbilis, T. Muster, R.G. Buchheit, Corrosion of aluminum alloys: Corrosion mechanisms in theory and practice, 3<sup>rd</sup> Ed., CRC Press, 2011, pp. 705-736.
- [2] G.S. Frankel, Journal of The Electrochemical Society, 145 (1998) 2186-2198.
- [3] Z. Szklarska-Smialowska, Corrosion Science, 41 (1999) 1743-1767.
- [4] N. Birbilis, R.G. Buchheit, Journal of The Electrochemical Society, 152 (2005) B140.
- [5] R.H. Jones, J.S. Vetrano, C.F. Windisch, Jr., Corrosion, 60 (2004) 1144-1154.
- [6] K.D. Ralston, N. Birbilis, M.K. Cavanaugh, M. Weyland, B.C. Muddle, R.K.W. Marceau, Electrochimica Acta, 55 (2010) 7834-7842.
- [7] K.A. Yasakau, M.L. Zheludkevich, S.V. Lamaka, M.G.S. Ferreira, Electrochimica Acta, 52 (2007) 7651-7659.
- [8] Z. Zhao, G.S. Frankel, Corrosion Science, 49 (2007) 3064-3088.
- [9] F.H. Scholes, S.A. Furman, A.E. Hughes, T.A. Markley, Corrosion Science, 48 (2006) 1812-1826.
- [10] J.R. Davis, Aluminum and Aluminum Alloys, ASM International, 1993.
- [11] J.R. Davis, Corrosion of aluminum and aluminum alloys, Materials Park, OH : ASM International, 1999.
- [12] R. Winston, Uhlig's corrosion handbook, 3 ed., Wiley, Hoboken, N.J, 2011.
- [13] N.J.H. Holroyd, G.M. Scamans, Metallurgical and Materials Transactions A, 44 (2013) 1230-1253.
- [14] I.J. Polmear, Light alloys : from traditional alloys to nanocrystals, 4th ed., Oxford ; Burlington, MA : Elsevier/Butterworth-Heinemann, 2006.
- [15] J.E. Hatch, Aluminum: properties and physical metallurgy, Metals Park, Ohio : American Society for Metals, 1984.
- [16] L.F. Mondolfo, J.G. Barlock, Metallurgical Transactions B, 6 (1975) 565-572.
- [17] R.K. Gupta, A. Deschamps, M.K. Cavanaugh, S.P. Lynch, N. Birbilis, Journal of The Electrochemical Society, 159 (2012) C492-C502.
- [18] S.P. Lynch, S.P. Knight, N. Birbilis, B.C. Muddle, "Stress corrosion cracking of Al-Zn-Mg-Cu alloys effects of composition and heat treatment" *Proc. Conf. 2008 International Hydrogen Conference - Effect of Hydrogen on Materials*, Jackson, WY, USA, 2009, pp. 243-250.
- [19] M.H. Larsen, J.C. Walmsley, O. Lunder, K. Nisancioglu, Journal of The Electrochemical Society, 157 (2010) C61-C68.
- [20] W.J. Liang, P.A. Rometsch, N. Birbilis, L.F. Cao, in: Corrosion And Prevention '12, Australasian Corrosion Association, Melbourne, Australia, 2012.
- [21] W.J. Liang, P.A. Rometsch, L.F. Cao, N. Birbilis, Corrosion Science, (2013).
- [22] K.D. Ralston, N. Birbilis, M. Weyland, C.R. Hutchinson, Acta Materialia, 58 (2010) 5941-5948.
- [23] M.K. Cavanaugh, PhD Dissertation, Materials Engineering Department, The Ohio State University, 2009.
- [24] R.K. Gupta, N.L. Sukiman, M.K. Cavanaugh, B.R.W. Hinton, C.R. Hutchinson, N. Birbilis, Electrochimica Acta, 66 (2012) 245-254.
- [25] Knovel (Firm) Handbook Committee, ASM Handbook: Volume 02 - Properties and selection: Nonferrous alloys and special purpose materials, 10<sup>th</sup> Ed., ASM International, Materials Park, OH, 1990.
- [26] [www.alcoa.com](http://www.alcoa.com)
- [27] C. Blanc, B. Lavelle, G. Mankowski, Corrosion Science, 39 (1997) 495-510.
- [28] G.S. Chen, M. Gao, R.P. Wei, Corrosion (Houston), 52 (1996) 8-15.

- [29] J.F. Li, Z. Ziqiao, J. Na, T. Chengyu, *Materials Chemistry and Physics*, 91 (2005) 325-329.
- [30] C.M. Liao, R.P. Wei, *Electrochimica Acta*, 45 (1999) 881-888.
- [31] T. Ramgopal, G.S. Frankel, *Corrosion*, 57 (2001) 702-711.
- [32] T. Suter, R.C. Aikire, *Journal of The Electrochemical Society*, 148 (2001) B36-B42.
- [33] A. Boag, A.E. Hughes, A.M. Glenn, T.H. Muster, D. McCulloch, *Corrosion Science*, 53 (2011) 17-26.
- [34] G.O. Ilevbare, O. Schneider, R.G. Kelly, J.R. Scully, *Journal of The Electrochemical Society*, 151 (2004) B453.
- [35] K.H. Na, S.I. Pyun, *Corrosion Science*, 50 (2008) 248-258.
- [36] J. Wloka, S. Virtanen, *Acta Materialia*, 55 (2007) 6666-6672.
- [37] B. Mazurkiewicz, A. Piotrowski, *Corrosion Science*, 23 (1983) 697-707.
- [38] K. Nisancioglu, *Journal of The Electrochemical Society*, 137 (1990) 69-77.
- [39] F. Øvari, L. Tomcsányi, T. Túrmezey, *Electrochimica Acta*, 33 (1988) 323-326.
- [40] M. Pourbaix, *Corrosion Science*, 14 (1974) 25-82.
- [41] A.R. Trueman, *Corrosion Science*, 47 (2005) 2240-2256.
- [42] R.G. Buchheit, N. Birbilis, *Electrochimica Acta*, 55 (2010) 7853-7859.
- [43] A. Conde, J. De Damborenea, *Electrochimica Acta*, 43 (1998) 849-860.
- [44] L. Speckert, G.T. Burstein, *Corrosion Science*, 53 (2011) 534-539.
- [45] T. Ramgopal, P.I. Gouma, G.S. Frankel, *Corrosion*, 58 (2002) 687-687.
- [46] P. Niskanen, T.H. Sanders, J.G. Rinker, M. Marek, *Corrosion Science*, 22 (1982) 283.
- [47] R.G. Buchheit, *Journal of The Electrochemical Society*, 142 (1995) 3994-3996.
- [48] R. Ambat, A.J. Davenport, G.M. Scamans, A. Afseth, *Corrosion Science*, 48 (2006) 3455-3471.
- [49] E.V. Koroleva, G.E. Thompson, G. Hollrigl, M. Bloeck, *Corrosion Science*, 41 (1999) 1475-1495.
- [50] F. Andreatta, H. Terryn, J.H.W. de Wit, *Electrochimica Acta*, 49 (2004) 2851-2862.
- [51] J.R. Scully, T.O. Knight, R.G. Buchheit, D.E. Peebles, *Corrosion Science*, 35 (1993) 185-195.
- [52] R.H. Jones, D.R. Baer, M.J. Danielson, J.S. Vetrano, *Metallurgical and Materials Transactions A: Physical Metallurgy and Materials Science*, 32 (2001) 1699-1711.
- [53] I.L. Muller, J.R. Galvele, *Corrosion Science*, 17 (1977) 995-1007.
- [54] M. Usta, M.E. Glicksman, R.N. Wright, *Metallurgical and Materials Transactions A: Physical Metallurgy and Materials Science*, 35 A (2004) 435-438.
- [55] L.P. Huang, K.H. Chen, S. Li, M. Song, *Scripta Materialia*, 56 (2007) 305-308.
- [56] R. Ambat, R.K. Prasad, E.S. Dwarakadasa, *Corrosion Science*, 37 (1995) 1253-1265.
- [57] J.F. Li, Z.Q. Jia, C.X. Li, N. Birbilis, C. Cai, *Materials and Corrosion*, 60 (2009) 407-414.
- [58] G. Svenningsen, M.H. Larsen, J.H. Nordlien, K. Nisancioglu, *Corrosion Science*, 48 (2006) 258-272.
- [59] D.K. Xu, N. Birbilis, D. Lashansky, P.A. Rometsch, B.C. Muddle, *Corrosion Science*, 53 (2011) 217-225.
- [60] R.G. Buchheit, R.P. Grant, P.F. Hlava, B. McKenzie, G.L. Zender, *Journal of The Electrochemical Society*, 144 (1997) 2621-2628.
- [61] P. Campestrini, E.P.M. van Westing, H.W. van Rooijen, J.H.W. de Wit, *Corrosion Science*, 42 (2000) 1853-1861.
- [62] A. Davoodi, J. Pan, C. Leygraf, S. Norgren, *Journal of The Electrochemical Society*, 155 (2008) C211.
- [63] H.C. Fang, K.H. Chen, X. Chen, H. Chao, G.S. Peng, *Corrosion Science*, 51 (2009)

2872-2877.

- [64] D.R. Baer, C.F. Windisch, M.H. Engelhard, M.J. Danielson, R.H. Jones, J.S. Vetrano, *Journal of Vacuum Science & Technology - Vacuum Surfaces and Films*, 18 (2000) 131-136.
- [65] F. Eckermann, T. Suter, P.J. Uggowitzer, A. Afseth, P. Schmutz, *Electrochimica Acta*, 54 (2008) 844-855.
- [66] R.K. Gupta, N.L. Sukiman, K.M. Fleming, M.A. Gibson, N. Birbilis, *ECS Electrochemistry Letters*, 1 (2012) B1-B3.
- [67] Y. Liu, Y.F. Cheng, *Materials and Corrosion*, 61 (2010) 211-217.
- [68] M. Cavanaugh, N. Birbilis, R. Buchheit, F. Bovard, *Scripta Materialia*, 56 (2007) 995-998.
- [69] R.G. Buchheit, F.D. Wall, G.E. Stoner, J.P. Moran, *Corrosion*, 51 (1995) 417-428.
- [70] Ø. Sævik, Y. Yu, J.H. Nordlien, K. Nisancioglu, *Journal of The Electrochemical Society*, 152 (2005) B334-B341.
- [71] B. Graver, A.M. Pedersen, K. Nisancioglu, *ECS Transactions*, 16 (2009) 55-69.
- [72] Anawati, S. Diplas, K. Nisancioglu, *Journal of The Electrochemical Society*, 158 (2011) C158-C163.
- [73] I.N. Ganiev, M.T. Norova, F.U. Obidov, *Russian Journal of Applied Chemistry*, 80 (2007) 78-82.
- [74] J.T.B. Gundersen, A. Aytac, S. Ono, J.H. Nordlien, K. Nişancıoğlu, *Corrosion Science*, 46 (2004) 265-283.
- [75] F. Eckermann, P.J. Uggowitzer, P. Schmutz, *Materials Science Forum*, 519-521 (2006), 635-640.
- [76] C. Blanc, G. Mankowski, *Corrosion Science*, 39 (1997) 949-959.
- [77] W.N. Garrard, *Corrosion*, 50 (1994) 215-225.
- [78] R. Ambat, E.S. Dwarakadasa, *Corrosion Science*, 33 (1992) 681-690.
- [79] M. Kannan, V.S. Raja, *Metallurgical and Materials Transactions A*, 38 (2007) 2843-2852.
- [80] Anawati, B. Graver, H. Nordmark, Z. Zhao, G.S. Frankel, J.C. Walmsley, K. Nisancioglu, *Journal of The Electrochemical Society*, 157 (2010) C313-C320.
- [81] G. Kumar, R.G. Buchheit, *Corrosion*, 64 (2008) 241-254.
- [82] Y. Lin, G.A. Cunningham, *IEEE Trans on fuzzy system*, 3(190) (1995) 190-197.
- [83] H. Jones, *Journal of Materials Science*, 19 (1984) 1043-1076.
- [84] H. Jones, *Aluminium*, 54 (1978) 274-281.
- [85] L.F. Mondolfo, *Aluminium Alloys: Structure and Properties*, Butterworths, 1976.
- [86] K.R. vanHorn, *Aluminium*, Volume 1 - Properties, Physical Metallurgy and Phase Diagrams, ASM, 1967.
- [87] M. Hansen, K. Anderko, *Constitution of binary alloys* 2nd ed., prepared with the cooperation of Kurt Anderko., McGraw-Hill, New York, 1958.
- [88] *Equilibrium Diagrams of Aluminium Systems*, The Aluminium Development Council, London, 1961.
- [89] S.P. Knight, N. Birbilis, B.C. Muddle, A.R. Trueman, S.P. Lynch, *Corrosion Science*, 52 (2010) 4073-4080.
- [90] O. Seri, K. Tagashira, *Keikinzoku/Journal of Japan Institute of Light Metals*, 36 (1986) 806-812.
- [91] M. Zamin, *Corrosion*, 37 (1981) 627-632.
- [92] T. Marlaud, B. Malki, C. Henon, A. Deschamps, B. Baroux, *Corrosion Science*, 53 (2011) 3139-3149.
- [93] R. Goswami, G. Spanos, P.S. Pao, R.L. Holtz, *Metallurgical and Materials Transactions A: Physical Metallurgy and Materials Science*, 42 (2011) 348-355.

- [94] F. Sato, R.C. Newman, *Corrosion*, 55 (1999) 3.
- [95] B.N. Padgett, PhD Dissertation, Materials Engineering Department, The Ohio State University, 2009.
- [96] C. Blanc, A. Freulon, M.C. Lafont, Y. Kihn, G. Mankowski, *Corrosion Science*, 48 (2006) 3838-3851.

# Chapter 5

## The role of chemistry in the general corrosion behaviour of Al-alloys

---

This chapter includes three distinct ‘sub-chapters’ which together provide a comprehensive empirical study on the role of alloying elements in the ensuing corrosion behaviour of Al-alloys.

**Section 5.1** is a research paper accepted (September 2013) in the journal ‘Corrosion Engineering, Science and Technology’. Following the outcomes in Chapter 4, the alloy used in this study is based on Al-4Mg-0.4Mn system with quaternary addition of various elements that includes Ti, Zn, Zr, Pb, Nd, Sn, Sr and Si. The aim of this work was to understand the effect of alloying elements on the (micron scale) microstructure of Al-4Mg-0.4Mn alloy in relation to the electrochemical response and subsequent corrosion morphology. The presence of levels of alloying elements (nominally below the maximum solid solubility limit) can influence the microstructure of the base alloy (by modification of  $\beta$ -phase as also described in the subsequent chapters) but also by the formation of dispersoids and additional intermetallic particles. In this work, the electrochemical response was characterised by potentiodynamic polarisation, supplemented by immersion testing and optical profilometry to determine the form and intensity of the localised corrosion. Microstructural characterisation was carried out by Scanning Electron Microscopy (SEM) and the chemical composition of the particles was analysed with energy dispersive X-ray (EDX) spectroscopy.

The present chapter also includes a section on the electrochemical behaviour and localised corrosion associated with the  $\text{Mg}_2\text{Si}$  particles in Al-alloys. **Section 5.2** is a research paper published in the journal ‘ECS Electrochemistry Letters’. As previously discussed in Chapter 4, there are several potential alloy systems to be explored throughout this project. The 6xxx series alloys have higher mechanical strength in comparison to the 5xxx (Al-4Mg-0.4Mn) series alloys due to the presence of fine  $\text{Mg}_2\text{Si}$  precipitates (which can be stimulated and grown by thermal exposure). This particle however increases the susceptibility to localised corrosion. In this work, the electrochemical behaviour of  $\text{Mg}_2\text{Si}$  was investigated over a

range of pH by carrying out potentiodynamic polarisation technique and supplemented by SEM and EDX. This was a unique set of work, because the electrochemical response of  $\text{Mg}_2\text{Si}$  was not previously reported in detail, owing to the great difficulty in preparation of bulk  $\text{Mg}_2\text{Si}$ . The result shows that in Al-alloys,  $\text{Mg}_2\text{Si}$  was found to be anodic (less noble) in acidic and neutral pH hence undergoes selective dissolution in the Al-matrix.

**Section 5.3** is a (collaborative) research paper published in the journal ‘Electrochimica Acta’. It was foundational in further validating, if not establishing, that as alloying elements are added to improve mechanical strength by increasing the microstructural heterogeneity, pitting susceptibility increased exponentially. Conventionally, pitting potential ( $E_{\text{pit}}$ ) is used to indicate pitting susceptibility; however this method lacks more useful information on size and frequency of the pits. A more effective way in characterising pitting propensity is by using current transient measurement during potentiostatic polarisation test. The current transient counted (metastable pitting) have better correlation with the actual number of pits formed as characterised by optical profilometry. The work is in its own right a complete study; however its relation to the present thesis is important on the basis of: a) it indicates the merit in selecting an alloys such as AA5083 as a platform for future work, b) it unequivocally indicates the microstructure-corrosion relationship as driven by microstructural heterogeneity.

## Monash University

### Declaration for Thesis Section 5.1

In the case of Section 5.1, the nature and extent of my contribution to the work was the following:

Nature of contribution	Extent of contribution (%)
Initiation, key ideas, experimental, development, results interpretations, writing up	85

The following co-authors contributed to the work. If co-authors are students at Monash University, the extent of their contribution in percentage terms must be stated:

Name	Nature of contribution	Extent of contribution (%) for student co-authors only
Nick Birbilis	Initiation, key ideas, experimental, development, results interpretations, writing up	5
Rajeev Gupta	Initiation, key ideas, experimental, development, results interpretations, writing up	5
Rudy Buchheit	Results interpretations, writing up	5

The undersigned hereby certify that the above declaration correctly reflects the nature and extent of the candidate's and co-authors' contributions to this work.

**Candidate's  
Signature**

	<b>Date</b> 18 June 2014
---	-----------------------------

**Main  
Supervisor's  
Signature**

	<b>Date</b> 18 June 2014
---	-----------------------------

# Influence of microalloying additions on Al–Mg alloy. Part 1: Corrosion and electrochemical response

N. L. Sukiman<sup>\*1,2</sup>, R. K. Gupta<sup>1</sup>, R. G. Buchheit<sup>3</sup> and N. Birbilis<sup>1</sup>

A range of custom alloys based on the Al–4Mg–0.4Mn system were produced with selected quaternary microalloying additions. Alloying elements studied include silicon, zinc, lead, titanium, tin, zirconium, strontium and neodymium. To characterise the corrosion response, electrochemical tests were carried out in 0.1M NaCl, supplemented by constant immersion tests and basic microstructural characterisation by means of scanning electron microscopy (SEM). Optical profilometry was used to determine the form and intensity of localised corrosion. The results indicate that low level quaternary alloying additions can have a marked influence on specific aspects of the first order correlation between chemistry, microstructure, hardness and corrosion.

**Keywords:** Corrosion, Hardness, Aluminium alloys, Alloying

## Introduction

The Al–Mg based alloys are commercially classified as the 5xxx series aluminium (Al) alloys. These alloys do not respond to age hardening and gain strength through solid solution strengthening and work hardening.<sup>1,2</sup> Al–Mg alloys such as AA5083 are typically used as materials in transportation where formability, weldability and moderate strength are necessary.<sup>2</sup> Owing to a comparatively more uniform microstructure and absence of precipitates, Al–Mg alloys possess better corrosion resistance (including pitting corrosion) than the other classes of Al alloys, such as the 2xxx and 7xxx series alloys.<sup>1</sup> In one study, Muller reported that addition of Mg to Al up to 5 wt-% does not change the pitting susceptibility.<sup>3</sup> Most of the commercial 5xxx series Al alloys are supersaturated with Mg, i.e. containing more Mg than the maximum solubility in Al at room temperature. This supersaturation can lead to the formation of  $\beta$ -phase ( $Mg_2Al_3$ ) during exposure to elevated temperatures (as low as 50 to  $\sim 220^\circ\text{C}$ ) for an extended period of time.<sup>4</sup> The occurrence of  $\beta$ -phase precipitation in the 5xxx series alloy is known as sensitisation, since the  $\beta$ -phase precipitation is deleterious to properties (depleting the matrix of solute without contributing to strength).  $\beta$ -phase tends to form at grain boundaries<sup>5,6</sup> and also readily precipitates heterogeneously in the presence of dislocations or adjacent to  $Al_6Mn$  constituent particles.<sup>7</sup>  $\beta$ -phase is electrochemically anodic to the Al matrix, capable of causing severe

intergranular corrosion (IGC) and contributing to stress corrosion cracking (SCC).<sup>4,8–10</sup> Minimising the extent of sensitisation in Al–Mg alloys has been reported in only limited investigations in the literature which included the addition of Zn, Cu, Ag and Nd to Al–Mg alloys.<sup>11–14</sup> The decrease in sensitisation was reported mainly due to modification of the chemical composition of  $\beta$ -phase and a decrease in the  $\beta$ -phase fraction.

The properties of Al–Mg alloys may be improved by small additions of alloying elements (microalloying) through formation of dispersoids and modification of the  $\beta$ -phase (to decrease anodic activity). Mn and Cr are added to 5xxx alloys to improve strength by dispersion hardening and may influence SCC by hindering recrystallisation.<sup>1,2,15–17</sup> Er is reported to improve mechanical properties without loss of corrosion performance. Sc is reported to be beneficial in improving both corrosion resistance and mechanical properties,<sup>18–20</sup> however, the use of Sc (whilst beneficial) is limited by cost considerations.<sup>21</sup>

As is appreciated, the corrosion rate of Al alloys generally increases with any attempt to significantly increase the alloy strength,<sup>1,22,23</sup> as the latter is nominally achieved via microstructural heterogeneity in precipitation hardening systems. Fine secondary phases on the order of  $\sim >4$  nm are capable of exhibiting unique electrochemical differences leading to localised corrosion.<sup>24–26</sup> The 5xxx series alloys are nominally free from precipitates, and hence this is what leads to this alloy class having the best compromise of strength and corrosion resistance. In the present work, we explore the effect of various alloying elements on the corrosion of Al–4Mg–0.4Mn (which is an analogue to commercial alloy AA 5083), and relate this to a simple mechanical metric of hardness, in order to simultaneously explore the alloy property space and if any attendant improvements can be achieved in the compromise between strength and corrosion rate. Herein, we

<sup>1</sup>ARC Centre of Excellence for Design in Light Metals, Department of Materials Engineering, Monash University, VIC. 3800, Australia

<sup>2</sup>Department of Mechanical Engineering, University of Malaya, Kuala Lumpur. 50603, Malaysia

<sup>3</sup>Department of Materials Science and Engineering, The Ohio State University, Columbus, OH 43210, USA

\*Corresponding author, email nazatul.sukiman@monash.edu



study the influence of the quaternary alloying additions including silicon, zinc, lead, titanium, tin, zirconium, strontium and neodymium. Part 1 of this study reports the specimen selection, production, electrochemical and corrosion response, while Part 2 of the study reports the sensitisation behaviour, together with phase analysis and sensitisation resistance.

The rationale for selection of the alloying elements studied herein has been abridged in Table 1, together with the maximum solid solubility for the respective elements. Each element has been studied on the basis of a first order hypothesised influence, which required experimental validation. As will be seen, several additions had adverse effects, however we believe still worthy of reporting. Some additional background information about the elements studied in the context of the Al–Mg alloys is given below.

In most of the 5xxx series alloys (and in most wrought Al alloys besides the 6xxx series), Si is present as an impurity. Excess Si can lead to the formation of  $Mg_2Si$  particles which are detrimental to corrosion,<sup>27</sup> whereby  $Mg_2Si$  is anodic to the matrix. The influence of  $Mg_2Si$  on the corrosion of Al–Mg alloys has been investigated<sup>28</sup> and it was shown that the enrichment of Si during selective dissolution of Mg caused the formation of  $Mg(OH)_2$  and  $SiO_2 \cdot nH_2O$  hydroxide that act as an additional barrier to stop the propagation from forming deep pits.

The addition of Zn in AA5083 has been reported to improve SCC and IGC resistance due to modification of  $\beta$ -phase.<sup>12,29</sup> Addition of Zn in Al–Mg alloys leads to the formation of a ternary intermetallic phase known as  $\tau$  phase  $[Mg_{32}(Al,Zn)_{49}]$ ,<sup>11,12</sup> which has apparently lower dissolution kinetics than  $\beta$ -phase hence reducing the susceptibility to SCC. Zn content is kept low so that formation of  $MgZn_2$  phase can be avoided.

Zr, Ti and Sc are noted as serving as grain refiners and may also contribute to an increment in strength by forming dispersoids.<sup>18,30</sup> The contribution to strength from grain refinement alone is not large in Al alloys (compared to say, steels or Mg alloys) as the Hall–Petch

coefficient is low.<sup>31</sup> The dispersoid  $Al_3Sc$  is reported to be beneficial to mechanical properties of Al–Mg alloys<sup>20,32,33</sup> and does not have significant effect on corrosion because of inability to support the cathodic reaction at high rates.<sup>18</sup> However, Sc additions are uncommon due to the high cost of Sc. Zr is known to form  $Al_3Zr$  dispersoids which are cathodic to the matrix, however, Birbilis and Buchheit, reported that cathodic current density sustained by  $Al_3Zr$  is relatively low and therefore Zr addition is expected to not significantly deteriorate the corrosion performance.<sup>34</sup> Ti has been used as potent grain refiner and is present in some of the 5xxx Al alloys (such as AA 5083 and AA 5356),<sup>35</sup> however, investigations comparing the effect of these alloying additions (particularly in some excess) on corrosion and mechanical properties remains scarce. The amount of Zr, Sc and Ti added to Al–Mg alloy in the present study is based on the nominal contents of these alloys in commercial Al alloy systems.

The presence of Pb and Sn in Al alloys can increase fluidity during production. Both Pb and Sn have almost negligible solubility in Al, and during heat treatment they can segregate.<sup>36–39</sup> These elements in particular have been noted as being able to also segregate to the alloy surface, beneath the aluminium oxide layer, where they can significantly weaken it.<sup>37,39–41</sup> In many aqueous electrolytes the anodic reaction rate thus increases rather dramatically, from the destabilisation of oxide layer, known as the ‘activation’ effect which has been well documented by the Nisancioglu group.<sup>37,38,40–44</sup> Sn is reported to have a higher activation effect than Pb. The activation effect of Sn can be seen at temperature as low as 300°C but significantly reduced when heated to 600°C where some Sn is dissolved into solid solution.<sup>43</sup> The addition of Pb to Al–Mg alloy reduces the activation temperature further than with Al–Pb binary alloys as Mg enhances Pb segregation on the surface. It has been posited that the presence of Mg is not influencing the activation effect since Mg segregates at low temperatures (450°C) and form passive thermal oxide of crystalline  $MgAl_2O_4$  spinel<sup>45</sup> which lessen the activation effect from

**Table 1** Maximum solubility of alloying elements in pure Al (compiled from<sup>57–60</sup>)

Element	Maximum solid solubility in Al C <sub>s</sub>	Rationale for selection of the element as an addition
Mg	17.40	Present in base alloy
Mn	1.80	Present in base alloy
Fe	0.05	Present as an impurity, not intentionally added
Si	1.65	High solubility in Al and can be added without stimulating additional phases
Ti	1.20	Added in an attempt to increase hardness and not compromise corrosion by formation of dispersoids
Zn	80.00	Added to contribute to solid solution and potentially reduce the effect of $\beta$ -phase by formation of ternary phase
Zr	0.28	Added in an attempt to increase hardness and not compromise corrosion by formation of dispersoids
Pb	0.17	Although known as an ‘activator’, was added to explore the influence on the cathodic kinetics of the alloy since the alloy is Mg rich and Pb has a low exchange current density for cathodic reaction.
Nd	0.05	Added to explore the influence of what is a previously unexplored micro-alloying addition on the basis that it may form electrochemically homogeneous phase ( $Al_4Nd_3$ )
Sn	0.06	Although known as an ‘activator’, was added to explore the influence on the cathodic kinetics of the alloy since the alloy is Mg rich and Sn has a low exchange current density for cathodic reaction.
Sr	0.00	Added to explore the influence of what is a previously unexplored microalloying addition on the basis that it may form dispersoids and electrochemically homogeneous ternary phase

Pb segregation.<sup>41</sup> In this study however, we wanted to test a hypothesis, concerning whether or not excess additions of Pb and Sn would have a beneficial impact on retarding cathodic kinetics, therefore added amounts of Pb and Sn are kept slightly above their respective maximum solid solubilities. The exchange current density of both Pb and Sn<sup>46</sup> is significantly lower than that of Al, and it was sought to observe if this may translate to lower corrosion. The expectation however, is that the effect of ‘activation’ will be unlikely to be overcome as it is a persistent phenomenon for obvious reasons. None the less, the addition of Pb and Sn on hardness and subsequent sensitisation for the Al–Mg–Mn contributes to making this a more holistic study.

In a recent report, the addition of Nd has been seen to reduce the sensitisation of an Al–5Mg alloy by modifying the  $\beta$ -phase composition and the co-precipitation of an  $\text{Al}_{11}\text{Nd}_3$  which was distributed as fine particles.<sup>14</sup> Additionally Nd was also incorporated into coarse constituent particles. In a separate study Nd was reported to increase recrystallisation temperature of an Al–Mg–Mn alloy.<sup>47</sup> These studies indicate Nd to be one of the potential alloying elements leading to an improvement in properties of Al–Mg alloys and therefore the influence of Nd was investigated.

The addition of Sr to Al–Mg alloys has not been previously reported. Sr has nominally been used as a modifier for eutectic Si in high Si containing Al–Si alloys,<sup>48–51</sup> which are nominally casting alloys. The properties of Al–Si alloys were improved due to modification of Si and also due to incorporation of Sr within the  $\text{Al}_5\text{FeSi}$  phase. The effect of Sr on Al–Mg alloys is investigated for the first time herein due to an anticipated ability to form dispersoids and potential for  $\beta$ -phase modification. Sr content of alloys in this study was kept similar to what it is used in Al–Si alloys as modifier.<sup>48–51</sup>

It is understood that the alloying explored herein is not oriented towards commercial products, particularly at such an elementary stage where processing is static, but allows for a previously unreported platform of information to more generally assess the corrosion of Al–Mg alloys and the role of chemical additions.

## Experimental

### Materials

The alloys tested in this study were produced by melting an Al–Mg–Mn master alloy (denoted as AMM in Table 2) with alloying elements either in their pure

form, or in some instances in the form of commercially available master alloys. The amounts of alloying are kept at a low level to limit the formation of precipitates. Commercially pure Mg and Al were added to balance the chemical compositions in cases where master alloys were used. Melting was carried out in a muffle furnace. Regular stirring of the melt was carried out, followed by casting into a preheated (at 300°C) graphite crucible. Cast alloys were homogenised below the liquidus temperature (nominally at 400°C) for two days, and then cold rolled to a 50% thickness reduction. The composition of the alloys produced was independently analysed using inductively coupled plasma – optical emission spectrometry (ICP-OES) at spectrometer services (Australia) and presented along with designation of the alloys in Table 2.

### Characterisation and physical testing

The microstructures were characterised using an FEI Quanta 200 scanning electron microscopy (SEM) to identify the presence and nature of particles within the microstructure. All samples were prepared by metallographic polishing down to a 1  $\mu\text{m}$  finish, followed by ultrasonic cleaning. The images were observed using backscattered electron (BSE) mode and the chemical composition of the particles was analysed with energy dispersive X-ray (EDX) spectroscopy. Vickers hardness testing was performed using a Duramin A300 Hardness Tester using a 1 kg load. This method of mechanical testing was preferred, as a large number of replicate measurements were possible, and the testing could be performed in-house on all specimens. The size of specimens produced prohibited a round robin of tensile tests.

### Corrosion testing

Specimens were ground to 1200 grit SiC paper under ethanol prior to electrochemical testing. All tests were carried out in 0.1M NaCl. Potentiodynamic polarisation tests were performed using a standard 3-electrode flat-cell (PAR) and a Biologic VMP3 potentiostat under the control of EC-Lab software. A saturated calomel electrode (SCE) was used as a reference electrode and platinum mesh was used as a counter electrode. Potentiodynamic polarisation tests were initiated using a scan rate of 1  $\text{mV s}^{-1}$  after 10 min at open circuit potential. This period of 10 min was determined to be sufficient for achieving a stable potential, whereby the potential did not subsequently alter by more than a few  $\text{mV min}^{-1}$ . A longer time at open circuit in dilute

**Table 2** Chemical composition from ICP-OES of alloys tested in this study/wt-%

Alloys	Alloying elements											
	Al	Mg	Mn	Si	Fe	Ti	Zn	Zr	Pb	Nd	Sn	Sr
AMM	Bal.	4.01	0.49	0.13	0.36	...	...	...	...	...	...	...
AMM+0.1Ti	Bal.	3.89	0.48	0.13	0.34	0.10	...	...	...	...	...	...
AMM+0.4Zn	Bal.	4.01	0.48	0.13	0.33	...	0.40	...	...	...	...	...
AMM+0.21Zr	Bal.	4.17	0.49	0.11	0.32	...	...	0.21	...	...	...	...
AMM+0.23Pb	Bal.	3.84	0.50	0.11	0.31	...	...	...	0.23	...	...	...
AMM+0.18Nd	Bal.	5.14	0.01	0.06	0.15	...	...	...	...	0.18	...	...
AMM+0.34Sn	Bal.	3.97	0.50	0.13	0.34	...	...	...	...	...	0.34	...
AMM+0.1Sr	Bal.	3.64	0.47	0.12	0.32	...	...	...	...	...	...	0.10
AMM+0.16Zr+0.12Sr	Bal.	4.02	0.45	0.14	0.33	...	...	0.16	...	...	...	0.12
AMM+0.1Si	Bal.	4.00	0.48	0.24	0.32	...	...	...	...	...	...	...

chloride electrolytes will ultimately lead to corrosion initiation following a finite period, after which any changes in the alloy surface do not reflect the response of the original surface. Additionally, electrochemical impedance spectroscopy (EIS) was also performed on all samples. EIS spectra were collected over the range of 500 kHz to 5 mHz in the potential range of OCP +/−10 mV, and analysed using EC Lab software.

Immersion (mass loss) tests were performed for samples immersed in 0.1M NaCl for 14 days. Following immersion, corrosion products were removed by a short immersion (~<10 s) and light rubbing in 7% nitric acid solution before final weighing. This solution was used in order to preserve the original morphology of the corrosion attack for subsequent profilometry (shown to be effective in Refs. 24 and 52). The morphology of the immersion samples were analysed using SEM and optical profilometry (Veeco Wyko NT1100). Pitting attributes such as average pit depth, number of pits and the volume of pits were calculated with the assistance of Veeco Vision software package.

All tests were repeated for at least three times for data reproducibility and standard deviation was used to generate error bars of the results.

## Results and discussion

### Effect of alloying on microstructure

The addition of the various alloying elements studied has an influence on the formation of second phase particles within the matrix, as shown by backscattered electron (BSE) images in Fig. 1. The chemical composition and solubility limit of the alloys studied are listed in Tables 1 and 2 respectively, for correlation. In this study, the particles were analysed on the microscale (not the nanoscale, as TEM studies were not employed), justified on the basis that alloys were not expected to precipitation harden and form a nanostructure in the quenched and wrought condition. As the particles imaged via SEM are larger than 1 µm, phase identification was achieved by energy dispersive X-ray (EDX). In general the particles which form are smaller than the constituent particles in the base alloy, and more evenly distributed. Of the types of intermetallic compounds identified; there was nominally some remnant constituent  $\beta$ -phase ( $Mg_2Al_3$ ), and the impurity based constituents  $Al_6(Mn,Fe)$ ,  $Al_{12}(Mn,Fe)$ ,  $Al-(Fe,Mn,Si)$  and  $Mg_2Si$  for each of the alloys characterised. There are appreciable amount of Fe and Si present as impurities, as the alloys are of commercial grade Al–Mg alloy. These constituent intermetallics identified herein are also nominally found in commercial AA5083.<sup>28,53</sup>

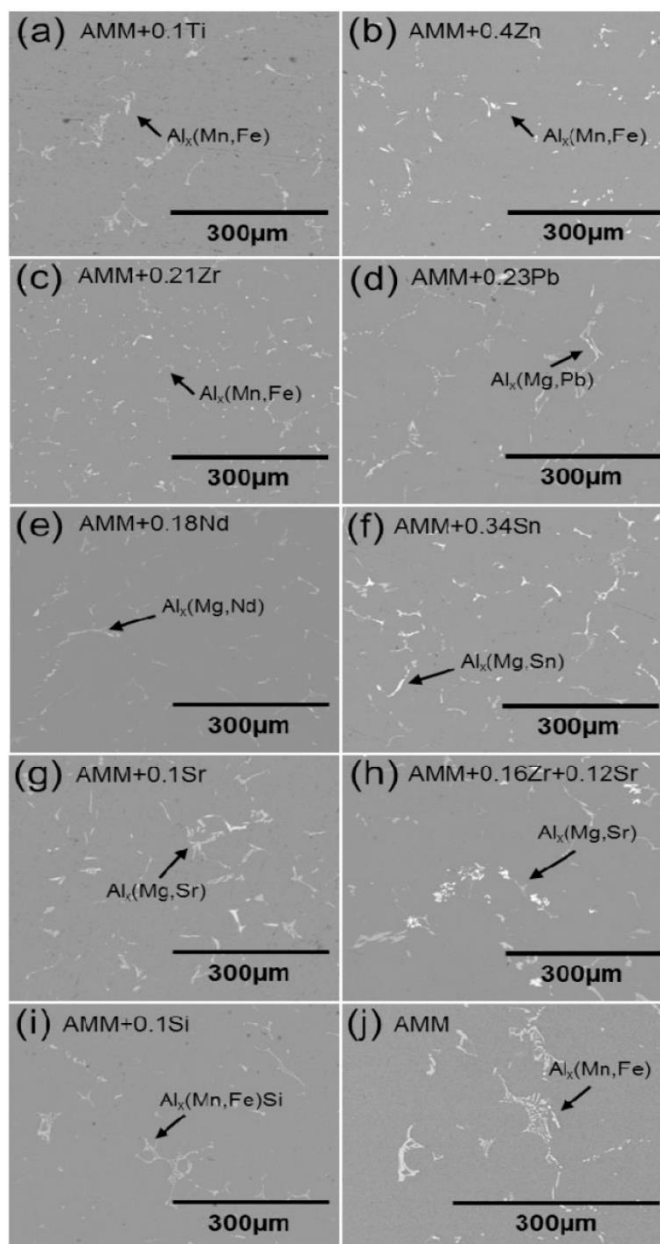
The addition of Zr and Ti are nominally added for the purpose of grain refinement, albeit in somewhat lower concentrations. For the concentrations tested herein, these elements were seen to stimulate the formation of  $Al_3Zr$  and  $Al_3Ti$  constituents (in addition to any nanometre scale dispersoids) as identified by EDX shown in Fig. 1a and c. The presence of Zr retards nucleation through substructure pinning of the fine precipitates and causing shape contractions in the as cast shape of eutectic constituents.<sup>16,54</sup> A limited amount of nuclei lowers recrystallisation which may also reduce corrosion rate by avoiding the formation of high angle grain boundaries.<sup>55</sup>

The addition of Sr in Al–Mg alloy changed the constituent morphology from branched dendrites to a less branched plate like intermetallics as shown in Fig. 1g. The use of Sr in Al–Si alloys is more common than in Al–Mg alloys but herein some modifying effect is also readily observed. EDX also traced the presence of Al–Sr intermetallic which we believe to be  $Al_4Sr$  but the size is too small for quantification be seen in SEM. Zn has a similar modifying effect as Sr, therefore the morphology of constituents is also changed to smaller and less branched than those observed in base alloy (Fig. 1j).<sup>12</sup> With regards to the rare earth element, Nd (Fig. 1e) what is observed is a reduced density of micrometre scale intermetallics compared to the base alloy. Previous study reports the formation of  $Al_{11}Nd_3$  intermetallics in an Mn free Al–Mg alloy,<sup>14</sup> however such quantification was done using TEM. Pb and Sn have low solubility limits in Al (Table 2) and EDX analysis confirms an appreciable amount of Al–Mg–Pb and Al–Mg–Sn constituent particles, which are nominally rich in, and most likely relatively pure, Pb and Sn in the microstructure seen in Fig. 1d and f. Detected Al and Mg levels are very small and most likely due to the overlap between the analysis volume and the surrounding matrix.

### General properties, hardness and mass loss

Optimisation of corrosion performance and mechanical strength is one of the biggest challenges in Al alloy design and therefore understanding simultaneous effect of alloying additions on hardness (a quick measure of strength) and corrosion performance is of great interest. The effect of alloying additions on corrosion (as presented in a first order sense by mass loss) and hardness of the alloys studied is shown in a combined representation in Fig. 2. Alloying additions to the base alloy did not cause a significant change in hardness. Nd and Zr additions lead to a slight increase in hardness, which may be attributed to the formation of fine dispersoids,<sup>20,32,56</sup> but the effect was subtle, whilst the presence of elements such as Pb, Si, Sr and Sn lead to a slight decrease in hardness. Formation of an additional phase with Mg (for example  $Mg_2Si$  in presence of Si and  $Al_{38}Mg_{58}Sr_4$  in case of Sr) would lead to a loss of Mg in solid solution, and consequently a decrease in hardness was observed. The individual effect of alloying elements in Al–Mg base alloy may be summarised as follows:

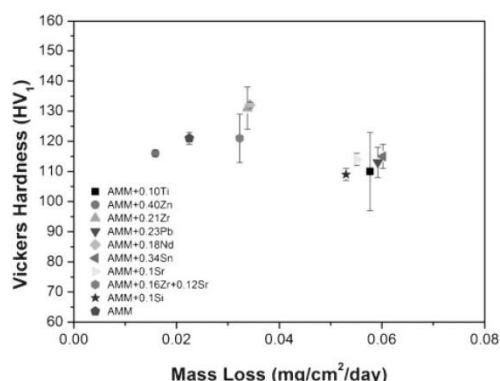
- (i) Zn caused a slight decrease in the corrosion rate (as assessed by mass loss) and hardness. This could be ascribed to the co-solubility of Zn in Al, and the reduction in the formation of second phases. Additionally Zn is reported to decrease the anodic activity of  $\beta$ -phase by depleting the Mg to form ternary phase,  $AlMgZn$  leading to improved corrosion resistance.<sup>12,29</sup>
- (ii) The alloy containing higher Si than the base alloy was observed to have a higher mass loss, but with lower hardness. This may be attributed to the presence of coarse  $Mg_2Si$ , depleting the matrix of Mg, but not contributing to hardness (since hardness contributions would be expected to occur by  $Mg_2Si$  on the nanoscale). Since the alloy was tested in the quenched and wrought condition, the precipitation of fine  $Mg_2Si$  is not expected.<sup>57</sup>



a AMM+0.1Ti; b AMM+0.4Zn; c AMM+0.21Zr; d AMM+0.23Pb; e AMM+0.18Nd; f AMM+0.34Sn; g AMM+0.1Sr; h AMM+0.16Zr+0.12Sr; i AMM+0.1Si; j AMM

1 Backscattered electron (BSE) images of alloys with various alloying elements in as cast condition

- (iii) Additions of Zr increased the hardness of the alloy as well as mass loss values. The formation of  $\text{Al}_3\text{Zr}$  dispersoids impedes dislocations movement hence higher hardness values, however the excess of Zr added herein has also apparently stimulated coarser  $\text{Al}_3\text{Zr}$  particles ( $>1\ \mu\text{m}$ ), which have led to increased levels of corrosion.<sup>58</sup>
- (iv) Ti significantly increased the mass loss value with a slight decrease in hardness. Similar to the effect of Zr, the increased in corrosion rate may be due to the excess of Ti and presence of coarse  $\text{Al}_3\text{Ti}$ .
- (v) Addition of Sr was observed to have significantly high mass loss with a slight decrease in hardness. The formation of coarse  $\text{Al}_4\text{Sr}$  has a



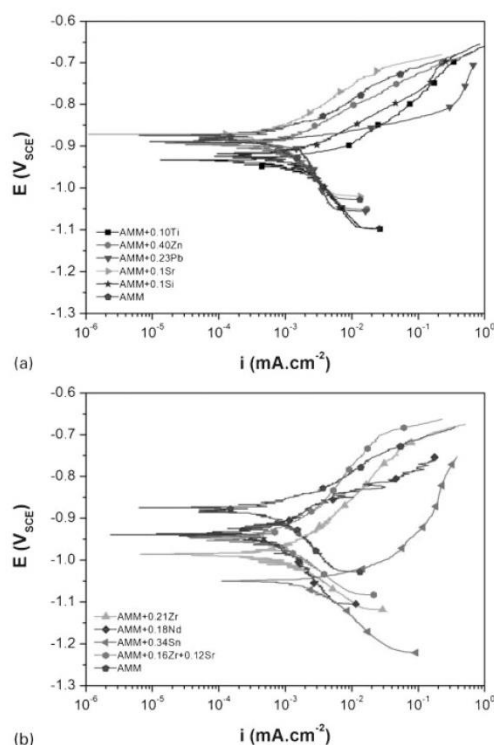
**2 Correlation between hardness and mass loss:** hardness was collected using 1 kg load; mass loss determined from 2 weeks exposure in 0.1M NaCl; error bars omitted for clarity

greater influence on corrosion rate than on hardness as it did not deplete Mg from the solid solution. The modifying effect of Sr on  $\beta$ -phase also unclear by mass loss evaluation.

- (vi) The addition of Nd enhanced the hardness with only a slight increase in mass loss than the base alloy. Formation of  $\text{Al}_{16}\text{Mg}_7\text{Nd}$  phase is reported to be responsible in impeding the movement of dislocation hence higher strength.<sup>47</sup> Nd is also reported to form fine Al rich phase,  $\text{Al}_{11}\text{Nd}_3$  which has lower electrochemical mismatch with the matrix that contributes to lower corrosion rate.<sup>14</sup>
- (vii) The addition of Pb and Sn were found to increase mass loss significantly without much influence on hardness. As Pb and Sn have extremely low solubility limit in Al, one could assert that they have segregated to the metal/oxide interface causing a large anodic activation,<sup>40–42</sup> described further below.

### Influence of chemistry on electrochemical response

The typical potentiodynamic polarisation curves for various alloys are shown in Fig. 3 which reveals the influence of alloying additions on the electrochemical characteristics. These include the corrosion potential  $E_{\text{corr}}$ , pitting potential  $E_{\text{pit}}$ , corrosion current density  $i_{\text{corr}}$  values, along with the relative rates of cathodic and anodic reactions. All the alloying additions, except Sr, shifted the  $E_{\text{corr}}$  to the less noble direction. Depending upon the alloying element the shift in  $E_{\text{corr}}$  was as much as 170 mV (for Sn). An overall shift of  $E_{\text{corr}}$  in the less noble direction as a result of alloying is expected either due to increase in the anodic reaction or decrease in cathodic reaction, or a combination of the change in the rates of the two reactions. Addition of Zn, Sr, Pb, Si and Ti did not lead to significant changes in the cathodic reaction rates. However, Sn, Nd and Zr lead to a rather marked decrease in the cathodic reaction rate. The effect of these alloying elements on anodic kinetics was significantly different than on cathodic kinetics. Additions of Sr decreased the anodic reaction slightly. All other alloying additions lead to increase in anodic kinetics and level of



**3 Typical polarisation curves of alloys in 0.1M NaCl which shows a alloying additions that increase or not changing cathodic reaction kinetics and b alloying additions that reduce cathodic reaction kinetics: both a and b include base alloy (AMM) as benchmark**

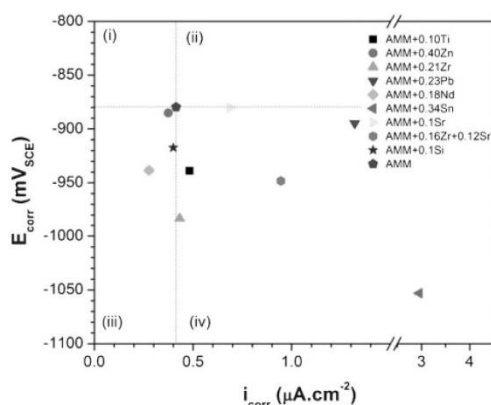
increment was dependent on alloying addition. Sn and Pb have the largest impact in increasing the anodic kinetics, a disproportionate increase concomitant with the phenomenon of anodic activation.<sup>37,39–41</sup>

All alloys tested show a distinct breakdown potential except for the alloys containing Sn, Pb, Ti and Si (Fig. 3). These alloys do not show any passivity windows for the testing herein in 0.1M NaCl. Si does not lead to a large increase in corrosion current density, however, Si can contribute to the formation of  $\text{Mg}_2\text{Si}$  particles which are anodic and increases local anodic reaction rates rather significantly, disrupting passivity.<sup>27</sup>

To interpret the electrochemical reactions that are dominating changes in the corrosion current density,  $E_{\text{corr}}$  was plotted with respect to  $i_{\text{corr}}$  and the plot was divided into four quadrants (Fig. 4). Each quadrant represents whether the cathodic or anodic reaction kinetics dominate changes in  $i_{\text{corr}}$  (see caption, Fig. 4). Most of the alloys are situated in the fourth quadrant which indicates increases in the anodic reaction, dominated over any changes in the cathodic reaction. Only two of the alloys (Nd and Zn containing alloys) fall in third quadrant which indicated that decrease in the cathodic reaction dominated over the change in anodic reaction kinetics.

Mass loss as measured after constant immersion tests was compared with the  $i_{\text{corr}}$  and polarisation resistance



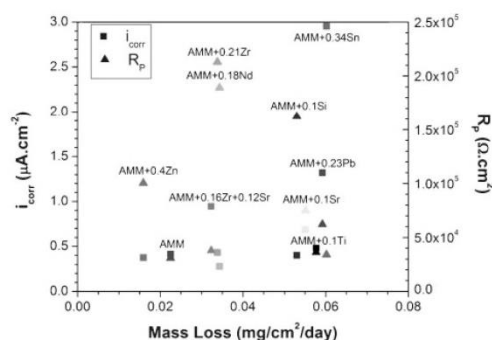


4 Relationship between  $i_{corr}$  and  $E_{corr}$  for alloys tested herein: each quadrant, relative to base alloy, represents: (i), overall reduction in cathodic reaction; (ii), overall increase in cathodic reaction; (iii), overall reduction in anodic reaction; (iv), overall increase in anodic reaction

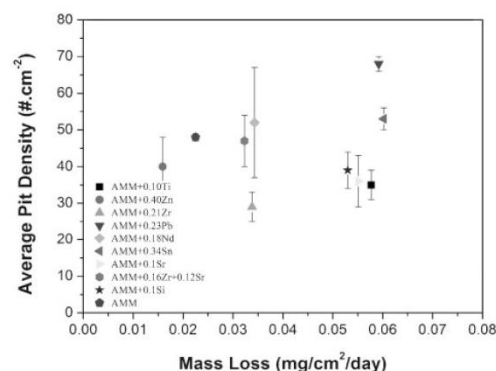
$R_p$  which is presented in Fig. 5. Mass loss as measured from the immersion tests was not linearly necessarily proportional to the electrochemical parameters with a low scatter, however generally speaking there is a correlation from these two independent tests (one being short term, the other long term). Further, the relatively subtle differences observed in mass loss herein mean that in the context of alloy corrosion overall, a relative narrow window of mass loss was observed. As expected  $R_p$  increased with decreased in  $i_{corr}$ .

#### Influence of microstructure on corrosion morphology

Mass loss only indicates the amount of metal dissolution during corrosion and not necessarily the severity of the localised attack that could be more vital in assessing the performance of structural materials in corrosive environments. Pitting susceptibility as measured using potentiodynamic polarisation tests sometimes may result in

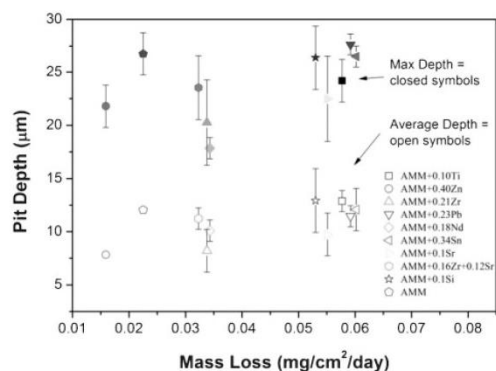


5 Correlation between  $i_{corr}$  and  $1/R_p$  with mass loss: electrochemical response was determined via potentiodynamic polarisation, PDP (for  $i_{corr}$ ) and via electrochemical impedance spectroscopy, EIS (for  $R_p$ ); PDP and EIS were conducted on independent samples following open circuit exposure of 10 min in 0.1M NaCl



6 Correlation between pit density and mass loss: pit density was determined using optical profilometry following 2 weeks exposure in 0.1M NaCl; error bars omitted for clarity

misleading information and therefore microscopic observation of pitting damage to corroborate findings also becomes necessary. In order to gauge the significance of the attack, surface characterisation by optical profilometry was carried out after immersion revealing the pitting characteristics relationship with mass loss as seen in Figs. 6 and 7. The amount of pits (known as the pit density) does not necessarily correlate linearly with the mass loss measurements, indicating that the different alloys tested had rather different localised corrosion morphologies. Alloys containing Nd, Pb and Sn form more pits than the base alloy. The alloys that populates in high mass loss spectrum have wide variation of pit density, with the Pb containing alloy yields the highest number of pits. This indicates that dissolution of metal does not necessarily point to the formation of pits in such cases, and that a correlation between particle density and damage may not be so relevant for 'activated' alloys where the surface film has been disrupted en masse. Again, the results seen here for pit density could be possibly related to differences in the constituent particle



7 Correlation between maximum pit depth and average pit depth with mass loss: pit depth was determined using optical profilometry following 2 weeks exposure in 0.1M NaCl; Opaque symbols indicate maximum pit depth and outlined symbols as average pit depth; error bars omitted for clarity

densities, with those having lower mass loss apparently having more pits arising due to there being more smaller constituents, however the relative scatter is rather small. Additionally, the pit density is not representative of pit depth, and hence the depth is analysed and presented separately.

The maximum and average pit depth varied rather slightly with alloying additions, however there is a statistically relevant difference, and it is apparent that there is a trend between mass loss and pit depth (albeit for the small range of space which these alloys occupy) as shown in Fig. 7. Alloys containing Sr, despite having high mass loss, did not form pits deeper than the base alloy and at par with Nd and Zr containing alloys which have much lower mass loss. As Sr is insoluble in Al, Al<sub>4</sub>Sr phase was expected to form,<sup>59</sup> it is however not visible in the SEM images shown in Fig. 1g and h. This indicates that the size is small (nanoscale) and localised attack was not associated with these particles. Sr also modifies the characteristics of intermetallic particles such as the  $\beta$ -phase, hence reducing probable sites for localised attack.<sup>49,60–62</sup> Alloy with Si has less pit density than the base alloy due to the formation of coarse Mg<sub>2</sub>Si precipitate. As Mg is a highly reactive element, Mg<sub>2</sub>Si tend dissolve selectively and severely leaving deeper pits (contribute to higher mass loss) than the base alloy. The segregation of Pb and Sn destabilises the oxide layer increases sites for localised attack as shown by the average pit density.<sup>39–41,63</sup> This followed by higher depth of the pits due to increase in the anodic activity. Other notable element is Zn which effectively lowered the pit depth and mass loss in comparison to the base alloy. This indicates that Zn is not only reduced the localised attack but also the general corrosion. It may be related to the modification of  $\beta$ -phase and formation of electrochemically homogeneous  $\tau$  phase.<sup>11,12</sup>

## Conclusions

1. From an electrochemical perspective, it was observed that alloying additions did not significantly alter the rates of the cathodic reaction. Of the influence on cathodic kinetics, the only statistically relevant change was the reduction in cathodic kinetics imparted by Sn additions, however this did not offset the concomitant increase in anodic kinetics by the activation effect.

2. The alloying elements Pb, Sn, Zn, Ti, Zr, Nd and Si showed an increase in anodic kinetics such that electrochemical corrosion rates were enhanced. This was attributed to activation in the case of Pb and Sn (noting that Sn was much more efficient at activation), but also due to microstructural disruption in the case of Zn, Ti, Zr, Nd and Si in this Al–Mg–Mn system. A more detailed discussion regarding the changes in microstructure and phase analyses in relation to heat treatment (sensitisation) are reported in Part II of this work. The impact of Sr was reported here for the first time and Sr additions were seen to reduce anodic kinetics in the base Al–Mg–Mn alloy.

3. The addition of Pb, Sn, Zn, Ti, Zr, Nd, Sr and Si had an influence on the hardness of the alloys tested. Of the elements tested, it appeared that Zr and Nd were able to impart a statistically relevant hardening effect,

whilst the elements Pb, Sn, Zn, Ti, Sr and Si did not have a significant impact on hardness.

4. In regards to moderating corrosion, from electrochemical testing, Nd and Zn indicated that a minor (but not significant) reduction in  $i_{\text{corr}}$  could be obtained, however in regards to mass loss tests, the data was rather inconclusive with the tests indicating (besides for the high corrosion rates imparted by Pb, Sn, Ti, Sr and Si) that most mass loss rates were similar. To assess any localisation of corrosion, profilometry revealed Pb formed highest number of pit and Zr the lowest, however again, the results are not varying largely between alloys (nominally values are within ~20% of one another).

## Acknowledgements

The Australian Research Council Centre of Excellence for Design in Light Metals is gratefully acknowledged. We also acknowledge the RMIT Microscopy & Microanalysis Facility and The Ohio State University CEOF (Prof. H. L. Fraser) for provision of SEM. NS acknowledges the Ministry of Higher Education, Malaysia for scholarship provision.

## References

1. J. R. Davis: 'Corrosion of aluminum and aluminum alloys'; 1999, Materials Park, OH, ASM International.
2. I. J. Polmear: 'Light alloys: from traditional alloys to nanocrystals', 4th edn, 2006; Burlington, MA, Elsevier/Butterworth-Heinemann.
3. I. L. Muller and J. R. Galvele: *Corros. Sci.*, 1977, **17**, 995–1007.
4. J. L. Searles, P. I. Gouma and R. G. Buchheit: *Mater. Sci. Forum*, 2002, **396–402**, 1437–1442.
5. D. R. Baer, C. F. Windisch, M. H. Engelhard, M. J. Danielson, R. H. Jones and J. S. Vetrano: *J. Vacuum Sci. Technol. A: Vacuum Surf. Films*, 2000, **18**, 131–136.
6. R. Goswami, G. Spanos, P. S. Pao and R. L. Holtz: *Mater. Sci. Eng. A*, 2010, **A527**, 1089–1095.
7. R. Goswami, G. Spanos, P. S. Pao and R. L. Holtz: *Metall. Mater. Trans. A: Phys. Metall. Mater. Sci.*, 2011, **42**, 348–355.
8. A. J. Davenport, Y. Yuan, R. Ambat, B. J. Connolly, M. Strangwood, A. Afseth and G. M. Scamans: *Mater. Sci. Forum*, 2006, **519–521**, 641–646.
9. I. Oguocha, O. Adigun and S. Yannacopoulos: *J. Mater. Sci.*, 2008, **43**, 4208–4214.
10. R. Goswami, G. Spanos, P. S. Pao and R. L. Holtz: *Metall. Mater. Trans. A*, 2010, **42A**, 348–355.
11. M. C. Carroll, P. I. Gouma, G. S. Daehn and M. J. Mills: *Mater. Sci. Eng. A*, 2001, **A319–A321**, 425–428.
12. M. C. Carroll, P. I. Gouma, M. J. Mills, G. S. Daehn and B. R. Dunbar: *Scr. Mater.*, 2000, **42**, 335–340.
13. N. Birbilis, R. Zhang, M. L. C. Lim, R. K. Gupta, C. H. J. Davies, S. P. Lynch, R. G. Kelly and J. R. Scully: *Corrosion*, 2013, **69**, 396.
14. R. K. Gupta, Y. Wang, R. Zhang, N. L. Sukiman, C. H. J. Davies and N. Birbilis: *Corrosion*, 2012, **69**, 4.
15. L. Lodgaard and N. Ryum: *Mater. Sci. Eng. A*, 2000, **A283**, 144–152.
16. J. S. Vetrano, S. M. Brummer, L. M. Pawlowski and I. M. Robertson: *Mater. Sci. Eng. A*, 1997, **A238**, 101–107.
17. A. K. Bhattamishra and K. Lal: *Mater. Des.*, 1997, **18**, 25–28.
18. M. Cavanaugh, N. Birbilis, R. Buchheit and F. Bovard: *Scr. Mater.*, 2007, **56**, 995–998.
19. V. S. Sinyavskii, V. D. Val'kov and E. V. Titkova: *Protect. Met.*, 1998, **34**, 549–555.
20. Z. Yin, Q. Pan, Y. Zhang and F. Jiang: *Mater. Sci. Eng. A*, 2000, **A280**, 151–155.
21. J. Røyset and N. Ryum: *Int. Mater. Rev.*, 2005, **50**, 19–44.
22. N. L. Sukiman, X. Zhou, N. Birbilis, A. E. Hughes, J. M. C. Mol, S. J. Garcia, X. Zhou and G. E. Thompson: 'Durability and corrosion of aluminium and its alloys: overview, property space, techniques and developments', 2012. dx.doi.org/41099
23. K. D. Ralston, N. Birbilis, M. Weyland and C. R. Hutchinson: *Acta Mater.*, 2010, **58**, 5941–5948.

24. R. K. Gupta, N. L. Sukiman, M. K. Cavanaugh, B. R. W. Hinton, C. R. Hutchinson and N. Birbilis: *Electrochim. Acta*, 2012, **66**, 245–254.
25. K. D. Ralston, N. Birbilis, M. K. Cavanaugh, M. Weyland, B. C. Muddle and R. K. W. Marceau: *Electrochim. Acta*, 2010, **55**, 7834–7842.
26. R. K. Gupta, A. Deschamps, M. K. Cavanaugh, S. P. Lynch and N. Birbilis: *J. Electrochem. Soc.*, 2012, **159**, C492–C502.
27. R. K. Gupta, N. L. Sukiman, K. M. Fleming, M. A. Gibson and N. Birbilis: *ECS Electrochem. Lett.*, 2012, **1**, B1–B3.
28. K. A. Yasakau, M. L. Zheludkevich, S. V. Lamaka and M. G. S. Ferreira: *Electrochim. Acta*, 2007, **52**, 7651–7659.
29. K. A. Unocic, P. Kobe, M. J. Mills and G. S. Daehn: *Mater. Sci. Forum*, 2006, **519–521**, 327–332.
30. J. S. Vetrano, C. H. Henager Jr, S. M. Brummer, Y. Ge and C. H. Hamilton: 'Use of Sc, Zr and Mn for grain size control in Al–Mg alloys', *Mater. Res. Soc. Sympos. Proceed.*, 1998, 89–98.
31. Z. Liu, Z. Li, M. Wang and Y. Weng: *Mater. Sci. Eng. A*, 2008, **A483–A484**, 120–122.
32. X. Wang, G. Chen, B. Li, G. Wu and D. Jiang: *Gongcheng/Rare Met. Mater. and Eng.*, 2010, **39**, 719–722.
33. F. Fazeli, W. J. Poole and C. W. Sinclair: *Acta Mater.*, 2008, **56**, 1909–1918.
34. N. Birbilis and R. G. Buchheit: *J. Electrochem. Soc.*, 2005, **152**, B140.
35. 'ASM handbook', Volume 02, 'Properties and selection: non-ferrous alloys and special-purpose materials'; 1990, Materials Park, OH, ASM International.
36. S. G. Song, J. S. Vetrano and S. M. Brummer: *Mater. Res. Soc.*, 1997, **458**, 237–242.
37. Y. W. Keung, J. H. Nordlien, S. Ono and K. Nisancioglu: *J. Electrochem. Soc.*, 2003, **150**, B547–B551.
38. J. C. Walmsley, Ø. Sævik, B. Graver, R. H. Mathiesen, Y. Yu and K. Nisancioglu: *J. Electrochem. Soc.*, 2007, **154**, C28–C35.
39. B. Graver, A. M. Pedersen and K. Nisancioglu: *ECS Trans.*, 2009, **16**, 55–69.
40. Ø. Sævik, Y. Yu, J. H. Nordlien and K. Nisancioglu: *J. Electrochem. Soc.*, 2005, **152**, B334–B341.
41. Z. Jia, B. Graver, J. C. Walmsley, Y. Yu, J. K. Solberg and K. Nisancioglu: *J. Electrochem. Soc.*, 2008, **155**, C1–C7.
42. J. T. B. Gundersen, A. Aytas, J. H. Nordlien and K. Nisancioglu: *Corros. Sci.*, 2004, **46**, 697–714.
43. B. Graver, A. M. Pedersen and K. Nisancioglu: *ECS Trans.*, 2009, **16**, (52), 55–69.
44. Anawati, B. Graver, H. Nordmark, Z. Zhao, G. S. Frankel, J. C. Walmsley and K. Nisancioglu: *J. Electrochem. Soc.*, 2010, **157**, C313–C320.
45. D. J. Field, G. M. Scamans and E. P. Butler: *Metall. Trans. A*, 1987, **18A**, 463–472.
46. J. O. M. Bockris, R. E. White and B. E. Conway: 'Modern aspects of electrochemistry (No. 31)'; 1998, Dordrecht, Springer.
47. H. Li, H. Wang, X. Liang, Y. Wang and H. Liu: *J. Mater. Eng. Perform.*, 2012, **21**, 83–88.
48. T. Song, X. Xu, Z. Fan, Z. Zhang, B. Wang and Y. Luo: *Chin. J. Rare Met.*, 2012, **36**, 196–200.
49. M. Timpel, N. Wanderka, R. Schlesiger, T. Yamamoto, N. Lazarev, D. Isheim, G. Schmitz, S. Matsumura and J. Banhart: *Acta Mater.*, 2012, **60**, 3920–3928.
50. C. Liao, J. Chen, Y. Li, R. Tu and C. Pan: *J. Mater. Sci. Technol.*, 2012, **28**, 524–530.
51. F. H. Samuel, A. M. Samuel, P. Ouellet and H. W. Doty: *Metall. Mater. Trans. A*, 1998, **29A**, 2871–2884.
52. M. K. Cavanaugh: 'Modelling the environmental dependence of localized corrosion evolution in AA7075-T651', PhD thesis, Ohio State University, 2009.
53. L. Tan and T. R. Allen: *Corros. Sci.*, 2010, **52**, 548–554.
54. J. S. Vetrano, S. M. Brummer and I. M. Robertson: *Mater. Res. Soc. Symp. Proceed.*, 1996, 177–182.
55. H. C. Fang, K. H. Chen, X. Chen, H. Chao and G. S. Peng: *Corros. Sci.*, 2009, **51**, 2872–2877.
56. Y. Wang, R. K. Gupta, N. L. Sukiman, R. Zhang, C. H. J. Davies and N. Birbilis: *Corros. Sci.*, 2013, **73**, 181.
57. F. Eckermann, T. Suter, P. J. Uggowitzer, A. Afseth and P. Schmutz: *Electrochim. Acta*, 2008, **54**, 844–855.
58. J. R. Scully, T. O. Knight, R. G. Buchheit and D. E. Peebles: *Corros. Sci.*, 1993, **35**, 185–195.
59. V. Raghavan: *J. Phase Equil. Diffus.*, 2007, **28**, 473–476.
60. P. Ashtari, H. Tezuka and T. Sato: *Mater. Trans.*, 2003, **44**, 2611–2616.
61. W. Eidhed: *J. Mater. Sci. Technol.*, 2008, **24**, 45–47.
62. M. H. Mulazimoglu, A. Zaluska, F. Paray and J. E. Gruzleski: *Metall. Mater. Trans. A: Phys. Metall. Mater. Sci.*, 1997, **28**, 1289–1295.
63. M. Kliškić, J. Radošević, S. Gudić and M. Šmith: *Electrochim. Acta*, 1998, **43**, 3241–3255.



## Monash University

### Declaration for Thesis Section 5.2

In the case of Section 5.2, the nature and extent of my contribution to the work was the following:

Nature of contribution	Extent of contribution (%)
Initiation, key ideas, experimental, development, results interpretations, writing up	40

The following co-authors contributed to the work. If co-authors are students at Monash University, the extent of their contribution in percentage terms must be stated:

Name	Nature of contribution	Extent of contribution (%) for student co-authors only
Nick Birbilis	Initiation, key ideas, experimental, development, results interpretations, writing up	5
Rajeev Gupta	Initiation, key ideas, experimental, development, results interpretations, writing up	40
Rudy Buchheit	Results interpretations, writing up	5
K.M. Fleming	Results interpretations, writing up	5
Mark Gibson	Results interpretations, writing up	5

The undersigned hereby certify that the above declaration correctly reflects the nature and extent of the candidate's and co-authors' contributions to this work.

**Candidate's  
Signature**

	<b>Date</b> 18 June 2014
---	-----------------------------

**Main  
Supervisor's  
Signature**

	<b>Date</b> 18 June 2014
---	-----------------------------



## Electrochemical Behavior and Localized Corrosion Associated with Mg<sub>2</sub>Si Particles in Al and Mg Alloys

R. K. Gupta,<sup>a,\*</sup> N. L. Sukiman,<sup>a</sup> K. M. Fleming,<sup>b</sup> M. A. Gibson,<sup>c</sup> and N. Birbilis<sup>a,\*</sup>

<sup>a</sup>Department of Materials Engineering, Monash University, Clayton, Victoria 3800, Australia

<sup>b</sup>Department of Materials Science and Engineering, University of Virginia, Charlottesville, Virginia 22904, USA

<sup>c</sup>CSIRO Process Science and Engineering, Melbourne, Victoria 3168, Australia

The electrochemical characteristics of Mg<sub>2</sub>Si in dilute NaCl over a range of pH values are presented. In this study, Mg<sub>2</sub>Si was carefully synthesized to permit the collection of its anodic and cathodic potentiodynamic polarization response. Difficulties in producing bulk Mg<sub>2</sub>Si means that such data remains scarce to date. Mg<sub>2</sub>Si is an important intermetallic that forms in Al and Mg alloys containing silicon. In this work, the electrochemical response of Mg<sub>2</sub>Si is interpreted (and contrasted) in the context of Al and Mg alloys that contain Mg<sub>2</sub>Si, revealing that Mg<sub>2</sub>Si is either a local anode or local cathode.

© 2012 The Electrochemical Society. [DOI: 10.1149/2.002201eel] All rights reserved.

Manuscript submitted February 17, 2012; revised manuscript received February 23, 2012. Published July 17, 2012.

The electrochemical properties of intermetallic phases (whether constituent or precipitated) present in aluminum (Al) and magnesium (Mg) alloys differ significantly from the matrix, rendering such alloys susceptible to localized corrosion.<sup>1-4</sup> A quantitative understanding of the electrochemical characteristics of the intermetallic phases which populate an alloy have been shown to be imperative in order to predict, determine and characterize the overall alloy corrosion behavior.<sup>5</sup>

Si is a common element present either as an impurity or as an alloying addition in both Al and Mg alloys.<sup>6</sup> In the context of Al-alloys, Si additions nominally form Mg<sub>2</sub>Si when Mg is also present (the amount required to form Mg<sub>2</sub>Si will depend on the Mg:Si ratio in the alloy, but may be as low as 0.2 wt%). Whilst Si is also present up to 10 wt% in Al casting alloys where a large population of Mg<sub>2</sub>Si is reported,<sup>7</sup> such alloys are not the principal focus in this work. However, wrought alloys based on the 6xxx series are critical in structural applications, since they are nowadays alloyed more heavily to induce precipitation hardening (via formation of Mg<sub>2</sub>Si) during paint baking of automotive panels.<sup>8</sup> Mg<sub>2</sub>Si has also been noted to form in hypoeutectic die cast Al-alloys.<sup>9</sup> In the context of Mg alloys, even small amounts of Si will form Mg<sub>2</sub>Si, with Si being largely insoluble at temperatures below 600°C.

In regards to electrochemical kinetics, little is known about the unique electrochemical behavior of Mg<sub>2</sub>Si, with the exception of one study that reported the electrochemical response over a range of chloride concentrations at neutral pH.<sup>2</sup> More recently the observations from a selection of experiments on the corrosion of Al-alloy 6061 brazed with Al-Si-(Cu) fillers indicated the ramification of Mg<sub>2</sub>Si in the microstructure.<sup>10</sup> The former study<sup>2</sup> employed the microcapillary technique where polarization tests were performed on Mg<sub>2</sub>Si particles (a few tens of microns in size) embedded in the heterogeneous bulk alloy matrix. Additionally, some detailed observations of the behavior of Mg<sub>2</sub>Si in Al-alloys were given by Jain,<sup>7</sup> who was amongst the first to suggest that in neutral bulk pH, Mg<sub>2</sub>Si dissolves by dealloying and preferential dissolution of Mg; which was later also confirmed by Eckermann and coworkers.<sup>11</sup> Given that the electrochemical response is heavily dependant on electrolyte pH, further tests are warranted, which is the aim of this study. The ability to elucidate the corrosion potential and dissolution/reduction kinetics of Mg<sub>2</sub>Si across the pH range will allow for assessment of whether Mg<sub>2</sub>Si is expected to behave as a local anode or cathode (along with the associated intensity of local currents it may sustain) in the context of alloys which it may populate. To do this, the electrochemical response of Mg<sub>2</sub>Si was compared with that of two common Al (AA6360-T6 and AA7075-T651) and a Mg alloy (AS31), all containing Mg<sub>2</sub>Si.

### Experimental

**Material.**— Mg<sub>2</sub>Si was synthesized by stacking alternating layers of thin sheets of pure Mg (99.9%) and Si (99.9%), and encapsulating the stack in a quartz tube backfilled with argon. This approach was designed to maximize the wetting of the Si during the melting of the Mg ( $T_{\text{melt}}(\text{Mg}) = 650^\circ\text{C}$ ). Given the large difference in the melting temperature of Mg and Si ( $T_{\text{melt}}(\text{Si}) = 1414^\circ\text{C}$ ), and the requirement to stay below the boiling point of Mg for safety concerns ( $T_{\text{boil}}(\text{Mg}) = 1091^\circ\text{C}$ ), quartz encapsulation allowed the stack to be held for extended periods at temperatures above  $T_{\text{melt}}(\text{Mg})$  the whilst avoiding oxidation and giving time for formation of the Mg<sub>2</sub>Si compound. Specimens were air-cooled.

To confirm the formation of Mg<sub>2</sub>Si, X-ray diffraction (XRD) was performed on the synthesized Mg<sub>2</sub>Si using Cu K<sub>α</sub> radiation ( $\lambda = 0.1541$  nm) at a scan rate of 0.5°/min and at 50 steps per degree (Philips 1130). Microstructural characterization was carried out using a JEOL-7001 field emission gun scanning electron microscope (SEM), equipped with energy dispersive x-ray spectroscopy (EDX).

**Electrochemical characterization.**— Separate anodic and cathodic potentiodynamic polarization experiments were conducted. Prior to each test, specimens were ground in ethanol to 2000 grit (SiC paper). All tests were conducted in quiescent 0.01 M NaCl (pH 2, 6 and 13) using a standard three-electrode flat cell (PAR), incorporating a saturated calomel electrode (SCE) and a platinum mesh counter electrode. A VMP3 Potentiostat (BioLogic) under the control of EC-lab software was used. Polarization commenced after monitoring the open circuit potential (OCP) for 30 minutes, and a scan rate of 1 mV/s was used. The exposed surface area of Mg<sub>2</sub>Si was about 15 mm<sup>2</sup>, acetone soluble red-lacquer was used for specimen masking. Experiments were independently repeated at least 5 times to ensure reproducibility. The tested specimens were examined under an optical microscope to verify that no crevice corrosion had occurred. Comparative open circuit potentials of AA6063-T6 (nominal composition wt% Al-0.6Mg-0.5Si), AA7075-T651 (nominal composition wt% Al-2.5Mg-6Zn-1.3Cu-0.2Si) and AS31 (nominal composition wt% Mg-3Al-1Si) are reported following 30 minutes immersion.

### Results and Discussion

The combination of XRD, SEM, and EDX confirmed the presence of single phase Mg<sub>2</sub>Si. The XRD revealed the cubic crystal structure of Mg<sub>2</sub>Si (space group Fm3m), however this structural result was also cross-validated from an EDX determined Mg to Si atomic ratio of ~2:1, where the EDX spectrum was collected at several points. Figure 1 shows a typical SEM image of a test sample and a photograph of as synthesized Mg<sub>2</sub>Si in the inset. The features in Figure 1 correspond to dimples and grinding marks that arise from the brittle nature of Mg<sub>2</sub>Si.

\*Electrochemical Society Active Member.

<sup>†</sup>E-mail: rajeev.gupta@monash.edu

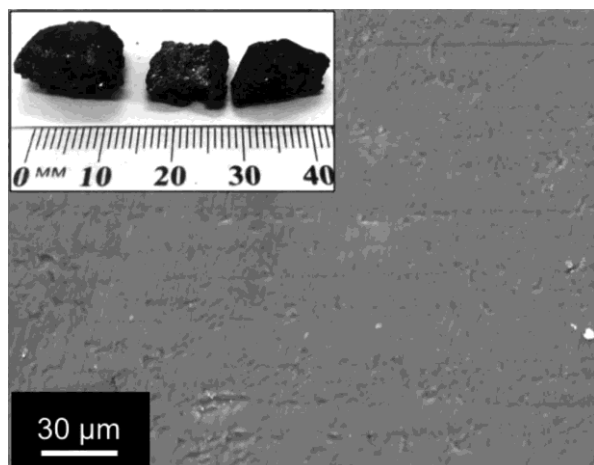
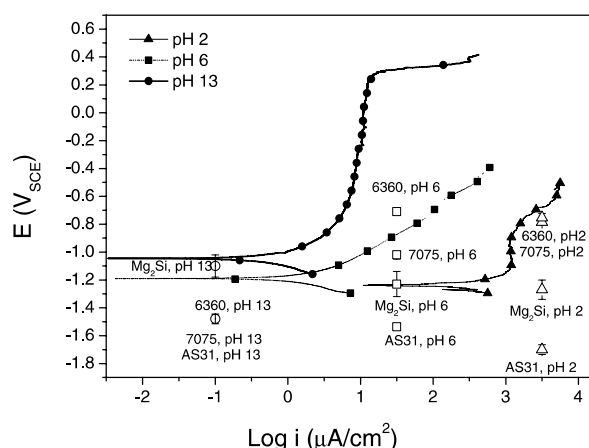


**Figure 1.** Backscattered SEM image of  $\text{Mg}_2\text{Si}$ . Inset shows a photograph of bulk  $\text{Mg}_2\text{Si}$  pieces cut from ingot. Dimples/scratches are remnants from the grinding of the brittle  $\text{Mg}_2\text{Si}$ .

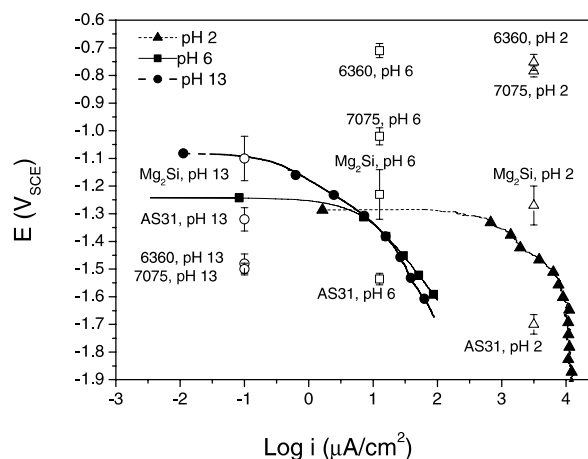
Anodic polarization curves of  $\text{Mg}_2\text{Si}$  in 0.01 M NaCl within a pH range of 2 to 13 are presented in Figure 2. Such curves indicate that the polarization response is strongly influenced by the electrolyte pH. Retardation of the anodic reaction kinetics are observed as pH increases from 2 to 6, accompanied by a slight ennoblement in corrosion potential. In alkaline pH,  $\text{Mg}_2\text{Si}$  exhibits a passive window (with a distinct breakdown at  $\sim 0.2 V_{\text{SCE}}$ ) associated with the passivity of Mg at this pH. Such passive behavior of  $\text{Mg}_2\text{Si}$  is not observed at neutral pH. In a qualitative sense, the polarization response of  $\text{Mg}_2\text{Si}$  follows that of Mg<sup>12</sup> as opposed to Si,<sup>2,13</sup> whereby current densities are highest and dissolution is rapid at low/acidic pH (i.e. 2), with dissolution slowing until a critical pH where the metal passivates.

Figure 3 shows cathodic polarization curves for  $\text{Mg}_2\text{Si}$ . In the potential range studied the cathodic reaction is water reduction (the rate of which was found to be independent of the level of aeration or oxygen concentration from unreported parallel tests). The cathodic response is essentially similar for neutral and alkaline pH, however cathodic kinetics are much more rapid under acidic conditions (which promote hydrogen evolution).

OCP of commercial alloys that contain a population of  $\text{Mg}_2\text{Si}$  have been overlaid on Figures 2 and 3. Of the Al-alloy OCPs overlaid in



**Figure 2.** Anodic polarization curves of  $\text{Mg}_2\text{Si}$  in quiescent 0.01 M NaCl at pH 2, 6 and 13. OCP for AS31, AA7075-T651 and AA6360-T6 are overlaid.



**Figure 3.** Cathodic polarization curves of  $\text{Mg}_2\text{Si}$  in quiescent 0.01 M NaCl at pH 2, 6 and 13. OCP for AS31, AA7075-T651 and AA6360-T6 are overlaid.

Figures 2 and 3 it is observed that at pH 2 and 6, the OCP of Al alloys is more noble than that of  $\text{Mg}_2\text{Si}$ . This implies that at such potentials  $\text{Mg}_2\text{Si}$  acts as an anodic site, undergoing a net anodic polarization within the Al-alloy matrix. At pH 13 however, the OCP of Al alloys is less noble (where Al undergoes rapid dissolution) than that of  $\text{Mg}_2\text{Si}$  and therefore at such elevated pH,  $\text{Mg}_2\text{Si}$  is polarized cathodically compared to the matrix. In the case of Mg-alloy AS31, we observe that although the OCP of AS31 becomes more noble with increasing in pH, OCP remains less noble than the  $\text{Mg}_2\text{Si}$  across the range of tested pH and therefore  $\text{Mg}_2\text{Si}$  was found to be a net cathode with respect to the Mg-matrix in AS31 in all cases.

We acknowledge that such first order determinations are more complex in dynamically corroding systems and alloys with complex surfaces (i.e. with additional second phases or intermetallic encapsulation). However, in order to validate the above assertions, the 6xxx series Al-alloy and AS31 were immersed in neutral 0.01 M NaCl for 90 minutes in order to observe the damage morphology that is associated with  $\text{Mg}_2\text{Si}$  (Figure 4).

It is observed that in the case of  $\text{Mg}_2\text{Si}$  in an Al-matrix, that the  $\text{Mg}_2\text{Si}$  site itself undergoes dissolution (independent of the matrix) as seen in Fig. 4a (secondary electron image). The damage accumulation takes the form of incongruent dissolution which is more obvious in Fig. 4b (backscattered electron image of Fig. 4a), revealing that dissolution occurs in a manner that leaves behind the (bright) Si. This is consistent with not only  $\text{Mg}_2\text{Si}$  serving as a local anode, but also in regards to the damage accumulation mode being incongruent, however the latter is more comprehensively described in.<sup>7,11</sup>

In the case of  $\text{Mg}_2\text{Si}$  in a Mg-matrix, the  $\text{Mg}_2\text{Si}$  appears to remain intact (Fig. 4c) and associated with dissolution of the surrounding matrix. The lack of incongruent (or any) dissolution of  $\text{Mg}_2\text{Si}$  itself is also seen in Fig. 4d, where the  $\text{Mg}_2\text{Si}$  is seen as the brighter particle surrounded by a matrix cavity. It appears that prolonged exposure may have led to the undermining of such an  $\text{Mg}_2\text{Si}$  particle in the more advanced stages of corrosion; and indeed surfaces analyzed from longer immersion times did not permit for ready determination of corrosion morphology (hence the short immersion time of 90 minutes was selected for such reactive systems). The electrochemical analysis with such simple observations indicate that  $\text{Mg}_2\text{Si}$  can be cathodically protected in Mg, which is consistent with work by Yamaguchi et al.<sup>14</sup> who suggested that  $\text{Mg}_2\text{Si}$  undergoes corrosion at rates lower than Mg-alloys; however in the context of Yamaguchi's work which involved  $\text{Mg}_2\text{Si}$  coatings, any coating defects would naturally have caused accelerated corrosion of the Mg substrate.

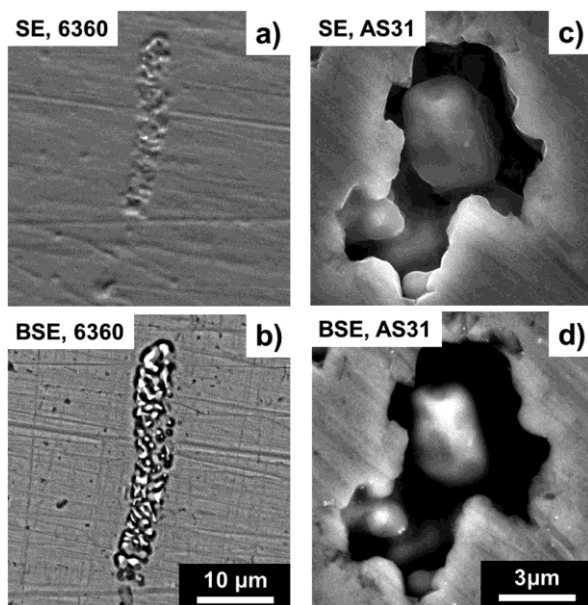


**Figure 4.** a) Secondary electron image showing dissolution of  $\text{Mg}_2\text{Si}$  in an Al-matrix; b) Backscattered electron image of a); c) Secondary electron image showing dissolution around  $\text{Mg}_2\text{Si}$  in an Mg-matrix; d) Backscattered electron image of c). Specimens exposed to quiescent 0.01 M NaCl pH6 for 90 minutes. Specimen preparation was 1  $\mu\text{m}$  diamond suspension; EDS was used to confirm presence of  $\text{Mg}_2\text{Si}$ .

### Conclusions

A suitable sample preparation technique made it possible to produce bulk and uniform  $\text{Mg}_2\text{Si}$  specimens for electrochemical testing.

The electrochemical/polarization behavior of  $\text{Mg}_2\text{Si}$  was investigated was found to be a function of pH, being highly active at acidic pH, active at neutral pH and passive under alkaline conditions.  $\text{Mg}_2\text{Si}$  was cathodic (more noble) with respect to Mg alloy AS31 for whole range of pH tested. Conversely,  $\text{Mg}_2\text{Si}$  was anodic (less noble) to Al alloys 6360 and 7075 in the acidic and neutral pH, but cathodic in alkaline conditions (where Mg is passive and Al dissolves). This study also lends support to the electrochemical response of  $\text{Mg}_2\text{Si}$  being dominated by Mg, and that  $\text{Mg}_2\text{Si}$  dissolves incongruently when it is a net anode.

### Acknowledgments

S.M. Zhu of the CAST-CRC is gratefully acknowledged for providing AS31 specimens. The Australian Research Council is also gratefully acknowledged for financial support. We acknowledge use of the Monash Center for Electron Microscopy.

### References

1. R. G. Buchheit, *J. Electrochem. Soc.*, **142**, 3994 (1995).
2. N. Birbilis and R. G. Buchheit, *J. Electrochem. Soc.*, **152**, B140 (2005).
3. N. Birbilis and R. G. Buchheit, *J. Electrochem. Soc.*, **155**, C117 (2008).
4. A. D. Südholz, N. T. Kirkland, R. G. Buchheit, and N. Birbilis, *Electrochemical and Solid-State Letters*, **14**, C5 (2011).
5. R. G. Buchheit and N. Birbilis, *Electrochimica Acta*, **55**, 7853 (2010).
6. I. J. Polmear, *Light Alloys*, 3rd ed., Arnold, London (1995).
7. S. Jain, PhD Thesis, The Ohio State University, 2006.
8. S. M. Hirth, G. J. Marshall, S. A. Court, and D. J. Lloyd, *Materials Science and Engineering A*, **319–321**, 452 (2001).
9. S. Otarawanna, C. M. Gourlay, H. I. Laukli, and A. K. Dahle, *Materials Chemistry and Physics*, **130**, 251 (2011).
10. K. M. Fleming, MSc Thesis, University of Virginia, 2011.
11. F. Eckermann, T. Suter, P. J. Uggowitzer, A. Afseth, and P. Schmutz, *Electrochimica Acta*, **54**, 844 (2008).
12. K. D. Ralston, G. Williams, and N. Birbilis, *Corrosion*, **68**, 507 (2012).
13. G. Zhang, *Electrochemistry of silicon and its oxide*, Kluwer, New York (2001).
14. T. Yamaguchi, T. Serikawa, M. Henmi, H. Oginuma, and K. Kondoh, *Materials Transactions*, **47**, 1026 (2006).

## Monash University

### Declaration for Thesis Section 5.3

In the case of Section 5.3, the nature and extent of my contribution to the work was the following:

Nature of contribution	Extent of contribution (%)
Initiation, key ideas, experimental, development, results interpretations, writing up	35

The following co-authors contributed to the work. If co-authors are students at Monash University, the extent of their contribution in percentage terms must be stated:


Name	Nature of contribution	Extent of contribution (%) for student co-authors only
Nick Birbilis	Initiation, key ideas, experimental, development, results interpretations, writing up	10
Rajeev Gupta	Initiation, key ideas, experimental, development, results interpretations, writing up	35
Mary Cavanaugh	Results interpretations, writing up	10
Bruce Hinton	Results interpretations, writing up	5
Chris Hutchinson	Results interpretations, writing up	5

The undersigned hereby certify that the above declaration correctly reflects the nature and extent of the candidate's and co-authors' contributions to this work.

**Candidate's  
Signature**

	<b>Date</b> 18 June 2014
---	-----------------------------

**Main  
Supervisor's  
Signature**

	<b>Date</b> 18 June 2014
---	-----------------------------





# Metastable pitting characteristics of aluminium alloys measured using current transients during potentiostatic polarisation

R.K. Gupta<sup>a,\*</sup>, N.L. Sukiman<sup>b</sup>, M.K. Cavanaugh<sup>a</sup>, B.R.W. Hinton<sup>a</sup>, C.R. Hutchinson<sup>a,b</sup>, N. Birbilis<sup>a,b</sup>

<sup>a</sup> Department of Materials Engineering, Monash University, VIC. 3800, Australia

<sup>b</sup> ARC Centre of Excellence for Design in Light Metals, Monash University, VIC. 3800, Australia

## ARTICLE INFO

### Article history:

Received 30 August 2011

Received in revised form 23 January 2012

Accepted 24 January 2012

Available online 2 February 2012

### Keywords:

Aluminium alloys

Corrosion

Passivity

Metastable pitting

## ABSTRACT

In this study we report a comparison between the metastable pitting observed upon AA2024-T3, AA5005-H34, AA5083-H116, AA6022-O, AA7075-T651 and pure Al, over a range of potentials. Metastable pitting increased with microstructural (hence electrochemical) heterogeneity of the alloys studied, which roughly correlates with hardness. In alloys exhibiting a low pitting propensity, metastable pitting activity completely ceased as the underpotential from  $E_{\text{pit}}$  was increased, whereas for corrosion prone alloys, metastable activity continued independently of underpotential. The selection of the test potential is also a key factor in using the method described herein. It is shown that the  $E_{\text{pit}}$  value bears little correlation with the number of pits formed during long-term exposure as measured using optical profilometry, whereas the metastable pitting rate bears a correlation to the actual pit density.

© 2012 Elsevier Ltd. All rights reserved.

## 1. Introduction

Pitting is the most common form of corrosion for aluminium (Al) and its alloys. Of the common electrochemical testing methods, potentiodynamic polarisation allows a determination of pitting susceptibility by revealing the pitting potential ( $E_{\text{pit}}$ ). Whilst  $E_{\text{pit}}$  is often used as an indication of pitting susceptibility [1], the  $E_{\text{pit}}$  value can however be misleading in the discrimination of pitting propensity between alloys. For example, if an alloy with a more noble  $E_{\text{pit}}$  is supposed to be less susceptible to pitting corrosion, such a judgement is made with no quantification of the number of pits or their relative size [2–4]. The determination of  $E_{\text{pit}}$  also fails to explain the mechanism or kinetics of pit initiation, and does not give any information about the metastable pitting which occurs in Al alloys at potentials well below the  $E_{\text{pit}}$  [5–11]. Furthermore, as indicated by Zavadil et al. [12] there are a number of ‘pre-pitting’ processes that can occur on aluminium. Therefore, an alternative quantification that provides information on the size and frequency of pitting in aluminium alloys is required. Previously, analysis and quantification of metastable pitting events has shown to be useful for discriminating between the pitting characteristics of different alloys or the same alloy processed in a different manner [6,7,13]. Such work follows studies upon ferrous alloys originally conducted by Williams et al. [14–16], who proposed that the probability of

stable pitting (i.e. pits which form and do not subsequently repassivate) was directly related to the occurrence of metastable pitting (i.e. pits which form and subsequently repassivate). It is therefore reasonable to study metastable pitting, since metastable events are not only easier to measure in a practical sense, but they occur more frequently and thence more relevant for a statistical study [2,5,6].

Metastable pitting can be characterised by current fluctuations (viz. transient spikes) when an alloy is held potentiostatically below  $E_{\text{pit}}$ . These transients correspond to the nucleation, growth and repassivation of metastable pits. Inclusions, intermetallic particles (coarse or fine), surface roughness and electrochemical potential are factors that influence the nucleation and growth of metastable pits [2,6]. In aluminium alloys, intermetallics may be in the form of constituent particles, precipitated phases, or dispersoids, as outlined in [4,17]. To date, most of the published work in this field is on stainless steels, with metastable pitting studies on Al and its alloys being less common. Cavanaugh suggested that the reason for this lack of attention is due to the larger frequency of metastable pitting events on Al alloys necessitating computer assisted analysis, and the increased complexity of such analysis [6]. A recent paper in regards to automated current transient analysis is given by Soltis et al. [18]. Pride et al. [5] were amongst the first researchers to investigate metastable pitting of pure Al by counting the current fluctuations in electrolytes of various chloride ion concentrations. That work revealed that the number of metastable pitting events increased with both chloride concentration and applied potential. The authors reported that the stabilisation of pits (i.e. a change from metastable to stable pitting) occurred when  $I_{\text{pit}}/r_{\text{pit}}$  was greater than  $10^{-2}$  A/cm, with metastable pit radii ( $r_{\text{pit}}$ ) estimated to be

\* Corresponding author. Tel.: +61 3 9905 5323; fax: +61 3 9905 4940.

E-mail addresses: [rajeev.gupta@monash.edu](mailto:rajeev.gupta@monash.edu), [gupt.rajeev@gmail.com](mailto:gupt.rajeev@gmail.com) (R.K. Gupta).

**Table 1**  
Designation and compositional analysis (weight%, balance Al) of alloys tested.

	Cu	Mg	Si	Zn	Cr	Fe	Mn
Pure Al	<0.05	<0.01	0.04	<0.01	<0.005	0.03	<0.005
AA2024-T3	4.4	1.5	0.50	0.25	0.1	0.50	0.6
AA5005-H34	0.2	0.8	0.30	0.25	0.10	0.70	0.20
AA5083-H116	0.10	4.5	0.40	–	0.1	0.40	0.5
AA6022-O	0.04	0.58	1.35	–	0.10	0.14	0.04
AA7075-T651	1.6	2.5	0.40	5.5	0.23	0.50	0.30

0.1 to 6  $\mu\text{m}$ . Inhibitors such as chromate were reported to be very effective in decreasing the extent of metastable and stable pitting, whereby Trueman [19] investigated the metastable pitting of 2024-T3 in NaCl solution and proposed a model for describing stable pitting by observing metastable pitting. Kim and Buchheit [20] used quantification of metastable pitting to investigate the effect of copper (Cu) on pitting of Al–Cu alloys; suggesting that the addition of Cu to Al (in solid solution form) may inhibit metastable pitting and shift  $E_{\text{pit}}$  in a more noble direction. Current transients collected at a constant applied potential (well below  $E_{\text{pit}}$ ) were analysed to compare the metastable pitting behaviour of Al and Al–Cu alloys. It was concluded that Cu additions diminished the metastable pitting rate. However, the applied potential for transient measurements was very close to the  $E_{\text{pit}}$  for pure Al and more than 100 mV below the  $E_{\text{pit}}$  for an Al – 2% Cu alloy, which may have influenced the conclusions of this work. The effect of applied potentiostatic potential with respect to  $E_{\text{pit}}$  is important, as suggested by Pride et al. [5], and further discussed in this work.

In a specific study that showcased the ability of metastable pit transients to give electrochemical information sensitive to nanoscale microstructural features in an age hardened Al–Cu–Mg alloy, Ralston et al. [7,8] were able to isolate critical precipitate sizes that led to a large increase in pit susceptibility. Davis et al. [10] used a similar technique to report that (1 1 1) crystal facets exhibited the highest number of metastable pits at a given potential, whilst metastable and stable pitting corrosion of aluminium modified with carbon was reported by Lensch et al. [11]. Speckert and Burstein [21] recently investigated current transients in pure Al, Al–0.35% Fe and Al–0.03% Ti alloys. Current transients appearing in these materials were distinguished by their unique size and shape, and the appearance of so-called cathodic transients was reported for the first time. The cathodic transients occurred exclusively in the Fe containing alloy and were attributed to the accelerated hydrogen evolution from the Fe rich pit nucleation site. However, the most comprehensive compilation of work to date is that of Cavanaugh [6], who investigated the effect of potential, time, temperature, pH, and chloride ion concentration on metastable pitting of AA7075-T651.

To date, there have been few comparisons of the metastable pitting behaviour of different Al alloys in a consolidated and systematic presentation. Except for the work of Pride et al. [5] and Cavanaugh [6], the dependence of metastable pitting events in Al systems upon the potentiostatic potential has not been sufficiently investigated in the literature. This paper presents a study on the comparison and quantification of metastable pitting of various Al alloys over a wide range of potentials and relates the metastable pitting to the alloy microstructure, whilst maintaining a broader and general view of the comparisons.

## 2. Experimental

### 2.1. Materials

The aluminium alloys tested in this study, along with their composition and designation (and temper [4]) are given in Table 1. For electrochemical testing, the alloys were cut into “matchstick”

working electrodes and cold mounted in epoxy resin with a wire connection at the rear. Specimens had an exposed surface of 1 mm  $\times$  1 mm. This working electrode size was selected on the basis that the number of pits measured (which scales with area) would be more manageable if the number to be analysed were regulated via the use of a small electrode area.

### 2.2. Electrochemical testing

Prior to each experiment, specimens were ground to a 2000 grit SiC paper finish under ethanol. All electrochemical experiments were carried out in 10  $\mu\text{M}$  NaCl using a standard three-electrode flat cell (available commercially from PAR), incorporating a saturated calomel electrode (SCE) and a platinum mesh counter electrode. A solution volume of 300 mL was used for each test. Prior to testing, the solution was purged with argon gas for at least 45 min to deaerate the solution. Deaeration was necessary so that the kinetics of the oxygen reduction reaction could be largely stifled, thus providing a large window of passivity for the interrogation of each alloy for most accurate determination of  $E_{\text{pit}}$ . In all cases, a VMP3 Potentiostat (BioLogic) under the control of EC-lab software was used for data collection. Anodic potentiodynamic polarisation (PDP) experiments were used to determine the pitting potential ( $E_{\text{pit}}$ ). PDP was commenced after 30 min at the open current potential (OCP) and scanned upwards at a rate of 1.0 mV/s.

Potentiostatic polarisation was employed to produce measurable current transients. Current transients were collected at applied potentials ranging from 25 to 175 mV below the average  $E_{\text{pit}}$ . In this study, to be counted as a pit, a transient event must last at least 1.5 s and experience a current increase of at least 0.4  $\mu\text{A}/\text{cm}^2$ . Current was recorded at a frequency of 4 Hz. After a transient event, if the current recovered to the baseline current (pre metastable event) value, then the pit was considered metastable, otherwise, it was deemed stable. Custom software to automate the counting of metastable (and incipiently, stable) pitting events was applied to all current records collected; details of the associated software macro have been reported previously and are outlined elsewhere [6,13,22].

### 2.3. Characterisation

In order to quantify pitting that occurred following constant immersion for 14 days, optical profilometry was performed upon each alloy, using a Veeco Wyko NT100. Prior to immersion, the specimens were ground to a 2000 grit finish. Following the exposure tests, specimens were cleaned in 7%  $\text{HNO}_3$  to remove corrosion products, with negligible attack of the substrate occurring from such cleaning. Profilometry measurements were carried out at least in triplicate. Depth resolution of optical profilometry was 0.1 nm. Microstructural characterisation of Al alloys was carried out using both transmission electron microscopy (Philips CM-20) and scanning electron microscopy (JEOL 840A). Hardness data was collected using a Struers Duramin A300 with an applied load of 1 kg, and reported hardness values are an average of 10 hardness tests.

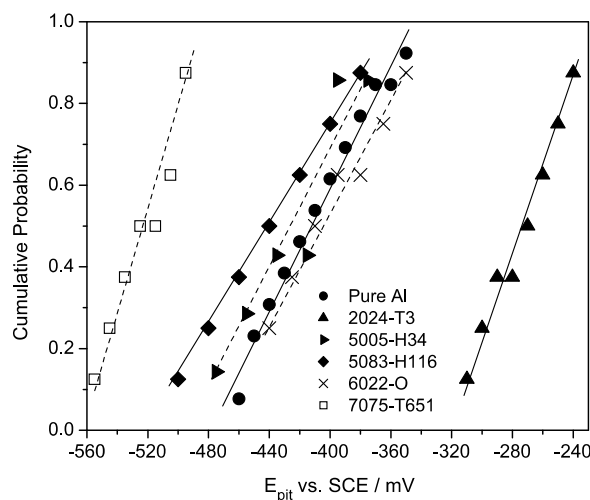


Fig. 1. Cumulative probability of pitting potentials ( $E_{\text{pit}}$ ) as determined by potentiodynamic polarisation in 10  $\mu\text{M}$  NaCl solution.

### 3. Results

#### 3.1. Pitting potential ( $E_{\text{pit}}$ ) of Al and Al alloys

Potentiodynamic polarisation was used to determine the pitting potential ( $E_{\text{pit}}$ ) of each alloy.  $E_{\text{pit}}$  is a distributed parameter [5,20], and in order to convey the variability in  $E_{\text{pit}}$ , a probability plot is presented (Fig. 1). The distribution as evident in Fig. 1 is consistent with what has been observed in Al systems [17,20] and supports the view of Shibata and Takeyama [23] that  $E_{\text{pit}}$  is a distributed parameter and probability of pitting potential can be determined as:  $P(E_{\text{pit}} < E(n)) = n/(N+1)$ , where  $N$  is the total number of samples studied and  $n$  is the number of samples that had pitted at a potential  $E$  or lower. The potential at  $P=0.5$  is a representative value of  $E_{\text{pit}}$  for a given alloy and surface preparation. In this work, we will use this single value of potential and term it the average  $E_{\text{pit}}$  ( $E_{\text{pit}}^*$ ), for the context of setting potentiostatic signals. Whilst Shibata and Takeyama [23] implied that pitting events are stochastic and unpredictable for a given sample, we see rather vividly that comparison of pitting across the range Al alloys studied is deterministic from the point of view that the microstructure and chemistry of the alloys will dictate the amount of pitting observed in a given environment.

#### 3.2. Some general observations of current transients appearing in pure Al and Al alloys

Metastable pitting rate was measured by applying potentials from 25 to 175 mV below  $E_{\text{pit}}^*$  at intervals of 25 mV. Representative raw current transients collected for the alloys (listed in Table 1) at an applied potential of 25 mV below  $E_{\text{pit}}^*$  for each alloy are shown in Fig. 2.

The shape, size and frequency of current transients depended strongly on the alloy tested. Current transients appearing in each material were described by a maximum current density ( $j_{\text{max}}$ ), a peak current density ( $j_{\text{peak}}$ ), a base current density ( $j_{\text{bc}}$ ), a pit growth time ( $t_g$ ) and a repassivation time ( $t_{\text{rp}}$ ). These parameters are defined in Fig. 3. Peak current density ( $j_{\text{peak}}$ ) is defined as,  $j_{\text{peak}} = j_{\text{max}} - j_{\text{bc}}$ . The total time for a metastable pitting event is given by  $t_{\text{pit}} = t_g + t_{\text{rp}}$ . The current densities as quoted here are

obtained by dividing the current by the total area of the test specimen, and therefore the reported current should not be confused by the current density as shown by a single metastable pit.

Generally the base current density ( $j_{\text{bc}}$ ) decayed rapidly following the commencement of the test and the rate of decay decreased with time. The difference in the  $j_{\text{bc}}$  just before the nucleation of a metastable pit and just after the repassivation was quite large in all alloys except AA2024-T3 and AA7075-T651, where the  $j_{\text{bc}}$  after pit repassivation was often greater than that at the beginning of event. This difference in the base current density may be due to simultaneous repassivation and initiation of metastable pits, or most probably a relatively higher number of stable pits (i.e. metastable pits not fully repassivating) in AA2024-T3 and AA7075-T651. Current transients appearing in pure Al were comparatively rare (Fig. 2a). In contrast, frequent, large current transients with larger  $j_{\text{peak}}$  and  $t_{\text{pit}}$  were observed in AA2024-T3; where it appeared as though transients in AA2024-T3 also overlapped one another. Transients occurred very frequently in AA7075-T651, but the  $j_{\text{peak}}$  and  $t_{\text{pit}}$  were small. This may be due to a large number of small metastable pits, or associated with the repetitive repassivation and growth of the same metastable pit. However, distinction of whether a current transient arises from the same metastable pit or from different metastable pit was not possible herein.

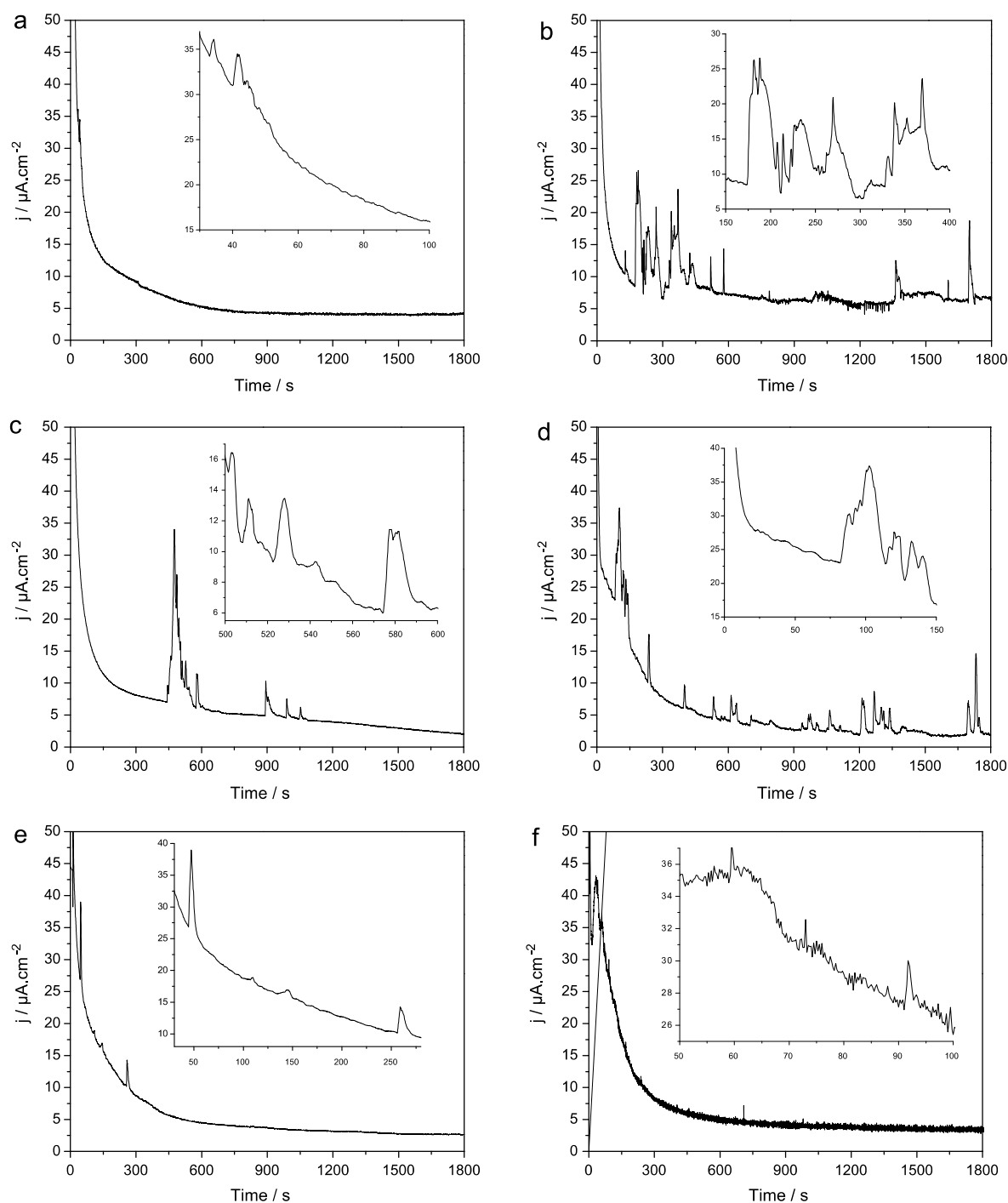
The current rise during pit growth for some of the metastable pitting events appearing in AA 5083-H116 were found to occur in steps which suggests the simultaneous repassivation and growth of metastable pits. Overlap of metastable pits seems less probable as repassivation after attaining peak current density is very sharp (Fig. 2d). Therefore, metastable pits appearing in AA5083-H116 are described to have a greater  $t_g$  than  $t_r$  (i.e. backwards to the normal expected shape, whereas for the other alloys, the  $t_r$  was greater than the  $t_g$ ). An attempt to correlate the size, shape and frequency of current transients observed in the different alloys with the microstructures is discussed in the following section.

#### 3.3. Quantification and comparison of metastable pitting

The number of metastable pits per unit area per minute (defined as the metastable pitting rate) is plotted as a function of potential below  $E_{\text{pit}}^*$  (i.e. the underpotential from  $E_{\text{pit}}^*$ ) in Fig. 4. Metastable pitting events occurred more frequently and with greater intensity as the potential approached  $E_{\text{pit}}^*$ . Pure Al had the highest resistance to metastable pitting rate over the entire range of applied potentials. The metastable pitting rate was greatest in AA7075-T651. Metastable pitting in pure Al, AA5005-H34, AA5083-H116 and AA6022-O alloys ceased at a critical underpotential ( $\sim 75$  mV below  $E_{\text{pit}}^*$ ), whereas metastable pitting was observed in AA2024-T3 and AA7075-T651 at underpotentials as low as  $E_{\text{pit}}^* - 175$  mV (in all cases ensuring that the current value was not negative). We note that 175 mV below  $E_{\text{pit}}^*$  falls well below the open circuit potential of these alloys in naturally aerated aqueous electrolytes (Table 2), which indicates that these alloys are capable of undergoing pitting at their respective open circuit potentials.

The frequency of metastable pitting events can be assessed by presenting data that is binned in 60 s intervals across the  $i$ - $t$  record of 30 min. This is presented for each alloy tested at an applied potential of  $E_{\text{pit}}^* - 25$  mV (Fig. 5). Metastable pit initiation rates for pure Al decreased with time and no metastable pitting event was observed after  $\sim 1000$  s (Fig. 5a). No metastable pit initiation was observed in the first 400 s for AA6022-O (Fig. 5c) but after this, intense metastable pitting occurred and then the frequency of pitting diminished with no metastable pitting observed after  $\sim 1100$  s. The decay of metastable pitting events with time is consistent





Current transients for: (a) pure Al, (b) AA2024-T3, (c) AA6022-O, (d) AA5083-H116, (e) AA5005-H34 and (f) AA7075-T651, obtained at 25 mV below  $E_{pit}^*$ . Insets show a region of interest that represents the typical transient features.

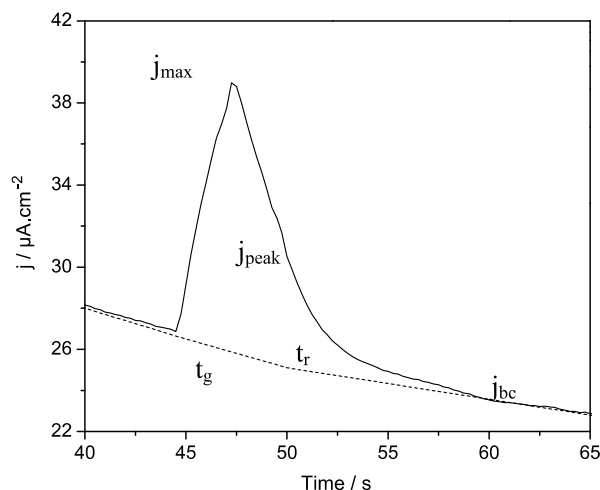
other findings reported in the literature [5,6,20]. However, the alloys (AA2024-T3, AA5005-H34, AA5083-H116 and AA7075-T651) (Fig. 5b,d–f) indicate that the metastable pitting rate did not vary with time, and a continual germination of pits is observed for up to at least 30 min. The notion that a steady rate of pit germination can persist with time was also previously suggested by the work of Cavanaugh for AA7075-T651 [6].

### 3.4. Pitting potential and extent of metastable pitting

A comparison of metastable pitting rate (collected at  $E_{pit}^* - 25$  mV) versus  $E_{pit}^*$  shows that, for the alloys studied in this work there was no obvious trend between these parameters (Fig. 6). This indicates that  $E_{pit}^*$  cannot be unambiguously used for assessing the intensity of pitting corrosion. For example, the metastable pitting

**Table 2**Pitting potentials and open circuit potentials of Al and Al alloys in 10  $\mu$ M NaCl solution.

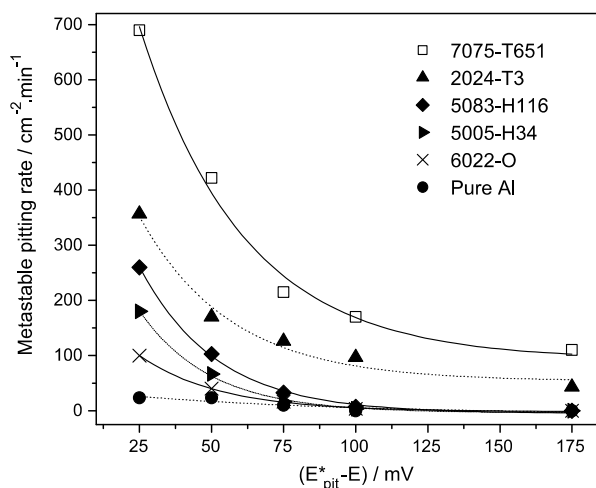
	$E_{\text{pit}}$ vs. SCE/mV	OCP vs. SCE/mV in deaerated solution	OCP vs. SCE/mV in quiescent solution
Pure Al	−416 ( $\pm 34$ )	−1390 ( $\pm 20$ )	−854 ( $\pm 18$ )
AA2024-T3	−279 ( $\pm 25$ )	−1100 ( $\pm 25$ )	−350 ( $\pm 30$ )
AA5005-H34	−433 ( $\pm 42$ )	−1220 ( $\pm 15$ )	−672 ( $\pm 14$ )
AA5083-H116	−433 ( $\pm 46$ )	−1250 ( $\pm 25$ )	−542 ( $\pm 19$ )
AA6022-O	−405 ( $\pm 41$ )	−1210 ( $\pm 10$ )	−621 ( $\pm 17$ )
AA7075-T651	−525 ( $\pm 20$ )	−1190 ( $\pm 26$ )	−521 ( $\pm 22$ )

**Fig. 3.** Typical transient seen on a current density versus time plot. The various parameters used to describe a current transient are labelled.

rate for AA 2024-T3—which displays the most noble  $E_{\text{pit}}^*$ , was  $\sim 200$  times more than that for pure Al in the same conditions.

### 3.5. Hardness vs metastable pitting

The corrosion behaviour of aluminium alloys is greatly affected by alloying elements [4]. These elements are deliberately added to tailor the mechanical properties of the alloy (i.e. strength, hardness, toughness, ductility, etc.). The strength of these alloys typically increases with the heterogeneity of the microstructure, and this

**Fig. 4.** Metastable pitting rate (defined following 30 min) for pure Al and various Al alloys as a function of potential below  $E_{\text{pit}}^*$ .

microstructural heterogeneity usually also corresponds to electrochemical heterogeneity [20]. As a result, it is reasonable to expect some correlation between alloy hardness and the propensity for pitting. Fig. 7 reveals the metastable pitting rate (for two applied potentials) as a function of alloy hardness. A correlation between the evolution of microstructure, mechanical properties and metastable pitting rate was given by Ralston et al. [8] for a model Al–Cu–Mg alloy. In that work the impact of precipitation from a solid solution to overaged condition was shown to have a significant affect on metastable pitting rate, which allowed a realisation of the metastable pitting rate vs. hardness relationship to be attained for a single alloy. Herein however, we represent a more general property space for the hardness of commercial alloys vs. metastable pitting rate to indicate a correlation exists more broadly, and emphasise that such a relationship can only be realised via the use of the metastable pitting rate parameter.

### 3.6. Charge transferred through metastable pits

The total charge emanating from metastable pitting events (i.e. the total area under all transient spikes) which accumulated over the 30 min test period was evaluated (with the aid of Origin Pro®). This charge is presented versus the metastable pitting rate (Fig. 8). The charge related to metastable pitting was the greatest for AA 2024-T3, and the least for pure Al. No direct correlation between charge transferred and metastable pitting rate was observed however, which indicates that pit size and shape may vary from one alloy to other. For example, the total charged transferred through metastable pits in AA2024-T3 is greater than that through AA7075-T651, whereas, metastable pitting rate of AA7075-T651 is greater. This indicates that metastable pit size for AA7075-T651 should be smaller than that for AA2024-T3 and similar trend should be applicable for all other alloys under consideration. A detailed study on this topic in the future will be very interesting.

### 3.7. Relationship between metastable pitting and stable pitting

The correlation between stable pitting and metastable pitting events has been reported in the literature [14–16] for stainless steel. Williams [14–16] proposed a linear relationship between the two; however, the existence of such a relationship for Al and Al alloys has yet to be established. Whilst it is not the goal to correlate Al with stainless steel (the systems being inherently different in many aspects), we opted to present the number of pits arising from a unit area after constant immersion of each alloy in quiescent NaCl solution for 14 days (as measured using optical profilometry) and plot this against the metastable pitting rate (collected at  $E_{\text{pit}}^* - 25$  mV) in Fig. 9. There appears to be a correlation between the values determined from short term potentiostatic testing and the longer-term immersion tests. The parameters are left in their native units to emphasise that they are fundamentally different in their evaluation and time scale, hence it is simply the revelation of a correlation that is being emphasised. It is evident from the images obtained from the optical profilometer (Fig. 9), that AA7075-T651

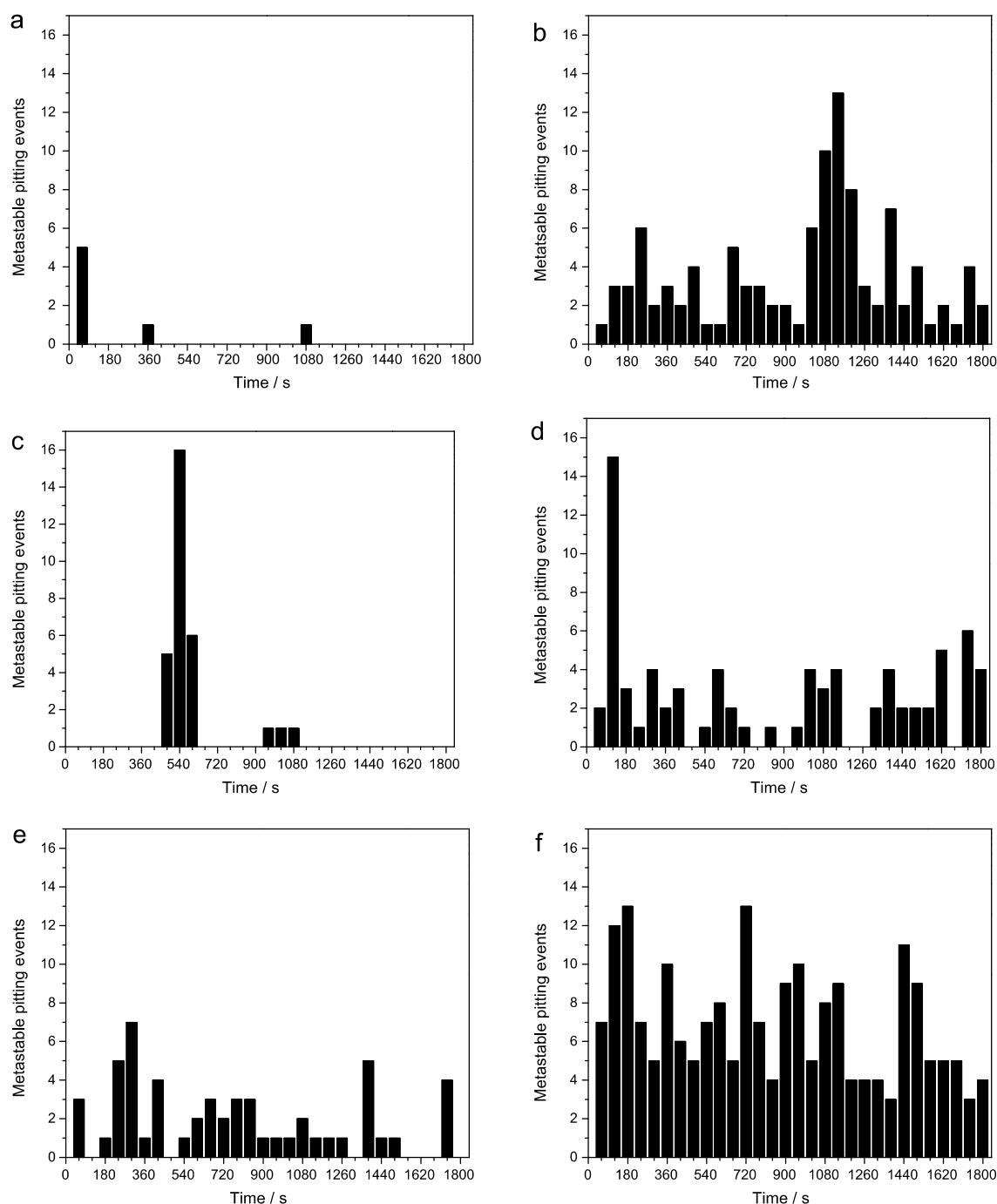


**Fig. 5.** Number of metastable pits occurring per 60 s in: (a) pure Al, (b) AA2024-T3, (c) AA6022-O, (d) AA5083-H116, (e) AA5005-H34 and (f) AA7075-T651, measured at 25 mV below  $E_{\text{pit}}^*$  of each respective alloy.

had a large number density of fine pits. AA2024-T3 had fewer pits, but they had a larger diameter and are deeper. It is also interesting to note that pure Al, AA5005 (not shown) and AA5083 had much fewer stable pits, however a small number of them grew to comparatively large depths ( $\sim 20 \mu\text{m}$ ) in 14 days. In service conditions, both size and number of metastable pits are important. In contrast, the density of stable pits, as measured by profilometry is plotted with against  $E_{\text{pit}}^*$  in the Fig. 10, which indicates no obvious

correlation between the two, suggesting (as in Fig. 6) that  $E_{\text{pit}}^*$  is not a good indication of propensity for pitting.

#### 4. Discussion

It was observed that the composition of the alloys tested played a significant role in the metastable pitting response. In order to give

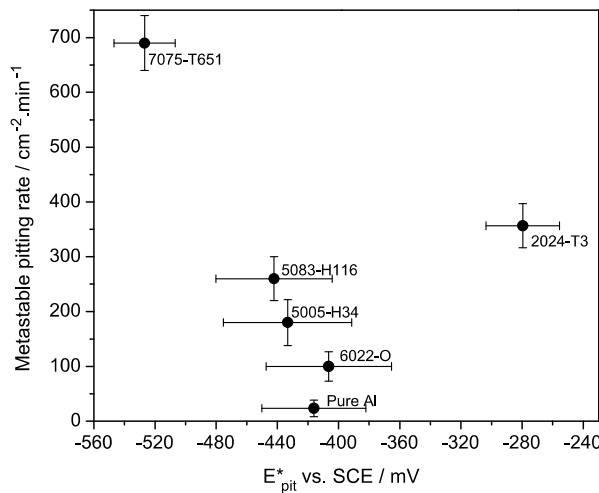


Fig. 6. Metastable pitting rate (measured at 25 mV below  $E_{pit}^*$ ) versus average pitting potential.

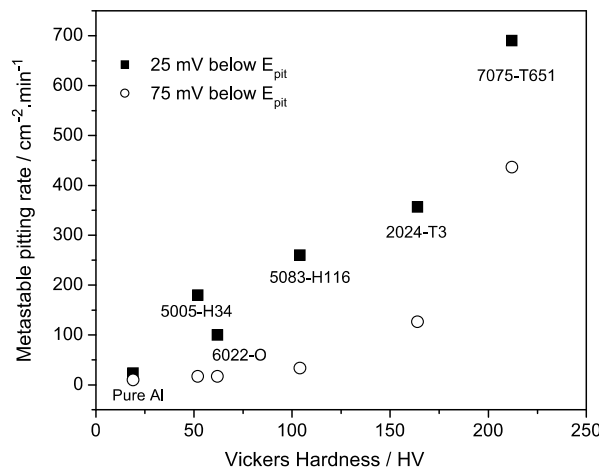


Fig. 7. Hardness versus metastable pitting rate collected at 25 mV and 75 mV below  $E_{pit}^*$ .

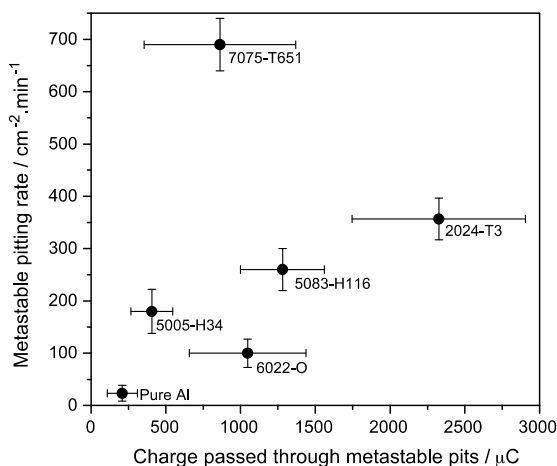


Fig. 8. Total charge measured arising from metastable pits during 30 min of potentiostatic polarisation at 25 mV below  $E_{pit}^*$ .

an overall account of the results of this study, selected microstructures of the alloys tested are presented (Fig. 11).

It was observed that for a 5xxx series alloy, as per typical Al-alloys, on the microscale a number of constituent particles from impurities and alloy production persist on the length scale of  $\sim 1\text{--}50\text{ }\mu\text{m}$ . However, the nanostructure is free of any features, with the alloy being a ‘solid solution’ alloy designed to be precipitate free and non-age hardenable (Fig. 11A, B, K and L). In the case of AA2024-T3 and AA7075-T651, we also observe the typical constituent particles on the micron scale, however we observe a large number density [24] of strengthening precipitates in the nanostructure; AA7075-T651 having the greater number density. It is important to emphasise that on the micron level, all the alloys have coarse constituent particles that are present from alloy production and insoluble (due to the high melting point of Fe, Mn containing intermetallics and coarse Cu and Si containing constituents [25]). Such constituents are there in all commercial alloys, and this must be appreciated.

The ability of fine changes in microstructure to dictate the metastable pitting response has been previously observed by Cavanaugh [6] in two contexts. In that work, it was shown that when AA7075-T651 was solution heat treated to dissolve all the nanoscale precipitates, that a decrease in the number of metastable pitting events was observed. However, that decrease was only one increment, and when compared with pure Al, a further decrease in the number of metastable pitting events was observed, suggesting that the composition of the solid solution also plays a role (as coarse insoluble constituents still remain after solution heat treatment). In the work of Cavanaugh, it was further shown that even fewer metastable pits were observed in ultra high purity Al, indicating that the constituent particles also have a role in metastable pitting events [6]. However, the case of highly pure Al was not studied in this present work, and all samples tested in this work have a constituent particle population. Further, the work of Ralston also shows that metastable pitting events increased with the number density and size of precipitates [7].

Bearing in mind the above, as a tentative summary, it is possible to postulate that based on the work herein:

- (1) The presence of nm scale precipitates dramatically increases the number of metastable pits observed.
- (2) The size and composition of the nm scale precipitates can influence the transient size and length, whilst the greatest number of metastable pitting events was observed in AA7075-T651, these events were also characterised by rapid repassivation time and comparatively low transient peak current density. In contrast, AA2024-T3 produced the largest current transients with large  $t_g$  and  $t_{rp}$ .
- (3) Coarse constituents that were present in all alloys did not play the major role in dictating pitting response. In AA5005-H34, and pure Al, where no precipitates exist, the current transients and repassivation time are small. We cannot comment on cases where ‘no constituents exist’ or ‘model solid solutions’ based on the work herein, however such fundamental works are in progress.
- (4) The metastable pitting rate bears correlation with the pitting damage measured following exposure testing, whereby the value of  $E_{pit}^*$  can be biased by bulk alloy chemistry and not necessarily correlate with the extent of pitting that evolves. Future work should emphasise the validation and development of higher fidelity correlations such as that seen in Fig. 9; given how important such relationships can be in the context of accelerated testing.
- (5) The observation that Cu can increase  $E_{pit}^*$  but also increase the pitting damage which evolves was also confirmed.

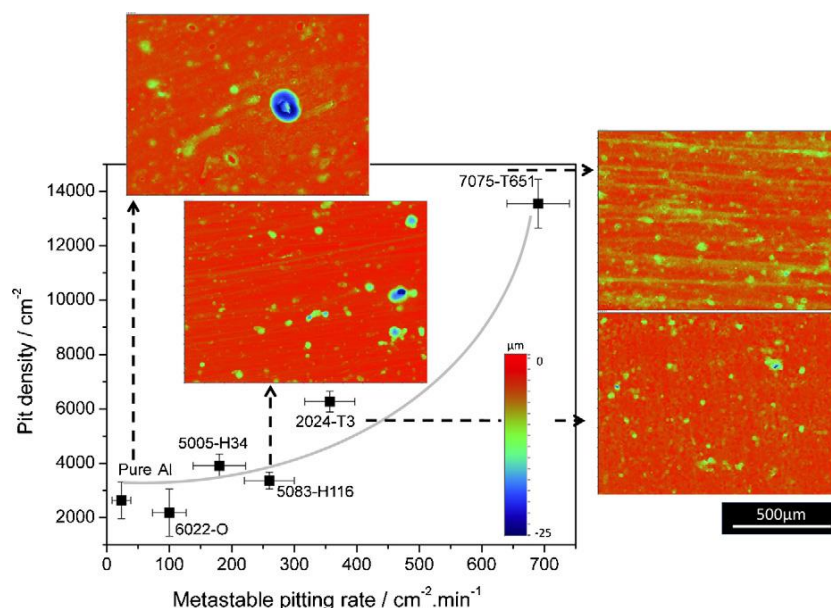


Fig. 9. Actual (i.e. stable) pit density as measured from profilometry (following 14 days of immersion) versus metastable pitting rate measured at 25 mV below  $E_{\text{pit}}^*$ .

Whilst not the focus of this paper, the purpose of which was to show a general utility of the potentiostatic transient method in the context of discrimination between alloys, it is apparent that the above findings can be used as a criterion for studying pitting susceptibility of Al alloys in a manner that can be directly related to microstructure in model systems which has only been exploited by Ralston et al. to date [7] when coupled with high-resolution microscopy. Such fundamental works may also shed light on some aspects related to current transient interpretation; for example a greater charge transfer through an individual metastable pitting event may suggest a larger metastable pit size, etc.

One critical outcome of the present work also indicates that the measured metastable pitting rate strongly depends on the applied potential (Fig. 4). Metastable pitting rate was highest at

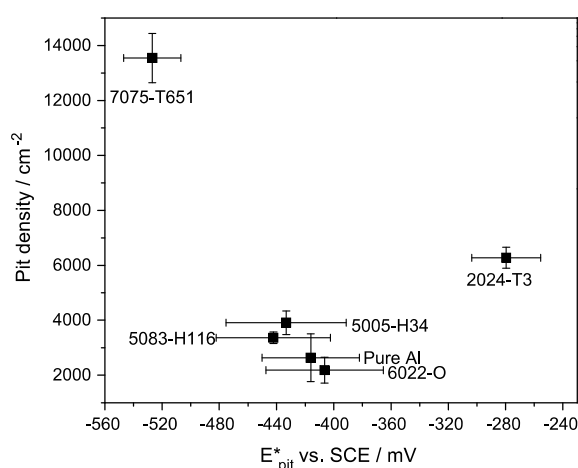
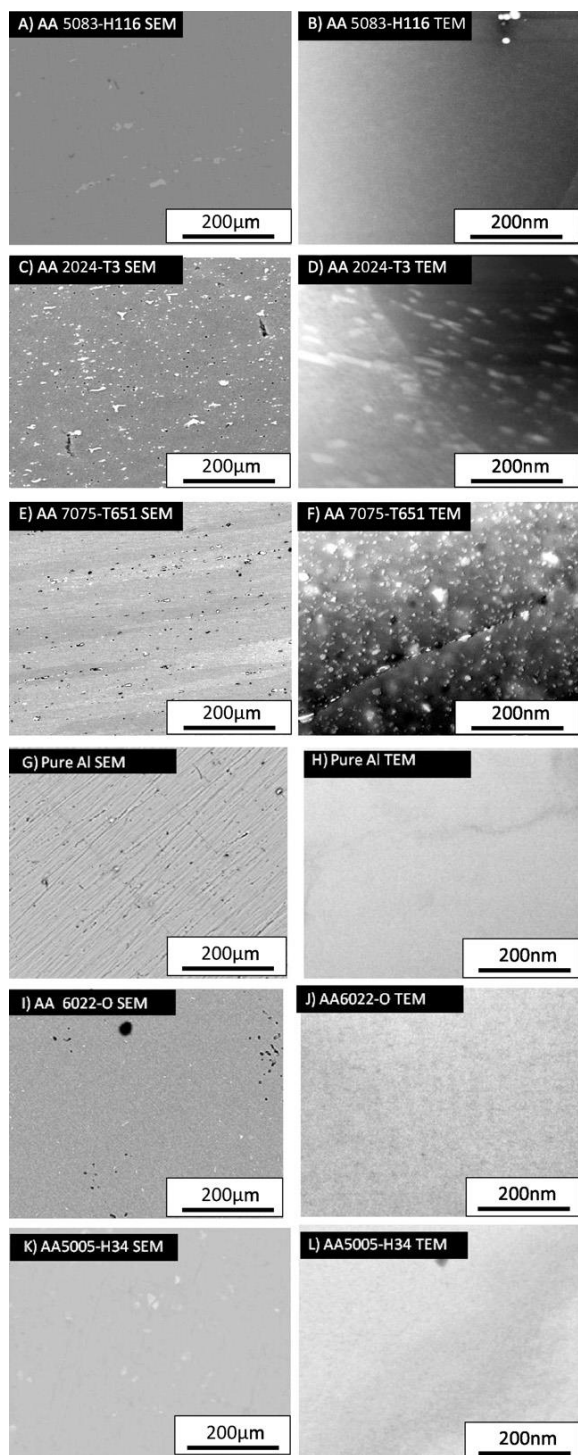
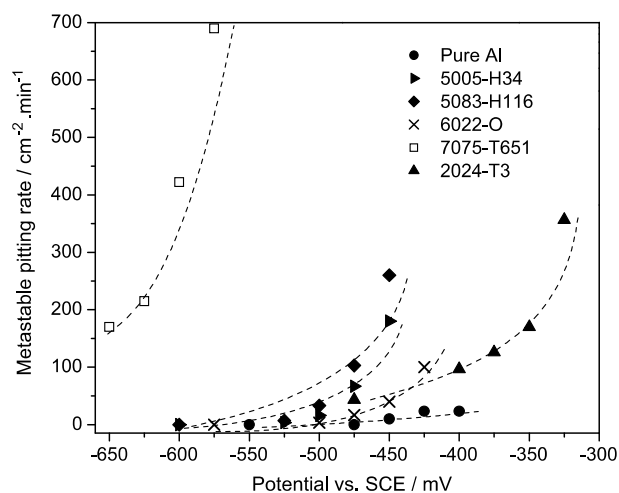


Fig. 10. Actual (i.e. stable) pit density as measured from profilometry versus  $E_{\text{pit}}^*$ .

potentials closest to the  $E_{\text{pit}}^*$  (where the driving force is the greatest). For a direct comparisons of the metastable pitting activity between alloys, the use of a constant underpotential from  $E_{\text{pit}}^*$  (i.e. constant driving force) may be more informative than applying a fixed value of potential (i.e. an isopotential versus a reference electrode). In prior works, most authors have used a standard isopotential with respect to reference electrode for comparison of the metastable pitting susceptibility of alloys with significantly different  $E_{\text{pit}}^*$ . For example Kim and Buchheit [20] compared the pitting susceptibility of Al with two Al–Cu alloys and established that the addition of Cu (in solid solution form) decreased the number of metastable pitting events compared with Al. However, this trend may not have been manifest if a constant driving force were employed; as the applied potential in that work was very close to the pitting potential of Al, and well below the  $E_{\text{pit}}^*$  of Al–2Cu. In other instances however, Cavanaugh [6] used an isopotential and a range of underpotentials from  $E_{\text{pit}}^*$  to study the effect of environmental variation on the same alloy (in that case AA7075-T651) which seems to be the most effective way to study the variation of environmental factors whilst not varying the substrate. Consequently, researchers have the ability to choose between constant driving force (from  $E_{\text{pit}}^*$ ) or isopotential tests, depending on the information they require/seek. In the present study, we have established that the choice of potential with respect to  $E_{\text{pit}}^*$  is critical to compare the metastable pitting frequency of different alloys (e.g. Fig. 12). At a potential of  $-475 \text{ mV}_{\text{SCE}}$ , the number of metastable pits occurring on the AA2024-T3 were less than those on AA5005-H34 and AA5083-H116. Therefore the comparison of the metastable pitting rate of AA5005-H34 and AA5083-H1115 against AA2024-T3 at an applied potential of  $-475 \text{ mV}_{\text{SCE}}$  may falsely give the impression that AA2024-T3 is less prone to pitting. However, profilometry and exposure measurements confirm that this was not the case. This observation establishes that the choice of applied potential for comparison of metastable pitting response between different alloys is a key parameter and should be chosen based on the respective  $E_{\text{pit}}^*$ .



**Fig. 11.** Microstructure of various alloys: (A) SEM image of AA5083-H116, (B) TEM image of AA5083-H116, (C) SEM image of AA2024-T3, (D) TEM image of AA2024-T3, (E) SEM image of AA7075-T651, (F) TEM image of AA7075-T651, (G) SEM image of Pure Al, (H) TEM image of Pure Al, (I) SEM image of AA6022-O, (J) TEM image of AA6022-O, (K) SEM image of AA 5005-H34 and (L) TEM image of AA5005H34.



**Fig. 12.** Metastable pitting rate as a function of applied potential.

## 5. Conclusions

1. Metastable pitting occurs upon Al and its alloys, and this may be quantified with good fidelity using current transients from potentiostatic polarisation. Metastable pitting rate data can allow one to discriminate between the pitting propensity of different alloys in a more relevant manner than that of the pitting potential alone. The  $E_{pit}^*$  values of individual alloys showed little correlation with the actual number of pits formed upon an Al-alloy surface following immersion test and profilometry, whereas there was a correlation between the number of metastable pitting rate and pitting density.
2. Metastable pitting has a strong correlation with the applied potentiostatic potential. The number of metastable pitting rate, and the size of the transients measured, continually increased as the applied potential approached  $E_{pit}^*$ . These characteristics of metastable pitting are alloy dependent. As a result, comparison between the response of alloys is best determined with testing at a constant underpotential below  $E_{pit}^*$ . In low to medium strength alloys, metastable pitting activity completely ceased as an applied potential is  $\sim 75$  mV below  $E_{pit}^*$ , while in high strength alloys metastable pitting occurred at potentials well below  $E_{pit}^*$ , even at 175 mV below  $E_{pit}^*$  (and as far down as could be practically measured). Such alloys have pitting susceptibility 'built in' to the alloy and will pit in most aqueous environments. This finding is an important revelation in the broader characterisation of Al-alloy corrosion, also revealing a criterion for when an alloy will be susceptible to pitting corrosion. This is defined by situations when the amount of metastable pitting does not cease at significant underpotentials from  $E_{pit}^*$ .
3. The metastable pitting rate observed tended to increase with electrochemical heterogeneity of the alloy studied; hence the metastable pitting rate was strongly dependent on the alloy composition. This sensitivity to alloy composition means that the determination of metastable pitting rate is capable of providing unique information. For example, this electrochemical method has a very good sensitivity to microstructure.
4. Increases in hardness were found to be proportional to the rate of metastable pitting observed, indicating rather vividly that a corrosion penalty that arises in commercial alloys as hardness increases. The density of stable pits determined after long-term immersion tests was well related to the number of metastable pitting events measured potentiostatically.



## Acknowledgements

The Australian Research Council and the DIIRD-funded Victorian Facility for Light Metals Surface Technology are gratefully acknowledged. We acknowledge the use of the Monash Centre for Electron Microscopy.

## References

- [1] Z. Szklarska-Smialowska, Pitting Corrosion of Metals, NACE, Houston, 1986, pp. 39–86.
- [2] P.C. Pistorius, G.T. Burstein, *Philosophical Transactions: Physical Sciences and Engineering* 341 (1992) 531.
- [3] G.S. Frankel, *Journal of the Electrochemical Society* 145 (1998) 2186.
- [4] G.M. Scamans, N. Birbilis, R.G. Buchheit, Corrosion of aluminum and its alloys, in: J.A.R. Tony (Ed.), *Shreir's Corrosion*, Elsevier, Oxford, 2010, 1974.
- [5] S.T. Pride, J.R. Scully, J.L. Hudson, *Journal of the Electrochemical Society* 141 (1994) 3028.
- [6] M.K. Cavanaugh, Modeling the Environmental Dependence of Localized Corrosion Evolution in AA7075-T651, The Ohio State University, 2009.
- [7] K.D. Ralston, N. Birbilis, M.K. Cavanaugh, M. Weyland, B.C. Muddle, R.K.W. Marceau, *Electrochimica Acta* 55 (2010) 7834.
- [8] K.D. Ralston, N. Birbilis, M. Weyland, C.R. Hutchinson, *Acta Materialia* 58 (2010) 5941.
- [9] Z. Szklarska-Smialowska, *Corrosion Science* 41 (1999) 1743.
- [10] B.W. Davis, P.J. Moran, P.M. Natishan, *Corrosion Science* 42 (2000) 2187.
- [11] O. Lensch, B. Enders, J. Knecht, W. Ensinger, *Nuclear Instruments and Methods in Physics Research Section B* 175–177 (2001) 683.
- [12] K.R. Zavadil, J.A. Ohlhausen, P.G. Kotula, *Journal of the Electrochemical Society* 153 (2006) B96.
- [13] M.K. Cavanaugh, N. Birbilis, R.G. Buchheit, *Electrochimica Acta* 59 (2012) 336.
- [14] D.E. Williams, J. Stewart, and P.H. Blackhill, *Proc. Symp. on Critical Factors in Localized Corrosion*, Phoenix (USA), G.S. Frankel and R.C. Newman (Editors), The Electrochemical Society PV 92-9 (1992), 36.
- [15] D.E. Williams, J. Stewart, P.H. Balkwill, *Corrosion Science* 36 (1994) 1213.
- [16] D.E. Williams, C. Westcott, M. Fleischmann, *Journal of the Electrochemical Society* 132 (1985) 1796.
- [17] N. Birbilis, R.G. Buchheit, *Journal of the Electrochemical Society* 152 (2005) B140.
- [18] J. Soltis, D.P. Krouse, N.J. Laycock, K.R. Zavadil, *Corrosion Science* 52 (2010) 838.
- [19] A.R. Trueman, *Corrosion Science* 47 (2005) 2240.
- [20] Y. Kim, R.G. Buchheit, *Electrochimica Acta* 52 (2007) 2437.
- [21] L. Speckert, G.T. Burstein, *Corrosion Science* 53 (2011) 534.
- [22] M.K. Cavanaugh, N. Birbilis, R. Buchheit, *ECS Transactions* 16 (2009) 1.
- [23] T. Shibata, T. Takeyama, *Corrosion* 33 (1977) 243.
- [24] M.K. Cavanaugh, R.G. Buchheit, N. Birbilis, *Engineering Fracture Mechanics* 76 (2009) 641.
- [25] J.R. Davis, *Corrosion of Aluminum and Aluminum Alloys*, ASM International, Materials Park, 1999, p. 25.

# Chapter 6

## The role of chemistry in intergranular corrosion of Al-4Mg-0.5Mn

---

This chapter includes a research paper accepted in the journal ‘Corrosion Engineering, Science and Technology’. Following the outcomes of Chapter 4 and Section 5.1, the same alloys produced which are based on Al-4Mg-0.4Mn system with quaternary addition of elements that including Ti, Zn, Zr, Nd, Sr and Si were studied. The purpose of this chapter was to elucidate the effect of microalloying additions on the intergranular corrosion susceptibility, and indeed in relating this to the  $\beta$ -phase characteristics. Exposure to elevated temperature for the sensitisation of the Al-Mg-Mn was carried out, as opposed to the experimental condition in Chapter 5. In the sensitised condition, Al-Mg-Mn alloy are nominally prone to intergranular attack, as the active  $\beta$ -phase tends to precipitate at the grain boundaries. Herein, the alloys were heat treated at 150°C followed by the Nitric Acid Mass Loss Test (NAMLTL) as outlined in ASTM G67-04. The results highlighted the effectiveness of Sr in minimising the intergranular corrosion by modifying the fraction of  $\beta$ -phase or reducing the amount of Mg available to form  $\beta$ -phase.



## Monash University

### Declaration for Thesis Section 6.1

In the case of Section 6.1, the nature and extent of my contribution to the work was the following:

Nature of contribution	Extent of contribution (%)
Initiation, key ideas, experimental, development, results interpretations, writing up	80

The following co-authors contributed to the work. If co-authors are students at Monash University, the extent of their contribution in percentage terms must be stated:

Name	Nature of contribution	Extent of contribution (%) for student co-authors only
Nick Birbilis	Initiation, key ideas, experimental, development, results interpretations, writing up	5
Rajeev Gupta	Initiation, key ideas, experimental, development, results interpretations, writing up	5
Ruifeng Zhang	Experimental, results interpretations	5
Rudy Buchheit	Results interpretations, writing up	5

The undersigned hereby certify that the above declaration correctly reflects the nature and extent of the candidate's and co-authors' contributions to this work.

**Candidate's Signature**

	<b>Date</b> 18 June 2014
---	-----------------------------

**Main Supervisor's Signature**

	<b>Date</b> 18 June 2014
---	-----------------------------

# Influence of microalloying additions on Al-Mg alloy. Part 2: Phase analysis and sensitisation behaviour

N. L. Sukiman<sup>\*1,2</sup>, R. K. Gupta<sup>1</sup>, R. Zhang<sup>1</sup>, R. G. Buchheit<sup>3</sup> and N. Birbilis<sup>1</sup>

A range of alloys based on the Al-4Mg-0.4Mn system were produced with selected quaternary microalloying additions. In Part 1 of this study, the electrochemical and corrosion response was studied. To characterise the sensitisation behaviour of these alloys, where sensitisation is the major mode of degradation of 5xxx alloys, heat treatment at 150°C was carried out and followed by the Nitric Acid Mass Loss Test (NAMLTL) according to ASTM G67-04. Herein the alloying elements studied include silicon, zinc, titanium, zirconium and strontium. The results indicate that strontium (Sr), silicon (Si) and titanium (Ti) have a significant influence in reducing intergranular corrosion (IGC) susceptibility.

**Keywords:** aluminium, alloying, aluminium alloys, sensitisation, intergranular corrosion

## Introduction

The aluminium–magnesium (Al-Mg) alloys are typically used in structural applications due to their strength to density ratio, good formability, weldability and their relatively exceptional corrosion resistance in many environments. The Al-Mg alloys are designated as the 5xxx series alloys. Of the 5xxx alloys, a common alloy in the rolled sheet and plate form in a structural context (particularly for marine vessels) is AA5083. The 5xxx alloys are non-age hardenable, strengthened by solid solution strengthening by Mg and strain hardening. Most 5xxx alloys contain a >3.5 wt-% Mg<sup>1</sup> to optimise strengthening and meet mechanical requirements. During the production and processing of 5xxx alloys, quenching of such alloys from elevated temperatures allows the retention of a supersaturation of Mg in the alloy. This can lead to in-service precipitation of  $\beta$ -phase ( $\text{Mg}_2\text{Al}_3$ ) which has no impact in increasing the mechanical properties,<sup>2-4</sup> but dramatically increases the susceptibility to intergranular corrosion (IGC) since the presence of  $\beta$ -phase precipitates typically at grain boundaries.<sup>5</sup> Reports of increased susceptibility to IGC and stress corrosion cracking (SCC) exist when 5xxx alloys have been exposed to elevated temperature (as low as 50°C).<sup>6-8</sup> The electrochemical characteristics of  $\beta$ -phase are not discussed in this paper but as reported previously,  $\beta$ -phase is a highly anodic with respect to the Al matrix.<sup>9-12</sup> In 5xxx alloys,  $\beta$ -phase is polarised anodically, and it has been shown that only a minor

anodic polarisation of  $\beta$ -phase (a few tens of mV) can result in large dissolution currents.<sup>11</sup>

In Part 1 of this work, the aim was to assess the electrochemical and corrosion influence of alloy additions on the Al-4Mg-0.4Mn system. Given that an important (and maybe dominant) mode of deterioration of alloys with this base composition (similar to that of AA5083) is due to sensitisation and subsequent intergranular corrosion; a holistic reporting of the performance of such alloys we believe also warrants testing and discussion relates to the sensitisation and IGC performance. More specifically, the ability of low level alloying additions to potentially reduce the susceptibility to IGC was sought to be evaluated. Microalloying with elements (<1 wt-%) to improve the properties of an alloy has been employed for decades. As suggested by Carroll, the addition of Zn to Al-Mg alloys can modify the  $\beta$ -phase by forming a less anodic ternary phase  $\text{AlMgZn}$  ( $\tau$  phase) and by thus potentially reducing the amount of Mg available to form  $\beta$ -phase.<sup>13</sup> Another study by Carroll incorporating Cu in conjunction with Zn also produces a similar result with Cu enriched  $\tau$  phase.<sup>14</sup> To ensure the addition of Cu and Zn is effective in reducing IGC, Unocic revealed that a higher amount of Cu and Zn increased the precipitation of  $\beta$ -phase within the grain instead of at the grain boundaries.<sup>15</sup> Sr is a less common type of alloying element in Al-Mg alloys. The effect of Sr in modifying the intermetallic phase in Al-Si is widely studied.<sup>16-18</sup>

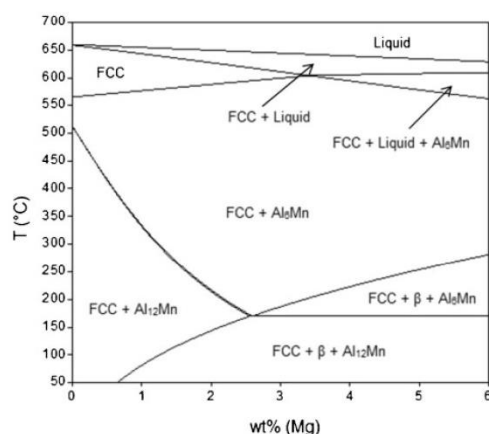
Herein, prior to describing the performance of the alloys in detail, some thermodynamic calculations were performed in order to assess *a priori* the phases that may form in the sensitised condition. This can then be related to the relative increase or decrease in measured IGC. The Nitric acid mass loss tests (NAMLTL) as per the ASTM G67-04 standard<sup>19</sup> was used herein as a method to evaluate the degree of sensitisation.

<sup>1</sup>ARC Centre of Excellence for Design in Light Metals, Department of Materials Engineering, Monash University, VIC. 3800. Australia

<sup>2</sup>Department of Mechanical Engineering, University of Malaya, Kuala Lumpur. 50603. Malaysia

<sup>3</sup>Department of Materials Science and Engineering, The Ohio State University, Columbus OH. 43210. USA

Corresponding author, email nazatul.sukiman@monash.edu



1 Calculated phase diagram for Al-xMg-0.4Mn calculated.  $\beta$ -phase represents  $Mg_2Al_3$

## Experimental

### Materials

The alloys tested in this study were produced by melting an Al-Mg-Mn master alloy (denoted as AMM in Table 1) with alloying elements either in their pure form, or in some instances in the form of commercially available master alloys. Pure Mg and Al were added to balance the chemical compositions in cases where master alloys were used. Melting was carried out in a muffle furnace. Regular stirring of the melt was carried out, followed by casting into a pre-heated (at 300°C) graphite crucible. Cast alloys were homogenised below the liquidus temperature (nominally at 400°C) for two days. The composition of the alloys produced was independently analysed using Inductively Coupled Plasma – Optical Emission Spectrometry (ICP-OES) by Spectrometer Services, Australia, and presented along with designation of the alloys in Table 1.

### Testing

The degree of sensitisation to intergranular attack of the alloys was determined by measuring the Nitric Acid Mass Loss Test (NAML T) values according to ASTM standard G67-04.<sup>19</sup> The samples were immersed in 5% NaOH solution at 80°C for 1 minute and rinsed with water. Then, a 30 seconds immersion in nitric acid was carried out. Finally the samples were rinsed and dried in air. This procedure was adapted from ASTM standard G67-04.<sup>19</sup> After this preparation, all samples were immersed in concentrated nitric acid (70 wt-%) for 24 hours at 30°C. Following immersion, corrosion products were removed by brushing of the samples. The test was repeated for three

times for data reproducibility and standard deviation was used to generate error bars of the results.

### Characterisation

The corrosion morphologies were characterised using an optical microscope (Olympus PMG3) to identify the degree of intergranular attack on the alloys. All samples were mounted in epoxy resin and micro polished to a 0.25  $\mu$ m diamond suspension finish, followed by ultrasonic cleaning.

To assist in interpretation of alloy characterisation, the phase analysis was conducted using Pandat® software package (CompuTherm LLC, Madison, WI).<sup>20</sup> This software is capable of calculating the most stable phase equilibrium without requiring prior knowledge of the diagram by mathematical analysis of thermodynamic properties between the Gibbs free energy and stable phase equilibrium.<sup>21</sup> The PanAluminum database was used for thermodynamic calculations in this work. This software has been previously used in literature to calculate phase diagram and fraction of phases present in Al based alloys.<sup>22–24</sup>

## Results & Discussion

### Calculated phase fractions

The equilibrium phase diagram for Al-xMg-0.4Mn as calculated by Pandat® software is presented in Figure 1. The diagram reveals the phases present at various composition of Mg as a function of temperature. From the phase diagram, when the alloy is sensitised at 150°C, presence of substantial amount of  $\beta$ -phase ( $Mg_2Al_3$ ) and  $Al_{12}Mn$  phase are predicted. The complete composition of the alloys studied and quaternary alloying elements in the Al-xMg-yMn alloy is listed in Table 1.

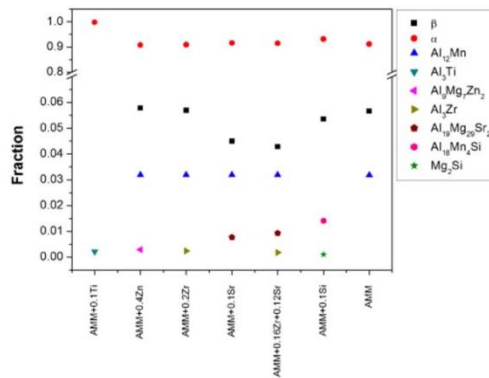
The addition of various elements can alter the existing phases and/or form additional phases. In Table 2, equilibrium phase fractions of the alloys produced (using the actual alloy compositions for calculations) were calculated at 150°C. We emphasise that these are equilibrium calculations reflecting an infinite time at 150°C, however we believe that they serve a great utility for interpretation of the response of the alloys studied herein.

The main cause for the increase in IGC susceptibility of 5xxx alloys is the formation of  $\beta$ -phase. A beneficial influence from any microalloying would be either to modify the composition of the  $\beta$ -phase to a less active state, or to minimise the fraction of this phase.

From Table 2, the relative influence of quaternary additions can be visually gauged. The addition of Sr has a significant impact in reducing the volume fraction of  $\beta$ -phase (also shown in Figure 2), with formation of additional Sr containing ternary phase,  $Al_{19}Mg_{29}Sr_2$ . The use of Sr as modifying agent typically in Al-Si alloys is widely known,<sup>16,18,25</sup> however a similar effect may be

Table 1 Chemical composition determined using ICP-OES for the alloys tested in this study. All values given in weight %

	Al	Mg	Mn	Si	Fe	Ti	Zn	Zr	Sr
AMM	~Bal	4.01	0.49	0.13	0.36				
AMM+0.1Ti	~Bal	3.89	0.48	0.13	0.34	0.10			
AMM+0.4Zn	~Bal	4.01	0.48	0.13	0.33		0.40		
AMM+0.2Zr	~Bal	4.17	0.49	0.11	0.32			0.21	
AMM+0.1Sr	~Bal	3.64	0.47	0.12	0.32				0.10
AMM+0.16Zr+0.12Sr	~Bal	4.02	0.45	0.14	0.33			0.16	0.12
AMM+0.1Si	~Bal	4.00	0.48	0.24	0.32				



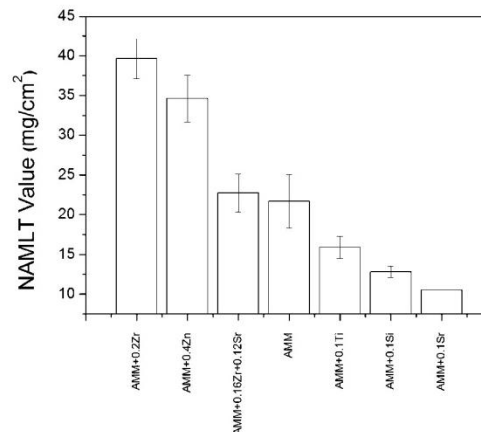
2 Calculated equilibrium fraction of phases present in the alloys at 150°C. The predicted phases are populated mainly by the  $\alpha$ -Al solid solution (FCC phase enriched in Mg),  $\beta$ -phase ( $\text{Mg}_2\text{Al}_3$ ) and  $\text{Al}_{12}\text{Mn}$ , however, the alloying addition are also able to impart additional intermetallics, and in some cases modify the fraction of the  $\beta$ -phase

gained in Al-Mg alloys as well. The addition of Zn is expected to have similar modifying effect to  $\beta$ -phase following the formation of ternary Mg containing phase.<sup>13</sup> However, based on the phase fraction analysis in Table 2, the formation of  $\text{Al}_3\text{Mg}_7\text{Zn}_2$  ( $\tau$  phase) does not reduce the amount of  $\beta$ -phase in the alloy, only a small amount of Zn ( $\sim 4.7$  wt-%) was found incorporated in the  $\beta$ -phase. The calculations however are conceded to not offer any further insight into morphology or location of  $\beta$ -phase that would result (i.e. whether it is displaced from grain boundaries). The addition of Si above the base level gives a slight reduction in  $\beta$ -phase following the formation of  $\text{Mg}_2\text{Si}$  intermetallics. As the amount of Si is more than 0.1 wt-%, Al-Mn dispersoids containing Si was also found.<sup>26</sup> In this case, the stoichiometry of the Mn containing intermetallic is  $\text{Al}_{18}\text{Mn}_4\text{Si}$  and the amount of Si present in the intermetallic is quite substantial. For other alloys in this work, there is no significant change in the amount of  $\beta$ -phase. Depending on the alloying elements, a small amount of other intermetallics (such as  $\text{Al}_3\text{Ti}$  and  $\text{Al}_3\text{Zr}$ ) were found. The following section will discuss how these phases affect the susceptibility to IGC.

### IGC performance as per ASTM G67-04

#### Degree of sensitisation

The resistance to IGC attack can be assessed by measuring the weight loss during nitric acid mass loss test (i.e.,



3 Results from ASTM G67-04 Nitric Acid Mass Loss Test (reported in mass loss per unit area) for alloys sensitised at 150°C for 7 days

NAMLT values). These values represent the degree of sensitisation; a higher value indicates higher susceptibility to IGC. From Figure 3, degree of sensitisation (DoS) for the baseline alloy was found to be 22 mg/cm<sup>2</sup>.

The influence of the quaternary alloying additions on the mass loss of the Al-xMg-yMn alloy is presented in the order of highest to lowest mass loss (Figure 3). Of the alloys tested, the highest mass loss was recorded from the AMM + 0.2Zr alloy (40 mg/cm<sup>2</sup>). The calculations suggest a slight increase in  $\beta$ -phase with Zr addition and also formation of an additional phase  $\text{Al}_3\text{Zr}$ . The rank followed by AMM+0.4Zn with mass loss valued at 35 mg/cm<sup>2</sup>, which indicates Zn as ineffective in reducing  $\beta$ -phase. This result is on contrary to previous research reporting possibility of improving sensitisation resistance of Al-Mg alloys by addition of Zn.<sup>13,27</sup>

A small addition of Si (0.1 wt-%) to the base alloy causes only a slight reduction in  $\beta$ -phase fraction. However, the mass loss value recorded as 13 mg/cm<sup>2</sup> is much lower than that for the base alloy. This indicates that the formation of  $\beta$ -phase might be less concentrated at the grain boundaries or this slight reduction in  $\beta$ -phase would have been enough to disrupt the continuous network of  $\beta$ -phase at grain boundaries. Experimental validation of this proposal using the electron microscopy is beyond the scope of this paper but on the basis of literature that the  $\beta$ -phase population within the grain and discontinuous

Table 2 Equilibrium fraction of phases present in the alloys produced, calculated at 150°C using Pandat® software. \*Denotes that these values may be subject to slight variations, as the calculations for Ti were conducted in isolation of Mg due to limitations of the PanAluminium database. This particular alloy was calculated in the basis of the binary Al-Ti system using the PanTitanium database

Alloy	Phase Fraction								
	$\alpha$ (Al)	$\beta$ ( $\text{Mg}_2\text{Al}_3$ )	$\text{Al}_{12}\text{Mn}$	$\text{Al}_3\text{Ti}$	$\text{Al}_3\text{Mg}_7\text{Zn}_2$	$\text{Al}_3\text{Zr}$	$\text{Al}_{19}\text{Mg}_{29}\text{Sr}_2$	$\text{Al}_{18}\text{Mn}_4\text{Si}$	$\text{Mg}_2\text{Si}$
AMM	Rem	0.0566	0.0319						
AMM+0.1Ti	Rem	0.0566*	0.0319*	0.0022*					
AMM+0.4Zn	Rem	0.0578	0.0319		0.0029				
AMM+0.2Zr	Rem	0.0569	0.0319			0.0024			
AMM+0.1Sr	Rem	0.0450	0.0319				0.0077		
AMM+0.16Zr+0.12Sr	Rem	0.0429	0.0319			0.0018	0.0092		
AMM+0.1Si	Rem	0.0536						0.0141	0.0010



formation along the grain boundary contribute to improving the resistance to IGC.<sup>28</sup>

Of the alloying additions studied, Sr had the most significant effect in reducing mass loss and improving resistance to IGC. The small addition of Sr (0.1 wt-%) was sufficient to reduce the IGC susceptibility to the lowest value of 11 mg/cm<sup>2</sup>. A drop in the amount of  $\beta$ -phase with the presence of Sr was observed following the formation of ternary phase, Al<sub>19</sub>Mg<sub>29</sub>Sr<sub>2</sub>. This phase is responsible in depleting the amount of Mg available to form  $\beta$ -phase hence the increase in IGC resistance.

Whilst the alloy containing Zr has the highest mass loss amongst the alloys tested, after Sr is added, the mass loss value (of Zr containing alloy) was reduced to almost half the value of only Zr containing alloy. This emphasises the effectiveness of Sr as modifying agent in Al-Mg alloys, and highlights an area of potential future work.

#### Intergranular corrosion

The severity of IGC attack was supplemented by optical images of the cross sections following nitric acid mass loss test as shown in Figure 4. According to ASTM G67-04, an alloy is highly susceptible to IGC if the mass loss is greater or equal to 25 mg/cm<sup>2</sup>. In this condition, a visibly significant attack on the grain boundaries is expected.

The alloy containing Zr (AMM+0.2Zr) had the highest nitric acid mass loss test value of 40 mg/cm<sup>2</sup>, indicating great susceptibility to IGC. The cross section image in Figure 4(d) shows a significant metal dissolution on the surface. Any fissures formation from IGC is no longer visible except for several of the fissures tails. The high mass loss is mainly contributed by IGC rather than general corrosion due to an increase in  $\beta$ -phase fraction compared to base alloy displayed in Figure 2.

Another alloy that is highly susceptible to IGC contains Zn (AMM+0.4Zn) with mass loss at 35 mg/cm<sup>2</sup>. The severity of IGC attack is evident in the cross section image in Figure 4(c). The fissures are deeper and more attack is observed on the surface forming a network of IGC resulting in rougher surface than the base alloy.

The alloys with highest resistance to IGC contain Si (AMM+0.1Si) and Sr (AMM+0.1Sr) with mass loss at 13 mg/cm<sup>2</sup> and 11 mg/cm<sup>2</sup> respectively. As shown in Figure 4(f) and 4(g), both alloys appear to have deep fissures on the surface. The occurrence however, is more isolated and the density of the attack is small leaving the surface smooth and hence an overall lower mass loss.

The presence of Sr in conjunction with Zr (AMM+0.16Zr+0.12Sr) has mass loss at almost half the value of the alloy with only Zr. It is apparent in Figure 4(e) that the fissures are shallow and narrow compared to AMM+0.2Zr in Figure 4(d). It has a very much similar cross section image of the base alloy in Figure 4(a). Alloy containing Ti further improves the resistance to IGC with mass loss smaller than base alloy at 16 mg/cm<sup>2</sup>. The cross section image in Figure 4(b) shows that there are some attacks on the alloy. However, the surface remained fairly smooth and the attacks occurred horizontally underneath the surface making it less likely due to IGC.

#### General discussion

The effort to improve resistance to IGC generally starts with modification of  $\beta$ -phase through alloying, heat

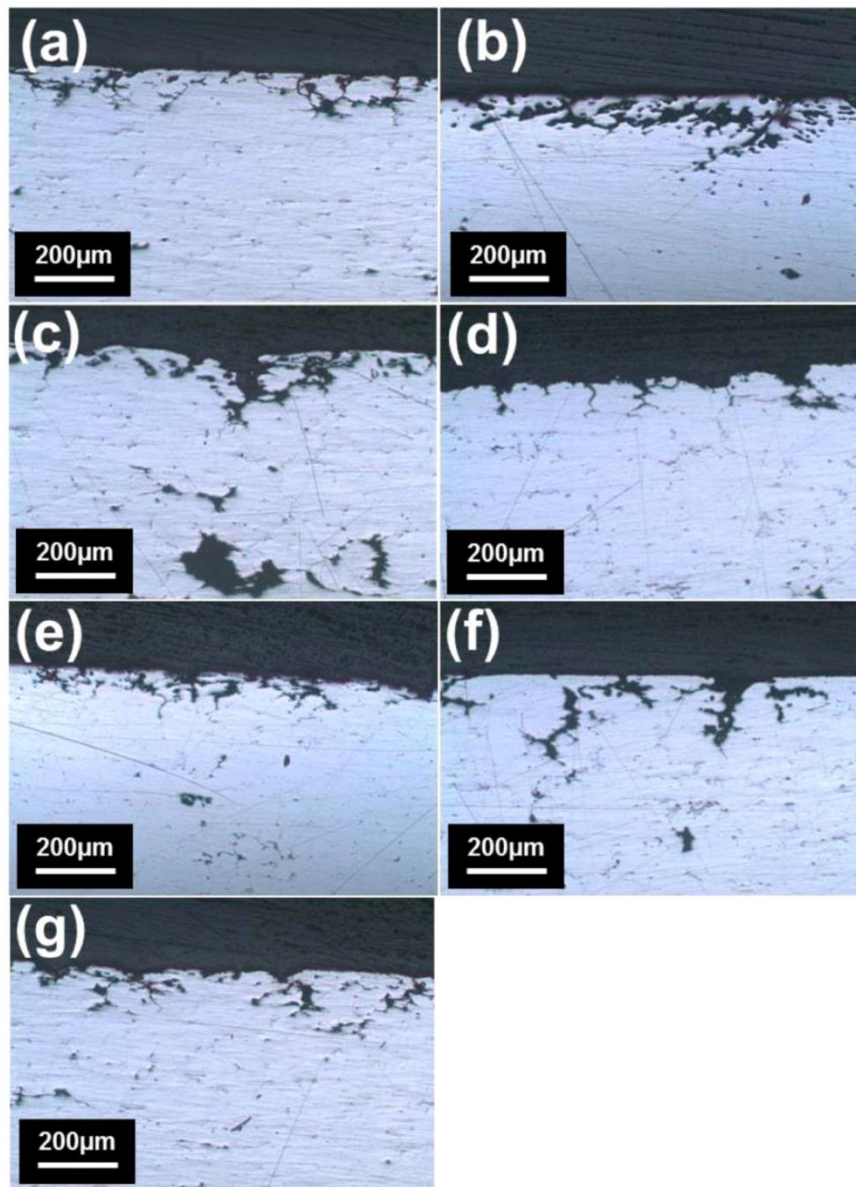
treatment or thermomechanical processing.<sup>15,29-31</sup> This work herein is focussed on alloying and the subsequent effect of changes in chemistry to the presence of  $\beta$ -phase.

The addition of Sr shows the most significant result in improving the IGC resistance to a value considered as highly resistant according to ASTM G67-04 compared to other elements. This enhancement is majorly owed to the ability of Sr to form a high Mg containing ternary phase, Al<sub>19</sub>Mg<sub>29</sub>Sr<sub>2</sub> at the expense of  $\beta$ -phase. Furthermore, Sr is also effective even with the presence of additional element such as Zr, lowering the amount of damaging phases as discussed in previous section and shown in Table 2. In normal condition, Zr containing alloy does not pose much threat to corrosion but after an extended period of exposure to elevated temperature, the morphology of Al<sub>3</sub>Zr dispersoid may change and consequently affecting the IGC resistance.

Addition of Zn was initially thought to have a positive effect in improving resistance to IGC<sup>13,27</sup> but the present study showed an increase in IGC susceptibility due to Zn addition which is in contrary to the previously reported work.<sup>12,19</sup> The phase analysis however point out that the stoichiometry of Zn containing ternary phase Al<sub>9</sub>Mg<sub>7</sub>Zn<sub>2</sub> has a much lower amount of Mg than Sr containing ternary phase Al<sub>19</sub>Mg<sub>29</sub>Sr<sub>2</sub>, rendering it less effective to significantly reduce the  $\beta$ -phase. An optimum amount of Zn might also play a role as previously reported,<sup>15</sup> before any conclusion can be made regarding the effectiveness of Zn. The degree of modification by alloying additions in Al-Mg phase is also influenced by the diffusion mechanism but the literature is still very limited, leaving opportunities for further work on this area in order to appropriately assess the effectiveness of these modifying agents in reducing  $\beta$ -phase and hence IGC.

Any excess additions of Si were seen to form the benign Al<sub>18</sub>Mn<sub>4</sub>Si phase avoiding the possibility of Si segregation at the grain boundaries leading to IGC. Unlike Zr, the addition of Ti mainly as grain refiner reduced the IGC susceptibility. Ti tend to form dispersoids such as Al<sub>3</sub>Ti, but they are less studied in terms of their role on corrosion.<sup>32</sup> However in the case herein, it is seen that such elements can have an impact on the subsequent precipitation of  $\beta$ -phase, which is relevant in the context of IGC for 5xxx series alloys, and may also influence the resistance to recrystallisation which was not studied herein.<sup>33</sup> Although the IGC initiation is not solely depending on the continuity of  $\beta$ -phase at the grain boundary, the  $\beta$ -phase may influence the severity of the attack.<sup>34-36</sup>

Further work is essential to thoroughly gauge the effect of an individual element to improve IGC resistance in Al-Mg alloy. As the composition dictates the type of phases present, a comprehensive work on varying amount of alloying elements is important to isolate chemical effects. Further, the precipitation in 5xxx alloys is also dictated by factors such as grain size, and level of prior cold work (given that  $\beta$ -phase can nucleate heterogeneously at dislocations, and that the grain size will dictate the fraction of boundary available for grain boundary precipitation). Transmission electron microscopy is essential to elaborate the details of the interaction between the alloying elements and phases. The need for IGC resistant Al-Mg alloys is increasing with wider application of Al-alloys, and any



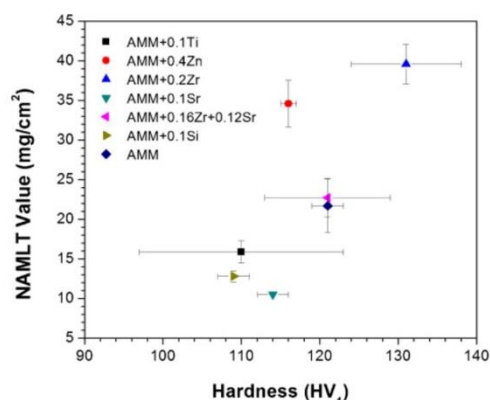
4 Optical images of cross sections following nitric acid mass loss testing and showing the extent of IGC for (a) AMM, (b) AMM+0.1Ti, (c) AMM+0.4Zn, (d) AMM+0.2Zr, (e) AMM+0.16Zr+0.12Sr, (f) AMM+0.1Si, and (g) AMM+0.1Sr

new alloys must consider strength as a first order of representation in this work, Figure 5 shows the relationship between nitric acid mass loss test value and hardness of the alloys (whereby hardness is a proxy to strength). The high IGC resistant alloys apparently populated at the low hardness spectrum and high hardness alloys have low IGC resistance. The main goal in the alloy design is to achieve high hardness and low mass loss. From Figure 5, alloy containing Zr and Sr has high potential to achieve this.

## Conclusions

1. The ability of low-level quaternary additions to Al-4Mg-0.4Mn (wt-%) was able to provide relatively significant differences in the degree of sensitisation and hence the IGC susceptibility. This is noteworthy, since the corrosion response of the alloys (in a general sense) in 0.1M NaCl was rather similar for the alloys tested. Further, equilibrium phase calculations also showed that some elements have a differing propensity for either





5 The property space for the Al-alloys tested in this work, presented as mass loss (NAMLT value) versus hardness

the stimulation of additional phases, or the modification of the  $\beta$ -phase fraction.

2. The addition of Ti, Si and Sr significantly reduce the IGC susceptibility, with nitric acid mass loss test values lower than that of the base alloy, and in the case of Sr, below that of what would be considered a hazardous nitric acid mass loss test value (i.e. greater than 25 mg/cm<sup>2</sup>). This is a significant finding, and is attributed to the ability of these elements to either modify the fraction of  $\beta$ -phase (Sr, Si) or reduce the amount of Mg to form  $\beta$ -phase (Sr, Si) or possibly modify the grain structure, orientation and grain size (Ti, Zr). We however acknowledge that the pursuit of more IGC resistant 5xxx alloys would necessitate significantly more research, including TEM and variation of the microalloying content, along with relevant thermomechanical variations; however the first order observation that singular additions can have such a significant impact on the performance of the alloy (with no corrosion or hardness penalty from Part 1) is noteworthy.

3. The presence of Sr in the Zr containing alloy significantly reduces the extent of  $\beta$ -phase formation via calculations, as compared to the additions of Zr alone, and this is reflected from the nitric acid mass loss test values. This suggests that the formation of a small fraction of Al<sub>19</sub>Mg<sub>29</sub>Sr<sub>2</sub> phase may be enough to significantly reduce  $\beta$ -phase fraction or continuity.

## Acknowledgements

The Australian Research Council Centre of Excellence for Design in Light Metals is gratefully acknowledged. NS acknowledges the Ministry of Higher Education, Malaysia for scholarship provision.

## References

- I. J. Polmear, Light alloys: from traditional alloys to nanocrystals, 4th ed., Oxford; Burlington, MA: Elsevier/Butterworth-Heinemann, 2006.
- R. K. Gupta, Y. Wang, R. Zhang, N. L. Sukiman, C. H. J. Davies, N. Birbilis, *Corrosion*, 2012, **69**, 4.
- M. L. C. Lim, J. R. Scully, R. G. Kelly, *Corrosion*, 2013, **69**, 35.
- R. Goswami, G. Spanos, P. S. Pao, R. L. Holtz, *Materials Science and Engineering: A*, 2010, **527**, 1089–1095.
- R. K. Gupta, R. Zhang, C. H. J. Davies, N. Birbilis, *Corrosion*, (2013). dx.doi.org/10.5006/0948
- J. L. Searles, P. I. Gouma, R. G. Buchheit, *Materials Science Forum*, 2002, **396–402**, 1437–1442.
- I. Oguocha, O. Adigun, S. Yannacopoulos, *Journal of Materials Science*, 2008, **43**, 4208–4214.
- R. Braun, B. Lenczowski, G. Tempus, *Materials Science Forum*, 2000, **331–337**, 1647–1652.
- N. Birbilis, R. G. Buchheit, *Journal of The Electrochemical Society*, 2005, **152**, B140.
- R. H. Jones, D. R. Baer, M. J. Danielson, J. S. Vetrano, *Metallurgical and Materials Transactions A: Physical Metallurgy and Materials Science*, 2001, **32**, 1699–1711.
- J. A. Lyndon, R. K. Gupta, M. A. Gibson, N. Birbilis, *Corrosion Science*, 2013, **70**, 290.
- K. A. Yasakau, M. L. Zheludkevich, S. V. Lamaka, M. G. S. Ferreira, *Electrochimica Acta*, 2007, **52**, 7651–7659.
- M. C. Carroll, P. I. Gouma, M. J. Mills, G. S. Daehn, B. R. Dunbar, *Scripta Materialia*, 2000, **42**, 335–340.
- M. C. Carroll, P. I. Gouma, G. S. Daehn, M. J. Mills, *Materials Science and Engineering: A*, 2001, **319–321**, 425–428.
- K. A. Unocic, P. Kobe, M. J. Mills, G. S. Daehn, *Materials Science Forum*, 2006, **519–521**, 327–332.
- M. Timpel, N. Wanderka, R. Schlesiger, T. Yamamoto, N. Lazarev, D. Isheim, G. Schmitz, S. Matsumura, J. Banhart, *Acta Materialia*, 2012, **60**, 3920–3928.
- C. Liao, J. Chen, Y. Li, R. Tu, C. Pan, *Journal of Materials Science & Technology*, 2012, **28**, 524–530.
- F. H. Samuel, A. M. Samuel, P. Ouellet, H. W. Doty, *Metallurgical and Materials Transactions A*, 1998, **29**, 2871–2884.
- ASTM G67-04, 'Standard test method for determining the susceptibility to intergranular corrosion 5xxx series aluminum alloys by mass loss after exposure to nitric acid (NAMLT test)' (West Conshohocken, PA: ASTM International 2004).
- in.
- S. L. Chen, S. Daniel, F. Zhang, Y. A. Chang, X. Y. Yan, F. Y. Xie, R. Schmid-Fetzer, W. A. Oates, *Calphad*, 2002, **26**, 175–188.
- W. Cao, S. L. Chen, F. Zhang, K. Wu, Y. Yang, Y. A. Chang, R. Schmid-Fetzer, W. A. Oates, *Calphad*, 2009, **33**, 328–342.
- C. Wolverton, X. Y. Yan, R. Vijayaraghavan, V. Ozoličs, *Acta Materialia*, 2002, **50**, 2187–2197.
- G. Wu, J. Zhang, Q. Li, K. Chou, X. Wu, *Metallurgical and Materials Transactions*, 2012, **43**, 198–205.
- P. Ashtari, H. Tezuka, T. Sato, *Materials Transactions*, 2003, **44**, 2611–2616.
- A. Davoodi, J. Pan, C. Leygraf, S. Norgren, *Journal of The Electrochemical Society*, 2008, **155**, C211.
- A. Halap, T. Radetić, M. Popović, E. Romhanji, in, 2012, pp. 387–392.
- A. J. Davenport, Y. Yuan, R. Ambat, B. J. Connolly, M. Strangwood, A. Afseth, G. M. Scamans, *Materials Science Forum*, 2006, **519–521**, 641–646.
- J. Gao, D. J. Quesnel, *Metallurgical and Materials Transactions A*, 2010, **42**, 356–364.
- A. P. Reynolds, J. Chrisfield, *Corrosion*, 2012, **68**, 913–921.
- M. C. Carroll, R. G. Buchheit, G. S. Daehn, M. J. Mills, Optimum trace copper levels for SCC resistance in a Zn-modified Al-5083 alloy, in: P. J. Gregson, S. J. Harris (Eds.) *Aluminum Alloys 2002: Their Physical and Mechanical Properties Pts 1–3*, 2002, pp. 1443–1448.
- J. R. Scully, T. O. Knight, R. G. Buchheit, D. E. Peebles, *Corrosion Science*, 1993, **35**, 185–195.
- H. C. Fang, K. H. Chen, X. Chen, H. Chao, G. S. Peng, *Corrosion Science*, 2009, **51**, 2872–2877.
- R. L. Holtz, P. S. Pao, R. A. Bayles, T. M. Longazel, R. Goswami, *Metallurgical and Materials Transactions*, 2012, **43**, 2839–2849.
- R. Goswami, R. L. Holtz, *Metallurgical and Materials Transactions A: Physical Metallurgy and Materials Science*, (2012) 1–11.
- E. Bumiller, R. G. Kelly, in: DoD Corrosion Conference, NACE, Palm Spring, CA, 2011.

# Chapter 7

## Alloying additions to improve the corrosion performance of Al-Mg-Mn alloys

---

This chapter includes three ‘sub-chapters’ for a more detailed study on the effect of Sr and Nd in improving the corrosion resistance of Al-Mg-Mn alloys, following the outcomes in Chapter 5 and 6.

**Section 7.1** is a research paper published in the ‘Journal of The Electrochemical Society’. The results from previous chapters highlighted the ability of strontium (Sr) to reduce corrosion attack whilst having minimal impact on hardness. This section provides a more detailed study on the microstructural aspects of this alloy and the critical amount of Sr to achieve the best result. The studies were carried out in the isolation of Mg in order to investigate the true effect of Sr in Al. In this work, the electrochemical response was characterised by potentiodynamic polarisation technique, supplemented by immersion test and optical profilometry to determine the form and intensity of the localised attack. Microstructural characterisation was carried out by SEM and the chemical composition of the particles was analysed with EDX. The results point to an increase in formation of  $\text{Al}_4\text{Sr}$  with Sr addition. The localised attack however was not associated with  $\text{Al}_4\text{Sr}$ , instead with Fe-containing constituent particles which present as impurities in commercial grade pure Al alloy used as the base metal. This is a very important finding, as outlined in Section 7.1.

The other promising element in improving corrosion performance of the Al-Mg alloy system as suggested in previous chapters is neodymium (Nd). This **section (7.2)** includes a research paper published in the journal ‘Corrosion Science’. Nd is a rare earth element that is an uncommon alloying addition in Al-alloys due to price. In this work, part of which was collaborative, low levels (up to 0.17 wt%) of Nd were added to an Al-5Mg alloy and the same experimental set up as in Section 7.1 was carried out. The results revealed a segregation of Nd to AlMnFe intermetallic particles and formation of apparently electrochemically homogeneous  $\text{Al}_{11}\text{Nd}_3$  particles that were not associated to intensifying localised attack of this alloy. The NAMLT values also point to better resistance to intergranular corrosion.

In order to further investigate the effect of Nd on the susceptibility to intergranular corrosion,



**Section 7.3**, a research paper published in 'Corrosion' journal, provides a study focussed on the sensitisation behaviour of the same alloy in Section 7.2. In this work, the alloys were heat treated at 150°C, followed by Nitric Acid Mass Loss Test (NAMLTL) as outlined in ASTM G67-04. The results highlighted that intergranular corrosion was reduced when the Nd content was more than 0.11 wt%. Even though the presence of Nd did not reduce the fraction of  $\beta$ -phase, Transmission Electron Microscopy (TEM) indicated the formation of fine  $\text{Al}_{11}\text{Nd}_3$  particles along with  $\beta$ -phase at the grain boundaries which may contribute to the improve intergranular corrosion resistance by disrupting the continuity of  $\beta$ -phase.

## Monash University

### Declaration for Thesis Section 7.1

In the case of Section 7.1, the nature and extent of my contribution to the work was the following:

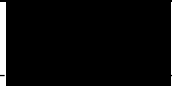
Nature of contribution	Extent of contribution (%)
Initiation, key ideas, experimental, development, results interpretations, writing up	80

The following co-authors contributed to the work. If co-authors are students at Monash University, the extent of their contribution in percentage terms must be stated:

Name	Nature of contribution	Extent of contribution (%) for student co-authors only
Nick Birbilis	Initiation, key ideas, experimental, development, results interpretations, writing up	5
Rajeev Gupta	Initiation, key ideas, experimental, development, results interpretations, writing up	5
Hanning Shi	Experimental, results interpretations	5
Rudy Buchheit	Results interpretations, writing up	5

The undersigned hereby certify that the above declaration correctly reflects the nature and extent of the candidate's and co-authors' contributions to this work.

**Candidate's Signature**

	<b>Date</b> 18 June 2014
---	-----------------------------

**Main Supervisor's Signature**

	<b>Date</b> 18 June 2014
---	-----------------------------



## Electrochemical and Corrosion Response of Commercially Pure Aluminum Alloyed with Binary Additions of Strontium

N. L. Sukiman,<sup>a,b,\*</sup> H. Shi,<sup>a</sup> R. K. Gupta,<sup>a</sup> R. G. Buchheit,<sup>c,\*\*</sup> and N. Birbilis<sup>a,\*\*\*</sup>

<sup>a</sup>ARC Centre of Excellence for Design in Light Metals, Department of Materials Engineering, Monash University, VIC 3800, Australia

<sup>b</sup>Department of Mechanical Engineering, University of Malaya, Kuala Lumpur 50603, Malaysia

<sup>c</sup>Department of Materials Science and Engineering, The Ohio State University, Columbus, Ohio 43210, USA

The influence of strontium (Sr) on the electrochemical response and corrosion of aluminum (Al) was studied over the range of 0 to 2.45 wt.% binary Sr additions. There is a paucity of prior information regarding the influence of Sr upon Al in any context, and the results herein revealed that corrosion attack is not predominantly associated with Sr containing phases, but rather Fe-rich constituents. Al<sub>4</sub>Sr intermetallic particles appear to be electrochemically homogeneous with the Al-matrix, which is both unique and important in the context of Al-alloy corrosion. The changes in corrosion rate with increasing Sr content are generally subtle, with a relative increase observed at approximately ~0.1 wt.% Sr, followed by a reduction in corrosion rate with increasing Sr.  
© 2013 The Electrochemical Society. [DOI: 10.1149/2.001308jes] All rights reserved.

Manuscript submitted February 20, 2013; revised manuscript received April 12, 2013. Published April 27, 2013.

Aluminum (Al) alloys are widely used as engineering materials due their strength to density ratio, toughness and corrosion resistance.<sup>1</sup> The physical properties of Al alloys can be improved by the addition of alloying elements in combination with appropriate heat-treatment or work hardening.<sup>2</sup> The addition of alloying elements produces a heterogeneous microstructure, which from a corrosion perspective contributes heavily to the increase in susceptibility to localized attack (e.g. pitting).<sup>3–6</sup> The difference in electrochemical properties of intermetallic particles (be it constituent particles, dispersoids or precipitates) that can populate the Al matrix<sup>1,2</sup> is rather diverse. The often multi-element and complex chemistry of intermetallic particles can render them either anodic (i.e. MgZn<sub>2</sub>, Mg<sub>2</sub>Si) or cathodic (i.e. Al<sub>2</sub>Cu, Al<sub>3</sub>Fe, Al<sub>7</sub>Cu<sub>2</sub>Fe) to the Al matrix. The relative potential of the intermetallics determines whether they will be polarized in the Al matrix to undertake the role of net anodes or cathodes, however it is the kinetics of the respective anodic and cathodic reactions at the equi-potential of the alloy which determines the extent of local attack that can occur.<sup>3,7,8</sup>

In an era of light-weighting for reduced energy consumption and for more advanced manufacturing, ongoing efforts are being carried out in attempt to improve the properties of Al alloys - particularly by chemistry modification. In the context of Al-Si alloys (which represent the family of Al-casting alloys), additions in the range of a few hundred ppm of Sr have been noted to significantly improve the properties of castings.<sup>9–12</sup> Al-Si alloys typically contain coarse needle-like eutectic Si phase and Fe-containing intermetallics, which are detrimental to mechanical properties. Traces of Sr transform these phases to fine fibrous structure by changing the solidification characteristics.<sup>11,13–16</sup> Sr is also noted to promote the formation of lower-Si containing intermetallics, modifying Al<sub>3</sub>FeSi to Al<sub>8</sub>Fe<sub>2</sub>Si,<sup>17–20</sup> leaving an excess of Si in the alloy available for precipitation of the strengthening Mg<sub>2</sub>Si phase. The effect of this chemical modification was discovered over 90 years ago,<sup>21</sup> and only decades later was it ascribed to modification of the Si-eutectic morphology. As indicated recently by Timpel and co-workers, the effect was however insufficiently understood until even more recently, aided by their study with atom probe tomography.<sup>22</sup> The detailed interaction between Sr and other elements in Al-alloys will not be covered here, however we emphasize the paucity of information available on the role of Sr on Al-alloys in any context outside of the Al-Si series of casting alloys, and there is no significant reports of the electrochemical influence of Sr in Al. Of the reports that exist in the context of Al-alloys where Sr has not been applied to modify Al-Si cast structures, there are some reports that Sr has been added

to the Li-containing high strength 2xxx and 7xxx with attendant improvement in some properties. As demonstrated by Xu and Song et al., microalloying (less than 0.1 wt.%) with Sr enhanced the resistance to intergranular and exfoliation corrosion, posited to be due to refining the microstructure and improving recrystallisation characteristics<sup>23,24</sup> – however the electrochemical impact of Sr remains unclear and essentially unstudied.

Sr is a reactive element, and largely insoluble in Al. According to the phase diagram, the Al<sub>4</sub>Sr phase is the intermetallic compound to form in the wide compositional range of when Sr content is below ~45 wt.%.<sup>25–27</sup> In this study we seek to determine the influence of binary Sr additions on the corrosion and electrochemistry of Al, revealing this information for what we believe is the first time. The rationale behind this fundamental study is several fold, however was conceived on the basis that: i) Sr may be a useful addition to a large number of Al-alloy classes in the context of controlling precipitate fraction and growth kinetics; ii) because of its reactivity it may be electrochemically compatible with Al and which remains unknown; iii) as a potential dispersoid that is cost effective in comparison with additions of elements such as scandium (Sc).

### Experimental

**Materials.**— The alloys tested in this study were produced by melting an Al-Sr master alloy (Al-2.45 wt.% Sr) with commercially pure aluminum (Alfa Aesar). The melting was carried out in a muffle furnace at ~720°C. Regular stirring of the melt was carried out over a period of about 2 hours, followed by casting into a pre-heated (to 300°C) graphite crucible. Cast alloys were homogenized below the liquidus temperature (nominally at 600°C) for two days. The composition of the alloys produced was independently analyzed using Inductively Coupled Plasma – Optical Emission Spectrometry (ICP-OES) at Spectrometer Services (Coburg, Australia) and presented along with designation of the alloys in Table I. The Si content in

Table I. Chemical composition from ICP-OES of the alloys tested in this study. All values in weight%.

Alloys	Alloying Elements			
	Al	Si	Fe	Sr
Pure Al	~Bal	0.06	0.14	0
Al-0.03Sr	~Bal	0.06	0.15	0.03
Al-0.11Sr	~Bal	0.06	0.13	0.11
Al-0.43Sr	~Bal	0.06	0.15	0.43
Al-0.85Sr	~Bal	0.06	0.15	0.85
Al-2.45Sr	~Bal	0.11	0.17	2.45

\*Electrochemical Society Student Member.

\*\*Electrochemical Society Fellow.

\*\*\*Electrochemical Society Active Member.

<sup>†</sup>E-mail: nick.birbilis@monash.edu

Al-2.45Sr specimen is higher than that in other specimens. The Al-2.45Sr alloy was the master alloy used herein, and it contained a fixed level of Si as a result of its initial production. As such, the Si content in the other alloys is slightly lower, as they were produced by diluting the Al-2.45Sr master alloy. Throughout the remainder of this manuscript, all alloy compositions are given in wt.%.

**Characterization.**— The microstructures developed were characterized using an FEI Quanta 3D-FEG scanning electron microscope to identify the presence and relative fraction of particles within the microstructure. All samples were prepared by metallographic polishing to a 0.05  $\mu\text{m}$  colloidal silica finish, followed by ultrasonic cleaning. Images were collected using back-scattered electron imaging, and the chemical composition of the particles was analyzed with energy-dispersive X-ray Spectroscopy (EDXS). Image analysis was conducted to determine actual phase fractions using Fovea Pro. To assist in interpretation of alloy characterization, the phase diagram and phase analysis was conducted using PANDAT software.

**Corrosion testing.**— Specimens were ground to a 1200 grit SiC finish under ethanol prior to electrochemical testing. All tests were carried out in quiescent 0.1M NaCl (pH 6). Potentiodynamic polarization tests were performed using a VMP3 potentiostat (BioLogic) under the control of EC Lab software. A standard 3-electrode flat-cell (PAR) incorporating a saturated calomel electrode (SCE) as the reference, and platinum mesh as the counter electrode, was used. Potentiodynamic polarization tests were conducted using a scan rate of 1.0 mV/s after a period of 10 minutes at the open circuit potential. This period of 10 minutes was determined to be sufficient for achieving a stable potential, whereby the potential did not subsequently alter by more than a few mV/min. A longer time at open circuit in dilute chloride electrolytes will ultimately lead to corrosion initiation following a finite period, after which any changes in the alloy surface do not reflect the response of the original surface. In this exploratory study, the anodic and cathodic scans were carried out separately in order to survey the true electrochemical response by avoiding the interference of prior polarization on electrode kinetics (i.e. the cathodic reaction produces hydroxyl ions that may subsequently influence the anodic reaction).

Values of  $i_{\text{corr}}$  were determined from a Tafel fit of the polarization data. Owing to the presence of a passive region, which frustrates the Tafel analysis of anodic polarization data, the reported values reflect the values of extrapolations from the cathodic data. In addition, to gain an unbiased and benchmark level of corrosion, immersion (mass loss) tests were also performed, with the samples immersed in quiescent 0.1M NaCl for 14 days. All tests were repeated at least three times. Following immersion, corrosion products were removed by a short exposure ( $\sim 15\text{s}$ ) and light rubbing in 7% nitric acid solution, prior to final weighing. This solution was used in order to preserve the original morphology of the corrosion attack.<sup>14</sup>

## Results and Discussion

**Influence of Sr on microstructure.**— The backscattered electron SEM images for the Al-Sr alloys produced are presented in Figure 1. It can be seen that there is clear evidence of a brighter second phase. To assist in determining the second phase from an equilibrium standpoint, PANDAT software was used to calculate the Al-Sr phase diagram for the compositional range of interest, revealing that the intermetallic observed in the micrographs is the  $\text{Al}_4\text{Sr}$  phase (Figure 2). The PANDAT calculations were also determined to ascertain the possibility of any precursor or additional intermetallics, which are however not predicted to form.

The volume fraction of the  $\text{Al}_4\text{Sr}$  intermetallic phase (as judged qualitatively by the inspection of the area fraction) increases with increasing in Sr content. Image analysis reveals there is approximately 8.5%  $\text{Al}_4\text{Sr}$  with 0.85 wt.% Sr additions, and  $\sim 14\%$   $\text{Al}_4\text{Sr}$  with 2.45 wt.% Sr additions. From EDX analysis, the intermetallics were found to contain the near stoichiometric proportions of Al and Sr,

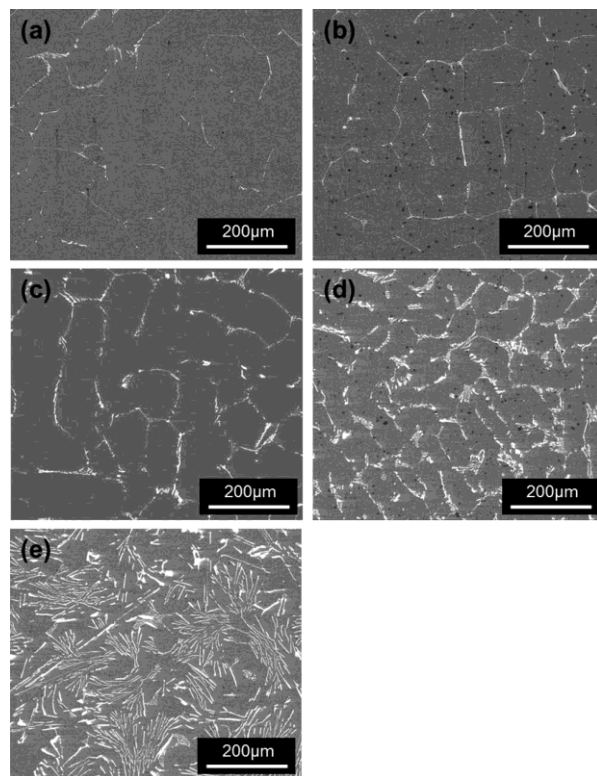


**Figure 1.** Back scattered electron (SEM) images of alloys with various content of Sr in as-cast condition. (a) Al-0.03Sr, (b) Al-0.11Sr, (c) Al-0.43Sr, (d) Al-0.85Sr, (e) Al-2.45Sr.

however it is also noted that a low fraction of constituent particles (concomitant with Fe, Si and Mn) are also present. The typical stoichiometry of such constituents is rather consistent across Al-alloy classes and their type and electrochemical influence has been covered in previous works.<sup>3,8,28–30</sup> Such constituent particles are present in essentially all Al-alloys, including commercially pure Al.<sup>1,2</sup> As commercial purity Al was used herein, Fe and Si impurities are also

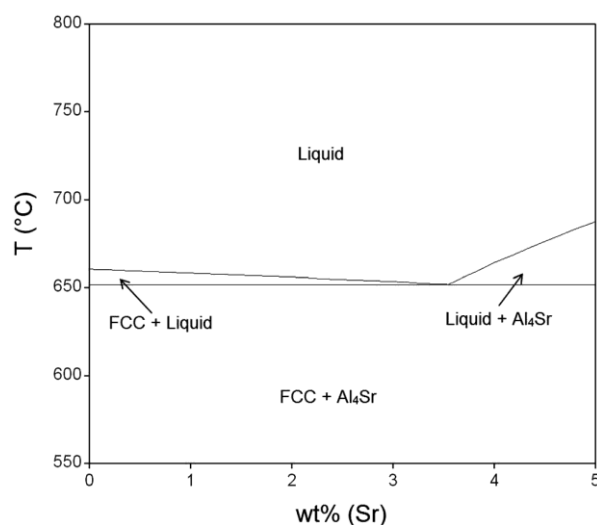


**Figure 2.** Phase diagram for Al-Sr calculated using PANDAT.

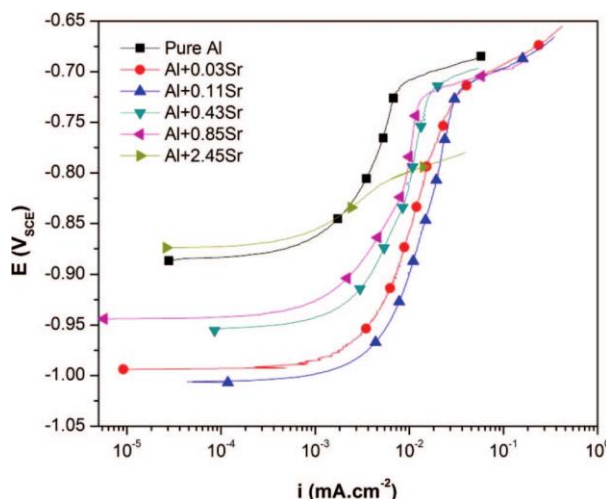


**Figure 3.** Anodic polarization curves for Al alloys with various amount of Sr in 0.1M NaCl using a scan rate of 1 mV/s.

present. Such constituents also appear as bright phases, and are difficult to isolate unless using EDX mapping (which is presented in the context of corrosion further below).

*Influence of Sr on electrochemical response of Al-Sr binary alloys.*—Given that there is no prior works on the influence of Sr on the electrochemical response of Al, the characteristic potentiodynamic polarization curves were conducted as separate anodic (Figure 3), and cathodic scans (Figure 4), to permit a more holistic interpretation. The polarization curves shown are representative of the typical response. We note that there is scatter between the  $E_{\text{corr}}$  values determined from the anodic and cathodic scans, and the total scatter for  $E_{\text{corr}}$  across all tests conducted was as high as 100 mV for a given sample, which we believe is within the statistical variation and depicted further below.

Inspection of the anodic polarization scans suggest that the low-level additions (0.03 and 0.11 wt.%) of Sr shift the corrosion potential ( $E_{\text{corr}}$ ) to less noble values whilst revealing an increased passive current density ( $i_{\text{pass}}$ ), of approximately  $10 \mu\text{A}/\text{cm}^2$ . The increase in passive

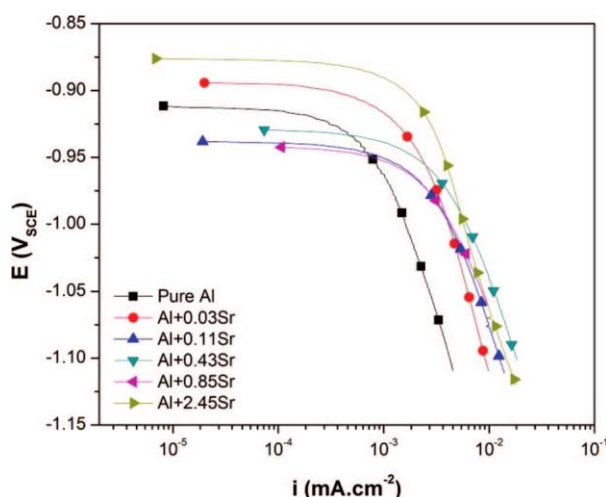


**Figure 4.** Cathodic polarization curves for Al alloys with various amount of Sr in 0.1M NaCl using a scan rate of 1 mV/s.

current density is rather marked, and in spite of this, the pitting potential ( $E_{\text{pit}}$ ) remains essentially unchanged. Interestingly, additions of Sr at higher concentrations (0.43 and 0.85 wt.%) also showed a very similar  $E_{\text{pit}}$  to pure Al, with an attendant decrease of the passive current density to values somewhere intermediate between pure Al and Al with 0.03 or 0.11% Sr. For Sr contents to 0.85 wt.%, windows of passivity in the range of  $\sim 300$  mV were seen in 0.1M NaCl, in spite of the presence of appreciable fractions of  $\text{Al}_4\text{Sr}$ . The highest addition of Sr (2.45 wt.%) revealed a passive current density essentially identical to that of pure Al, however with a comparatively lower  $E_{\text{pit}}$ . The  $E_{\text{pit}}$  of Al-2.45Sr was  $\sim -800$  mV<sub>SCE</sub>, about 100 mV less noble than that of pure Al.

In regards to cathodic kinetics, the polarization curves (Figure 4) indicate that the cathodic reaction rates are rather similar for all the Al-Sr alloys, irrespective of the relatively large difference in the alloy content and relatively dramatic difference in microstructure. The rates of cathodic reaction are somewhat faster with Sr additions, as opposed to commercially pure Al. The differences in the respective  $E_{\text{corr}}$  values are not interpreted to a large extent here, as we believe these values are largely dictated by shifts in the anodic kinetics.

A first order interpretation of the polarization kinetics would suggest that in instances where Al is alloyed with Sr, even in the case where relatively significant fractions of intermetallic exist, that Al-Sr alloys are spontaneously passive, indicating that dissolution of the  $\text{Al}_4\text{Sr}$  is not expected to be rapid. Further, if the  $\text{Al}_4\text{Sr}$  phase is to take the role of supporting cathodic reactions, the attendant rates are only slightly higher than those upon pure Al and apparently insensitive to increasing Sr content. This is in contrast to the influence of most other alloying additions to Al, which tend to have a monotonic effect (i.e. one classic example is that Cu increases cathodic kinetics in a manner that scales with the amount of alloying).<sup>31,32</sup>

To bridge the results in Figures 3 and 4, the electrochemically determined corrosion current density ( $i_{\text{corr}}$ ) and pitting potential ( $E_{\text{pit}}$ ) are plotted against alloy content and the determined  $\text{Al}_4\text{Sr}$  volume fraction (which was determined from repeated analysis of  $\text{Al}_4\text{Sr}$  area fractions via image analysis of BSE-SEM images) in Figure 5. The  $i_{\text{corr}}$  values were obtained by Tafel extrapolation and the standard deviation was used to generate the error bars. BSE-SEM images were taken in three different areas to appropriately represent the variation of  $\text{Al}_4\text{Sr}$  volume fraction on the surface of the alloys. Whilst the data is reported along with the relative scatter, it appears as though the corrosion current density ( $i_{\text{corr}}$ ) increases with low levels of Sr, after which at a critical Sr value the  $i_{\text{corr}}$  decreases. This trend is also reproduced when described in terms of %  $\text{Al}_4\text{Sr}$ . It should however be mentioned that all of the  $i_{\text{corr}}$  values for the Al-Sr alloys are relatively low compared with commercial Al-alloys such as the age-hardenable alloys (which display  $i_{\text{corr}}$  values of several  $\mu\text{A}/\text{cm}^2$ ), and the variation between all samples is not necessarily high. The pitting potential ( $E_{\text{pit}}$ ) also shows a small scatter between 20 mV except for the highest amount of Sr. The trend in  $i_{\text{corr}}$  and  $E_{\text{pit}}$  values is unique, and one explanation may be the modification of impurity based constituent particles is sensitive to some critical Sr increase. Since the data gathered from electrochemical tests has only small variation, mass loss was carried out to holistically evaluate the corrosion response.

To further understand the rate controlling reaction, Figure 6 shows the  $E_{\text{corr}}$  plotted with respect to  $i_{\text{corr}}$ . In order to capture the range of  $E_{\text{corr}}$  at various OCP, an average of  $E_{\text{corr}}$  extracted from the anodic and cathodic polarization curves are used to generate the plot, and the error bars reflect the standard deviation. From Figure 6, it is seen that electrochemical kinetics appear to be controlled by the anodic reaction as opposed to the cathodic reaction rate, whereby increases in corrosion rate are accompanied by less noble  $E_{\text{corr}}$  values.

*Influence of Sr on corrosion.*—Following immersion testing in 0.1M NaCl for 14 days, the mass loss values are presented as a function of Sr content (Figure 7). A very minor, but not negligible increase in mass loss is observed with Sr, with the exception of the Al-0.11Sr sample. Whilst not reported more widely herein, the specimens were also characterized using optical profilometry, which indicates the



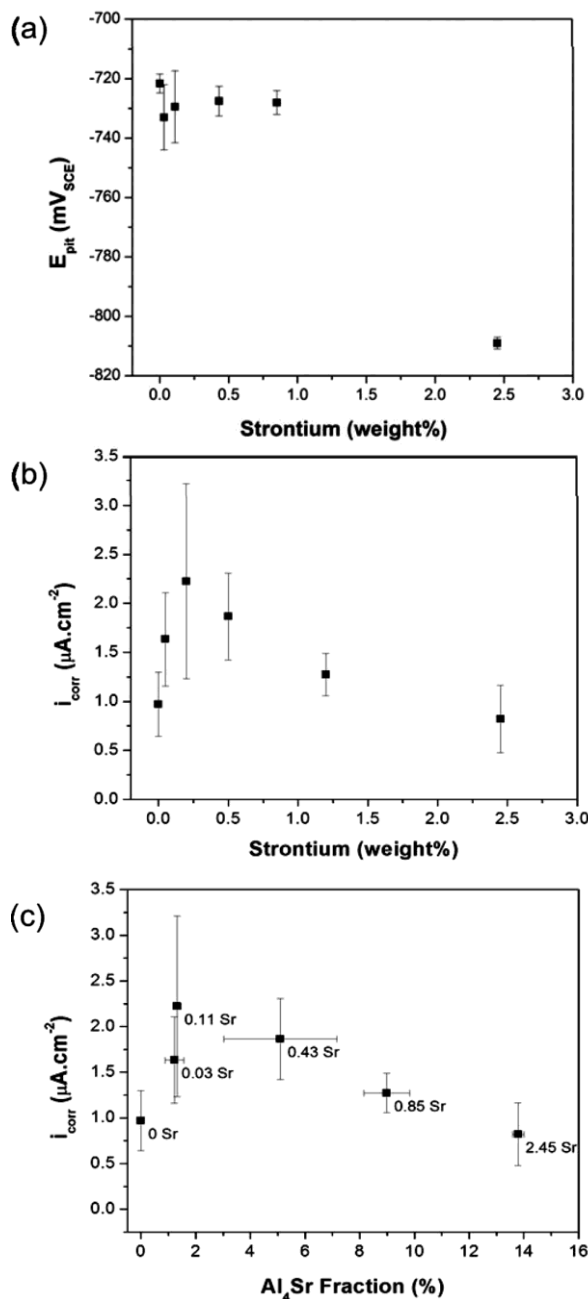


**Figure 5.** Effect of Sr content (a) on pitting potential and (b) on corrosion current density, and (c) effect of Al<sub>4</sub>Sr fraction on corrosion current density as in 0.1M NaCl.

corrosion morphology was essentially localized (as seen in the inset of Figure 7 for the specimen with the highest mass loss). The relatively low levels of mass loss, and the relative similarity in range of values with pure Al is also consistent with the electrochemical tests.

The similarity from tests with higher levels of Sr would tend to suggest that the mass loss is rather independent of the Sr and Al<sub>4</sub>Sr content. In order to validate this, post immersion SEM was carried out, revealing profound results. Figure 8 shows the form of corrosion on the alloy surface after exposure to 0.1M NaCl, and it is revealed that in spite of a significant volume fraction of Al<sub>4</sub>Sr intermetallic, that

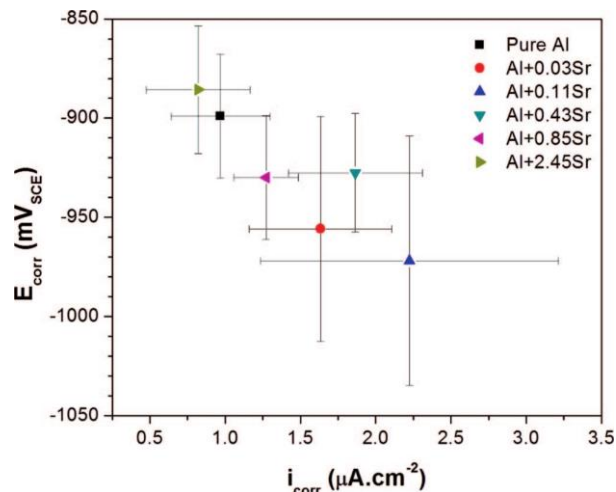


**Figure 6.** The relationship between  $i_{corr}$  and  $E_{corr}$  extracted from potentiodynamic polarization curves of the alloys determined at open circuit potential after 10 minutes in 0.1M NaCl using a scan rate of 1 mV/s.

the corrosion is not localized at, on, or adjacent to the Al<sub>4</sub>Sr. In all instances observed, corrosion was localized, and tended to be localized at constituent-type particles that were rich in Fe (from Fe impurity), which is particularly evident in Figure 8b. In fact, the identification of where the constituent phases exist was possible after corrosion had occurred, whereby the localisation of corrosion with constituent particles made it obvious how to discriminate from the Al<sub>4</sub>Sr. Validation that corrosion was associated with regions of high Fe concentration (i.e. Fe-bearing constituents) is given in Figure 9 via the EDX maps. It is evident that the sites of corrosion are associated with the Fe. It is also very interesting however to note that regions containing Sr, also tended to have an association with segregated Si (which is nominally always present in low levels in commercially pure Al). In fact, there is a significant richness in the data in Figures 8 and 9, suggesting that Si mobilizes with Sr, and also that the form of the constituent particles rich in Fe are modified by addition of Sr. On causing corrosion, it appears

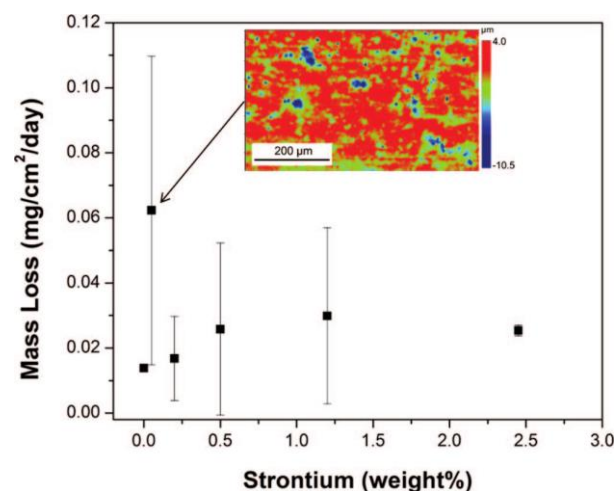


**Figure 7.** Effect of Sr content on the corrosion rates as determined by mass loss test in 0.1M NaCl for 14 days. As a comparison, in the same conditions 2024-T3 is 0.0582 mg/cm<sup>2</sup>/day and 7079-T6 is 0.707 mg/cm<sup>2</sup>/day. Inset shows the localized nature of the corrosion attack on the specimen with the highest mass loss, via Optical Profilometry imaging.

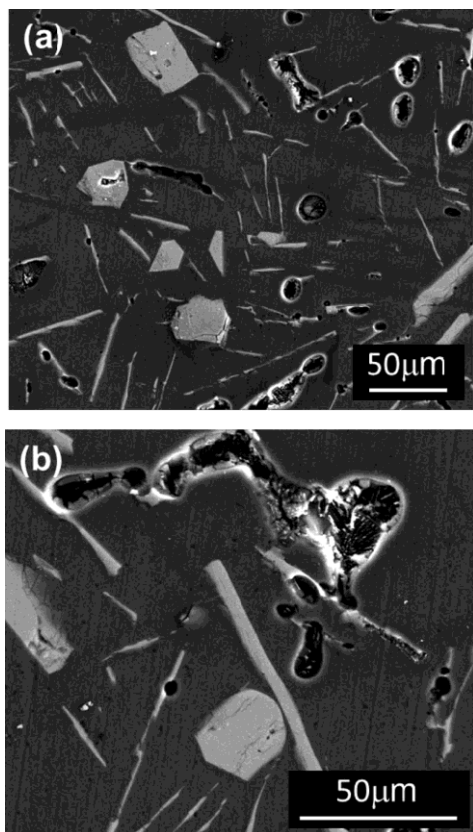


**Figure 8.** Scanning electron (SEM) images of Al-2.45Sr alloy after immersion in 0.1M NaCl for 5 hours showing (a) the extent of pitting on the surface and (b) close up observation of the pit.

as though the Fe rich particles are somewhat attacked themselves, and the remnants indicate a complex structure of needles. This is not synonymous with the classic ‘trenching’ observed around whole (i.e. non-needle like Fe-constituents) observed in Sr-free systems<sup>30,33–37</sup> and noteworthy in itself. The apparent electrochemical heterogeneity of intermetallics in the Al-matrix was previously shown for the case of Sc additions leading to  $\text{Al}_3\text{Sc}$  intermetallic particles.<sup>38,39</sup> The cost of Sc prohibits its use in commercial alloys, however a similar effect is observed herein with the addition of Sr.

If Sr can in fact modify the constituent particles, this may explain why at the lowest Sr content the highest mass loss was observed possibly linked with insufficient Sr to cause significant constituent modification. In any case, the modification of constituent particles by Sr would require dedicated study on the basis of isolating when the modification occurs (i.e. is it during the molten state) and the impact on the constituent chemistry and structure, which is beyond this study. Whilst the present work was largely focused on revealing the electrochemical and corrosion aspects of binary Sr additions, it appears that the rather general observation that Sr has the potential to modify particles and segregation in systems outside of the Al-Si casting alloys may be maintained. In the authors’ opinion, there remains significant future work in elucidating the more detailed electrochemical mechanisms at play involving the additions of Sr to Al. Certainly the apparent electrochemical heterogeneity, and its influence in localized corrosion and propagation will require a more dedicated appraisal. Further, the increased passive current density with Sr additions, however without a diminished  $E_{\text{pit}}$ , also merits further investigation.

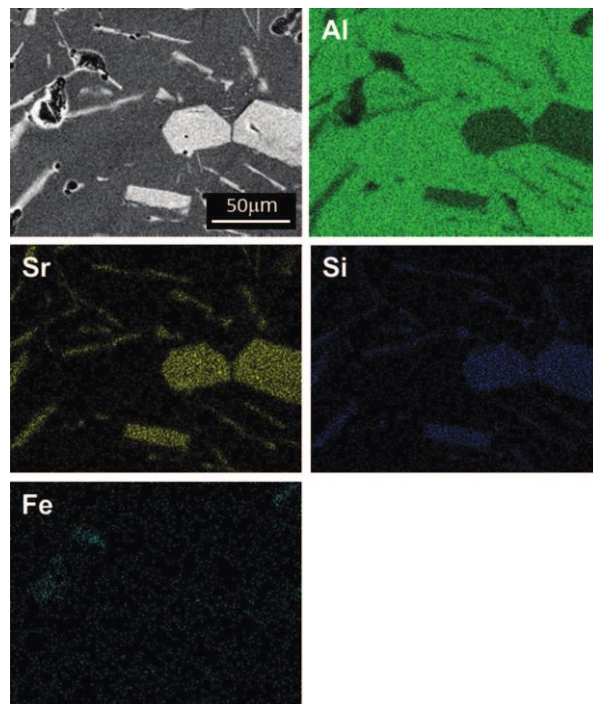


**Figure 9.** High magnification observations and EDS element mapping analysis of Al-2.45Sr alloy after immersion in 0.1M NaCl for 5 hours showing Fe enrichment inside the pits and no attack was observed on Sr containing intermetallics.

### Conclusions

1. The addition of Sr to Al led to the formation of the  $\text{Al}_4\text{Sr}$  intermetallic phase, which increased in volume fraction as Sr content increased. The level of electrochemical corrosion remains low, irrespective of Sr content, and the associated mass loss is also low and largely independent of the Sr and  $\text{Al}_4\text{Sr}$  content.
2. The SEM images after exposure to a dilute chloride electrolyte indicate that localized corrosion is associated with Fe-containing constituent particles, whilst  $\text{Al}_4\text{Sr}$  particles were un-attacked.
3. Pitting potentials ( $E_{\text{pit}}$ ) for Sr containing alloys are identical to pure Al despite an increase in passive current density, except for the highest Sr content studied (2.45 wt.%).
4. Cathodic reaction rates for Al-Sr alloys are slightly higher than pure Al but similar regardless of the alloy content and microstructure. This indicates that increasing  $\text{Al}_4\text{Sr}$  fraction did not support rapidification of cathodic kinetics.
5. The corrosion current density ( $i_{\text{corr}}$ ) increases with low levels of Sr but decreased after adding more than 0.11 wt.% Sr. A similar trend was observed with the volume fraction of  $\text{Al}_4\text{Sr}$ . This implies that there might be a critical amount of Sr required to significantly modify the constituent particles hence lowering corrosion rate. Significant future work is needed to fully interpret the mechanisms imparted by Sr additions, however the findings are unique in the context of particle induced localized corrosion of Al and its alloys. They are highly reproducible and indeed we believe merit wider dissemination for a general assessment by the field.

### Acknowledgments

The Australian Research Council is acknowledged for establishing the Center of Excellence for Design in Light Metals. The Monash

Center for Electron Microscopy is gratefully acknowledged and we thank Emeritus Professor I.J. Polmear for interesting discussions.

### References

1. J. R. Davis, *Corrosion of Aluminum and Aluminum Alloys*, Materials Park, OH: ASM International, (1999).
2. I. J. Polmear, *Light Alloys: from Traditional Alloys to Nanocrystals*, 4th ed., Oxford: Burlington, MA: Elsevier/Butterworth-Heinemann, (2006).
3. N. Birbilis and R. G. Buchheit, *Journal of The Electrochemical Society*, **152**, B140 (2005).
4. R. H. Jones, J. S. Vetrano, and C. F. Windisch, Jr., *Corrosion*, **60**, 1144 (2004).
5. K. D. Ralston, N. Birbilis, M. K. Cavanaugh, M. Weyland, B. C. Muddle, and R. K. W. Marceau, *Electrochimica Acta*, **55**, 7834 (2010).
6. K. A. Yasakau, M. L. Zheludkevich, S. V. Lamaka, and M. G. S. Ferreira, *Electrochimica Acta*, **52**, 7651 (2007).
7. C.-M. Liao and R. P. Wei, *Electrochimica Acta*, **45**, 881 (1999).
8. R. G. Buchheit and N. Birbilis, *Electrochimica Acta*, **55**, 7853 (2010).
9. S. McDonald, M. Dargusch, G. Song, and D. StJohn, Unintentional effects of Sr additions in Al-Si foundry alloys in *SHAPE CASTING: 2nd International Symposium*, Orlando, FL, pp. 59–66 (2007).
10. M. M. Haque and V. Kondic, in: C. Suryanarayana, P. M. Prasad, S. L. Malhotra, and T. R. Anantharaman (Eds.), Influence of Sr on solidification of Al-Si alloys in Trans Tech Publication, Varanasi, India, pp. 159–170 (1985).
11. M. Djurdjevic, T. Stockwell, and J. Sokolowski, *International Journal of Cast Metals Research*, **12**, 67 (1999).
12. K. Nogita, S. D. McDonald, and A. K. Dahle, *Philosophical Magazine*, **84**, 1683 (2004).
13. P. Ouellet and F. H. Samuel, *Journal of Materials Science*, **34**, 4671 (1999).
14. S. S. Sreeja Kumari, R. M. Pillai, T. P. D. Rajan, and B. C. Pai, *Materials Science and Engineering A*, **460–461**, 561 (2007).
15. W. Eidhed, *Journal of Materials Science and Technology*, **24**, 45 (2008).
16. N. Fat-Halla, *Journal of Materials Science*, **24**, 2488 (1989).
17. P. Ashtari, H. Tezuka, and T. Sato, *Materials Transactions*, **44**, 2611 (2003).
18. H. C. Liao, Y. Ding, and G. X. Sun, *Transactions of Nonferrous Metals Society of China (English Edition)*, **12**, 409 (2002).
19. F. H. Samuel, A. M. Samuel, P. Ouellet, and H. W. Doty, *Metallurgical and Materials Transactions A*, **29**, 2871 (1998).
20. M. H. Mulazimoglu, A. Zaluska, F. Paray, and J. E. Gruzleski, *Metallurgical and Materials Transactions A: Physical Metallurgy and Materials Science*, **28**, 1289 (1997).
21. R. S. Archer and L. W. Kempf, *Transactions of the American Institute of Mining and Metallurgical Engineers*, **73**, 581 (1926).
22. M. Timpel, N. Wanderka, R. Schlesiger, T. Yamamoto, N. Lazarev, D. Isheim, G. Schmitz, S. Matsumura, and J. Banhart, *Acta Materialia*, **60**, 3920 (2012).
23. T. Song, X. Xu, Z. Fan, Z. Zhang, B. Wang, and Y. Luo, *Xiyou Jinshu/Chinese Journal of Rare Metals*, **36**, 196 (2012).
24. X. J. Xu, G. C. Wu, B. Wang, F. B. Zhang, Y. Luo, T. Song, C. Cheng, L. Pan, and X. N. Cheng, *Cailiao Rechuli Xuebao/Transactions of Materials and Heat Treatment*, **32**, 22 (2011).
25. C. Liao, J. Chen, Y. Li, R. Tu, and C. Pan, *Journal of Materials Science & Technology*, **28**, 524 (2012).
26. C. Wang, Z. Jin, and Y. Du, *Journal of Alloys and Compounds*, **358**, 288 (2003).
27. C. Wolverton, X. Y. Yan, R. Vijayaraghavan, and V. Ozoliņš, *Acta Materialia*, **50**, 2187 (2002).
28. R. Ambat, A. J. Davenport, G. M. Scamans, and A. Afseth, *Corrosion Science*, **48**, 3455 (2006).
29. J. T. B. Gundersen, A. Aytaç, S. Ono, J. H. Nordlien, and K. Nişancioğlu, *Corrosion Science*, **46**, 265 (2004).
30. G. O. Ilevbare, O. Schneider, R. G. Kelly, and J. R. Scully, *Journal of The Electrochemical Society*, **151**, B453 (2004).
31. A. Boag, A. E. Hughes, A. M. Glenn, T. H. Muster, and D. McCulloch, *Corrosion Science*, **53**, 17 (2011).
32. T. J. R. Leclère and R. C. Newman, *Journal of The Electrochemical Society*, **149**, B52 (2002).
33. O. Schneider, G. O. Ilevbare, J. R. Scully, and R. G. Kelly, *Journal of The Electrochemical Society*, **151**, B465 (2004).
34. J. O. Park, C. H. Paik, Y. H. Huang, and R. C. Alkire, *Journal of The Electrochemical Society*, **146**, 517 (1999).
35. O. Seri, *Corrosion Science*, **36**, 1789 (1994).
36. R. M. Rynders, C. H. Paik, R. Ke, and R. C. Alkire, *Journal of The Electrochemical Society*, **141**, 1439 (1994).
37. N. Birbilis and R. G. Buchheit, *Journal of The Electrochemical Society*, **155**, C117 (2008).
38. M. Cavanaugh, N. Birbilis, R. Buchheit, and F. Bovard, *Scripta Materialia*, **56**, 995 (2007).
39. F. Fazeli, W. J. Poole, and C. W. Sinclair, *Acta Materialia*, **56**, 1909 (2008).



**Monash University**  
**Declaration for Thesis Section 7.2**

In the case of Section 7.2, the nature and extent of my contribution to the work was the following:

<b>Nature of contribution</b>	<b>Extent of contribution (%)</b>
Initiation, key ideas, experimental, development, results interpretations, writing up	30

The following co-authors contributed to the work. If co-authors are students at Monash University, the extent of their contribution in percentage terms must be stated:

<b>Name</b>	<b>Nature of contribution</b>	<b>Extent of contribution (%) for student co-authors only</b>
Nick Birbilis	Initiation, key ideas, experimental, development, results interpretations, writing up	5
Rajeev Gupta	Initiation, key ideas, experimental, development, results interpretations, writing up	5
Yuan Wang	Initiation, key ideas, experimental, development, results interpretations, writing up	50
Ruifeng Zhang	Results interpretations, writing up	5
Chris Davies	Results interpretations, writing up	5

The undersigned hereby certify that the above declaration correctly reflects the nature and extent of the candidate's and co-authors' contributions to this work.

<b>Candidate's Signature</b>		<b>Date</b> 18 June 2014
------------------------------	---	-----------------------------

<b>Main Supervisor's Signature</b>		<b>Date</b> 18 June 2014
------------------------------------	---	-----------------------------



## Influence of alloyed Nd content on the corrosion of an Al–5Mg alloy

Y. Wang<sup>a</sup>, R.K. Gupta<sup>a,\*</sup>, N.L. Sukiman<sup>a,b</sup>, R. Zhang<sup>a</sup>, C.H.J. Davies<sup>a,c</sup>, N. Birbilis<sup>a</sup>

<sup>a</sup> ARC Centre of Excellence for Design in Light Metals, Department of Materials Engineering, Monash University, Clayton, Australia

<sup>b</sup> Department of Mechanical Engineering, University of Malaya, Kuala Lumpur, Malaysia

<sup>c</sup> Department of Mechanical & Aerospace Engineering, Monash University, Clayton, Australia

### ARTICLE INFO

#### Article history:

Received 7 November 2012

Accepted 29 March 2013

Available online 10 April 2013

#### Keywords:

A. Alloy

A. Aluminium

C. Intergranular corrosion

B. Polarisation

B. SEM

### ABSTRACT

The influence of neodymium (Nd) additions from 0 to 0.17 wt.% on the electrochemical response, corrosion, and hardness of a model 5xxx alloy (Al–5Mg) was studied. The combination of SEM, polarisation, constant immersion and nitric acid mass loss testing, followed by optical profilometry, revealed that Nd had no significant effect on pitting or general corrosion of Al–5Mg; however with Nd additions the extent of intergranular corrosion following sensitisation was decreased substantially. Nd additions also increased alloy hardness and thus microalloying with Nd was shown to improve the properties of Al–5Mg.

© 2013 Elsevier Ltd. All rights reserved.

### 1. Introduction

The 5xxx series (Al–Mg) aluminium alloys are weldable wrought alloys with good corrosion resistance, generally used in transport and marine applications [1–3]. Al–Mg alloys do not respond to age hardening and their strength is due to the combination of work hardening and solid solution strengthening [1–4]. The properties of 5xxx aluminium alloys can be marginally enhanced by the addition of small amount of elements (microalloying additions), which can form fine dispersoids [1,5,6]. The addition of alloying elements to what are nominally solid solution alloys requires relatively careful selection of the element to be added, and the concentration in which it is added, since the electrochemical properties of any additional phases are likely to be rather different than those of the Al–Mg matrix [7–9]. Some less common alloying additions including the rare earth elements and transition metals (such as Sc, Er, Zr, Ce, Mn, Cr, and Ag) are believed to improve mechanical properties without deteriorating corrosion performance [10–22]. Al–Mg–Ag alloys with elevated Mg content can be age hardened [21]. Additions of Mn, Zr, and Sc have been suggested to increase mechanical properties as well as SCC resistance of Al–Mg alloys by hindering recrystallisation [23,24]. Er addition to Al–Mg alloys is reported to improve corrosion performance in

chloride containing solution [25]. Sc is reported to improve mechanical properties without significant loss in corrosion properties [26–29]. Small amounts of Sc increase ductility and strength of 5xxx Al alloys due to the formation of fine Al<sub>3</sub>Sc precipitates which not only refines grains, but also provides some precipitation hardening [23,30–32]. Moreover Sc has been reported to also permit superplasticity in Al–Mg alloys [33]. To date, no significant deleterious effect of Sc additions on general corrosion or pitting corrosion behaviour of Al–Mg alloys has been reported [27,28] which is attributed to inability of Sc to sustain a large cathodic current density [28]. These combinations of the influence of Sc suggest that Al–Mg–Sc alloys are promising for use in high performance sports equipment and aerospace applications [26,34].

However, in spite of beneficial effects of Sc in improving properties of Al–Mg alloys, the prohibitive high cost of Sc (whilst fluctuating, is presently several hundreds of thousands of US Dollars per ton) limits applications, and any cheaper alternative alloying additions of similar effectiveness are desirable. Pursuit of this goal is topical, and in one instance the addition of Zr along with Sc was reported to be effective in improving properties whilst decreasing the Sc content for the equivalent mechanical properties obtained from a high Sc content. In search of a substitute for Sc, the effect of erbium (Er) on properties of Al-alloys has been investigated in detail by the group of Nie, who reported that Er imparts an improvement in mechanical properties without significant loss in corrosion performance [12,25,35,36]. Nd was reported to be effective in increasing the recrystallisation temperature of Al–Mg–Mn alloy as well as grain refinement [37]. Additions of Nd to an Al–Mg

\* Corresponding author. Tel.: +61 3 9905 5323; fax: +61 3 9905 4940.  
E-mail address: [gupt.rajeev@gmail.com](mailto:gupt.rajeev@gmail.com) (R.K. Gupta).



**Table 1**

Composition (wt.%) of alloys tested in this study, as determined by inductively coupled plasma–optical emission spectrometry (ICP–OES).

	Mg	Nd	Fe	Si	Al
Al–5Mg	5.17	0	0.18	0.07	Bal.
Al–5Mg–0.06Nd	4.89	0.06	0.15	0.07	Bal.
Al–5Mg–0.11Nd	5.07	0.11	0.16	0.06	Bal.
Al–5Mg–0.17Nd	5.14	0.17	0.15	0.06	Bal.

alloy were also reported to increase yield strength and elongation simultaneously. However, the systematic effect of Nd on the corrosion of Al–Mg alloys has not been reported in literature.

When exposed to elevated temperatures for extended periods (~50–200 °C), Al–Mg alloys can become susceptible to intergranular corrosion (IGC) as a result of the formation of  $Mg_2Al_3$  along the grain boundaries.  $Mg_2Al_3$  is anodic in nature and can lead to a preferential dissolution path at grain boundaries [38–42]. This phenomenon is termed ‘sensitisation’ and has attracted considerable research attention in recent years [38–43]. Some strategies for minimising the extent of sensitisation in Al–Mg alloys have been recently discussed, and include decreasing  $Mg_2Al_3$  content, altering the chemical composition of  $Mg_2Al_3$  to make it less electrochemically active, and introducing additional particles to disrupt the continuous network of  $Mg_2Al_3$  [43–45]. Zn, Cu in combination with Zn and Ag were reported to improve sensitisation resistance of Al–Mg alloys [46–49]. Preliminary work suggests theoretically and experimentally that the addition of Nd to an Al–Mg alloy is effective in improving sensitisation resistance from a metallurgical perspective as determined by nitric acid mass loss tests (NAMLIT) [45]. To date however, the influence of Nd on the electrochemical properties, or general corrosion and physical properties of Al–Mg alloys is yet to be reported – and the purpose of this study.

## 2. Experimental

### 2.1. Materials

Al–5Mg–xNd (wt.%) alloys used in this investigation were prepared by melting pure Al (99.9%), pure Mg (99.9%) and an Mg–Nd master alloy in a muffle furnace. Initially the pure Al was melted at ~720 °C, after which the other elements were added to the melt and stirred. Regular stirring of the melt was carried out over 60 min in the molten state, followed by casting into a pre-heated (to 300 °C) graphite crucible. Alloys were homogenised just below the liquidus temperature for 2 days, followed by solution treatment at 450 °C for 1 h, then water quenched, then cold rolled to a 50% thickness reduction. Compositions of these alloys were analysed by inductively coupled plasma–optical emission spectrometry (Spectrometer Services, Coburg, Victoria, Australia) and are presented in Table 1.

### 2.2. Corrosion tests

Prior to each experiment, specimens were ground to a 2000 grit SiC paper finish under ethanol and dried with air. All the corrosion tests were carried out in quiescent 0.01 M NaCl using a standard three-electrode flat cell (PAR), incorporating a saturated calomel electrode (SCE) and a platinum mesh counter electrode. A VMP3 potentiostat (BioLogic) under the control of EC-lab software was used for potentiodynamic polarisation tests that were initiated after 10 min at open current using a scan rate of 1.0 mV/s. All tests were repeated at least five times.

Mass loss was measured after constant immersion of test coupons in 0.01 M NaCl solution for 14 days, followed by chemical cleaning of corrosion products with 15%  $HNO_3$ . Optical profilometry (Veeco Wyko NT-1100) was used to measure number and depth

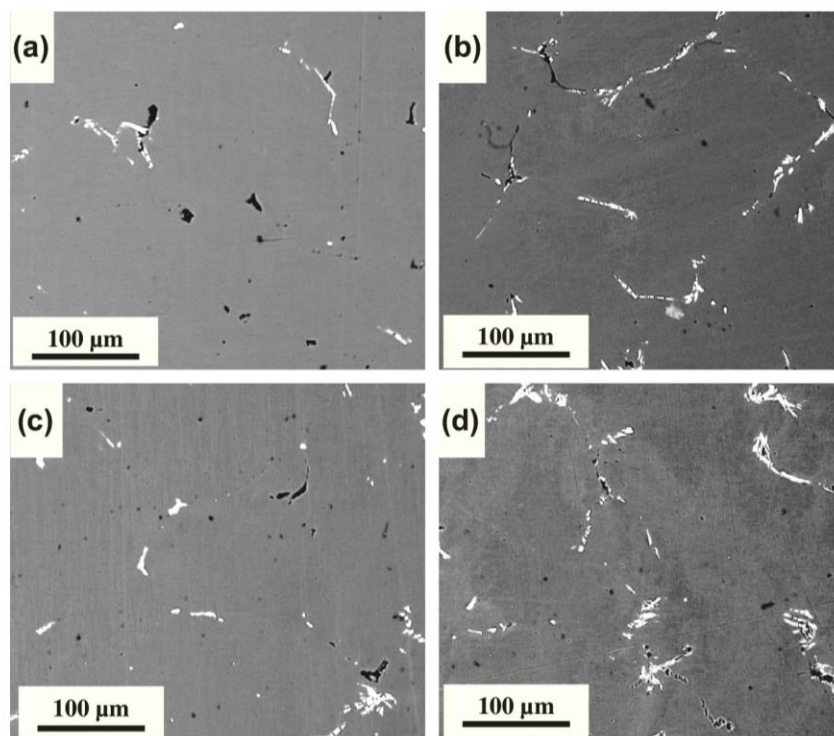


**Fig. 1.** Typical back-scattered electron images of (a) Al–5Mg, (b) Al–5Mg–0.06Nd, (c) Al–5Mg–0.11Nd and (d) Al–5Mg–0.17Nd alloys.

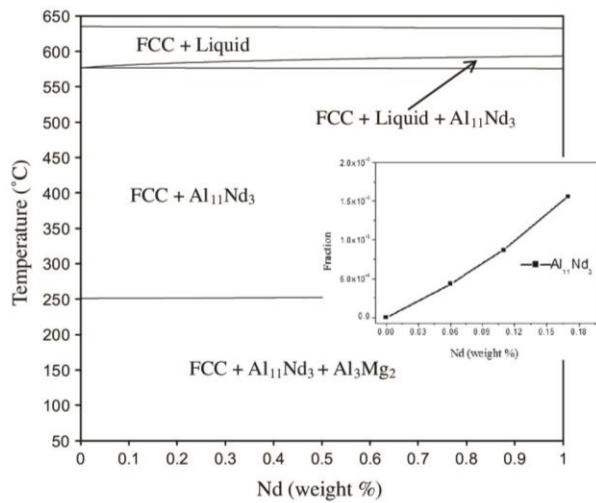


Fig. 2. Phase diagram of Al–5Mg–xNd alloy as calculated using Pandat [51]. Inset shows phase fraction of  $\text{Al}_{11}\text{Nd}_3$  as a function of Nd content.

of pits after constant immersion tests. A scan area of  $1.2 \times 0.9 \text{ mm}^2$  was used.

IGC susceptibility was measured in terms of mass loss per unit area ( $\text{mg}/\text{cm}^2$ ) adopting the Nitric Acid Mass Loss Test (NAMLT) as specified in ASTM G-67 [50]. All experiments were conducted three times and the average values are reported with the standard deviation. To artificially sensitise the alloys, isothermal heat treatment was carried out at  $150^\circ\text{C}$  for 7 days.  $150^\circ\text{C}$  was used to accelerate the sensitisation kinetics for this laboratory studies. The degree of sensitisation at  $150^\circ\text{C}/7$  days is approximately equivalent to that achieved from  $100^\circ\text{C}/100$  days or  $60^\circ\text{C}/220$  days.

### 2.3. Characterisation

Hardness was measured using Struers Duramin A300 with a 1 kg load. Reported hardness values in this paper are an average of ten measurements. Back scattered electron imaging and energy dispersive X-ray spectroscopy mapping were conducted via an FEI-Quanta 3D FEG scanning electron microscope. Specimens used for SEM were polished to  $0.05 \mu\text{m}$  (Beuhler Masterprep) finish followed by ultrasonic cleaning.

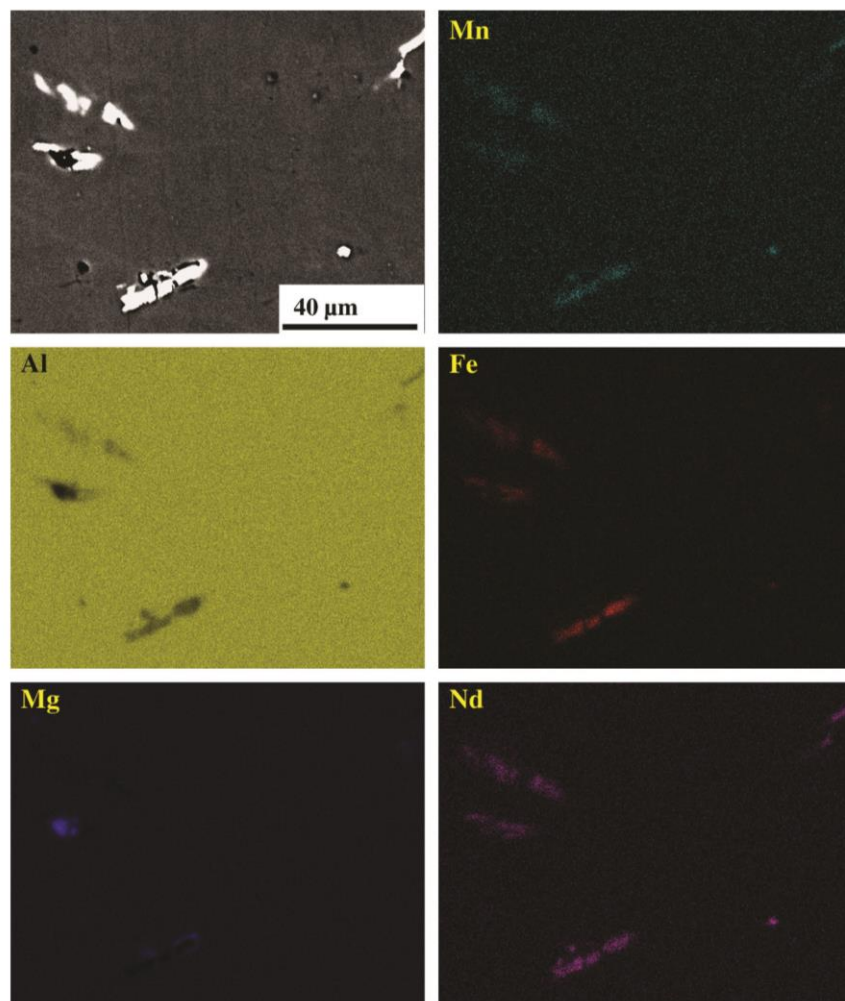


Fig. 3. High magnification observations and EDS element mapping analysis of the Al–5Mg–0.17Nd alloys showing Nd enrichment of Al–Fe–Mn types of intermetallic.



### 3. Results and discussion

#### 3.1. Effect of Nd on the microstructure of Al–5Mg

SEM images for the Al–5Mg–xNd alloys produced are presented in Fig. 1.

The microstructures in Fig. 1 reveal similar morphologies of the coarse intermetallic phases present, irrespective of Nd content. To rationalise the observations, the phase diagram of Al–5Mg–xNd alloys was calculated using PANDAT [51] and is presented in Fig. 2. From calculations, it is predicated that the presence of an  $\text{Al}_{11}\text{Nd}_3$  phase may occur. The relative volume fraction of the  $\text{Al}_{11}\text{Nd}_3$  phase is expected to increase with Nd content (Fig. 2), whilst overall existing in a low volume fraction of 0.157% for 0.17 wt.% Nd. Like a constituent phase,  $\text{Al}_{11}\text{Nd}_3$  phase is stable to elevated temperatures (Fig. 2), and its fraction does not have a dependence on solution treatment or aging temperature. From SEM investigations coupled with EDXS, no  $\text{Al}_{11}\text{Nd}_3$  phase could be detected using SEM. This suggests that either few  $\text{Al}_{11}\text{Nd}_3$  particles were formed, or those which formed were very fine. Further investigation of elemental distributions in the micron scale range revealed (via EDXS element mapping) that Nd was also incorporated in AlMnFe coarse constituent intermetallic particles (Fig. 3). Such segregation has

not been previously reported, and any change in the electrochemical properties of AlMnFe due to Nd incorporation is unknown and will require further work.

#### 3.2. Effect of Nd on the hardness of Al–5Mg

Vickers microhardness testing was carried out and has been reported in Fig. 4. It was observed that the hardness of the alloys increased with Nd content. The increase in hardness was observed both in as quenched and cold rolled samples, with the relatively minor addition of 0.17 wt.% Nd leading to an increase in hardness of  $\sim 10\%$ . This increase is rather significant given the amount of Nd present is  $\sim 1$  in 1000 atoms. The fraction of  $\text{Al}_{11}\text{Nd}_3$  increases with Nd content (inset of Fig. 2) which is expected to contribute in strengthening if a fine dispersion on the nanoscale is present (however this will need future TEM analysis to validate). An increase in hardness is consistent with some reported effects of Nd on properties of pure Al used in electronic applications [36].

#### 3.3. Effect of Nd on the electrochemical response and corrosion of Al–5Mg

Potentiodynamic polarisation tests were carried out to reveal the effect of Nd additions on the electrochemical response of Al–5Mg. Representative polarisation curves for Al–5Mg–xNd alloys are presented in Fig. 5, revealing that Nd additions ( $\geq 0.11$  wt.%)

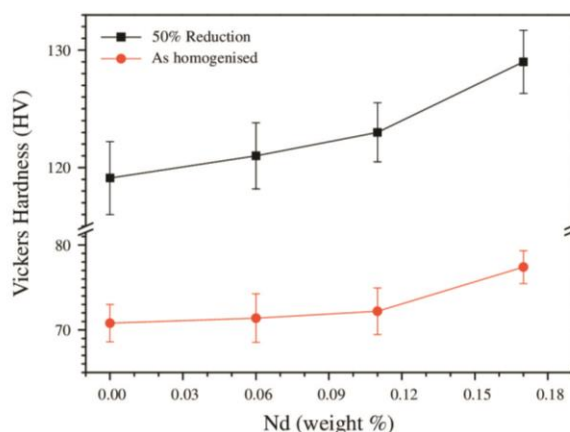


Fig. 4. Effect of Nd content on the Vickers hardness (measured using a 1 kg load) of Al–5Mg alloy.

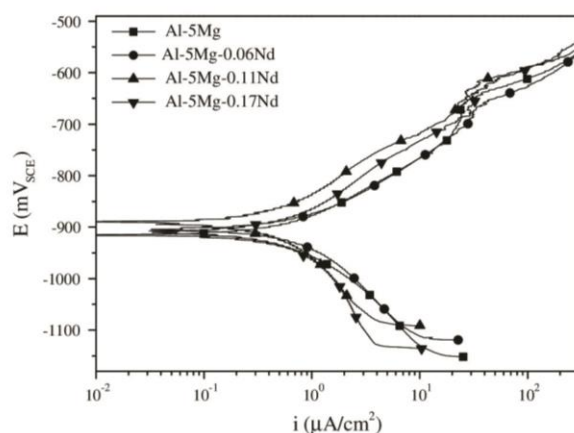


Fig. 5. Potentiodynamic polarisation curves for Al–5Mg–xNd alloys in quiescent 0.01 M NaCl using a scan rate of 1 mV/s.

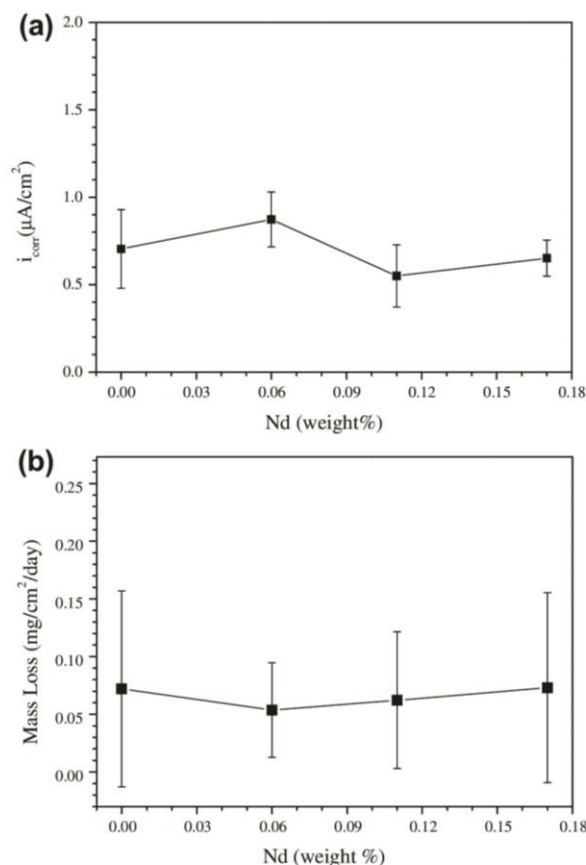


Fig. 6. Effect of Nd on corrosion of Al–5Mg alloy as measured in terms of (a) corrosion current density in 0.01 M NaCl as determined from Tafel extrapolation, and (b) mass loss per unit area per day following 14 days immersion in 0.01 M NaCl and subsequent cleaning of corrosion products.

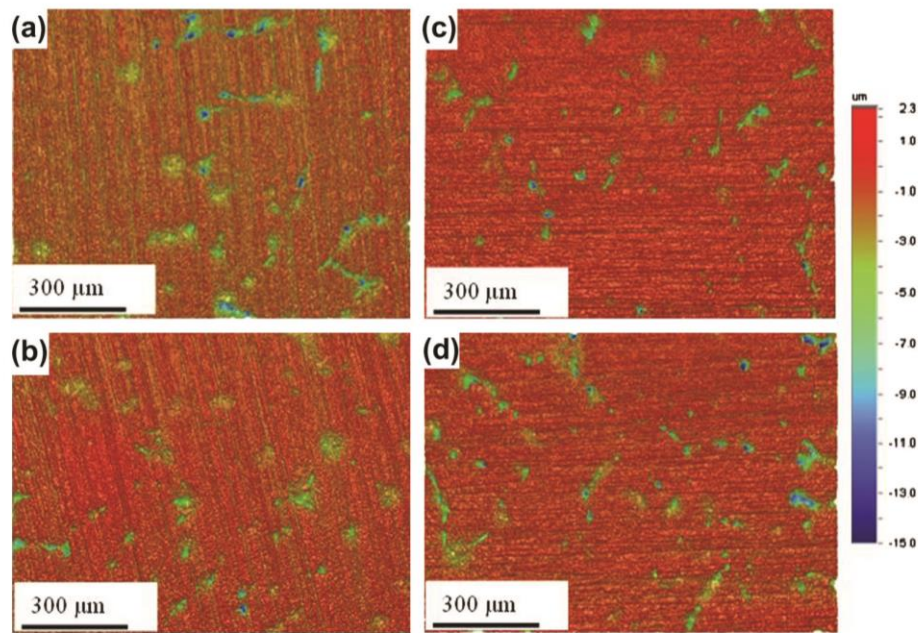


Fig. 7. Three dimensional optical profilometry images followed by constant immersion test (in 0.01 M NaCl for 14 days) and cleaning of corrosion products for (a) Al-5Mg-0Nd; (b) Al-5Mg-0.06Nd; (c) Al-5Mg-0.11Nd; and (d) Al-5Mg-0.17Nd.

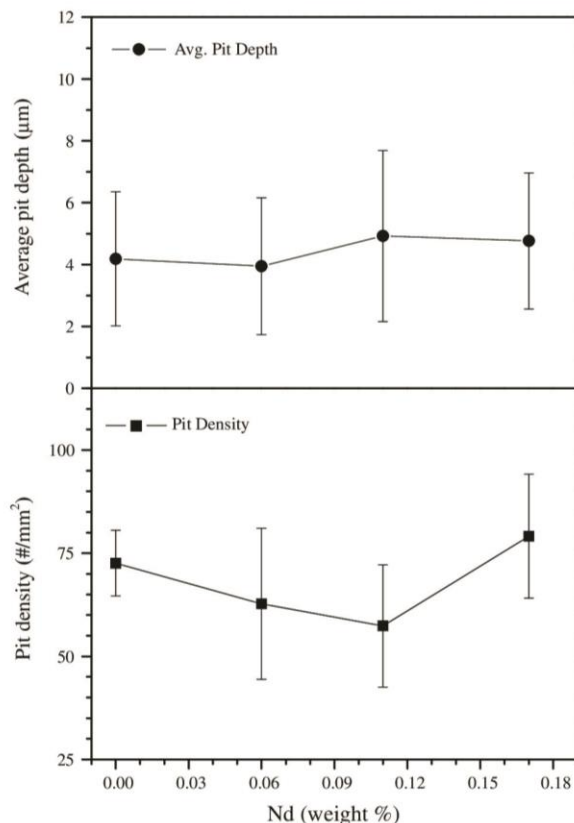


Fig. 8. Effect of Nd content on average pit depth and pit density as measured from optical profilometry after constant immersion tests in 0.01 M NaCl solution following cleaning of corrosion products.

lead to a slight decrease in anodic as well as cathodic kinetics – whilst corrosion potential ( $E_{\text{corr}}$ ) remained essentially unaltered. Corrosion current densities ( $i_{\text{corr}}$ ) were obtained from the Tafel extrapolation and are presented in Fig. 6.  $i_{\text{corr}}$  values for all alloys were in the range of 0.55–0.87  $\mu\text{A}/\text{cm}^2$ . If we consider the combined factors such as; the relatively small comparative difference in  $i_{\text{corr}}$ , the inherent difficulty in Tafel fitting, and the qualitative observation that all alloys displayed an  $i_{\text{corr}}$  of  $<1 \mu\text{A}/\text{cm}^2$ , we are able to suggest that the Nd additions did not lead to any increase in corrosion rate. Rather a marginal decrease in  $i_{\text{corr}}$ , albeit not outside the scatter, was noticed for higher Nd content ( $\geq 0.11 \text{ wt.}\%$ ) however no statistically relevant change in  $i_{\text{corr}}$  and  $E_{\text{corr}}$  values due to Nd additions can be concluded from this work alone. This response following the Nd additions to Al-5Mg indicates two possibilities, in that either the electrochemical characteristics of formed  $\text{Al}_{11}\text{Nd}_3$  phase are compatible with the Al-Mg matrix or the size of this  $\text{Al}_{11}\text{Nd}_3$  phase is too small to cause any significant change in electrochemical response as judged by potentiodynamic polarisation.

Mass loss after constant immersion tests in 0.01 M NaCl followed by chemical cleaning of corrosion products for alloys with varying Nd contents as presented in Fig. 6 exhibits similar mass loss throughout the composition range. This is consistent with potentiodynamic polarisation test results and indicates that up to 0.17 wt.% Nd does not influence corrosion of Al-5Mg alloy.

Pitting susceptibility of the Al-5Mg-xNd alloys was investigated by counting number and depth of pits using optical profilometry. Three dimensional surfaces of various alloys as presented in Fig. 7 show that size, shape and number of pits are similar in all the alloys. Average number and depth of pits (Fig. 8) revealed that Nd addition did not affect pitting corrosion. Pitting corrosion is largely influenced by presence of secondary phases, i.e., constituents, dispersoids or precipitates, and a relatively similar distribution of intermetallics for the alloy compositions tested herein explains the similar pitting behaviour of alloys. It is important to note that number, size and composition of the secondary phase particles are important in causing pitting corrosion [52,53].



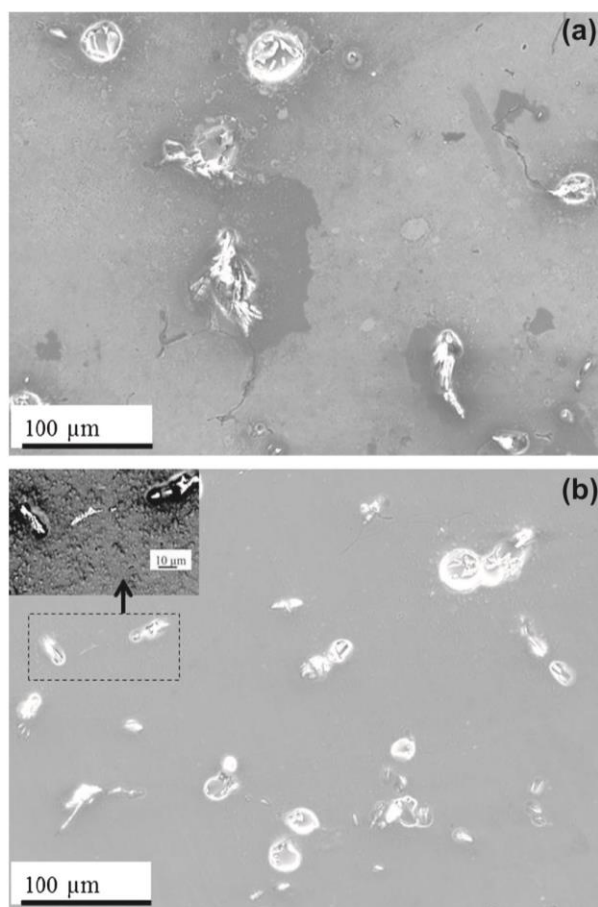


**Fig. 9.** SEM images for (a) Al-5Mg and (b) Al-5Mg-0.17Nd alloys after constant immersion test in 0.01 M NaCl for 2 days showing severe localised corrosion due to Fe containing intermetallics. Inset of Fig. 9b shows BSE image of  $\text{Al}_{11}\text{Nd}_3$  constituent particle which did not cause any localised corrosion.

A selection of Nd containing alloys were analysed using SEM following constant immersion tests for 2 days. The representative SEM images of Al-5Mg and Al-5Mg-0.17Nd after immersion testing are seen in Fig. 9, which reveals localised corrosion occurring around the coarse constituent intermetallics (Al-Fe-Mn type). The incorporation of Nd into coarse constituent intermetallics (which occurs 0.17Nd), did not seem to moderate the ability of constituents to cause localised corrosion. The  $\text{Al}_{11}\text{Nd}_3$  phase, which could not be easily detected via SEM of well polished sample (Fig. 1), was able to be identified in a low number density in specimens following immersion testing, due to no evident corrosion around these particles. The chemical composition was confirmed using EDXS, and the backscattered electron image (BSE) in the inset of Fig. 9b, indicates the presence of this phase. We note that the occurrence of  $\text{Al}_{11}\text{Nd}_3$  particles was rare and only evident in the in 0.17 wt.% Nd containing alloys. This indicates that  $\text{Al}_{11}\text{Nd}_3$  particles are most likely present as very fine dispersoids, whilst the  $\text{Al}_{11}\text{Nd}_3$  phase did not appear to cause any significant localised corrosion in Al-5Mg.

#### 3.4. Effect of Nd on hardness and IGC of Al-5Mg

Improving sensitisation resistance of Mg containing Al alloys, prone to IGC caused by sensitisation during prolonged service

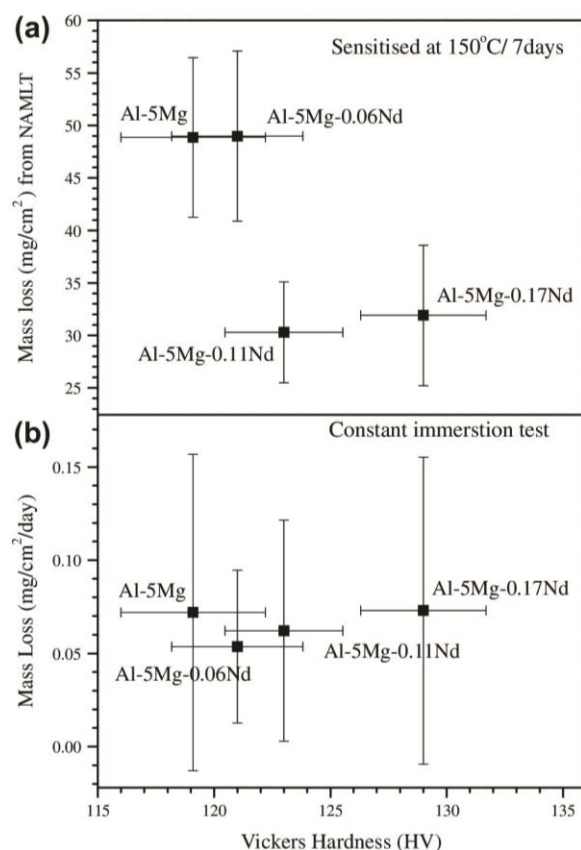


**Fig. 10.** Simultaneous effect of Nd on corrosion and hardness of an Al-5Mg alloy as represented by: (a) mass loss after NAMLT, a measure of IGC, versus hardness, and (b) mass loss (measured after 14 days constant immersion in 0.01 M NaCl following cleaning of corrosion products) versus hardness.

conditions, is one of the major challenges in engineering application of the alloys. The degree of sensitisation can be measured in terms of NAMLT values as described in [50]. Fig. 10 presents effect of Nd content on IGC and hardness simultaneously which reveals that  $\geq 0.17$  wt.% Nd is very effective in improving sensitisation resistance. It is interesting to note that 0.05 wt.% Nd content did not cause a significant change in NAMLT value. A significant decrease (by  $\sim 40\%$ ) in NAMLT value was observed due to addition of 0.11 and 0.17 wt.% Nd. Fig. 10 demonstrates that it is possible to increase hardness and a resistance to sensitisation simultaneously. For example, simultaneous reduction in degree of sensitisation (by 40%) and increase in hardness (by 10%) was caused by 0.17 wt.% Nd addition. This improvement in properties could be attributed to formation of  $\text{Al}_{11}\text{Nd}_3$  on grain boundaries potentially disrupting the  $\text{Mg}_2\text{Al}_3$  network, or incorporation of Nd in  $\text{Mg}_2\text{Al}_3$ , or even by altering the  $\text{Mg}_2\text{Al}_3$  formation kinetics [45], however the precise mode will need future work. A focused study on influence of Nd upon sensitisation resistance can be found in [45], which also reveals that alloyed Nd has no effect on NAMLT values of unsensitised (i.e. solution treated and quenched) alloys.

Fig. 10 also presents the relationship between corrosion (indicated by mass loss following by constant immersion tests) and hardness which also showed that Nd addition lead to increase in corrosion rate while not deteriorating corrosion resistance. This is an important finding demonstrating that the beneficial effects of Nd addition can be exploited without significant loss in corrosion performance of alloy.



### 3.5. General discussion

Improving physical properties without the loss of corrosion performance for Al alloys is of great industrial interest, as corrosion rate is nominally increased with any increase in hardness. Only a limited examples reporting simultaneous increase in hardness and corrosion performance are available in the literature. Nd additions to Al–5Mg alloys in this study indicated a possibility of improving strength and sensitisation resistance simultaneously while pitting corrosion (as presented in terms of number and depth of pits) and general corrosion (as presented by polarisation and mass loss data) remained unaffected. This interesting corrosion performance, hardness and Nd content relationship will need further investigation, as will the phenomenon which is possibly capable of being imparted by other rare earth elements and yet to be reported. The electrochemical characteristics of the  $\text{Al}_{11}\text{Nd}_3$  phase are not known, however, work herein indicates that if  $\text{Al}_{11}\text{Nd}_3$  formed, was not deleterious for corrosion and further investigations will be required to understand role of Nd and the electrochemical behaviour of the  $\text{Al}_{11}\text{Nd}_3$  phase more precisely. More generally, Nd could be a cost effective candidate to Sc, and further detailed studies could confirm if Nd could be a substitute for Sc or may be used in combination with Sc to improve properties of various Al alloys.

### 4. Conclusions

1. A range of custom alloys containing variable levels of Nd added to a model Al–5Mg composition were successfully produced.
2. Alloying with Nd did not affect the morphology of coarse (constituent type) intermetallics significantly. However, Nd microalloying did tend to reveal some segregation of Nd to coarse  $\text{AlMnFe}$  intermetallic particles. There was no evidence of Nd-rich intermetallics from SEM observations in alloys with Nd content  $\leq 0.11$  wt.%. Only a few  $\text{Al}_{11}\text{Nd}_3$  particles were detected in Al–5Mg–0.17Nd alloy.
3. For the range of compositions tested, Nd addition to Al–5Mg alloy leads to significant improvement in sensitisation resistance and a notable increase in hardness.
4. From an electrochemical perspective, microalloying additions of Nd statistically had a rather negligible effect on the  $E_{\text{corr}}$  and  $i_{\text{corr}}$  values realised, in addition to no significant alteration of anodic or cathodic kinetics. Post immersion SEM indicated that the  $\text{Al}_{11}\text{Nd}_3$  phase did not contribute to localised corrosion. The addition of Nd also had no significant effect on the general and pitting corrosion of Al–5Mg from mass loss testing, which suggests that the beneficial effect of Nd (on sensitisation resistance and hardness) can be exploited without loss in corrosion performance.

### Acknowledgments

Financial support from the Office of Naval Research and Office of Naval Research Global (with Dr. Airan Perez and Dr. Joseph Wells as Scientific Officers) is gratefully acknowledged. The Australian Research Council is acknowledged for establishing the Centre of Excellence for Design in Light Metals and the DP scheme.

### References

- [1] I.J. Polmear, *Light Alloys*, fourth ed., Butterworth-Heinemann, Oxford, 2005. pp. 97–204.
- [2] C. Vargel, M. Jacques, M.P. Schmidt, *Corrosion of Aluminium*, Elsevier, Amsterdam, 2004. pp. 61–69.

- [3] R.K. Gupta, N.L. Sukiman, M.K. Cavanaugh, B.R.W. Hinton, C.R. Hutchinson, N. Birbilis, *Electrochim. Acta* 66 (2012) 245–254.
- [4] J.R. Davis, *ASM Handbook*, vol. 2, ASM, Metals Park, OH, 1990. p. 29.
- [5] D.L. Olmsted, L.G. Hector Jr., W.A. Curtin, *J. Mech. Phys. Solids* 54 (2006) 1763–1788.
- [6] V.S. Zolotarevsky, N.A. Belov, M.V. Glazoff, *Casting Aluminum Alloys*, Elsevier, Amsterdam, 2007. pp. 397–447.
- [7] N. Birbilis, R.G. Buchheit, *J. Electrochem. Soc.* 152 (2005) B140–B151.
- [8] R.G. Buchheit, *J. Electrochem. Soc.* 142 (1995) 3994–3996.
- [9] N. Birbilis, R.G. Buchheit, *J. Electrochem. Soc.* 155 (2008) C117–C126.
- [10] X. Wang, S. Lin, J. Yang, Z. Tang, Z. Nie, G.C. Yao, *Rare Metals* 31 (2012) 237–243.
- [11] H. Shen, H. Liang, W.D. Yang, B.X. Liu, T.S. Li, G.C. Yao, *Adv. Mater. Res.* 314–316 (2011) 1449–1455.
- [12] Z. Nie, H. Huang, K. Gao, B. Li, W. Wang, Z. Chen, L. Rong, S. Wen, H. Li, T. Zuo, *Mater. Sci. Forum* 706–709 (2012) 329–334.
- [13] M. Kubota, *Mater. Trans.* 46 (2005) 2437–2442.
- [14] I.J. Polmear, I.F. Bainbridge, *Improved aluminium–magnesium casting alloys*, Australian provisional Patent Number 37271/63 (1963).
- [15] I.J. Polmear, K.R. Sargent, *Nature* 200 (1963) 669–670.
- [16] Y.A. Filatov, V.I. Yelagin, V.V. Zakharov, *Mater. Sci. Eng., A* 280 (2000) 97–101.
- [17] V. Ocenasek, M. Slamova, *Mater. Charact.* 47 (2001) 157–162.
- [18] Z. Yin, Q. Pan, Y. Zhang, F. Jiang, *Mater. Sci. Eng., A* 280 (2000) 151–155.
- [19] J.K. McBride, R.E. Sanders Jr., H.G. Reavis, *JOM* 48 (1996) 18–21.
- [20] M. Conserva, M. Leoni, *Metall. Trans. A* 6 (1975) 189–195.
- [21] M. Kubota, J.F. Nie, B.C. Muddle, *Mater. Trans.* 45 (2004) 3256–3263.
- [22] R.B. Inturi, Z. Szklarska-Smialowska, *Corros. Sci.* 34 (1993) 1201–1212.
- [23] J.S. Vetrano, S.M. Brummer, L.M. Pawlowski, I.M. Robertson, *Mater. Sci. Eng., A* 238 (1997) 101–107.
- [24] C.B. Fuller, A.R. Krause, D.C. Dunand, D.N. Seidman, *Mater. Sci. Eng., A* 338 (2002) 8–16.
- [25] F. Rosalbino, E. Angelini, S. De Negri, A. Saccone, S. Delfino, *Intermetallics* 11 (2003) 435–441.
- [26] A. Heinz, A. Haszler, C. Keidel, S. Moldenhauer, R. Benedictus, W.S. Miller, *Mater. Sci. Eng., A* 280 (2000) 102–107.
- [27] Z. Ahmad, A. Ul-Hamid, B.J. Abdul-Alim, *Corros. Sci.* 43 (2001) 1227–1243.
- [28] M.K. Cavanaugh, N. Birbilis, R.G. Buchheit, F. Bovard, *Scripta Mater.* 56 (2007) 995–998.
- [29] Y.L. Wu, F.H. Froes, C. Li, A. Alvarez, *Metall. Mater. Trans. A* 30 (1999) 1017–1024.
- [30] B.A. Parker, Z.F. Zhou, P. Nolle, *J. Mater. Sci.* 30 (1995) 452–458.
- [31] J. Ryset, N. Ryum, *Int. Mater. Rev.* 50 (2005) 19–44.
- [32] V.G. Davydov, T.D. Rostova, V.V. Zakharov, Y.A. Filatov, V.I. Yelagin, *Mater. Sci. Eng., A* 280 (2000) 30–36.
- [33] S. Komura, Z. Horita, M. Furukawa, M. Nemoto, T.G. Langdon, *J. Mater. Res.* 15 (2000) 2571–2576.
- [34] Z. Ahmad, *JOM* 55 (2003) 35–39.
- [35] T.J.Z. Nie, J. Fu, G. Xu, T.Z.J. Yang, *Mater. Sci. Forum* 396–402 (2002) 1731–1736.
- [36] C.H. Cui, K.Y. Gao, Z.R. Nie, S.P. Wen, H. Huang, *Corros. Prot.* 32 (2011) 94–98.
- [37] H. Li, H. Wang, X. Liang, Y. Wang, H. Liu, *J. Mater. Eng. Perform.* 21 (2012) 83–88.
- [38] G.M. Scamans, N.J.H. Holroyd, C.D.S. Tuck, *Corros. Sci.* 27 (1987) 329–347.
- [39] S. Jain, M.L.C. Lim, J.L. Hudson, J.R. Scully, *Corros. Sci.* 59 (2012) 136–147.
- [40] R.H. Jones, D.R. Baer, H.J. Danielson, J.S. Vetrano, *Metall. Mater. Trans. A* 32 (2001) 1699–1711.
- [41] M.L.C. Lim, J.R. Scully, R.G. Kelly, *Corrosion* 69 (2013) 35–47.
- [42] J.A. Lyndon, R.K. Gupta, M.A. Gibson, N. Birbilis, *Corros. Sci.* 70 (2013) 290.
- [43] R.L. Holtz, P.S. Pao, R.A. Bayles, T.M. Longazel, R. Goswami, *Metall. Trans. A* 43 (2012) 2839–2849.
- [44] N. Birbilis, R. Zhang, M.L.C. Lim, R.K. Gupta, C.H.J. Davies, S.P. Lynch, S.P. Lynch, R.G. Kelly, J.R. Scully, *Corrosion* 69 (2013) 396.
- [45] R.K. Gupta, Y. Wang, R. Fang, N.L. Sukiman, C.H.J. Davies, N. Birbilis, *Corrosion* 69 (2013) 4–8.
- [46] M.C. Carroll, P.I. Gouma, M.J. Mills, G.S. Daehn, B.R. Dunbar, *Scripta Mater.* 42 (2005) 335–340.
- [47] M.C. Carroll, P.I. Gouma, G.S. Daehn, M.J. Mills, *Mater. Sci. Eng., A* 319–321 (2001) 425–428.
- [48] M.C. Carroll, R.G. Buchheit, G.S. Daehn, M.J. Mills, *Mater. Sci. Forum* 396–402 (2002) 1443–1448.
- [49] I. Gheorghe, V.B. Dangerfield, *Aluminium–magnesium–silver based alloys*, United States Patent, US2008030500A1 (2008).
- [50] ASTM G 67-04, Standard Test Method for Determining the Susceptibility to Intergranular Corrosion of 5xxx Series Aluminum Alloys by Mass Loss After Exposure to Nitric Acid (NAML Test), ASTM International, West Conshohocken, PA, 2004.
- [51] Pandat® software, Pandat and PanAl databases, CompuTherm LLC. <http://www.compuTherm.com>.
- [52] K.D. Ralston, N. Birbilis, M.K. Cavanaugh, M. Weyland, B.C. Muddle, R.K.W. Marceau, *Electrochim. Acta* 55 (2010) 7834–7842.
- [53] R.K. Gupta, A. Deschamps, M.K. Cavanaugh, S.P. Lynch, N. Birbilis, *J. Electrochem. Soc.* 159 (2012) C492–C502.



## Monash University

### Declaration for Thesis Section 7.3

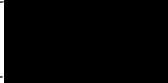

In the case of Section 7.3, the nature and extent of my contribution to the work was the following:

Nature of contribution	Extent of contribution (%)
Initiation, key ideas, experimental, development, results interpretations, writing up	30

The following co-authors contributed to the work. If co-authors are students at Monash University, the extent of their contribution in percentage terms must be stated:

Name	Nature of contribution	Extent of contribution (%) for student co-authors only
Nick Birbilis	Initiation, key ideas, experimental, development, results interpretations, writing up	5
Rajeev Gupta	Initiation, key ideas, experimental, development, results interpretations, writing up	30
Yuan Wang	Initiation, key ideas, experimental, development, results interpretations, writing up	25
Ruifeng Zhang	Initiation, key ideas, experimental, development, results interpretations, writing up	5
Chris Davies	Results interpretations, writing up	5

The undersigned hereby certify that the above declaration correctly reflects the nature and extent of the candidate's and co-authors' contributions to this work.

Candidate's Signature		Date 18 June 2014
Main Supervisor's Signature		Date 18 June 2014

# Imparting Sensitization Resistance to an Al-5Mg Alloy via Neodymium Additions

R.K. Gupta,<sup>†,\*</sup> Y. Wang,<sup>\*</sup> R. Zhang,<sup>\*</sup> N.L. Sukiman,<sup>\*\*\*</sup> C.H.J. Davies,<sup>\*\*\*</sup> and N. Birbilis<sup>\*</sup>

## ABSTRACT

Low-level Nd additions, up to 0.17 wt%, were added to Al-5Mg to explore the impact on the subsequent degree of sensitization. Following heat treatment at 150°C for 1 day and 7 days, nitric acid mass loss (NAML) tests revealed that additions of >0.11% Nd were effective at decreasing the amount of subsequent intergranular attack.

**KEY WORDS:** 5xxx aluminum alloys, aluminum, intergranular corrosion, neodymium, sensitization

## INTRODUCTION

5xxx series Al alloys are non-heat-treatable and work-hardenable alloys based on the Al-Mg(-Mn) system.<sup>1</sup> Alloys of this series are generally regarded as corrosion-resistant and used in a range of applications, including marine structures.<sup>1-4</sup> When Mg is present in levels greater than ~3.5 wt%,<sup>1-3</sup> intergranular corrosion (IGC) and stress corrosion cracking (SCC) can occur if the alloy has been exposed to elevated service temperatures (ranging from ~50°C to 200°C). This is because of the insidious precipitation of Mg<sub>2</sub>Al<sub>3</sub> (β phase) at grain boundaries,<sup>2,4-5</sup> which is anodic in

nature.<sup>4-6</sup> Dissolution associated with the presence of grain boundary β phase is a key contributor to IGC and SCC,<sup>7-8</sup> in addition to propagation by a hydrogen embrittlement mechanism.<sup>9-10</sup> A deeper insight into the factors involved and mechanism of IGC and SCC in Al-Mg alloys has been provided.<sup>11-12</sup>

In spite significant research in understanding and quantifying the IGC of 5xxx alloys arising from sensitization,<sup>7-17</sup> comparatively limited attention has been given to the development of 5xxx alloys with greater resistance to IGC.<sup>18-29</sup> The methods available to achieve greater resistance include:

- (1) Reduction in the amount of Mg present. This, however, ultimately leads to reduced strength and hence is not a universal option.
- (2) Rendering β phase “less anodic” by micro-alloying (and doping of the β phase).
- (3) Introduction of secondary precipitates (other than β phase) at grain boundaries to interrupt the β-phase network and potentially reduce IGC attack.
- (4) Alloying to decrease the volume fraction of β-phase precipitates.
- (5) Thermomechanical treatment to stabilize the microstructure rendering it less prone to sensitization. Such a microstructure may correspond to a structure that contains discontinuous β phase.<sup>18-19</sup>

Of the above approaches, (2), (3), and (4) have not been pursued or reported to an appreciable extent, and provide an area where significant future work is required. Some notable exceptions include parcels of

Submitted for publication: September 7, 2012. Revised and accepted: October 14, 2012. Preprint available online: October 26, 2012, <http://dx.doi.org/10.5006/0833>.

<sup>†</sup> Corresponding author. E-mail: [rajeev.gupta@monash.edu](mailto:rajeev.gupta@monash.edu).

<sup>\*</sup> ARC Centre of Excellence for Design in Light Metals, Department of Materials Engineering, Monash University, Clayton, Australia.

<sup>\*\*</sup> Department of Mechanical Engineering, University of Malaya, Kuala Lumpur, 50603, Malaysia.

<sup>\*\*\*</sup> Department of Mechanical and Aerospace Engineering, Monash University, Australia.

work carried out since the late 1950s,<sup>20-29</sup> to recent patents that indicate improved resistance to sensitization may occur with Cu additions (up to 0.43 wt%), while also indicating the relevance of appropriate thermomechanical treatment.<sup>20-21</sup>

Caroll, et al.,<sup>22-23</sup> showed that addition of Zn, and a combination of Cu and Zn (in the range of ~0.15 wt% to ~0.7 wt%), to Al-Mg alloys can modify  $\beta$  phase to form  $Mg_{32}(Al,Zn)_{49}$ , which was posited as less susceptible to anodic dissolution at grain boundaries. In a separate study, Caroll, et al.,<sup>24</sup> showed that the addition of Zn, and Cu with Zn, can suppress SCC by modification of the  $Mg_2Al_3$  precipitate chemistry, and that co-precipitation of an Al-Mg-Zn phase enriched with Cu may occur at grain boundaries. Unocic, et al.,<sup>25</sup> reported that higher levels of Cu and Zn decrease the IGC of AA5083 (Al~4.4Mg-0.5Mn [UNS A95083]<sup>(1)</sup>). Trace amounts of Ag were reported to improve IGC resistance by decreasing the amount of grain boundary precipitates.<sup>26</sup> Some pioneering work by Polmear and coworkers<sup>27-28</sup> also had indicated that addition of Ag was beneficial to Al-Mg alloys, minimizing the extent of sensitization by exploiting that a strengthening component from Ag could be accompanied by lower Mg levels for an equivalent strength.

In this study, the effect of Nd additions upon the sensitization of an Al-5Mg model alloy are investigated and reported. Nd additions were selected on the basis of studying the impact of the presence of an additional  $Al_{11}Nd_3$  phase, which, being Al-rich, would have a presumably lower electrochemical mismatch with the matrix phase. The alloy phases were determined from thermodynamic analysis (Figure 1) revealing the relative fraction of equilibrium phases present at 150°C, using Pandat<sup>†</sup> software (Pandat<sup>†</sup> and PanAl<sup>†</sup> databases, CompuTherm LLC, <http://www.compu-therm.com>).

## EXPERIMENTAL PROCEDURES

Al-5Mg-xNd alloys with varying Nd content (listed in Table 1) were prepared by melting pure Al (99.99%) ingot, commercially pure Al shot (99%), pure Mg (99.9%), and an Mg-Nd master alloy (99.9%) in a muffle furnace. The resulting alloys were cast into molds in air. The chemical composition of the alloys was analyzed using inductively coupled plasma-optical emission spectrometry (ICP-OES) (Spectrometer Services, Coburg, Victoria, Australia). Alloys were homogenized at 450°C for 3 days. Prior to testing, alloys were solution-treated for 1 h in a salt bath, quenched, and rolled to a 50% thickness reduction.

To sensitize the alloys artificially, isothermal heat treatment was carried out at 150°C for 1 day and

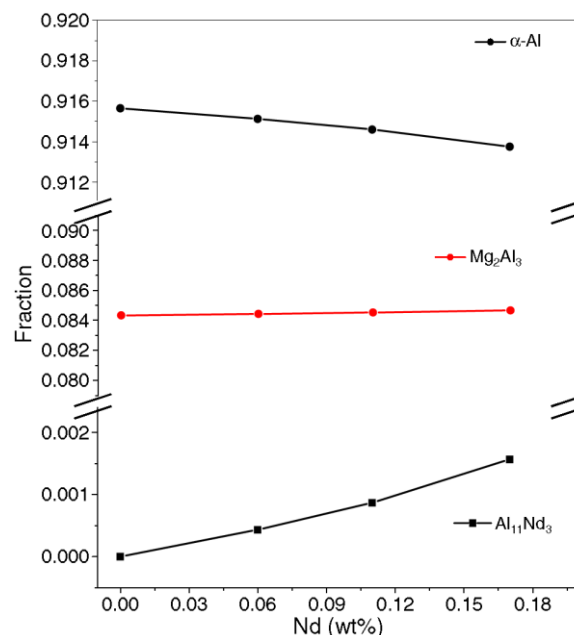


FIGURE 1. Equilibrium fraction of phases present in Al-5Mg-xNd alloy calculated at 150°C using Pandat<sup>†</sup>. The phases predicted are the  $\alpha$ -Al solid solution (face-centered cubic [fcc] phase enriched in Mg), the  $Mg_2Al_3$   $\beta$  phase, and the  $Al_{11}Nd_3$  phase.

TABLE 1  
Composition (wt%) of Alloys, as Determined  
Using Inductively Coupled Plasma-Optical  
Emission Spectroscopy

	Mg	Nd	Fe	Si	Mn	Al
Al-5Mg	5.17	0	0.18	0.07	0.03	Bal.
Al-5Mg-0.06Nd	4.89	0.06	0.15	0.07	0.02	Bal.
Al-5Mg-0.11Nd	5.07	0.11	0.16	0.06	0.02	Bal.
Al-5Mg-0.17Nd	5.14	0.17	0.15	0.06	0.02	Bal.

7 days. IGC susceptibility was measured in terms of mass loss per unit area ( $mg/cm^2$ ), adopting the nitric acid mass loss test (NAMLT) as specified in ASTM G67.<sup>30</sup> All experiments were conducted three times, and the average values are reported with the standard deviation. To quantify IGC that occurred following NAMLT and for verification of differences in the extent of IGC, cross sections of the alloys were examined using optical microscopy. Optical profilometry of exposed surfaces also was performed using a Veeco Wyko NT-1100<sup>†</sup>.

Grain size of the alloys was determined optically following polishing to a 0.05 micron surface finish followed by etching in Keller's reagent. Transmission electron microscopy (TEM) was carried out upon 3 mm disks electropolished at -13 V in a 30% nitric acid-70% methanol (30%  $HNO_3$ -70%  $CH_4O$ ) solution and at -30°C, and imaged in high-angle annular dark-field scanning TEM mode using an FEI TF-20<sup>†</sup>.

<sup>(1)</sup> UNS numbers are listed in *Metals and Alloys in the Unified Numbering System*, published by the Society of Automotive Engineers (SAE International) and cosponsored by ASTM International.

<sup>†</sup> Trade name.

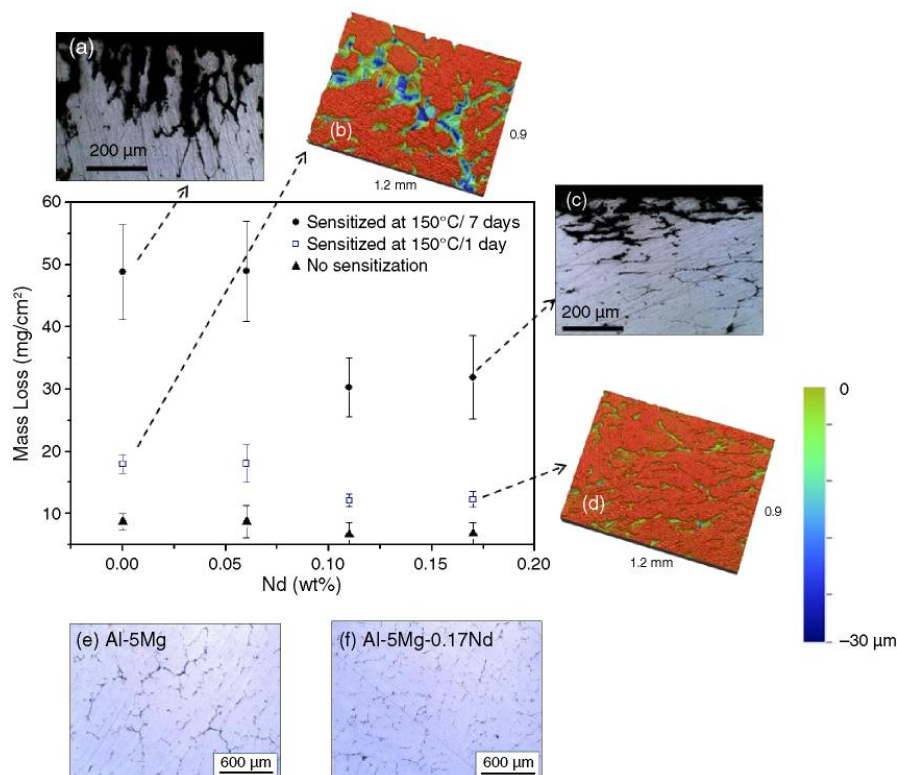


**FIGURE 2.** Results from ASTM G69 NAMLT (reported in mass loss per unit area) as a function of Nd content for unsensitized and sensitized at 150°C for 1 day and 7 day specimens. Optical images of cross sections following NAMLT testing and showing extent of IGC for (a) Al-5Mg and (c) Al-5Mg-0.17Nd alloy, sensitized at 150°C/7 days. Surface profiles after NAMLT are presented for (b) Al-5Mg and (d) Al-5Mg-0.17Nd sensitized at 150°C for 1 day. Optical microscopy images showing the grain size for (e) Al-5Mg and (f) Al-5Mg-0.17Nd.

## RESULTS AND DISCUSSION

The NAMLT results (Figure 2) indicate the effect of varying Nd contents for three sensitization conditions, namely, unsensitized and sensitized at 150°C for 1 day and 7 days. Mass loss per unit area values for unsensitized alloys were less dependent on Nd content, although a slight decrease in mass loss was observed for  $\text{Nd} \leq 0.11$  wt%. The NAMLT values were, however, highly dependent upon the Nd content for samples sensitized at 150°C. In fact, the effect of Nd on NAMLT values (which correlate with IGC susceptibility) of Al-5Mg alloys can be seen clearly after sensitization for compositions with  $\text{Nd} \geq 0.11$  wt%. In the case of 1 day at 150°C, the NAMLT value was nearly halved for alloys with  $\geq 0.11$  wt% Nd. This trend also remains for specimens treated for 7 days at 150°C. A NAMLT value of 150°C/7 days is equivalent to about 100°C/100 days and about 60°C/220 days (for AA5083). These results indicate that Nd is effective in suppressing the IGC susceptibility of Al-Mg alloys during sensitization at elevated temperatures—an effect that has not been reported previously for Nd additions.

Relating this to the thermodynamic calculations, we observe that the addition of Nd should not affect the fraction of  $\beta$  phase (Figure 1). In fact, the  $\beta$ -phase fraction remains essentially unchanged with increasing Nd content, with rather the fraction of  $\text{Al}_{11}\text{Nd}_3$  increasing linearly (and a concomitant minor decrease in the fraction of  $\beta$ -Al). As such, the decrease in mass loss per unit area values of Al-5Mg alloy as a result of the Nd addition may be attributed to either:

- incorporation of Nd into  $\beta$  phase, which may decrease the activity of this phase,
- coexistence of  $\text{Al}_{11}\text{Nd}_3$  particles on grain boundaries interrupting the network of  $\beta$  phase, or
- retardation of the  $\beta$ -phase growth kinetics.

Theoretical analysis, which was based on current thermodynamic databases ([www.computherm.com](http://www.computherm.com)), suggests that essentially no Nd can be substituted into the  $\beta$  phase, and that the Nd content in the  $\alpha$ -Al is  $\sim 1 \times 10^{-10}$  wt%.

Grain size as determined via optical microscopy indicates that Nd has only a minor effect on grain refinement (Figure 2). The average grain size for Al-5Mg, Al-5Mg-0.06Nd, Al-5Mg-0.11Nd, and Al-5Mg-0.17Nd was 200, 165, 152, and 155  $\mu\text{m}$ , respectively.

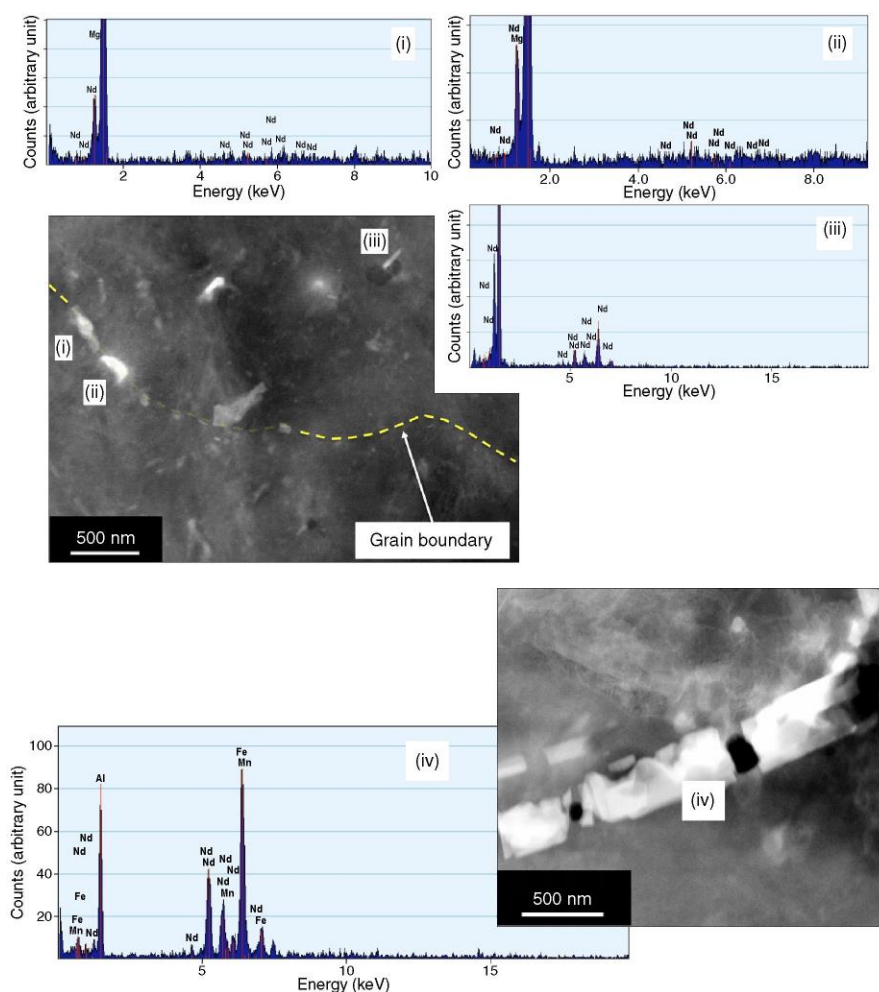


**FIGURE 3.** High-angle annular dark field scanning transmission microscopic (HAADF-STEM) images of an Al-5Mg-0.17Nd specimen held at 150°C for 7 days, revealing (top) the grain boundary nanostructure, and (bottom) a coarse constituent particle. Corresponding EDXS spectra indicate (i) and (ii) low Nd levels appearing to be incorporated in grain boundary  $\beta$  phase, (iii) an  $\text{Al}_{11}\text{Nd}_3$  particle, and (iv) obvious Nd segregation in a coarse Al-Fe-Mn constituent particle.

Comparison between grain size and NAML values indicates that NAML values can vary as a result of compositional changes for a similar grain size, which supports the basis of the study (i.e., the difference between Al-5Mg-0.06Nd and Al-5Mg-0.11Nd). However, more detailed studies are required more generally in regard to the effect of grain size on sensitization.

To probe further the possible mechanism of such decreased rates of NAML values, transmission electron microscopy (TEM) was used (Figure 3). TEM indicated the random presence of relatively fine  $\text{Al}_{11}\text{Nd}_3$  particles (Figure 3, inset [iii]) along with  $\beta$  phase on grain boundaries (Figure 3, insets [i] and [ii]). The associated energy-dispersive x-ray spectroscopy (EDXS) spectra are included. While EDXS is only semi-quantitative, elemental ratios reveal that there

was reproducibly detectable Nd in the  $\beta$  phase at the level of ~3 at% to 5 at%, even though this was not predicted. One possible reason is that the Nd may be associated with the  $\text{Mg}^{31}$  and possibly can segregate with and substitute for Mg, although this would need to be validated in future work, such as 3D atom probe studies. Nd presence in  $\beta$  phase also could be a factor in the reduced NAML values. An additional characteristic of the Nd-containing alloys is that the Nd had also segregated (in all cases tested by EDXS) to Al-Fe-Mn-type constituent particles (Figure 3, inset [iv]); however, this is not expected to have a great impact on IGC. Analysis to date has revealed that low-level Nd additions are potent at reducing IGC susceptibility; however, further work is needed—and underway—to isolate the specific mechanism, which could be associated with the following:



- the Nd presence in  $\beta$  phase as indicated herein
- changes in the  $\beta$ -phase size distribution
- changes in the kinetics of  $\beta$ -phase formation (each of these being a dedicated study)

## CONCLUSIONS

❖ This study has revealed that the addition of low levels of Nd can decrease the IGC susceptibility of an Al-5Mg alloy that was sensitized at 150°C. Of the concentrations studied, this beneficial effect was observed when Nd was present at  $\geq 0.11$  wt%, with a maximum tested Nd concentration of 0.17 wt%. The microstructure revealed a very low fraction of isolated  $\text{Al}_{11}\text{Nd}_3$  phase. However, the incorporation of Nd into  $\beta$  phase was observed, and this is conjectured to contribute to the decreased IGC rates. Nd was also incorporated into the Al-Fe-Mn constituent phases surveyed.

## ACKNOWLEDGMENTS

Financial support from the Office of Naval Research and Office of Naval Research Global (with A. Perez and J. Wells as scientific officers) is gratefully acknowledged. The Australian Research Council is acknowledged for establishing the Centre of Excellence for Design in Light Metals. We also thank the Bio21 Institute for access to TEM.

## REFERENCES

1. I.J. Polmear, *Light Alloys*, 3rd ed., (London, U.K.: Arnold, 1995).
2. J. Davis, *Corrosion of Aluminum and Aluminum Alloys* (Materials Park, OH: ASM International, 1999).
3. J.E. Hatch, *Aluminium: Properties and Physical Metallurgy* (Materials Park, OH: ASM International, 1984).
4. R.K. Gupta, N.L. Sukiman, M.K. Cavanaugh, B.R.W. Hinton, C.R. Hutchinson, N. Birbilis, *Electrochim. Acta* 66 (2012): p. 245.
5. E.H. Dix, W.A. Anderson, M.B. Shumaker, *Corrosion* 15 (1959): p. 19.
6. N. Birbilis, R.G. Buchheit, *J. Electrochem. Soc.* 152 (2005): p. B140.
7. J.L. Searles, P.I. Gouma, R.G. Buchheit, *Metall. Mater. Trans. A* 32 (2001): p. 2859.
8. R.H. Jones, D.R. Baer, H.J. Danielson, J.S. Vetrano, *Metall. Mater. Trans. A* 32 (2001): p. 1699.
9. G.M. Scamans, N.J.H. Holroyd, C.D.S. Tuck, *Corros. Sci.* 27 (1987): p. 329.
10. R.H. Jones, J.S. Vetrano, C.F. Windisch, Jr., *Corrosion* 60, 12 (2004): p. 1144, doi: <http://dx.doi.org/10.5006/1.3299228>.
11. G. Scamans, "Low Temperature Sensitization of AA5xxx Alloys," Technical Report IR07-197, Innoval, Oxon, U.K., 2008.
12. R.H. Jones, *JOM* 55 (2003): p. 42.
13. S. Jain, M.L.C. Lim, J.L. Hudson, J.R. Scully, *Corros. Sci.* 59 (2012): p. 136.
14. M.L.C. Lim, J.R. Scully, R.G. Kelly, "Intergranular Corrosion Penetration in an Al-Mg Alloy as a Function of Electrochemical and Metallurgical Conditions," *Corrosion*, doi: <http://dx.doi.org/10.5006/0722>, in press.
15. R.L. Holtz, P.S. Pao, R.A. Bayles, T.M. Longazel, R. Goswami, *Metall. Mater. Trans. A* 43 (2012): p. 2839.
16. R. Goswami, G. Spanos, P.S. Pao, R.L. Holtz, *Metall. Mater. Trans. A* 42 (2011): p. 348.
17. N. Birbilis, R. Zhang, M.L.C. Lim, R.K. Gupta, C.H.J. Davies, S.P. Lynch, R.G. Kelly, J.R. Scully, "Quantification of Sensitization in AA5083-H131 via Imaging Ga-Embrittled Fracture Surfaces" *Corrosion* (2012), doi: <http://dx.doi.org/10.5006/0804>, in press.
18. E. Bumiller, "Intergranular Corrosion in AA5XXX Aluminum Alloys with Discontinuous Precipitation at the Grain Boundaries" (Ph.D. thesis, The University of Virginia, 2011).
19. E. Bumiller, R.G. Kelly, "Intergranular Corrosion in AA5XXX: A Case for Continuous Attack with a Discontinuous Active Path," 2011 DoD Corrosion Conf. (Houston, TX: NACE International, 2011).
20. J.M. Newman, F.S. Bovard, R.R. Sawtell, "5xxx Aluminium Alloys, and Methods for Producing the Same," United States Patent, US2012/0103476A1, 2012.
21. D.C. Mooy, R.J. Rioja, R.R. Sawtell, S. Bovard, G.B. Venema, D.A. Lindle, "5xxx Aluminium Alloys and Wrought Aluminium Alloy Products Made from Therefrom," United States Patent, US2011/0017055A1, 2011.
22. M.C. Carroll, P.I. Gouma, M.J. Mills, G.S. Daehn, B.R. Dunbar, *Scr. Mater.* 42 (2005): p. 335.
23. M.C. Carroll, P.I. Gouma, G.S. Daehn, M.J. Mills, *Mater. Sci. Eng. A* 319-321 (2001): p. 425.
24. M.C. Carroll, R.G. Buchheit, G.S. Daehn, M.J. Mills, *Mater. Sci. Forum* 396-402 (2002): p. 1443.
25. K.A. Unocic, P. Kobe, M.J. Mills, G.S. Daehn, *Mater. Sci. Forum* 519-521 (2006): p. 327.
26. I. Gheorghe, V.B. Dangerfield, "Aluminium-Magnesium-Silver Based Alloys," United States Patent, US2008030500A1, 2008.
27. I.J. Polmear, I.F. Bainbridge, "Improved Aluminium-Magnesium Casting Alloys," Australian Provisional Patent Number 37271/63, 1963.
28. I.J. Polmear, K.R. Sargent, *Nature* 200 (1963): p. 669.
29. C.L. Briant, K.S. Kumar, Z. Wang, P. Wang, "The Effect of Microstructure on the Polarization and Stress Corrosion Cracking in Al-5Mg Alloys," paper no. 00373, CORROSION/2000 (Houston, TX: NACE 2000).
30. ASTM G67-04, "Standard Test Method for Determining the Susceptibility to Intergranular Corrosion of 5XXX Series Aluminum Alloys by Mass Loss After Exposure to Nitric Acid (NAMLT Test)" (West Conshohocken, PA: ASTM International, 2004).
31. L.L. Rokhlin, *Magnesium Alloys Containing Rare Earth Metals* (London, U.K.: Taylor & Francis, 2003).

# Chapter 8

## Discussion and Future Works

---

### 8.1 General Discussion

A review of the literature highlighted a deficiency of archival public domain works that have focused on the aim of rationalising a scientific approach for the development of more corrosion resistant Al-alloys (both in the compositional selection but also in the attendant rationale). This is in contrast to the body of work that evolved some decades ago regarding stainless steels, and modified ferrous alloys. In contrast to the Al-alloy development work, there is, in contrast, significant (hundreds) of works that have focused on corrosion of existing commercial alloys (such as AA7075-T6 or AA2024-T3) [1-8]. The works carried out in this project herein, were based on the hypothesis that by controlling chemistry (and hence microstructure) it is possible to alter the corrosion rate (a logical notion which is appreciated from the literature in itself) with a view to development Al-alloys that are more corrosion resistant for equivalent or better mechanical properties. Whilst it is appreciated and emphasised that a single dissertation can only contribute part way to this endeavour, there is a large amount of scientific learning which comprises this thesis, that has been elucidated and is original. As such, this chapter will discuss/consolidate some of the key findings from the body of work in Chapters 4 to 7 in relation to the Research Aims set at the beginning of this project.

As for contributing towards foundational information, Research Aim 1 is focused on establishing (if not, revealing) the corrosion rate vs. hardness property space. There are some caveats here, in that hardness was used as a proxy to strength. This was justified on the basis that many of the commercial alloys don't have the dimensions to permit tensile testing (i.e. 3xxx alloys are very thin sheet, destined for can-stock, etc.). Further the corrosion rate vs. hardness property space was really represented to serve as a baseline to rationalise (and identify the relevant property space for) the development of new Al-alloys with improved corrosion resistance. Consequently, various commercial Al-alloys were tested and the results provided a significant amount of consolidated information of the corrosion behaviour of Al-alloys – rather generally. There was a realisation of a correlation between higher mass loss

being associated with alloys that have higher measured hardness. The presentation of the so-called ‘property space’ also allowed some rather obvious – but not previously reported – aspects to become obvious. For example, alloys that contain beyond a critical concentration of Cu - which can contribute to strengthening of Al-alloys such as the 2xxx series and modifying the 7xxx series alloys - occupy the high corrosion, high mass loss space. The tests also indicated that AA5083, which is a medium strength alloy, displays low corrosion rates, and can be rationalised to be the best compromise alloy for the strength and corrosion performance of the alloys surveyed. This in itself justifies the empirical evidence which suggests AA5083 is the benchmark (industrially) for Al-alloys corrosion – and hence the benchmark herein for what can be further developed; serving as a baseline in assessing the improvement of corrosion performance for the experimental alloys produced from this point forward.

Research Aim 2 centres on understanding the effect of alloying elements in relation to electrochemical response of Al-alloys. In Chapter 4, extensive potentiodynamic polarisation tests were carried out on various types of commercial Al-alloys whilst Chapter 5 (Section 5.1) covers the Al-4Mg-0.4Mn alloys with regards to the addition of elements including Ti, Zn, Zr, Pb, Nd, Sn, Sr and Si. An important criterion in discussing the electrochemical response is the anodic and cathodic reactions kinetics. From the results, the value of  $E_{\text{corr}}$  was seen to vary with the presence of alloying elements. Variation was dictated by either an alteration in the anodic reaction or cathodic reaction, or a combination of the change in the rates of the two reactions. As such, the value of  $E_{\text{corr}}$  alone was seen to be a crucial parameter in the assessment of the corrosion performance. An exception is in high strength commercial Al-alloys that contain significant Cu, where the  $E_{\text{corr}}$  is ennobled but not associated with reduced corrosion (with significant pitting observed during subsequent exposure and profilometry). From a mechanistic perspective, attention is given to the anodic and cathodic reaction kinetics (more specifically, their relative shifts with alloying) where the rate of reaction associated with electrochemical kinetics is better explained. Section 5.1 (Chapter 5) highlighted that microalloying did not have major impact in the anodic/kinetic reaction rate compared to the base alloy, where only a handful of elements have a statistically significant impact. For instance, the presence of Sn, Nd and Zr were able to reduce the cathodic reaction rate which is in itself considered good; however this phenomenon was offset by high mass loss in the case of Sn addition, mainly contributed to the anodic activation effect [9-12], also



demonstrated by a massive increase in anodic reaction kinetics in the potentiodynamic polarisation curve. Such results were interesting from a scientific perspective, because they highlighted some fundamental challenges. The reduction in cathodic kinetics which may be derived from the utility of alloying elements with a low exchange current density, has a deleterious second order effect. This can thus rule such elements out in terms of alloy design, perhaps in itself a contribution (from a negative result). In a (very) positive sense, the presence of Sr was able to reduce the anodic reaction rate, whilst the cathodic reaction rate remained unchanged; the mass loss value however was not however significantly reduced in comparison to other alloys, but none the less a useful result (particularly when considering sensitisation), as where all the reported results in a unique manner) – which will not be repeated in their entirety here.

In order to elucidate the results from different types of corrosion tests, emphases on the understanding of the microstructural aspect of the alloys are given in Research Aim 3 and 4. Microstructural heterogeneity, gained from alloying elements and heat treatments, contribute to the increase in strength for commercial Al-alloys (generally). Chapter 4 demonstrated that high strength alloys have high mass loss values and high average pit density observed after long term immersion tests. This indicates that improvement in strength caused susceptibility to localised corrosion – deterministically linked to the increased presence of intermetallic particles. For 2xxx series Al-alloys, such particles are  $\text{Al}_2\text{CuMg}$  (S-phase) and  $\text{Al}_2\text{CuLi}$  ( $T_1$ ). Whilst in the 7xxx series Al-alloys, they are  $\text{MgZn}_2$ , whilst many alloys include a range of constituent particles such as  $\text{Al}_7\text{Cu}_2\text{Fe}$ ,  $\text{Mg}_2\text{Si}$ ,  $\text{Al}_6\text{Mn}$  and  $\text{Al}_2\text{Cu}$  (to name but a few). This justifies the electrochemical tests discussed above, perhaps pointing to the notion that one path to developing more corrosion resistance Al-alloys is to minimise the use of Cu as alloying element where possible.

In Section 5.1 (Chapter 5), microalloying Al-4Mg-0.4Mn alloys did not result in significant changes in heterogeneity of the microstructure. Therefore the hardness gained by the alloys had only a small variation. The caveat is made that limited TEM was conducted to report the nanostructure due to constraints related to breadth versus depth. The polarisation tests also revealed that small additions of alloying elements did not cause significant alterations in the electrochemical response of the alloys.

In regards to the morphology of corrosion that occurred, as stated in Research Aim 4, for the

Al-alloys studied herein and in the electrolyte used throughout (0.1M NaCl), corrosion attack was observed to be largely in the form of pitting. Corrosion localisation was associated with the presence of intermetallic particles and obviously aided by the 0.1M NaCl. There was some unique interactions reported, as described in Section 5.2 (Chapter 5), pitting associated with  $\text{Mg}_2\text{Si}$  was manifest as attack localised to the  $\text{Mg}_2\text{Si}$  causing the formation of deep pits as verified by profilometry work (Section 5.1, Chapter 5). It was revealed in such instances that there was a more diffuse correlation between pit depth, pit density and mass loss value. It was demonstrated by Ti containing Al-4Mg-0.5Mn alloy that has high mass loss value, the pit density however was low and pit depth was high. This is perhaps the form of attack that is most typical with instances that are dictated by more rapid cathodic kinetics as a result of alloying (providing better electrochemical support for pits to deepen). Again, such discussion points are being made to reveal the number of complex factors that are of relevance in Al-alloy corrosion and corrosion morphology. The revelation of a number of factors, some of which were better explored than others, is not considered a weakness – but a progress – on the basis that there exists a catalogue of considerations. The original parts of the work have been summarised in the respective papers, but also in the conclusions.

The susceptibility of pitting which is typically / nominally related to the  $E_{\text{pit}}$  obtained from polarisation curves, was seen to not be able to estimate the pitting propensity in the most efficient manner. Section 5.3 (Chapter 5) highlighted the application of current transient measurements to quantify metastable pits. In this work, the potential was held at a constant, (under)potential below  $E_{\text{pit}}$ . The current transient counts were found to correlate with the actual pits that formed after a long-term immersion as characterised as demonstrated by profilometry images, and also scale with the microstructural heterogeneity. This parallel work was also a good rationalisation of the initial research aims as they relate to general understanding.

In slight deviation, but in theme with the study of 5xxx alloys, a propagation form for corrosion (subsequent to pitting) is intergranular attack of sensitised microstructures. This was described as the deleterious precipitation which can occur for the 5xxx series alloys (with an excess of Mg) during operation or exposure at an elevated temperature. A parallel assessment was made of intergranular attack via nitric acid mass loss testing (NAMLt). The works related to this aspect was covered in Chapter 6, using the same alloys as in Section 5.1. With the aide of phase analysis and NAMLt, alloys which displayed a lower susceptibility to

intergranular corrosion contained Sr, Ti and Si. This realisation was a significant finding, and was attributed to the ability of these elements to either modify the fraction of  $\beta$ -phase or to modify the  $\beta$ -phase itself. However, from a discussion perspective, perhaps one of the more universal outcomes of that line of work, was that it revealed the ability of calculated phase diagrams (i.e. CALPHAD packages) to provide a desktop experiment in regards to aspects which are noted to dictate corrosion and corrosion propagation. As such, there is ahead a blue-sky for similar approaches to be used to aide in tackling the development of Al-alloys for future applications – as they pertain to unique applications. A demonstration was however seen here, no less, whereby calculations were useful in the selection elements for sensitisation resistance – demonstrating the approach and its potential utility.

Information gained in Chapter 4 to Chapter 6 was useful in elucidating several of the key critical factors in the corrosion of Al-alloys more generally, and can be used as foundational knowledge towards assisting the design of new Al-alloy compositions as listed in Research Aim 5. This leads to a shortlist of elements that are potentially able to moderate corrosion behaviour by minimising pitting (as well as intergranular corrosion), in the context of this work. This distinction was made on the basis that we rationalised the research boundaries on the basis of leaning towards the 5xxx (non-heat treatable) path. There is perhaps likely to be unique aspects yet to be un-earthed in the context of the identified 6xxx series (heat treatable alloy) path. Herein, the promising elements Sr and Nd were further explored in Chapter 7, by incremental additions to the baseline 5xxx (Al-Mg-Mn) composition. The results pointed towards optimised / critical values of Sr and Nd which were effective from a corrosion perspective – as summarised in the attendant manuscripts.

## 8.2 Future Work

The findings from this project revealed a considerable amount of future work. The amount of future work can be reported to be very extensive, or instead – as done herein – can be rationalised towards a few focused aspects. There are indeed two paths for future work, which include (i) several new opportunities to improve corrosion performance of Al-alloys, whilst being sympathetic to mechanical aspects, and (ii) fundamental aspects which can be further explored in depth following some of the empirical revelations of the general work herein. In focusing on the former (i.e. (i)), some of the following are two suggestions that can be explored:

### **1. An extensive study on the effect of Sr and Nd in Al-Mg-Mn alloys (and more widely in commercial Al-alloys as a functional modification):**

- Investigation of electrochemical response of previously un-studied intermetallics on a phase-by-phase basis.

Addition of alloying elements at or above the solubility limit in Al will introduce heterogeneity in the microstructure (which is essential to achieve certain level of strength for commercial use). The downside of heterogeneity is the increase in pitting susceptibility. The findings in Chapter 7 revealed that corrosion attack was not associated with the  $\text{Al}_4\text{Sr}$  and  $\text{Al}_{11}\text{Nd}_3$  intermetallics. This is interesting in regards to imparting so called ‘passive heterogeneity’ into the microstructure - which be useful in exploiting the corrosion-strength relationship. The project stopped short of understanding if such  $\text{Al}_4\text{Sr}$  and  $\text{Al}_{11}\text{Nd}_3$  intermetallics are effective in strengthening (or other properties, both positively and negatively). In particular if this effect is understood, alternate elements that behave similarly – or perhaps more beneficially across a range of properties - may also be deployed. Information on the characteristics of  $\text{Al}_4\text{Sr}$  and  $\text{Al}_{11}\text{Nd}_3$  is still limited in the literature. A complete microstructural level characteristic can be done by microelectrochemical testing supplemented by higher level of electron microscopy including TEM.

- Modification of  $\beta$ -phase by the formation of ternary phase

The addition of Zn to Al-Mg(-Mn) alloys was previously reported to improve resistance against intergranular corrosion due to the formation of an Al-Mg-Zn ( $\tau$  phase) instead of  $\text{Al}_3\text{Mg}_2$  ( $\beta$  phase). This project demonstrates similar, in fact enhanced, results can be achieved by the addition of Sr and Nd. There was limited advanced characterisation herein, but extensive studies of the microstructure (in a quantitative sense) at a deeper level will help to improve the understanding on the segregation of these elements in either modifying the fraction of  $\beta$ -phase or the ability of other co-precipitated intermetallics to reduce the amount of Mg available in the alloy to form  $\beta$ -phase. Other factors that have to be considered in reducing intergranular corrosion are the location of the additional (or perhaps ternary) phase; whether by functioning by interrupting the continuity of  $\beta$ -phase or removing the  $\beta$ -phase from grain boundaries.

## **2. Formation of sub-critical features in the microstructure of Al-alloys as stimulated by heat treatments**

The key factor in 5xxx series alloys with regards to retention of corrosion resistance is a result of the ability of aluminium and magnesium to form a solid solution over a wide range of compositions. Solid solution alloys are good candidates for more corrosion resistant Al-alloys; however the limitation in the strength they can achieve is one technical barrier to their potential wider usage. As was revealed by Ralston and co-workers, careful low aging time heat treatments can stimulate early or pre-precipitation processes which lead to re-organisation of the solid solution but with insufficient driving force for en masse nucleation and growth to form large precipitates. This so-called engineered or heterogeneous solid solution is effective at increasing strength, but not deteriorating corrosion performance. Although the alloy system used in the work by Ralston contained Cu (which our work and all evidence has suggested is an element to avoid), it is a good indication of possibility that this concept may be viable for non-copper containing alloy. The reorganisation of solute

atoms can be explored for systems containing Mg or Si – however this would require dedicated future work.

## References

- [1] M.K. Cavanaugh, N. Birbilis, R.G. Buchheit, *Electrochimica Acta*, 59 (2012) 336-345.
- [2] J.G. Brunner, N. Birbilis, K.D. Ralston, S. Virtanen, *Corrosion Science*, 57 (2012) 209-214.
- [3] D.K. Xu, N. Birbilis, D. Lashansky, P.A. Rometsch, B.C. Muddle, *Corrosion Science*, 53 (2011) 217-225.
- [4] T. Marlaud, B. Malki, C. Henon, A. Deschamps, B. Baroux, *Corrosion Science*, 53 (2011) 3139-3149.
- [5] A.E. Hughes, A. Boag, A.M. Glenn, D. McCulloch, T.H. Muster, C. Ryan, C. Luo, X. Zhou, G.E. Thompson, *Corrosion Science*, 53 (2011) 27-39.
- [6] A. Boag, A.E. Hughes, A.M. Glenn, T.H. Muster, D. McCulloch, *Corrosion Science*, 53 (2011) 17-26.
- [7] S.P. Knight, N. Birbilis, B.C. Muddle, A.R. Trueman, S.P. Lynch, *Corrosion Science*, 52 (2010) 4073-4080.
- [8] K.-H. Na, S.-I. Pyun, *Corrosion Science*, 50 (2008) 248-258.
- [9] Y.W. Keuon, J.H. Nordlien, S. Ono, K. Nisancioglu, *Journal of The Electrochemical Society*, 150 (2003) B547-B551.
- [10] Z. Jia, B. Graver, J.C. Walmsley, Y. Yu, J.K. Solberg, K. Nisancioglu, *Journal of The Electrochemical Society*, 155 (2008) C1-C7.
- [11] B. Graver, A.M. Pedersen, K. Nisancioglu, *ECS Transactions*, 16 (2009) 55-69.
- [12] J.T.B. Gundersen, A. Aytaç, J.H. Nordlien, K. Nişancıoğlu, *Corrosion Science*, 46 (2004) 697-714.

# Chapter 9

## Conclusions

---

It can be summarised that the work in this thesis was an evolution of learnings from the initial to the final experiments. The work relates to the technological issue, which is the development of more corrosion resistant Al-alloys. From conducting a comprehensive literature review, there is an evident paucity of the reported archival work that has focused on the development of more corrosion resistant Al-alloys, particularly in regards to compositional selection or balancing industrially useful properties, in spite of the wide usage of Al-alloys. This may not reflect the extent of industry knowledge; however such information is not openly available, nor may it be related to the underlying science. Herein, it was hypothesised that by controlling chemistry and microstructure it is possible to develop Al-alloys that are more corrosion resistant for equivalent or better mechanical properties. The individual tasks carried out in this thesis, presented as unique papers / reports, in their own right each provide new information of scientific significance. As described previously, it was decided that following initial work defining the primitive property space, and the subsequent rationalisation in terms of structure and electrochemical properties, the remainder of the work would focus on the non-heat treatable 5xxx Al-Mg-Mn system (i.e. a finite endeavour).

Whilst the relevant conclusion have been presented within the relevant reports / papers included in this dissertation, some key conclusions drawn from this work is summarised as the following:

- The presence of alloying elements contributes to the increase in strength by the formation of a heterogeneous microstructure. This also leads to an increase in the susceptibility to localised attack. The corrosion rate vs. hardness property space revealed that medium-to-high strength commercial Al-alloys (i.e. 2xxx and 7xxx series) populate the high corrosion rate spectrum. The presence of Cu in these alloys enhances precipitation hardening (in 2xxx alloys) hence increasing the localised attack sites. In the case of 7xxx alloys, an  $\text{MgZn}_2$  precipitate (along with often appreciable amounts of Cu) is a known issue. However, the low strength commercial Al-alloys (i.e. 3xxx and 5xxx series alloys) populate the low corrosion rate spectrum.

The alloying elements in these alloys are typically Mg and Mn, that have appreciable solubility in Al. The strength is gained from solid solution strengthening therefore the microstructure is homogeneous.

- The mode of corrosion attack observed after long-term immersion testing in 0.1M NaCl was mainly localised, in particular, pitting. In general, an increase in microstructural heterogeneity arising from increased alloying increases the pit density. However, the composition and size of the particles also influence the formation of pits. For instance,  $\text{Al}_3\text{Zr}$ ,  $\text{Al}_6\text{Mn}$  and  $\text{Al}_3\text{Ti}$  present as evenly distributed nano-scale dispersoids were not found to cause appreciable corrosion. The  $\text{Al}_4\text{Sr}$  intermetallics that typically exist as coarse branched constituents were not associated with the formation of pits due the unique effect (and electrochemical homogeneity) of Sr. In order to assess pitting susceptibility of Al-alloys, potentiostatic measurement of metastable pitting events was found to be effective in estimating the number of pits that will subsequently form following open circuit exposure. The metastable pits measured using current transients from potentiostatic polarisation correlates with the number of stable pits that were observed after long-term immersion tests. This validates that the technique can be used with higher confidence in the future.
  
- In the Al-4Mg-0.4Mn alloy system, microalloying with Sr, Zn, Nd, Zr, Si, Ti, Pb and Sn, increased the anodic reaction kinetics (in an ascending order). The increase in anodic reaction kinetics was associated to the presence of  $\beta$ -phase ( $\text{Mg}_2\text{Al}_3$ ),  $\text{Mg}_2\text{Si}$  and impurity based constituent particles  $\text{Al}_x(\text{Mn,Fe})$  (i.e.  $\text{Al}_6\text{Mn}$ ,  $\text{Al}_{12}\text{Mn}$  and  $\text{Al}_3\text{Fe}$ ). In the case of Pb and Sn containing alloys, a significant increase in the anodic reaction rate was ascribed to the anodic activation phenomenon. The cathodic reaction kinetics however showed no significant changes with microalloying except for alloys containing Nd, Sn, Sr and Zr. In the case of Sn, the reduction in cathodic reaction rate was offset the anodic activation effect that lead to a significant increase in  $i_{\text{corr}}$ . The addition of Nd, Sr and Zr reduced the size of constituent particles and evenly distributed within the matrix. This lead to lower cathodic reaction rates overall.
  
- The mass loss values from long-term immersion tests of Al-4Mg-0.4Mn microalloyed with Nd, Pb, Si, Sn, Sr, Ti, Zn and Zr showed a very weak correlation to the number



of pits formed. For instance, the average number of pits for Si containing alloy was lower than the Al-4Mg-0.4Mn base alloy whilst mass loss value was amongst the highest compared to the other alloys tested. This was due attributed to the formation of coarse  $\text{Mg}_2\text{Si}$  particles (in the as-cast condition) that lead to severe localised attack when exposed to dilute chloride solution. The selective dissolution phenomenon of reactive Mg in coarse  $\text{Mg}_2\text{Si}$  particle left significantly deeper/larger pits that contribute to higher mass loss with less number of pits.

- With regards to intergranular corrosion (IGC) in the Al-4Mg-0.4Mn alloy system, the addition of Si, Sr and Ti had a positive effect. The nitric acid mass loss test (NAMLTL) revealed that these alloying elements yield better IGC resistance than the Al-4Mg-0.4Mn alloy alone. The most significant reduction in mass loss was the addition of Sr. This addition (Sr) indicates enhanced resistance to IGC, due to the ability of Sr to cause appreciable modification of the  $\beta$ -phase volume fraction. This finding was supported by phase fraction calculations that showed the formation of a small fraction of  $\text{Al}_{19}\text{Mg}_{29}\text{Sr}_2$  phase that may be significant enough to reduce  $\beta$ -phase fraction or continuity. This is relevant in the context of developing more IGC resistant 5xxx series Al-alloys that are typically exposed to elevated temperature during operation. The strength of the improved 5xxx series Al-alloys must also be considered. In this work, the high IGC resistant alloys were populated at the low hardness spectrum. With the exception of alloy containing Zr and Sr, which has slight potential to improve IGC resistance whilst maintaining the hardness, it is apparent that more research in this area is essential.
  
- In the development of 5xxx series Al-alloys with improved corrosion resistance, it is important to find a balance between improving corrosion resistance to different types of attack. After considering the outcomes of the corrosion response of different alloying elements, it can be concluded that the addition of Nd and Sr were found to have a good balance between reducing the susceptibility to localised attack and IGC. Both elements improved the corrosion resistance by forming electrochemically homogeneous phases that are not associated with the localised attack that occurred.
  
- The addition of Sr in commercially pure Al alloy formed a coarse  $\text{Al}_4\text{Sr}$  intermetallic

phase that increased in volume fraction as the Sr content increased. On exposure to dilute chloride solution, it was observed that the localised corrosion was not associated with the presence of the  $\text{Al}_4\text{Sr}$  intermetallic particles but rather the Fe-containing constituent particles. In addition, the pitting potential ( $E_{\text{pit}}$ ) for Sr containing alloys was identical to pure Al, indicating enhanced localised corrosion resistance to a level similar to that of pure Al. A decreased in  $i_{\text{corr}}$  was observed for alloys with more than 0.11 wt.% Sr, this implies that there might be a critical amount of Sr required to effectively reduce the corrosion rate.

- The addition of Nd in the Al-5Mg alloy system did not significantly affect the morphology of coarse intermetallics particles. However, phase fraction analysis revealed the presence of  $\text{Al}_{11}\text{Nd}_3$  phase. Hardness values increased with the increase of Nd content. On exposure to dilute chloride solution, a slight decrease in anodic and cathodic reaction kinetics was observed whilst no significant changes in the  $E_{\text{corr}}$  and  $i_{\text{corr}}$  with varying Nd content. The electrochemical response suggests the possibility of  $\text{Al}_{11}\text{Nd}_3$  phase is compatible with Al-Mg matrix and/or the size of  $\text{Al}_{11}\text{Nd}_3$  phase is too small to cause any significant changes. The mass loss values after long-term immersion tests showed no statistically significant changes than the base Al-5Mg alloy. Subsequent optical profilometry analysis of the surface confirmed that Nd addition did not influence pitting corrosion.
  
- Alloys containing Sr and Nd significantly reduced the susceptibility to IGC. Both elements increased the resistance to IGC by modifying the volume fraction of  $\beta$ -phase. For the addition of Nd, it was observed that some segregation of Nd to coarse AlMnFe particles and  $\beta$ -phase did occur. The incorporation of Nd into  $\beta$ -phase changed the electrochemical characteristic of the  $\beta$ -phase, leading to a decrease in the possibility of corrosion attack hence increasing the resistance to IGC. For the addition of Sr, shows the most significant result in improving the IGC resistance to a value considered as highly resistant compared to other elements. This enhancement is majorly owed to the ability of Sr to form a high Mg containing ternary phase,  $\text{Al}_{19}\text{Mg}_{29}\text{Sr}_2$  at the expense of  $\beta$  phase.

